A Thesis for the Degree of Ph.D. in Engineering

Integration of Ionophore-Based Ion-Selective Optodes into Paper-Based Sensing Platforms for Optical Cation Detection

July 2019

Graduate School of Science and Technology

Keio University

SHIBATA, Hiroyuki

Table of Contents

Chapter 1

General introduction to ionophore-based ion-selective optodes and paper-based sensing platforms

1.1. Ion-selective optodes (ISOs)

1.1.1. Short history of the origin in the academic field

The quantification of ion species undoubtedly plays an important role for many years in the various analytical fields, such as medical diagnosis, environmental monitoring, food chemistry, and biochemical research.[1-5] In distinction from other analytical techniques, such as electrochemistry, atomic (flame) emission spectrometry (AES), and capillary electrophoresis (CE), optical chemical sensors have been expected to replace conventional analytical methods because of their common multiple advantages: (i) easy to miniaturize instruments, (ii) inexpensiveness to manufacture, and (iii) potential of compatibility with other techniques.[6-10] Their optical detection can be accomplished with an indicator chromogen generating the spectral information (e.g. absorbance and/or fluorescence, reflectometry), based on an interaction between analytes and analyte-specific receptors. However, common indicators for ion species suffer from modest selectivity and flexibility in the term of their dynamic response range.[7]

For this issue, ionophore-based ion-selective optodes (ISOs) have extensively gained as more powerful optical chemical sensors along with a electrochemical counterpart of ion-selective electrodes (ISEs), because they can tune the analytical performances of both their selectivity and their dynamic range by changing the sensing components (refer to later section for the working principle). Typically, ionophore-based ISOs are composed of following lipophilic sensing reagents: chromoionophore (colorimetric pH indicator), ionophore (ion-specific receptor), and ion-exchanger (organic salt to maintain electroneutrality, if necessary), and their working principle is based on the ion-exchange reaction for cation detection or the co-extraction for anion

detection as illustrated in **Figure 1-7**.[6-7, 9] In both cases, the ISO-based reaction refers to protons of H^+-responsive chromoionophores as reference ions together with optically-silent ionophores. For a comprehensive review of ionophores for all kinds of ionic species, the excellent review was reported by Bühlmann *et al.*[11]

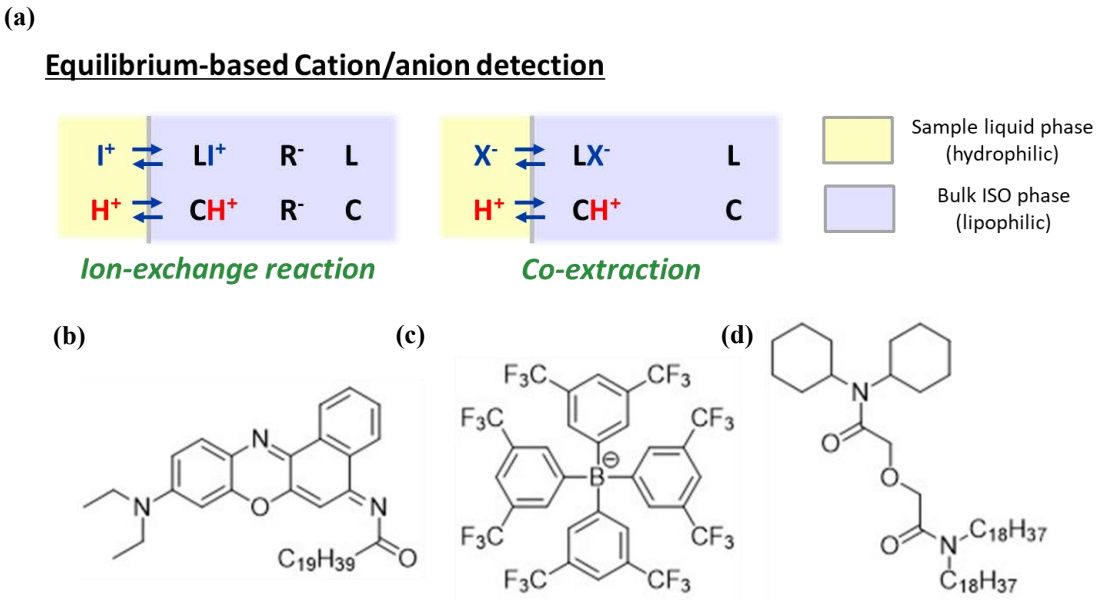

Figure 1-1. (a) Schematic reaction scheme of ISOs for equilibrium-based cation/anion determination. The legends of I^+/X^-, L, C, and R^- represent cationic/anionic analytes, ionophores, chromoionophores, and ion-exchanger, respectively. Increasing the concentration level of I^+/X^- results in the promotion of the rightward reaction (*i.e.* deprotonation/ protonation of chromoionophores for cation/anion detection); (b)-(d) examples of cation-sensing components of ISOs; (b) chromoionophore (chromoionophore I), (c) ion-exchanger (TFPB: tetrakis[3,5-bis(trifluoromethyl)phenyl]borate); (d) ionophore (calcium ionophore IV).

The first concept of resembled modern ISOs was introduced by Charlton *et al.* in 1982, based on the co-extraction of both a cationic analyte (K^+) and an anionic dye (erythrosine B) with a K^+-selective ionophore (valinomycin)[12]. A solid-type test strip containing ionophores was soaked into the sample liquid solution prepared by diluting with the cationic dye solution, followed by generating the optical signal corresponding to the analyte concentration. However, the academic research on ISOs did not progress rapidly until 1990s when Simon's research group developed a new class of a lipophilic colorimetric pH indicator, now commonly referred to as a chromoionophore[13]. Afterward, Simon's research group also established the detection principle of modern neutral carrier-based ISOs for determination of ammonia[14] and calcium[15] (detailed working

principle will be demonstrated in following **section 1.1.2.**). Since the development of the original chromoionophore by Simon research groups at ETHZürich[16], most of the ionophore-based ISOs have relied on Nile blue derivatives, which are commercialized as chromoionophore/ETH series by Sigma Aldrich.

1.1.2. Theory of working principle

1.1.2.1. Response function for the cation detection

The working principle of equilibrium-based ISOs is well-established for the optical detection of cations/anions. Their detection mechanism is typically based on an equilibrium reaction between a water-immiscible polymeric membrane and an aqueous sample phase as shown in **Figure 1-1**.[6-7] Selective recognition of the ion species of interest is achieved by an ion-specific receptor (*i.e.* ionophore) doped into the organic polymeric membrane. To data, various materials for bulk membrane substrates have been applied, such as cellulose acetate, polyvinyl chloride (PVC), ethylcellulose, poly(vinyl alcohol), nafion, polyurethane, poly(alkyl methacrylate).[6, 9] Among them, PVC is the most popular polymer matrix because it has great capacity of membrane solvent (*i.e.* plasticizer). Extraction of the target ion into the organic phase is accompanied by either protonation (for anionic target ions) or deprotonation (for cationic target ions) of a co-doped chromoionophore, generating an optical signal from the ISO membrane. Their advantageous features, including high selectivity and ease of optical signal detection, gave birth to a variety of ISO configurations such as thin membrane films, particles, and suspension.[6-10, 17]

In this context, the current thesis intends to describe the only cation detection with carrier-based ISOs. For anion detections, as a number of excellent review articles are available[6-9], and thus, its detailed working principle will not be repeated here. In the term of the cation detection, the observable optical signal is based on the degree of deprotonation of the H^+-sensitive chromoionophore (α), corresponding to the concentration level of cationic analytes. **Figure 1-2** shows an overview of popular combinations of the following chemical components, such as a chromoionophore (C), an ionophore (L), an ion-exchanger (R), for the determination of

cations. Since only chromoionophores and ionophores cannot maintain electroneutrality during the ISO-based reaction (*e.g.* ***a*** and ***e*** in **Figure 1-2**), ion-exchangers (R^- or R^+) must be doped into the organic optode phase.[6-7] Most of the studies on ISOs have exploited the detection principle with a neutral ionophore and a neutral chromoionophore (***e*** in **Figure 1-2**). On the other hand, in the term of "***c***" and "***f***" in **Figure 1-2**, the used ionophore itself must generate optical signal relying on the analyte concentration level.

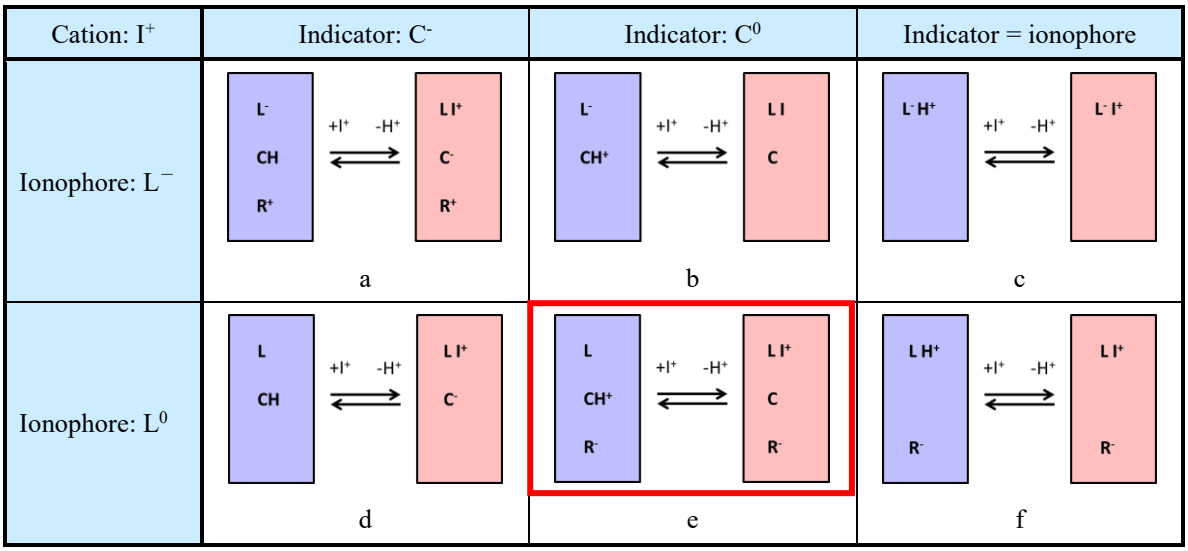

Figure 1-2. An overview of popular combinations of the following ISO components for the equilibrium-based determination of cations (I^+): a chromoionophore (C), an ionophore (L), an ion-exchanger (R^-/R^+). Adapted with permission from Ref. 7.

In the current thesis, the stepwise process for ion-exchange equilibrium reaction (**Figure 1-2e**) will be demonstrated. Selective extraction of cationic analytes (I^{z+}) into the organic optode phase triggers a release of protons of chromoionophores (H^+) into the sample liquid phase to maintain electroneutrality in the organic optode phase. The working principle can be expressed in a simplified manner based on the ion-exchange equilibrium reaction using **eq (1)**.[6-7]

$$I^{z+}(aq) + nL(org) + zCH^+(org) + zR^-(org) \rightleftharpoons L_nI^{z+}(org) + zC(org) + zH^+(aq) + zR^-(org) \quad (1)$$

$$I^{z+}(aq) + nL(org) + zCH^+(org) \rightleftharpoons L_nI^{z+}(org) + zC(org) + zH^+(aq) \quad (1)'$$

where, subscripts of (org) and (aq) designate the organic optode phase and the aqueous sample liquid phase, respectively; L is a neutral ionophore; C is a neutral chromoionophore; R^- is an ion-exchanger; z represents a valent of the analyte ion; n represents the stoichiometry ratio of the analyte-ionophore complex. For corresponding cation with charge z, an equivalent number of protons is necessary to be released from the organic phase. Because ion-exchangers are not involved in the ion-exchange reaction (see **eq (1)'**), the overall equilibrium constant of the reaction (K_{exch}) can be given by using the corresponding concentrations/activities as shown in **eq (2)**.[6-7]

$$K_{\mathrm{exch}} = \frac{[\mathrm{C}]^z (a_{\mathrm{H}})^z [\mathrm{L}_n \mathrm{I}^{z+}]}{[\mathrm{CH}^+]^z [\mathrm{L}]^n a_{\mathrm{I}}} \tag{2}$$

where, a_{H} and a_{I} represent the activity of the proton (H^+) in the aqueous phase and the free cation analytes in the aqueous phase, respectively. Here, because we cannot find the concentrations of ISO components after the ion-exchange equilibrium reaction, the unknown terms should be replaced by the experimental parameters. Firstly, **eq (3)** involving the degree of deprotonation of the chromoionophores (α) is essential to make a correlation between an experimental optical signal and a_{I}.

$$1 - \alpha = \frac{[\mathrm{CH}^+]}{C_{\mathrm{T}}} \tag{3}$$

where, C_{T} represents the total concentration of the used chromoionophore in organic phase (known from the optode preparation). On the other hands, since mass balance must not be changed during ISO-based reaction, each sensing components of ISOs can be expressed with **eqs (4) to (6)**, representing the total concentrations of the corresponding sensing reagents.

$$R_{\mathrm{T}} = [\mathrm{CH}^+] + z[\mathrm{L_n I}^{z+}] \tag{4}$$

$$L_{\mathrm{T}} = [\mathrm{L}] + n[\mathrm{L_n I^{z+}}] \tag{5}$$

$$C_{\mathrm{T}} = [\mathrm{C}] + [\mathrm{CH^+}] \tag{6}$$

where, R_{T} and L_{T} represent the total concentration of the used ion-exchanger and ionophore in organic phase, respectively (known from the optode preparation). Here, the unknown concentrations in **eq (2)** can be replaced by using experimentally observable terms (e.g. R_{T}, L_{T}, C_{T}, $[\mathrm{CH^+}]$) according to **eqs (4) to (6)**.

$$[\mathrm{L}] = L_{\mathrm{T}} - \frac{n}{z}(R_{\mathrm{T}} - [\mathrm{CH^+}]) \tag{7}$$

$$[\mathrm{C}] = C_{\mathrm{T}} - [\mathrm{CH^+}] \tag{8}$$

$$[\mathrm{L}_n\mathrm{I}^{z+}] = \frac{R_{\mathrm{T}} - [\mathrm{CH^+}]}{z} \tag{9}$$

Then, **eqs (3), (7) to (9)** are inserted into **eq (2)** to estimate the K_{exch}, and **eq (2)** is solved for a_{I} in order to obtain response function: [6-7]

$$a_{\mathrm{I}} = \frac{1}{zK_{\mathrm{exch}}}\left(\frac{\alpha}{1-\alpha}a_{\mathrm{H}}\right)^{\mathrm{z}} \times \frac{R_{\mathrm{T}} - (1-\alpha)C_{\mathrm{T}}}{\{L_{\mathrm{T}} - (R_{\mathrm{T}} - (1-\alpha)C_{\mathrm{T}})(n/z)\}^n} \tag{10}$$

Here, α can be calculated according to **eq (11)** based on the experimentally determined absorbance of the chromoionophore in the optode phase.[6-7]

$$\alpha = \frac{A_{\mathrm{P}} - A}{A_{\mathrm{P}} - A_{\mathrm{D}}} \tag{11}$$

where A represents the experimentally measured absorbance at any given protonation state; A_{P} and A_{D} stand for the absorbance in the fully protonated and deprotonated states, respectively.

1.1.2.2. The overall equilibrium constant (K_{exch}) explained by the complexation constants

The overall equilibrium constant (K_{exch}) represents the whole reaction process of **eq (1)**, containing the acidity of the used chromoionophore (K_a) and analyte-ionophore complex formation constant ($\beta_{L_nI^{z+}}$). Each ion-exchange equilibrium reaction during the cation assay is illustrated in **Figure 1-3** to consider the concentration of the single protons and analyte ions in both the organic optode phase ($[H^+]$, $[I^{z+}]$) and the aqueous phase (a_H, a_I).[6-7] Because the primary ions in the aqueous sample phase (*i.e.* I^{z+}, H^+) cannot directly form the complex with the receptors (*i.e.* ionophore, chromoionophore), it is essential that the transportation of the primary ions from the aqueous phase to the organic phase as shown in **Figure 1-3**.

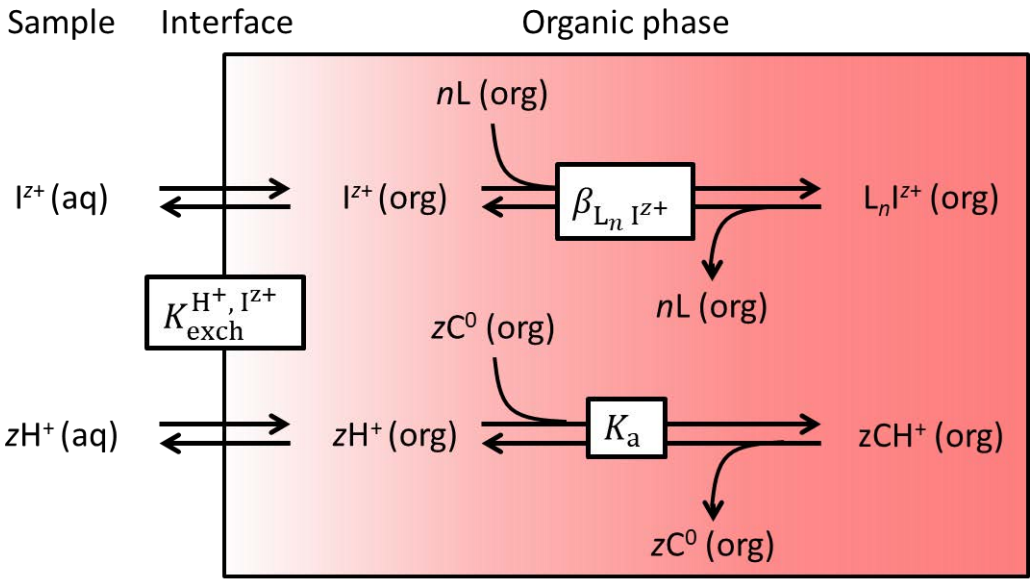

Figure 1-3. Schematic detailed ion-exchange equilibrium reaction scheme for cation detection with the typical ISO sensing components; subscripts of "(org)" and "(aq)" designate the organic phase and the aqueous phase respectively; L, C, and R represent an ionophore, a chromoionophore, and an ion-exchanger, respectively; K_a is the acidity of the used chromoionophore; $\beta_{L_nI^{z+}}$ is the constant of analyte-ionophore complex formation; $K_{exch}^{H^+,I^{z+}}$ represents the exchange constant for the naked ions. Adapted with permission from Ref. 7.

Then, we will consider an ion-exchange constant for the naked ions on the surface between the aqueous sample phase and the organic optode membrane ($K_{exch}^{H^+,I^{z+}}$). Based on **Figure 1-3**, $K_{exch}^{H^+,I^{z+}}$ can be expressed with **eq (12)**.

$$K_{\mathrm{exch}}^{\mathrm{H}^+,\mathrm{I}^{z+}} = \frac{(a_{\mathrm{H}})^z[\mathrm{I}^{z+}]}{[\mathrm{H}^+]^z a_{\mathrm{I}}} \tag{12}$$

On the other hands, the acidity constant (K_a) and the complex formation constant ($\beta_{\mathrm{L_nI}^{z+}}$) can be given as follows:

$$z\mathrm{CH}^+(\mathrm{org}) \rightleftharpoons z\mathrm{C}(\mathrm{org}) + z\mathrm{H}^+(\mathrm{org})$$

$$(K_{\mathrm{a}})^z = \frac{[\mathrm{C}]^z[\mathrm{H}^+]^z}{[\mathrm{CH}^+]^z} \tag{13}$$

$$n\mathrm{L}(\mathrm{org}) + \mathrm{I}^{z+}(\mathrm{org}) \rightleftharpoons \mathrm{L_nI}^{z+}$$

$$\beta_{\mathrm{L_nI}^{z+}} = \frac{[\mathrm{L_nI}^{z+}]}{[\mathrm{I}^{z+}][\mathrm{L}]^n} \tag{14}$$

Therefore, the overall ion-exchange constant ($K_{\mathrm{exch}}^{\mathrm{overall}}$) can be estimated by multiplying above constants of **eqs (12) to (14)**.

$$K_{\mathrm{exch}}^{\mathrm{overall}} = (K_{\mathrm{a}})^z \beta_{\mathrm{L_nI}^{z+}} K_{\mathrm{exch}}^{\mathrm{H}^+,\mathrm{I}^{z+}} = \left(\frac{[\mathrm{C}]a_{\mathrm{H}}}{[\mathrm{CH}^+]}\right)^z \frac{[\mathrm{L_nI}^{z+}]}{[\mathrm{L}]^n a_{\mathrm{I}}} \tag{15}$$

In addition, obtained equation of **eq (15)** is identical to **eq (2)**, representing that K_{exch} in **eq (2)** (*i.e.* $K_{\mathrm{exch}}^{\mathrm{overall}}$ in **eq (15)**) may be replaced by K_{a}, $\beta_{\mathrm{L_nI}^{z+}}$, and $K_{\mathrm{exch}}^{\mathrm{H}^+,\mathrm{I}^{z+}}$ as follows:[6-7]

$$a_{\mathrm{I}} = \frac{1}{z(K_{\mathrm{a}})^z \beta_{\mathrm{L_nI}^{z+}} K_{\mathrm{exch}}^{\mathrm{H}^+,\mathrm{I}^{z+}}} \left(\frac{\alpha}{1-\alpha} a_{\mathrm{H}}\right)^{\mathrm{z}} \times \frac{R_{\mathrm{T}} - (1-\alpha)C_{\mathrm{T}}}{\{L_{\mathrm{T}} - (R_{\mathrm{T}} - (1-\alpha)C_{\mathrm{T}})(n/z)\}^n} \tag{16}$$

The working function for the cation detection with ISOs is predictable by using a commercial available software (e.g. Mathematica, Matlab, Excel or others) based on **eq (16)**.[6-7] Furthermore, the response function can be moderated by changing the chemical properties of the used chromoionophores or/and ionophores.

Although this approach is very useful to simulate ISO-based sensor response, direct calculation of $K_{\mathrm{exch}}^{\mathrm{H}^+,\mathrm{I}^{z+}}$ is basically challenging. Therefore, eq (16) is often applied to estimate $K_{\mathrm{exch}}^{\mathrm{H}^+,\mathrm{I}^{z+}}$ when both K_{a} and $\beta_{\mathrm{L_nI}^{z+}}$ are experimentally known by other individual experiments. In contrast to ISO-based measurement, electrochemical approach without ionophores and chromoionophores (*i.e.* ion-selective electrodes: ISEs) is more convenient for the direct estimation of $K_{\mathrm{exch}}^{\mathrm{H}^+,\mathrm{I}^{z+}}$.[6-7]

1.1.2.3. Response in the presence of interfering ions

The working principle for the cation detection as mentioned above is the ideal reaction model in the absence of the interfering ions. Although these equations are very useful for the development of ISO-based sensors, we have to attend to consider the potentially interfering ions in real sample matrix. The response function in the presence of the secondary interfering ion (J^{z+}) can be expanded in the same manner with the theory of cation detections of interest.[6-7] Separated exchange equilibria and its overall equilibrium constant (K_{exch}) for each ion can be given as follows:

$$\mathrm{I}^{z_\mathrm{I}+}(\mathrm{aq}) + n_\mathrm{I}\mathrm{L}(\mathrm{org}) + z_\mathrm{I}\mathrm{CH}^+(\mathrm{org}) \rightleftharpoons \mathrm{I}^{z_\mathrm{J}+}\mathrm{L}_{n_\mathrm{J}}(\mathrm{org}) + z_\mathrm{J}\mathrm{C}(\mathrm{org}) + z\mathrm{H}^+(\mathrm{aq}) \tag{17}$$

$$K_{\mathrm{exch}}^{\mathrm{CH}^+,\mathrm{L}_n\mathrm{I}^{z_\mathrm{I}+}} = \frac{[\mathrm{C}]^{z_\mathrm{I}}(a_\mathrm{H})^{z_\mathrm{I}}[\mathrm{L}_n\mathrm{I}^{z_\mathrm{I}+}]}{[\mathrm{CH}^+]^{z_\mathrm{I}}[\mathrm{L}]^{n_\mathrm{I}}a_\mathrm{I}(\mathrm{IJ})} \tag{18}$$

$$\mathrm{J}^{z_\mathrm{J}+}(\mathrm{aq}) + n_\mathrm{J}\mathrm{L}(\mathrm{org}) + z_\mathrm{J}\mathrm{CH}^+(\mathrm{org}) \rightleftharpoons \mathrm{J}^{z_\mathrm{J}+}\mathrm{L}_{n_\mathrm{J}}(\mathrm{org}) + z_\mathrm{J}\mathrm{C}(\mathrm{org}) + z_\mathrm{J}\mathrm{H}^+(\mathrm{aq}) \tag{19}$$

$$K_{\mathrm{exch}}^{\mathrm{CH}^+,\mathrm{L}_n\mathrm{I}^{z_\mathrm{J}+}} = \frac{[\mathrm{C}]^{z_\mathrm{J}}\left(a_\mathrm{J}\right)^{z_\mathrm{J}}[\mathrm{L}_n\mathrm{I}^{z_\mathrm{J}+}]}{[\mathrm{CH}^+]^{z_\mathrm{J}}[\mathrm{L}]^{n_\mathrm{J}}a_\mathrm{J}(\mathrm{IJ})} \tag{20}$$

where, "(IJ)" written after the activity represents the activity in the aqueous liquid solution containing both primary and interfering ions ($\mathrm{I}^{z_\mathrm{I}+}$, $\mathrm{J}^{z_\mathrm{J}+}$). On the other, mass balance of the ion-exchanger (**eq (4)**) and the ionophores (**eq (5)**) in the presence of the secondly ion can be given as follows:

$$R_\mathrm{T} = [\mathrm{CH}^+] + z_\mathrm{I}\left[\mathrm{L}_{n_\mathrm{I}}\mathrm{I}^{z_\mathrm{I}+}\right] + z_\mathrm{J}\left[\mathrm{L}_{n_\mathrm{J}}\mathrm{I}^{z_\mathrm{J}+}\right] \tag{21}$$

$$L_{\mathrm{T}} = [\mathrm{L}] + n_{\mathrm{I}}\left[\mathrm{L}_{n_{\mathrm{I}}}\mathrm{I}^{z_{\mathrm{I}}+}\right] + n_{\mathrm{J}}\left[\mathrm{L}_{n_{\mathrm{J}}}\mathrm{I}^{z_{\mathrm{J}}+}\right] \quad (22)$$

Next, a selectivity coefficient for the primary ion compared with the secondary ion (k_{IJ}) is defined by using the ratio of both ions as follows:[6-7]

$$k_{\mathrm{IJ}} = \frac{a_{\mathrm{I}}(\mathrm{I})}{a_{\mathrm{J}}(\mathrm{J})} \quad (23)$$

$$\log k_{\mathrm{IJ}} = \log a_{\mathrm{I}}(\mathrm{I}) + \log a_{\mathrm{J}}(\mathrm{J}) \quad (24)$$

Here, this legalism k_{IJ} of **eq (24)** corresponds to the difference of the sigmoidal response curve for the primary and the secondary ions at 50% deprotonation of the chromoionophore (*i.e.* $\alpha = 0.5$) as shown in **Figure 1-4**. [6-7]

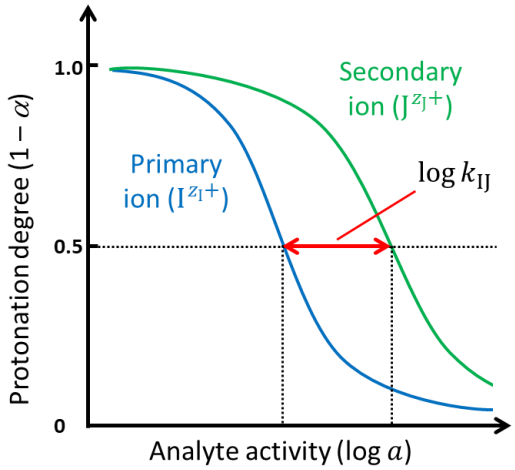

Figure 1-4. Estimation of a selectivity coefficient (k_{IJ}) by the use of the response curves for the primary ions ($\mathrm{I}^{z_{\mathrm{I}}+}$) in the presence of the secondary ions ($\mathrm{J}^{z_{\mathrm{J}}+}$).[6-7]

On the other hands, the activity of the primary ion the aqueous liquid solution containing both primary and interfering ions ($a_{\mathrm{I}}(\mathrm{IJ})$) can be expressed with **eq (25)**.

$$a_{\mathrm{I}}(\mathrm{IJ}) = a_{\mathrm{I}}(\mathrm{I}) - k_{\mathrm{IJ}}\, a_{\mathrm{J}}(\mathrm{IJ}) \quad (25)$$

Then, **eq (16)** can be expand by using **eq (25)** to estimate the correlation of $a_{\mathrm{I}}(\mathrm{IJ})$ and the ion-exchange constant for the naked ions on the surface between the aqueous sample phase and the organic optode membrane ($K_{\mathrm{exch}}^{\mathrm{H}^+,\mathrm{I}^{z+}}$) as follows:[6-7]

$$a_{\mathrm{I}} = \frac{1}{z_{\mathrm{I}}(K_{\mathrm{a}})^{z_{\mathrm{I}}}\beta_{\mathrm{L}_n\mathrm{I}^{z+}}K_{\mathrm{exch}}^{\mathrm{H}^+,\mathrm{I}^{z+}}}\left(\frac{\alpha}{1-\alpha}a_{\mathrm{H}}\right)^{z_{\mathrm{I}}} \times = \frac{R_{\mathrm{T}} - (1-\alpha)C_{\mathrm{T}}}{\{L_{\mathrm{T}} - (R_{\mathrm{T}} - (1-\alpha)C_{\mathrm{T}})(n_{\mathrm{I}}/z_{\mathrm{I}})\}^{n_{\mathrm{I}}}} - k_{\mathrm{IJ}}\, a_{\mathrm{J}}(\mathrm{IJ}) \qquad (26)$$

Here, k_{IJ} can be estimated by using the ratio of each activity as follows:

$$\begin{aligned} k_{\mathrm{IJ}} &= \frac{a_{\mathrm{I}}(\mathrm{I})}{a_{\mathrm{J}}(\mathrm{J})} \\ &= \frac{z_{\mathrm{J}}(K_{\mathrm{a}})^{z_{\mathrm{J}}}\beta_{\mathrm{L}_{n_{\mathrm{J}}}\mathrm{I}^{z_{\mathrm{J}}+}}K_{\mathrm{exch}}^{\mathrm{H}^+,\mathrm{I}^{z_{\mathrm{J}}+}}}{z_{\mathrm{I}}(K_{\mathrm{a}})^{z_{\mathrm{I}}}\beta_{\mathrm{L}_{n_{\mathrm{I}}}\mathrm{I}^{z+}}K_{\mathrm{exch}}^{\mathrm{H}^+,\mathrm{I}^{z_{\mathrm{I}}+}}}\left(\frac{1}{K_{\mathrm{a}}}\frac{a_{\mathrm{H}}\alpha}{1-\alpha}\right)^{z_{\mathrm{I}}-z_{\mathrm{J}}} \times \frac{\{L_{\mathrm{T}} - (R_{\mathrm{T}} - (1-\alpha)C_{\mathrm{T}})(n_{\mathrm{J}}/z_{\mathrm{J}})\}^{n_{\mathrm{J}}}}{\{L_{\mathrm{T}} - (R_{\mathrm{T}} - (1-\alpha)C_{\mathrm{T}})(n_{\mathrm{I}}/z_{\mathrm{I}})\}^{n_{\mathrm{I}}}} \end{aligned} \qquad (27)$$

1.1.2.4. Response time of equilibrium-based ISOs

For equilibrium-based ISOs, the time required for the extraction of target analytes into the bulk optode basically is much longer than other comparable surface- or interface-based techniques (e.g. ISEs).[6-7] This is because the limiting step for the ISO system is dominated by the diffusion within the bulk membrane (*i.e.* plasticized PVC membrane), representing that response time strongly depends on the membrane thickness except for extremely thin membranes. By introduction of a mean concentration-independent diffusion coefficient (D_{m}), a simple correlation between membrane thickness (d) and the time needed to achieve 95% of the steady state response (t_{95}) can be given by **eq (28)**:[6-7]

$$t_{95} = 1.13\frac{d^2}{D_{\mathrm{m}}} \qquad (28)$$

In the term of a typical plasticized PVC-based membrane, a response time for the diffusion of ion species can be found to be approximately 1 s for a membrane film of 1-μm thickness (in the case: $D_m \approx 10^{-8}$ cm^2 s^{-1}). In order to improve the prolonged response time, many researchers have attempted to increase the surface/volume ratio by minimizing ISOs as nanoparticles (refer to the later **section of 1.1.3** for nanoscale optodes).[6-7] However, the limitation of the diffusion in the bulk membrane phase is given only at relatively high analyte concentration.[7] Regarding the nanoscale ISO suspension, this issue will be potentially overcome by sufficiently mixing. Apart from the use of nanoscale ISOs, reducing the amount of active compounds in bulk ISOs also serves to improve the prolonged response time, but lower sensor sensitivity will occur due to the limitation of a molecular absorbance coefficient (ε) of colorimetric dyes. For this issue, a limit of detection (LOD) of absorbance-based measurements, in particular definitely depends on instrumentation-relying sensitivity, thus, fluorescent dyes were sometimes used because of their intrinsically higher sensitivity.[7]

1.1.3. From the bulk to the nanoscale

1.1.3.1. Overview of academic studies on miniaturized ISOs

While classical film-based ISOs have been applied to various analytical platforms, such as fiber optics[18], flow cells[15], waveguide devices[19], and microchip[20-21], they are too bulky for challenging applications with a small volume of sample (e.g. living cells).[8] Thus, miniaturized ISOs in the form of micro- or nanosphere have emerged to expand their analytical applications. Kopelman and co-workers introduced optical ion nanosensors in 1990s, which were regarded as PEBBLEs (probes encapsulated by biologically localized embedding).[22-27] PEBBLE sensors are mainly composed of cross-linked acrylamide and water-soluble optical proves targeting intracellular ions of interest, and they are not so sensitive to sample pH. Although an average size of these particles sizes is relatively small (300 to 700 nm, see **Figure 1-5a**), however, the usable lifetime is limited to several hours due to the leakage of the sensing components (*i.e.* chromoionophore, ionophore, and ion-exchanger). In addition, the preparation of PEBBLE-based sensors was relatively complicated and time-consuming. Following this studies, Clark's research group has improved this issue by the introduction of

polymeric Na^+-selective nanosensors with an average diameter of approximately 120 nm (**Figure 1-5b**).[28] The lifetime of this particle was roughly 1 week in solution, and it can be easily prepared under sonication. The polymeric cores, which consisted of traditional optode materials (*i.e.* plasticized PVC, chromoionophore, ionophore, and ion-exchanger), were coated with PEG-lipid molecules for stabilization in solution. Afterward, the same research group also reported on biodegradable Na^+-selective nanosensors composed of polycaprolactone (PCL) and a citric acid ester plasticizer.[29] The preparation of the particles was performed by a displacement method followed by centrifugation and washing. These nanosensors provide an average diameter of approximately 260 nm and a lifetime of at least 14 days at physiological temperature.

During the same period, micrometer and submicrometer-sized ISOs composed of conventional polymetric materials (*i.e.* plasticized PVC) were reported by Shvarev's (**Figure 1-5c**)[30-31] and Bakker's research group[32-41]. These particles were fabricated by the solvent displacement method with a sonicated/stirred reservoir solution. The obtained micro-spherical ISOs provided the function in a similar way to traditional film-based bulk optodes and monodispersity in aqueous solutions. Although nonionic surfactants (e.g. PEG: polyethylene glycol, Brij) were necessary for the stabilization in the optode suspension, the ISO microspheres were still too large size, causing aggregation.

On the other hands, commercialized polymeric beads were used as templates to fabricate miniaturized ISOs. For instance, the surface of micrometer-sized polystyrene particles was modified based on a simple adsorption of traditional ISO components (*i.e.* chromoionophore, ionophore, and ion-exchange).[42-43] As seen in **Figure 1-5d**, the modification occurred only on the surface of polystyrene particles because diffusion of chemical reagents within polystyrene is extremely slow.[42]

While the majority of micro- and nanoscale ISOs relies on sonication, polymerization, centrifugation, dialysis, or similar procedures, their fabrication procedure was relatively time-consuming and complicated (refer to comprehensive review on miniaturized ISOs for further works[8]). For this issue, a solvent displacement, also called precipitation, has been expected to the alternatives to these techniques for the fabrication of miniaturized ISOs. In 2013, Xie *et al*. successfully introduced a new precipitation-based

approach to yield monodisperse optode nanospheres, also called nano-emulsions, with an average size of 40 to 100 nm (see **Figure 1-5e**).[44] All ISO components (*i.e.* chromoionophore, ionophore, ion-exchanger) are encapsulated in a surfactant-composed micelle, leading water mono-dispersibility. The preparation of the nanosphere suspension was simply accomplished by mixing a cocktail containing sensing reagents, plasticizers, and nonionic surfactants (e.g. Pluronic F127) with an aqueous solution, followed by removal of the cocktail solvent (e.g. tetrahydrofuan) by blowing compressed non-reactive air (see **Figure 1-6**). Moreover, no further experimental steps, such as purification and filtration, were required. To date, Xie *et al*. demonstrated the unique feasibilities of optode nanospheres over classical film-based ISOs not only for ion sensing[45-50] but also for light controlled ion concentration perturbations[51], titration[10, 52-55], and equipment-free blood determination[56].

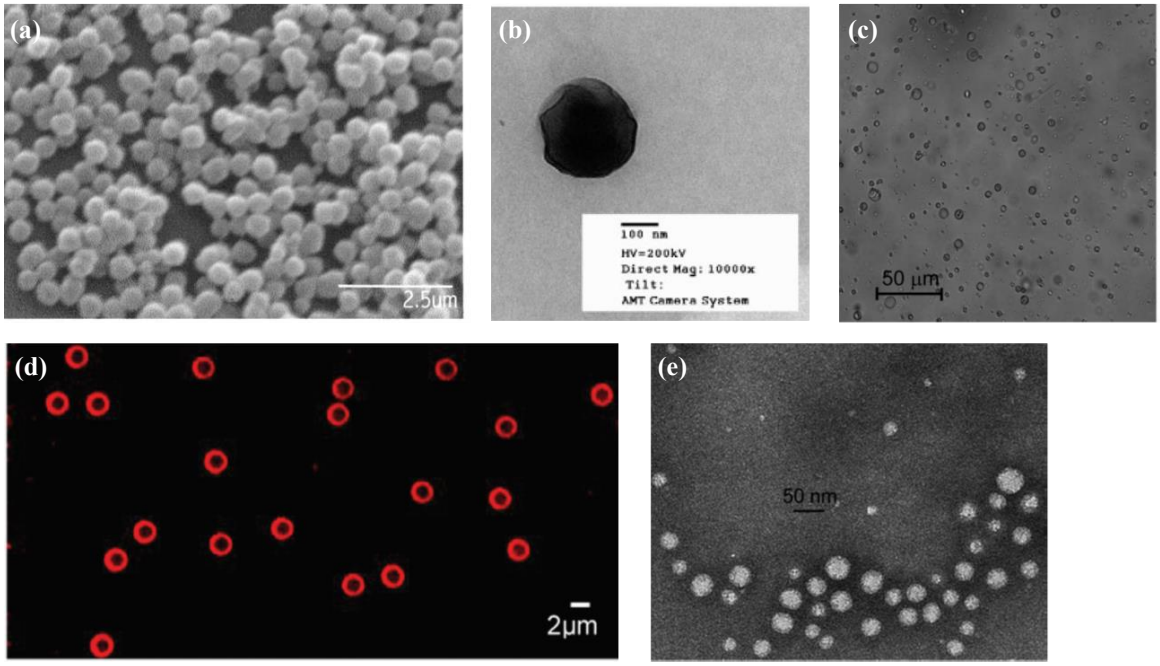

Figure 1-5. Microscope images of different miniaturized ISOs; (a) scanning electron microscope (SEM) image of K^+-selective PEBBLE sensors. Adapted with permission from M. Brasuel; R. Kopelman; T. J. Miller; R. Tjalkens; M. A. Philbert, *Anal. Chem.*, 2001, **73**, 10, 2221-2228 (ref. 24). Copyright 2012 American Chemical Society; (b) transmission electron microscope (TEM) image of Na^+-selective nanosensors. Adapted with permission from J. M. Dubach; D. I. Harjes; H. A. Clark, *Nano Lett.*, 2007, **7**, 6, 1827-1831 (ref. 28). Copyright 2007 American Chemical Society; (c) bright field image of the plasticized PVC-composed particles prepared by a solvent displacement method. Adapted with permission from V. Bychkova.; A. Shvarev, *Anal. Chem*., 2009, **81**, 6, 2325-2331 (ref. 31). Copyright 2009 American Chemical Society.; (d) confocal fluorescence image of surface-modified polystyrene particles. Adapted from Ref. 42 with permission from The Royal Society of Chemistry; (e) TEM image of Na^+-selective optode nanospheres in the form of

surfactant-based micelles. Adapted from X. Xie.; G. Mistlberger; E. Bakker, *Anal. Chem.*, 2013, **85**, 20, 9932-9938 (ref. 44). Copyright 2013 American Chemical Society).

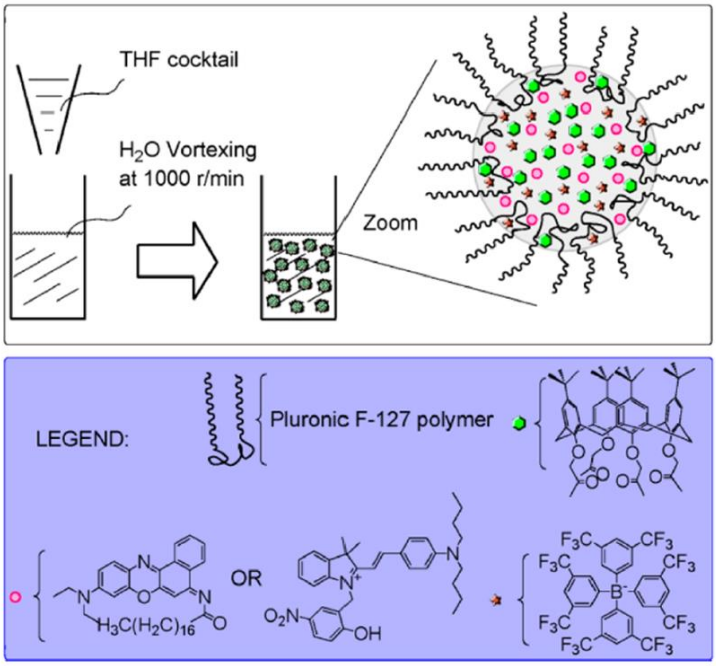

Figure 1-6. Typical schematic procedure for fabrication of Na^+-selective optode nanospheres forming micelles with surfactants (Pluronic F127) and the simple microscopic structure; gray spherical background represents plasticizer acting as a solvent for other sensing components; green symbols represent Na^+-selective ionophores; pink symbols represent chromoionophores; blown symbols represent ion-exchanger. Adapted from X. Xie; J. Zhai; E. Bakker, *Anal. Chem.*, 2014, **86**, 6, 2853-2856 (ref. 46). Copyright 2014 American Chemical Society.

1.1.3.2. Detection mode: equilibrium vs. exhaustive

As mentioned before (see **section 1.1.2**), the ISO response is associated with the redistribution of analyte ions together with H^+ between two immiscible phases, therefore, the sample pH must be controlled or separately measured prior to the optical detection.[6-7] Recently, Xie *et al*. reported that this pH dependence can be overcome by means of an "exhaustive" detection mode (refer to **Figure 1-7**).[45-46] In case the analyte ions in the aqueous sample will completely consumed by the receptors (*i.e.* ionophores), the sensor response will only depend on not analyte concentrations (strictly, activities) but the total amount of the analytes, which potentially enables calibration-free analysis. Moreover, exhaustive-based reaction no longer depends on the sample pH at the limited range of analyte concentration as shown in **Figure 1-7b**. In the term of equilibrium

mode (**Figure 1-7a**), it is often assumed that the sample concentration is not changed before and after exposure to ISO-based sensors. In contrast, the exhaustive detection mode can only occur in the presence of excess binding sites in the sensing phase compared to the total amount of analyte ions in the aqueous sample phase (**Figure 1-7b**).[7-8, 45] To achieve exhaustive detection mode with classical film-based ISOs, both a thin ISO membrane and a thin layer of sample liquid are required since the use of large sample volumes will cause in extremely long response times.[8] For this reason, suspensions of micro- or nanospheres are useful thanks to a massively increased surface/volume ratio and significantly smaller diffusion distances for the reaction.

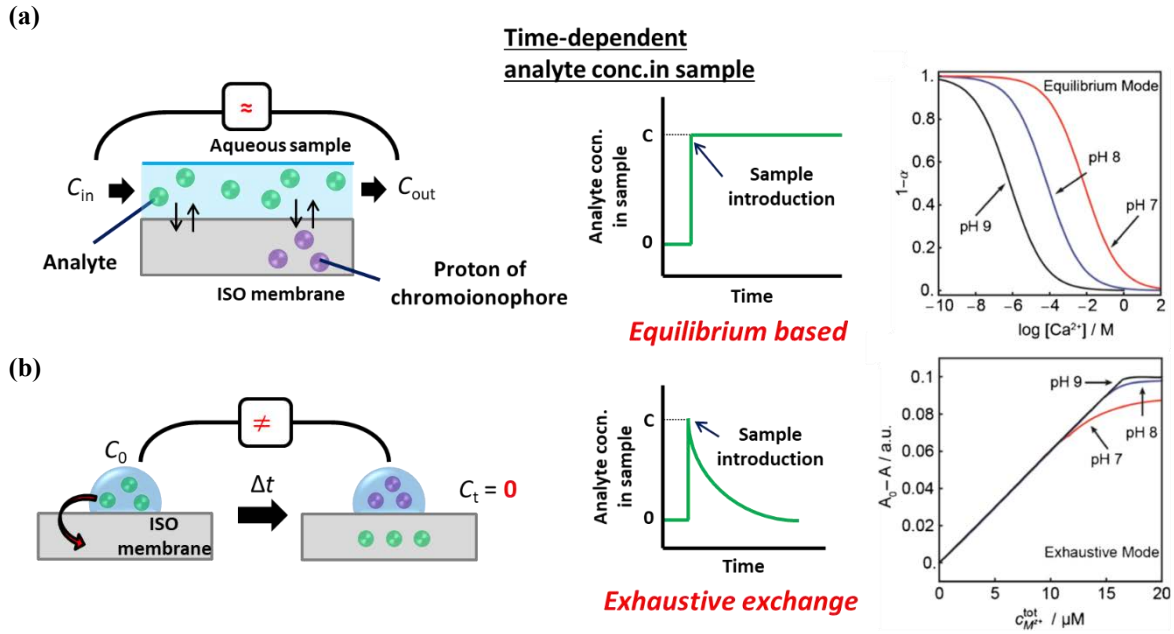

Figure 1-7. Schematic working principles and theoretical response curves for Ca^{2+} at different pH: (a) equilibrium-based, (b) exhaustive-exchange detection. Adapted with permission from refs. 7 and 8.

1.1.4. Renovating the chromoionophores and the detection modes for ISOs

Another option to overcome pH dependence during ISO-based assay is the replacement of chromoionophores with solvatochromic dyes (SDs), also called polarity-sensitive dyes, since the root of this issue is caused by the use of H^+-responsive chromoionophores (refer to **Figure 1-8** for comparison of signal transducing principle between traditional ISOs and SD-based ISOs).[17] Optical properties of SDs (*i.e.* absorbance/emission spectra, and hence, color) are varied, corresponding to the solvent polarity

(solvatochromic effect).[57-58] Wolfbeis and co-workers first introduced SDs to hydrogel-based ISOs instead of conventional H^+-sensitive chromoionophores.[59-63] Unlike classic ISOs, the sensor exhibited pH-independent response under the condition of a certain pH range. Recently, positively-charged SDs were rediscovered by Bakker's research group for applications to carrier-based ISOs.[17, 43, 47-49, 64] Surprisingly, these optical sensors were composed of not membrane films but nanospheres with massively increased surface/volume ratio as stated previous section. Generating optical signal from SD-based ISOs is based on the repartition of analyte cations in the aqueous sample phase with positively-charged SDs (see **Figure 1-8**), therefore the sensor response was no longer accompanied with the sample pH.

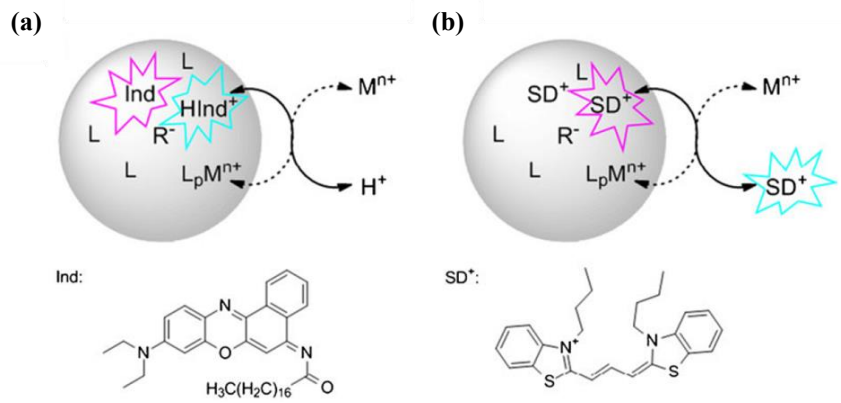

Figure 1-8. A comparison of the signal transducing principle: (a) traditional ISOs with H^+-sensitive chromoionophore and (b) SD-based ISOs; M^{n+}, L, L_pM^{n+}, R^-, and SD^+ represent an analyte cation, an analyte-free ionophore, an analyte-ionophore complex, an ion-exchanger, and a solvatochromic dye, respectively; Ind and $HInd^+$ represent a deprotonated and protonated chromoionophore, respectively; The purple and blue color represent different absorption/fluorescence spectra. Adapted from Ref. 17 with kind permission from Springer Science and Business Media.

1.1.5. Readout mode for the estimation of the ISO response function

Quantitative evaluation for the function of ISO response has been originally performed by means of spectral information (e.g. absorbance, reflectance, and fluorescence).[6-7, 9] The majority of ISO studies has exploited visible absorbance/reflectance because colorimetric signal can be easily acquired in comparison to fluorescent signal. Our research group introduced digital color analysis (DCA) to quantify the colorimetric response of a plasticized PVC film-based optodes instead of the conventional optical methodology (*i.e.*

spectrometry). [65-66] In these studies, DCA has served to evaluate the visual sensor response for the Li^+ detection. For instance, mixing ratio of two chromoionophores with different pK_a values and different color variations can be optimized by means of hues, to acquire an appreciated visual color change over the whole Li^+ concentration range.[66]

By the way, why are most of the color spaces (e.g. red-green-blue: RGB, hue-saturation-value: HSV, and others) defined by the use of three component representation? This is because they follow the human vision system as Helmholtz has stated about the trichromatic theory of color.[67] Among them, RGB color space is undoubtedly the most common in DCA since it works in a similar way to the human visual system.[67] Although RGB color space has been applied for the evaluation of ISO response[56, 68], RGB-based data processing is often affected by the concentration of chromogens or membrane thickness (*i.e.* optical path length).[69] In contrast, a hue value of HSV color space shows excellent robustness against signal interferences from chromogen concentration, membrane thickness, detector spectral responsivity and illumination.[9, 69] In addition, a hue coordinate commonly corresponds to the dominant wavelength of the spectral radiance of a color (see **Figure 1-9**).[67, 70] Hence, hue values have been frequently used for the quantitative evaluation of the colorimetric response from ISOs (see **Figure 1-10**).[69, 71-79] However, it should be noted that deprotonation degrees of chromoionophores (α) experimentally obtained from absorbance and from hue color coordinates are not necessarily identical as shown in **Figure 1-10b**.

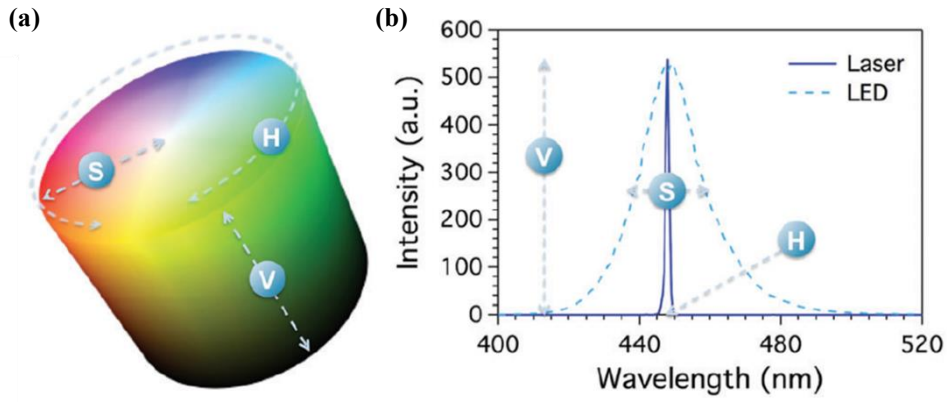

Figure 1-9. (a) Schematic illustration of cylindrical hue-saturation-value (HSV) color space coordinates; (b) Correlation between HSV coordinates and the emission spectra of two different light sources with same hue and value but different saturation; a solid line and a dashed line represent blue laser and a blue LED, respectively. Adapted from Ref. 70 with permission from The Royal Society of Chemistry.

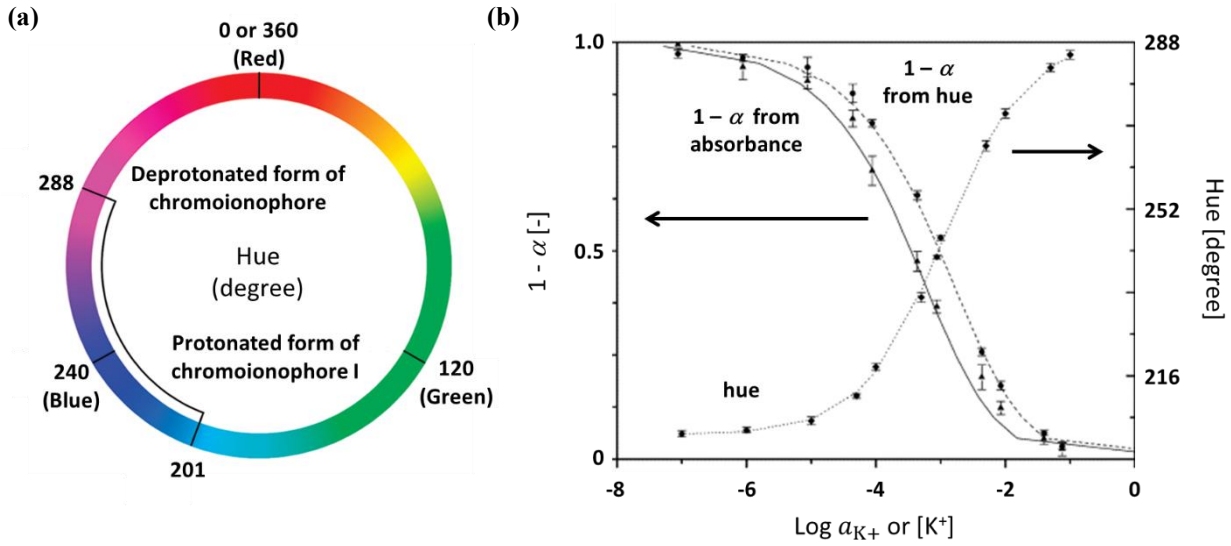

Figure 1-10. (a) An example of color ring indicating the range of possible hue values in the term of K^+-selective ISO with chromoionophore I; other coordinate (e.g. saturation and value) are maintained constant at 1; The values of the H coordinate for the K(I); (b) Response curves obtained from different analytical parameters; the plots of triangles and circles represent the protonation degrees of the used chromoionophores (1-α) obtained from absorbance measurement and hue values, respectively; diamond plots represent concentration response for K^+ based on hue-based quantification; the solid and dashed lines represent the simulated theoretical curves. Adapted from K. Cantrell; M. Erenas; I. de Orbe-Payá; L. F. Capitán-Vallvey, *Anal. Chem.*, 2009, **82**, 2, 531-542 (ref. 69). Copyright 2009 American Chemical Society.

In the DCA process, ISOs potentially suffer from two specific challenges: (i) interference of sample color (e.g. biological fluids) and (ii) light condition affected by a light source and a detector. To reduce the interference of biological fluid color on the pH/Na^+ optodes, the optical measurement setup arranged with LED- and grayscale detectors has been applied for cation assay with optodes.[80] Interestingly, a hydrogel layer containing white beads was immobilized between the sample liquid and the optode sensing membrane. Although this work is not related to ISO-based sensing, color manipulation is one of the simple and effective strategies to enhance sensor sensitivity in hue analysis (**Figure 1-11**).[81] While the effectiveness of this tinting method *via* colorimetric detection depends on the reaction system, this strategy has excellent potential for broad application to any analyte-of-interest. Moreover, the tinting method enabled to distinguish between subtle or monotonal (colorless-to-coloed) color change to improve limits of H_2O_2 detection. On the other hands, sensor sensitivity in DCA-based ion sensing depends on the selection of digital color model. In previously published

study[82], the sensor signal for colorimetric detection of irons with classical indicators varie, depending on used coordinates of color model (e.g. RGB, HSV, $L^*a^*b^*$, and others). Under the optimized condition, analytical performance, such as calibration linearity, a slope of response curve, a limit of detection (LOD) and a limit of quantification (LOQ), was successfully enhanced.

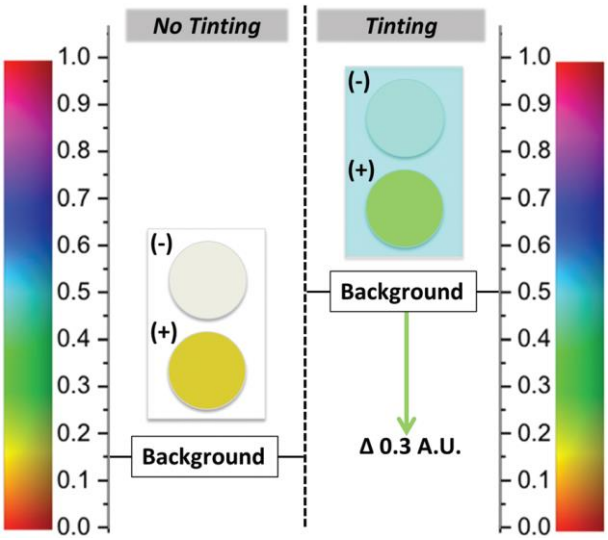

Figure 1-11. Schematic illustration of the tinting strategy by color manipulation. Color association with thr y-axis for a hue value in arbitrary unites (A. U.) represents colorimetric reaction for H_2O_2 assay with a chromogen (not ISOs). Adapted from Ref. 81 with permission from The Royal Society of Chemistry.

1.2. Paper as a sensor substrate

1.2.1. Short history of paper in the science field

Paper has accompanied the progress of science for many years because of the multiple advantageous features as a sensor substrate: (i) inexpensiveness, (ii) abundance, (iii) safe disposability with incineration, (iv) mass productivity, and (v) high chemical/physical stabilities.[83-88] Surprisingly, the long history of paper-based assay can be track back to a litmus paper in 17th century[89], which has been used for the simple colorimetric test of acidity (*i.e.* pH) even now (refer to **Figure 1-12a** for an example of a commercialized product). Later, "dry chemistry" has drawn significant attention to develop test papers and dipsticks for the diagnostic application.[83] In the 1950s, a dipstick-type paper test was first established for urinary metabolite assays (e.g. glucose)[90-91], followed by its commercial introduction to the consumer market in the 1960s[83-84]. Urinary dipsticks allow screening of multiple analytes by simple single dipping of plastic-backed testing paper pads containing colorimetric indicators, to diagnose individual health conditions, such as diabetes, kidney disease, and hydration state (refer to **Figure 1-12b** for an example of a commercialized product). Semi-quantitative readout is also achievable by visual comparison of a resultant color with a color-code chart after the defined incubation time corresponding to the analytes of interest. Parallel to the development of dipstick tests, a paper-based lateral-flow format has been established for immunochromatographic assays in the 1980s.[92-93] To date, this platform is undoubtedly common in commercial pregnancy testing and influenza diagnosis, among others in the field targeting food monitoring, veterinary, environmental assessment, and drug monitoring (refer to **Figure 1-12c** for an example of a general latera-flow paper devices). As mentioned above, paper-based assay, which is successfully penetrated into the commercial market, has often provided semi-quantitative screening of just one analyte per one sample (e.g. yes/no answer, comparison with color-coded chart) until a few years back. Recently, optical electronic readout systems have been applied to some commercial paper dipsticks and lateral flows, which allow quantitative and reliable result in the comparison the simple visual inspection.

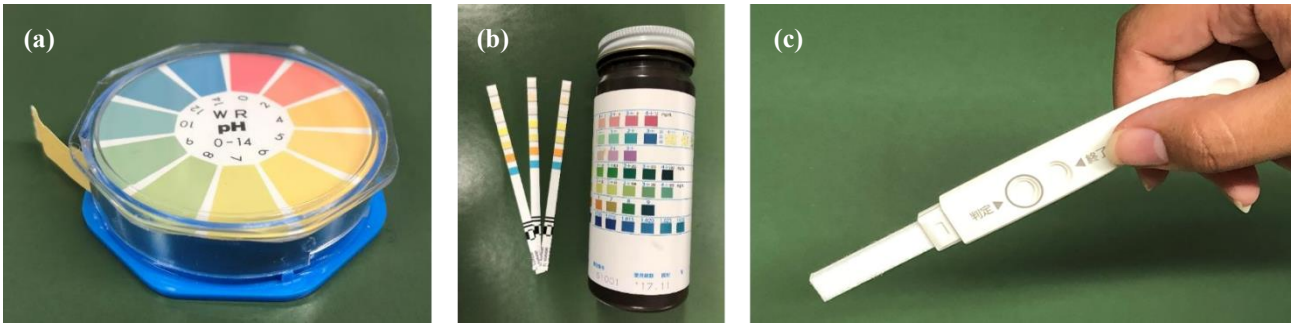

Figure 1-12. Examples of paper-based analytical devices in the commercial market: (a) a colorimetric pH test paper; (b) a urinary dipstick paper; (c) a lateral-flow format test kit for an immunochromatographic pregnancy test.

The first emergence of patterned paper in the analytical chemistry was in the 1930s, when a spot test for colorimetric detection of metal ions (**Figure 1-13a**).[94] Following this study, a microfluidically-patterned paper was reported for the chromatographic separation and refractometric detection of dyes/pigments in the 1940s (**Figure 1-13b**).[95] In both studies, hydrophobic walls were fabricated by the use of a paraffin wax, which was originally used to prevent cross contamination of each reaction zone[96]. In 2007, the Whitesides research group established a photographically-patterned paper-based microfluidic as a new chemical assay platform, targeting colorimetric detection of urinary pH and proteins (**Figure 1-13c**).[97] Now it has been commonly referred to as a microfluidic paper-based analytical device (μPAD).[98] The porous structure and hydrophilic nature of cellulose-composed paper enable passive sample transportation by capillary action, in contrast to conventional microfluidic systems requiring active pumping. Thanks to its feasibility as a sensor substrate, a wide variety of detection principles, such as colorimetry, fluorescence, chemiluminescence, and electrochemistry, electrochemiluminescence, and others, has been adapted to paper-based sensing platforms targeting medical diagnosis, environmental analysis and food quality monitoring, among others. [99-107] **Figure 1-13** shows an comparison of various assessments on the analytical performance and handling of paper-based biosensor products, based on SWOT (strengths, weaknesses, opportunities, and threats) analysis.[104]

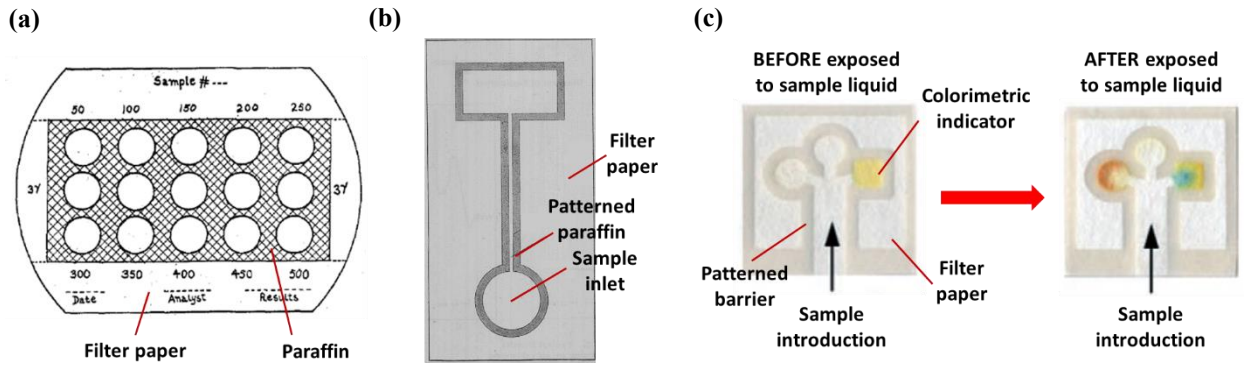

Figure 1-13. Schematic designs of the earliest filter paper patterned by the use of a paraffin wax: (a) a simple patterned spot test for the colorimetric detection of metal ions (adapted from H. Yagoda, *Ind. Eng. Chem. Anal. Ed*., 1937, **9**, 2, 79-82 (ref. 94)). Copyright 1937 American Chemical Society); (b) a microfluidically-patterned filter paper for the chromatographic separation and refractometric detection of dyes and pigments (adapted from R. H. Müller; D. L. Clegg, *Anal. Chem.* 1949**,** **21**, 9, 1123-1125 (ref. 95)). Copyright 1949 American Chemical Society); (c) a photographically-patterned filter paper as the chemical sensing platform (reproduced with permission from ref. 97. Copyright© 2007 Wiley-VCH Verlag GmbH & Co. KGaA, Weinheim).

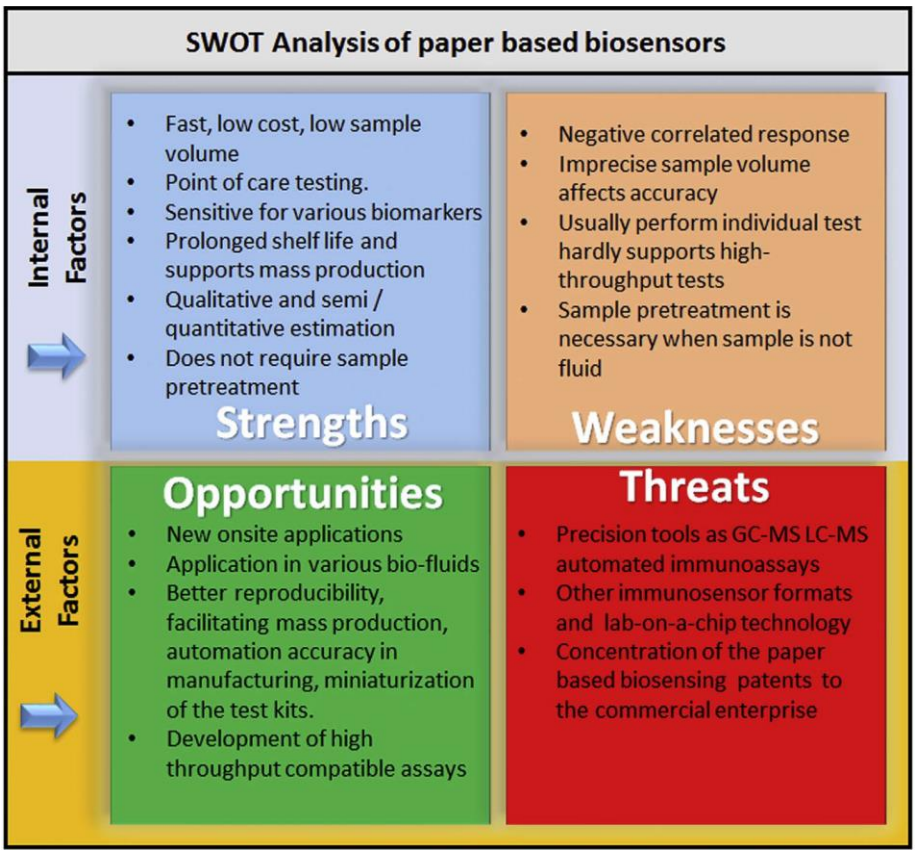

Figure 1-13. SWOT (strengths, weaknesses, opportunities, and threats) analysis of paper-based biosensors. Adapted from Biosens. Bioelectron., 96, K. Mahato; A. Srivastava; P. Chandra, "Paper based diagnostics for personalized health care: Emerging technologies and commercial aspects", 246-259, (ref. 104), Copyright 2017, with permission from Elsevier.

1.2.2. The potential of paper for microfluidics

1.2.2.1. Comparison with other conventional microfluidic materials

As mentioned in the above section, paper has numerous advantages as a sensor substrate to consider the alternative to the conventional materials (refer to **Table 1-1** for comparison with other conventional microfluidic materials: glass, silicon, PDMS).[84, 108-110] Especially, inexpensive material cost and white background have supported the motivation of scientific research for developing (μ)PADs, emerged as promising microfluidic substrate in the field of analytical chemistry.

In spite of their excellent and unique characters, paper also has some weaknesses. For instance, some of paper products contain chemical additives (e.g. calcium carbonate: $CaCO_3$, sizing reagents) to improve light scatting, ink absorbency, smoothness, water resistance, and mechanical strength.[110] Therefore, these impurities may potentially cause interference with (bio)chemical assay on a paper substrate. For this issue, a chromatographic or filter paper, which is mainly composed of high-quality pure cellulose without chemical reagents, is often used for the development of μPADs.[111] The other character is that the physical properties can easily vary, depending on ambient conditions (e.g. relative humidity and temperature).[110] Although the hydrophilic feature of natural cellulosic paper enable passive transport of sample liquid with a capillary force, the amount of moisture around the surface of paper fibers is increased, corresponding to the relative humidity[112-113]. This saturation moisture content depends on the paper structure and the number of polar groups (e.g. hydroxyl groups), and the absorption water leads a reduced physical strength, swelling, and a change in pore size distribution, which influences on microfluidic transport of applied sample liquid.[110-111] The surrounding water can be categorized as unbound (or bulk) and bound water, depending on the strength of interaction between water molecule and the surface of cellulosic surface as illustrated in **Figure 1-14**.[114-115] Furthermore, the bound water can be divided into two categories: freezing water (in the pores of the fiber wall) and nonfreezing water (chemically bonded to the hydrophilic groups). [114-115]

Table 1-1. Features of paper as a sensor substrate in comparison with traditional materials (glass, Silicon, and PDMS: polydimethylsiloxane). Reprinted from Ref. 84 with kind permission from Springer Science and Business Media.

Property	Material			
	Glass	Silicon	PDMS	Paper
Surface profile	Very low	Very low	Very low	Moderate
Flexibility	No	No	Yes	Yes
Structure	Solid	Solid	Solid, gas-permeable	Fibrous
Surface-to-volume ratio	Low	Low	Low	High
Fluidic flow	Forced	Forced	Forced	Capillary action
Sensitivity to moisture	No	No	No	Yes
Biocombability	Yes	Yes	Yes	Yes
Disposability	No	No	No	Yes
Biodegradability	No	No	To some extent	Yes
High-throughput fabrication	Yes	Yes	No	Yes
Functionalization	Difficult	Moderate	Difficult	Easy
Spatial resolution	High	Very high	High	Low to modulate
Homogeneity of the material	Yes	Yes	Yes	No
Price	Moderate	High	Moderate	Low
Initial investment	Moderate	High	Moderate	Low

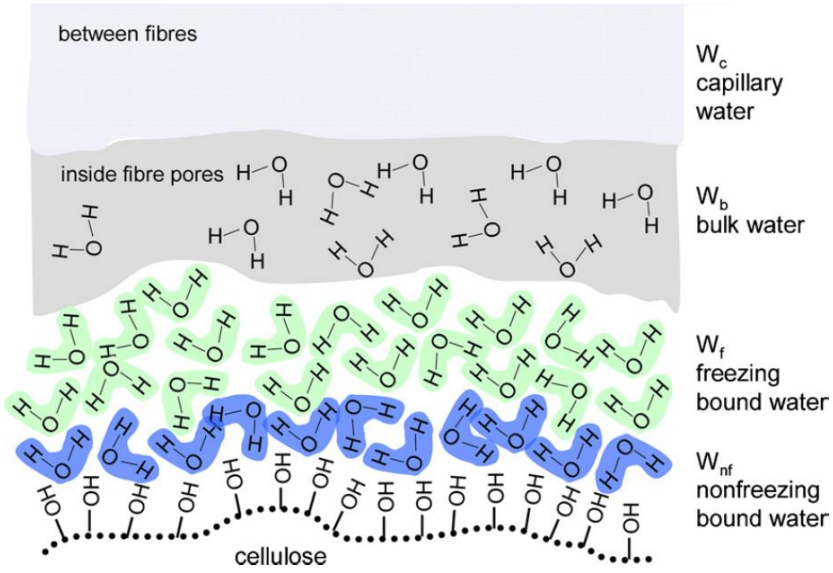

Figure 1-14. A three-dimensional structure of water absorption around the surface of cellulosic paper: capillary water (bulk water: W_c); bulk water (cluster: W_b); freezing bound water (W_f); nonfreezing water (W_{nf}). Adapted from Carbohydr. Polym., T. Bechtold; A. P. Manian; H. B. Öztürk; U. Paul; B. Široká; J. Široký; H. Soliman; L. T. Vo; H. Vu-Manh, 93, "Ion-interactions as driving force in polysaccharide assembly", 1, 316-323, (ref. 115), Copyright 2013, with permission from Elsevier.

1.2.2.2. Chemistry of papers

Paper is a flexible thin sheet of material produced by pressing together cellulosic fibers. The raw sources for the production of paper are selected corresponding to the intended purpose: wood for printing paper, cotton for filter and chromatographic papers, jute or flax for linen, and others.[111] For the development of the μPADs, the physical and chemical properties of paper (e.g. surface characters, flow rate for liquid transport, pore size, porosity, thickness) are significantly important because they are critical parameters in the analytical performance of μPADs (*i.e.* sensitivity, specificity, and reproducibility).[111] To date, various grades of paper have been applied for (bio)chemical assays with (μ)PADs, selection of the appreciate paper substrate is still challenging, relying on the used techniques (e.g. fabrication, designing, and detection principle).[106] Most of studies have exploited Whatman No. 1 filter paper, which is a smooth surface, uniformity on both sides, medium flow rate, and the thickness which can be applied to printing technology.[84, 111]

Cellulose is the simplest structure among polysaccharides, which is composed a linear, polydisperse and syndiotactic chain of *β*-D-glucopyranose (**Figure 1-15**).[116-117] The chain length, also called the degree of polymerization (DP), is expressed as the number of anhydroglucose unit (AGU), relying on not only but the origin of the raw material but also the extraction treatments during manufacturing (e.g. cotton: 800 to 10 000).[116] In addition, both ends of the cellulose chain are different as shown in **Figure 1-15**.[116] At a non-reducing group, the glucose unit is still a closed ring, displaying an original C4-OH group. At the other end (*i.e.* a reducing end group), both pyranose ring structures (cyclic hemiacetal) provide the reducing feature due to the equilibrium between an original C1–OH group and an aldehyde structure.

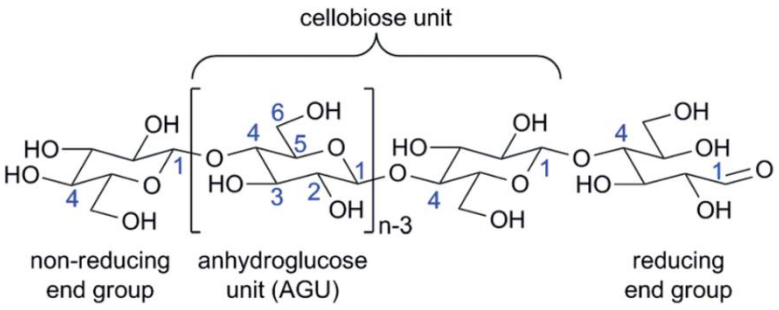

Figure 1-15. Chemical molecular structure of cellulose; *n* represents degree of polymerization (DP). Adapted from ref. 116 with permission from the Royal Society of Chemistry.

Since cellulose contains abundant hydroxyl groups (-OH) as shown in **Figure 1-15**, cellulosic paper shows the hydrophilic surface character as mentioned before. If that is so, then why does cellulose provide insolubility in the aqueous media? Before answering this question, we should consider the intra- and inter-molecular hydrogen bounding (**Figure 1-16**). For a detailed principle, the some excellent reviews are avairable[114, 116-117], and thus, brief of chemical interaction will be here described in this thesis. The primary intra-molecular hydrogen bond in the cellulose is the OH(3)-O(5') bound, which is shared by most allomorphs, and OH(2)-O(6') hydrogen bonds also occur in some allomorphs(**Figure 1-16a**).[116, 118] On the other hands, the supramolecular distinction (*i.e.* inter- and intra-molecular hydrogen bonds) is expressed as show in **Figure 1-16b**, resulting in different packings: parallel (cellulose I) and anti-parallel (cellulose II).[116, 119] The primary intra-molecular OH(3)-O(5') hydrogen bond is shared by both polymorphs, and the intra-molecular OH(2)-O(6) hydrogen bond only occurs in cellulose I in **Figure 1-16b**. Furthermore, inter-molecular hydrogen bonds of OH(6)-O(3'') and OH(6)-O(2'') in cellulose I and II, respectively.[116, 119]

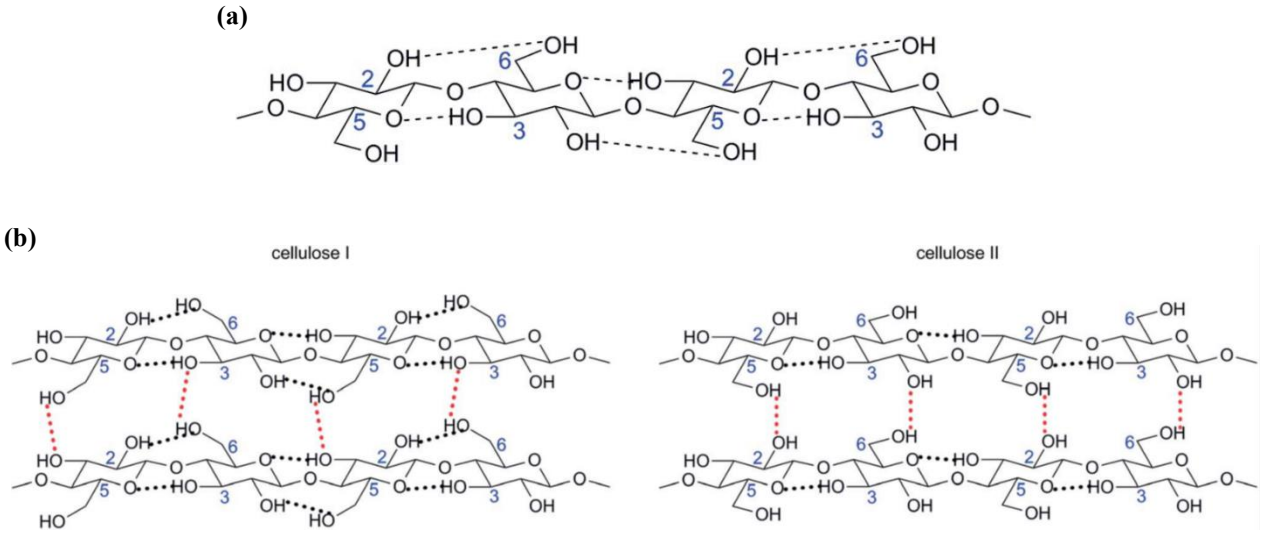

Figure 1-16. Intra- and inter-molecular hydrogen bounding of cellulose: (a) Intra-molecular hydrogen bonding in cellulose; (b) different packings models: parallel (cellulose I) and anti-parallel (cellulose II). Adapted from Ref. 116 with permission from the Royal Society of Chemistry.

Abundant hydroxyl groups of cellulose serve the chemical functionalization, however, inherent chemical reactivities of three hydroxyl groups in AGU (*i.e.* OH(2), OH (3), and OH(6) in **Figure 1-15**) are different due

to the involvement in supramolecular structure (*i.e.* the hydrogen bond network).[116, 120] Therefore, the relative chemical reactivity of the hydroxyl groups in cellulose can be basically described in the following order: OH(6) >> OH(2) > OH(3).[120]

1.2.3. Fabrication technique for microfluidically patterning

The first introduction of a microfluidically-patterned paper for (bio)chemical assay was based on a photolithographic and etching techniques in the same manner with the fabrication of silicon/glass-based microfluidics. In general, a hydrophilic microfluidic channel is defined by bonding with hydrophobic walls, and the reported patterning methods can be categorized the following groups: (i) indirect pattering and (ii) direct patterning (see **Figure 1-17**).[121] In the term of (i) indirect patterning (e.g. lithography), a paper substrate is often soaked into hydrophobic components forming a wall (e.g. polymer), followed by removal of formed coating chemical components to define a hydrophilic microfluidic channel. These techniques are relatively high-resolution, but they are expensive and complicated manufacture process (e.g. mask, phonologist, and clean room). In addition, the hydrophilic channel area of paper substrate once coated with the hydrophobic polymer solution may have the potential of interfering (bio)chemical assays. In contrast, direct patterning (e.g. printing, stamping, and others) serves to pattern a microfluidic channel with simple equipment, which does not require pre-exposure of the microfluidic channel area to chemical reagents. For the detailed characters of laboratory-based patterning technique some excellent reviews were reported.[86, 122-123] Briefly, most of the studies on μPADs depend on wax-printing methods for patterning of microfluidic channels because of the multiple advantageous features (as shown in **Figure 1-18**): (i) simplicity (printing, followed by heating for 30 s at 135°C[124]), (ii) relatively inexpensiveness including initial introduction of a wax printer, and (iii) high-throughput (30 pages of A4-sized paper in 1 min[124]), (iv) the feasibility to combine with other techniques (especially, printing technology because the same graphic software is adaptable for the deposition of chemical reagents).[103]

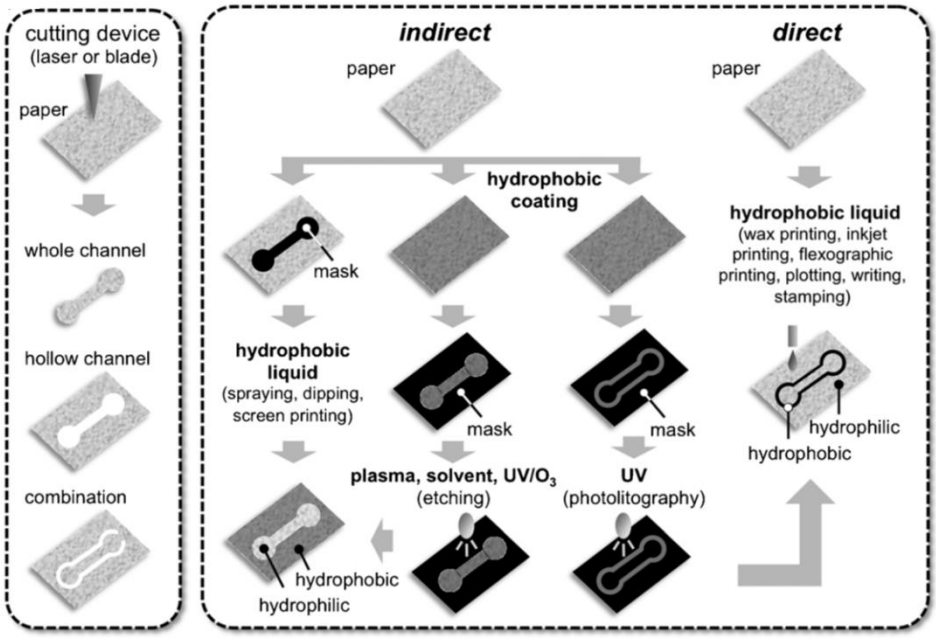

Figure 1-17. Classification of patterning techniques to fabricate microfluidic channels on paper substrates: (i) indirect and (ii) indirect patterning. Reproduced with permission from ref. 121. Copyright© 2015 Wiley-VCH Verlag GmbH & Co. KGaA, Weinheim.

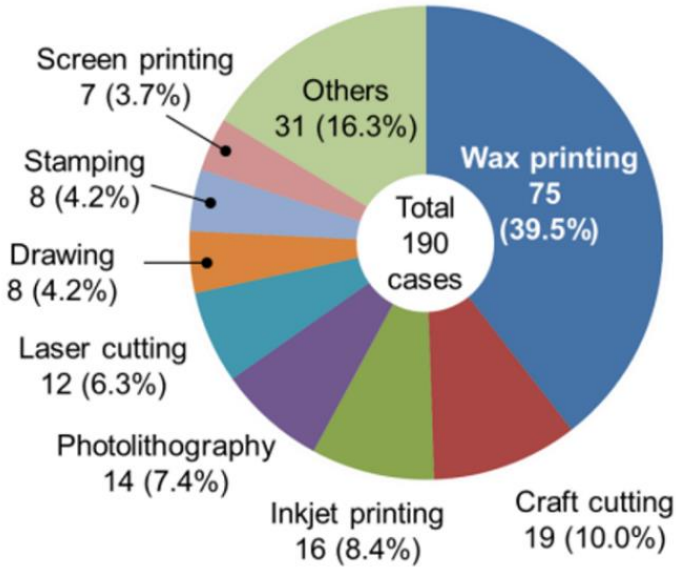

Figure 1-18. Classification of literature publications on μPADs for medical application according to the implemented patterning technique. Adapted from Ref. 103 with permission from The Royal Society of Chemistry.

In the same manner with patterning techniques, automation of reagent deposition is also appreciated to improve the reproducibility of μPAD manufacture (*i.e.* device sensitivity and selectivity). To date, the reagent

deposition originally performed by manual pipetting onto a paper substrate (typically less than 10 μL) has been replaced by printing-based dispensing since our research group introduce inkjet-printing technology for the fabrication of μPADs[125-126]. Especially, inkjet-printing technology plays a significantly essential role because defined contactless deposition of assay reagents is achievable with tiny sample volumes (pL order).[103, 121] For comprehensive reviews on inkjet-printed μPADs, some excellent reviews are available[121, 127], and further discussion is not described here. Not surprisingly, inkjet-printing technology enables to dispense wide varieties of chemical assay reagents, such as organic/inorganic molecule, polymer, nanoparticles, proteins, and others.[125-126]. Therefore, it can be concluded that inkjet printing is already penetrated as a routine tool for the R&D on μPADs, and that novel applications are being continuously developed.

1.3. Paper-based ion sensing

1.3.1. Paper-based colorimetric ion sensing with classical indicators

In the academic field targeting paper-based ion sensing, several detection principles have been applied to (μ)PADs, such as colorimetry, fluorescent, electrochemistry, electrochemiluminescence, chemiluminescence, and others. In the term of general paper-based assay, colorimetry is the most popular detection principle as shown in **Figure 1-19** assay (note that "electrochemistry" in **Figure 1-19** may include amperometry, voltammetry, potentiometry, and electrochemical impedance spectrochemistry detection)[86], and it is regarded as the most appropriate detection technique for paper-based assay.[128] Not surprisingly, the detection principle of colorimetric transduction typically have relied on mature reactions: classic indicators, nanoparticles, redox reaction, acid-base reaction, and others.[111, 128-131] Although colorimetry is simple and capability with low-cost instruments, it suffers from poor sensitivity, which does not meet the sensitivity of traditional analytical technique (e.g. UV-Vis spectroscopy). In addition, application of optical paper sensors to biological fluid (e.g. blood, urine) is significantly challenging because body fluids often have their own color. Therefore, additional sample preparation steps (e.g. sample dilution, matrix simplification) are very important prior to the colorimetric assay with biological fluid.

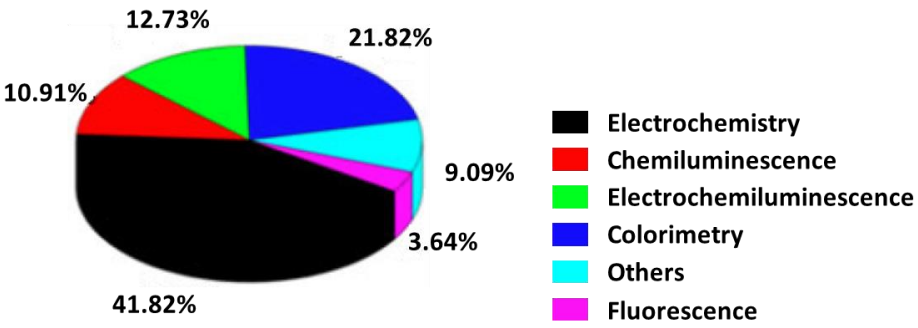

Figure 1-19. Classification of each detection principle in the analytical field targeting (μ)PAD-based assay. Adapted from Ref. 86 with kind permission from Springer Science and Business Media.

In contrast to ion sensing with biological fluids, colorimetric paper devices plays an important role for the quality control of water and processing of foods and beverages in the fields of both academic studies and industrial manufacturing.[107, 130-133] For example, Macherey-Nagel and Merks Millipore have commercialized colorimetric paper dipsticks for various ion species: Al^{3+}, Ar^{5+}, Ca^{2+}, CO_3^{2-}, Cl^-, Co^{2+}, CrO_4^{2-}, CN^-, Fe^{3+}, Ni^{2+}, Mo^{2+}, Pb^{2+}, Ni^{2+}, Mn^{2+}, NO^{2-}, NO^{3-}, K^+, PO_4^{3-}, SO_4^{2-}, SO_3^{2-}, Sn^{2+}, Zn^{2+}, and total hardness, of interest.[134-135] Most of these ion sensing also rely on well-establish recognitions: classical indicators, redox reactions, Griess reaction (NO^{3-}, NO^{2-}) and Gutzeit reaction (Ar^{5+}). Not surprisingly, the major focus of colorimetric dipsticks is on the heavy metal detection since classical indicators for the selective detection of heavy metals are abundant. Moreover, in academic studies on (μ)PADs targeting ion sensing, classical colorimetric indicators also lead to determine heavy metals (refer to **Table 1-2** and **1-3** for the summary of colorimetric μPADs for the determination of ion species). Apart from heavy metal detections, it can be seen that research on nitrite detection with (μ)PADs is also well-reported. This is because Griess reaction promises reliable nitrite detection, which can be used for not only environmental and food monitoring but also clinical application (e.g. urinary analysis).[103, 111] On the other hand, (μ)PADs for alkali and alkaline-earth metals are much less plentiful, because no selective classical colorimetric indicators are available for these ion species. Alternatively, metal-chelating fluorophores[136] and a DNAzyme coupled with chromogenic enzymatic reaction[137] enable μPAD-based quantification of tear electrolytes (Na^+, K^+, Ca^{2+}) and serum K^+, respectively.

Table 1-2. Summary of colorimetric indicators/chromogens for the detection of heavy metals with (μ)PADs

Heavy metals	**Indicator/chromogen**	**Quantification method**	**Ref**
Cadmium	Thiourea	Intensity	138
Chromium	Diphenylcarbazide (DPC)	Intensity	138-148
Cobalt	Chrysoidine-G	Intensity	148
	1-(2'-pyridylazo)-2-naphthol (PAR)	Intensity	149
	1-Nitroso-2-naphthol	Distance	150
Copper	Bathocuproine	Intensity	141-143, 147, 151
	Diethyldithiocarbamate	Intensity	138-139
	D2EHPA and 1-(2'-pyridylazo)-2-naphthol (PAR)	Intensity	152
	Dithiooxamide,	Intensity	148
		Distance	153
	Zincon	Intensity	154
		Distance	155
	Polyethyleneimine	Intensity	156
	1-(2-pyridylazo)-2-naphthol (PAN)	Counting	157
	Diethyldithiocarbamate trihydrate (DDTC)	Intensity	158
	Diphenylcarbazide (DPC)	Intensity	159
Iron	Aminophenol	Intensity	160
	Bathophenanthroline	Intensity	158
		Distance	153, 155, 161
	Ferene S	Intensity	154
	Phenanthroline	Intensity	141-142, 148, 151, 162-164
	2,4,6-Tri(2-pyridyl)-1,3,5-triazine (TPTZ)	Intensity	159
	Thiocyanate	Intensity	165
Lead	Sodium rhodizonate	Intensity	160, 166
		Distance	167
Manganese	1-(2'-pyridylazo)-2-naphthol (PAR)	Intensity	148
Mercury	Michler's thioketone (MTK)	Intensity	146, 149
	Zincon	Intensity	139
	Pyridylazo dye	Intensity	168
	HOTT	Intensity	169
	Dithizone	Distance	170
Nickel	Dimethylglyoxime (DMG)	Intensity	138-139, 141-143, 146-148, 151, 158, 165, 171-172
		Distance	153, 173-174
	Zincon	Intensity	175
	Nitro-PAPS	Intensity	176
Zinc	Zincon	Intensity	154, 177
	Dithizone	Distance	160

D2HEPA: di(2-ethlyhexyl)phosphoric acid, HOTT: 6-hydroxy-3-(2-oxoindolin-3-ylideneamino)-2-thioxo-2*H*-1,3-thiazin-4(3*H*)-one, Nitro-PAPS: 2-(5-Nitro-2-pyridylazo)-5-[*N*-n-propyl-*N*-(3-sulfopropyl)amino] phenol

Table 1-3. Summary of colorimetric indicators/chromogens for the detection of ion species (except for heavy metals) with (μ)PADs.

Analyte	Indicator/chromogen	Quantification method	Ref
Alkaline-earth metals			
Barium	Sodium rhodizonate	Intensity	160
Calcium	Eriochrome Black T/Xylidyl blue (Chelating titration)	Intensity	178
	Eriochrome Black T/Calcon (Chelating titration)	Counting	179
Magnesium	Eriochrome Black T/Xylidyl blue (Chelating titration)	Intensity	178
	Xylidyl blue	Intensity	160
	Eriochrome Black T/Calcon (Chelating titration)	Counting	179
Strontium	Chrysoidine-G	Intensity	180
Other metals			
Aluminum	Aluminon/Ammonium acetate	Intensity	160
Antimony	Sodium sulfide	Intensity	160
Other ions			
Ammonia	Bromothymol blue (acid-base reaction)	Intensity	181
	3-nitrophenol (acid-base reaction)	Intensity	181-182
	Nessler reagent	Intensity	182-183
	Berthelot reagent	Intensity	184
Bromide	Phenol red	Intensity	185
Boric acid	Brilliant green	Distance	186
Nitrite	Griess reagent	Intensity	164, 183, 187-204
Phosphate	Molybdenum blue	Intensity	205-206
Fluoride	SPADNS	Intensity	203
	Methylene blue	Intensity	183

SPADNS: 2-(4-Sulfophenylazo)-1,8-dihydroxy-3,6-naphthalenedisulfonic acid,

For the colorimetric detection, most of quantitative readout are performed based on digital color analysis by the use of color intensity (e.g. **Figure 1-20a**). However, intensity-based interpretation is often affected by inhomogeneous color development of indicators and/or ambient conditions (e.g. illumination condition). In addition, calibrations cannot be integrated with paper devices, which require conventional digital color analysis or visual comparison of the resultant color with a reference color-coded guide. To simplify quantification steps for point-of-care testing (POCT), equipment-free detection models have been investigated

by the introduction of direct distance-based (**Figure 1-20b**), ladder-bar (**Figure 1-20c**), counting-based (**Figure 1-20d**), and timing-based readout (**Figure 1-20e**).[207]

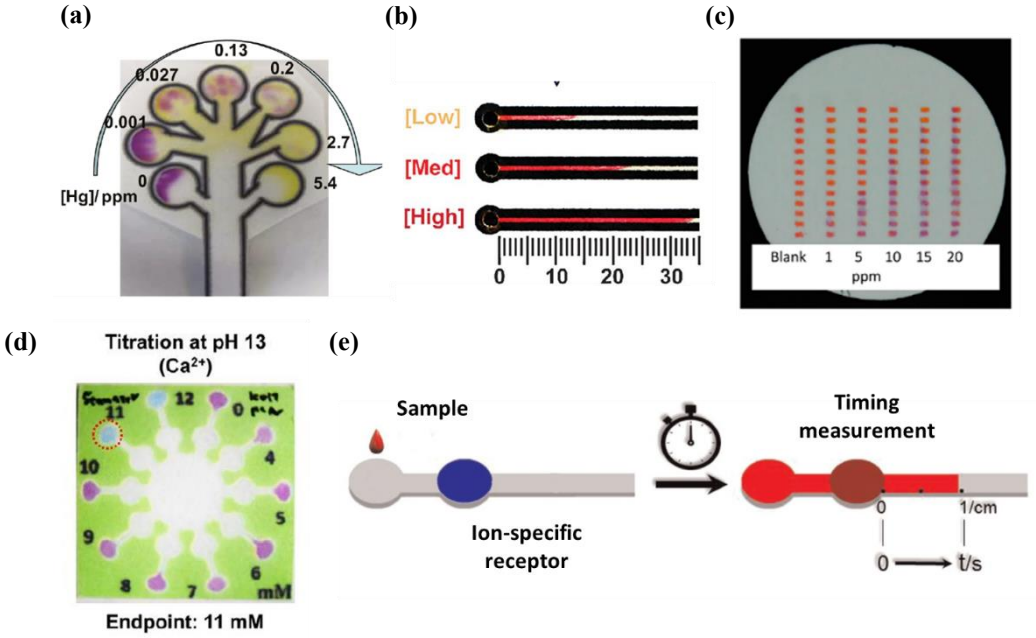

Figure 1-20. Examples of reported colorimetric μPADs targeting ion sensing: (a) intensity-based readout model for the colorimetric detection of Hg^{2+}. Adapted from S. M. Z. Hossain; J. D. Brennan, *Anal. Chem.*, **2011**, *83*, 22, 8772-8778. (ref. 139) with permission. Copyright 2011 American Chemical Society; (b) direct distance-based readout model. Adapted from Ref. 173 with permission from The Royal Society of Chemistry; (c) ladder-bar readout for the colorimetric detection of Cu^{2+}. Adapted from G. C. Bandara; C. A. Heist; V. T. Remcho, *Anal. Chem.*, **2018**, *90*, 4, 2594-2600 (ref. Adapted from 157). Copyright 2018 American Chemical Society; (d) counting-based readout model for a complexometric titration. Adapted from Anal. Chim. Acta, S. Karita; T. Kaneta, 924, "Chelate titrations of Ca^{2+} and Mg^{2+} using microfluidic paper-based analytical devices". 60-67 (ref. 177). Copyright 2014, with permission from Elsevier; (e) timing-based readout model for the colorimetric detection of K^+. Adapted from Biosens. Bioelectron., Y. Zhang; J. Fan; J. Nie; S. Le; W. Zhu; D. Gao; J. Yang; S. Zhang; J. Li, 73, "Timing readout in paper device for quantitative point-of-use hemin/G-quadruplex DNAzyme-based bioassays", 73, 13-18 (ref. 137). Copyright 2015, with permission from Elsevier.

The first introduction of distance-based readouts to μPAD-based assay is accomplished by Henry's research group, based on concentration-dependent visual spatial distribution of the resultant signal along the flow channel (see **Figure 1-20b**).[173] The marks preprinted beside the colorimetric detection region serves to calibration-free semi-quantification without any optical instruments. Due to the feasibility of distance-based readouts, this quantification model has been applied to various microfluidic substrate (e.g. glass, PDMS, and

cotton thread).[208] Ladder-bar quantification model is relatively similar to direct distance-based readout, relying on counting the number of the discrete detection regions of color-developed indicators (**Figure 1-20c**).[157] Although the number of resultant visual bars can be semi-quantitatively translated to the analyte concentration, the observer-dependent errors will potentially occur during the semi-quantification. In contrast, radial-bar readout (*i.e.* counting-based readout) targeting ion sensing is inspired by the classical titration (*i.e.* complexometric titration with EDTA (ethylenediaminetetraacetate) and semi-selective indicators).[179] Compared to linear rudder-bar readout, dynamic range of paper devices can be tuned by changing the amount of chelating reagents (*i.e.* EDTA). Although, calibration-free detection is achievable for both rudder-bar and counting-based readouts, however, resolution of detectable analyte is relatively limited.[103] Finally, a complementary readout model is based on "time" requiring for the ion assay, which is similar to distance-based readout (**Figure 1-20d**).[137] Note that this research used a DNAzyme coupled with chromogenic enzymatic reaction to detect K^+. This model potentially results in quantitative readout, however, the devices force users to pay attention not to miss the resultant time during the assay.[103, 207] For this issue, timing-based readout can be automatically performed by introduction of the a smartphone, and it serves to reduce observer-dependent errors.[207]

1.3.2. Implementation of the ionophore-based sensing system into a (μ)PAD

As mentioned before, focus has mostly been on the detection of heavy metal cations and nitrite due to the presence of excellent colorimetric indicators. Despite the necessity of detecting biologically abundant electrolytes (e.g. Na^+, K^+, Cl^-), (μ)PADs targeting these electrolytes are much less plentiful, because no classical colorimetric indicators are available. For this issue, the function of ionophore-doped chemical sensors, which are based on not only optical detection (*i.e.* ISOs) but also electrochemical detection, has been attempted to apply to paper-based sensing platforms. The concept of ion-selective electrodes (ISEs), often regarded as electrochemical counterparts of ISOs, have been adapted to disposable paper sensors earlier than

ISOs, because paper has historically accompanied potentiometric measurement as a mechanically supporting substrate for sensing membrane and electrolyte solution over the past three decades[209-211].

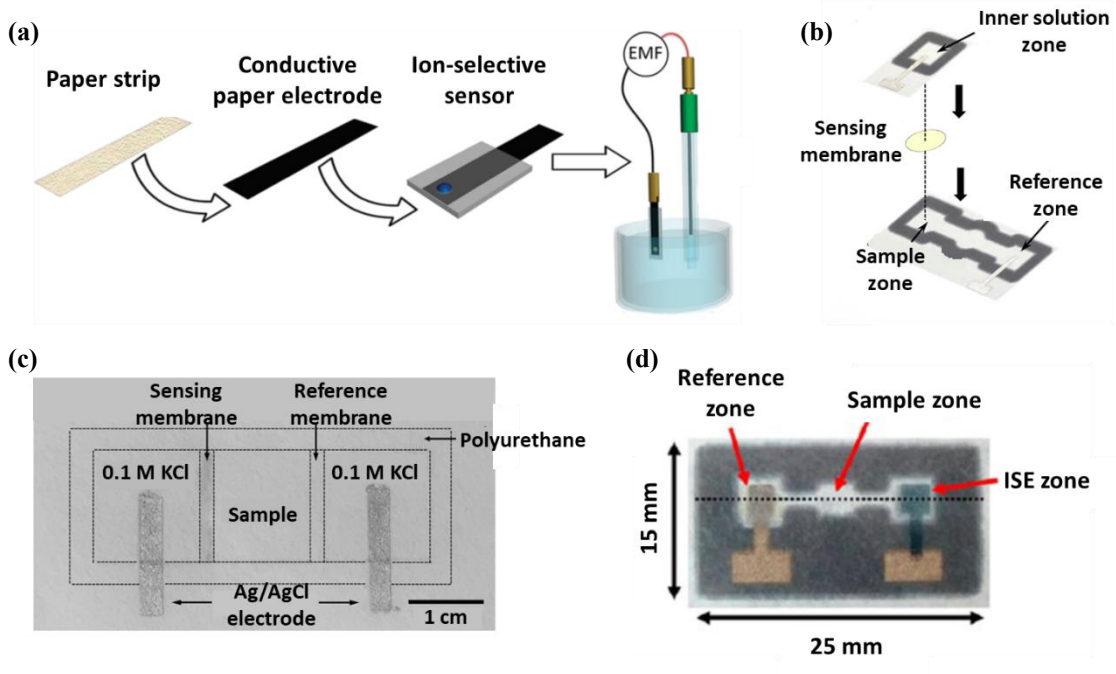

Figure 1-21. Designs of paper-based analytical devices for potentiometric ion sensing: (a) a planar strip-type paper-based ion selective electrode (ISE) and a separated commercial reference electrode. Adapted from M. Novell; M. Parrilla; G. A. Crespo; F. X. Rius; F. J. Andrade, *Anal. Chem.*, 2012, **84**, 11, 4695-4702 (ref. 212). Copyright 2012 American Chemical Society); (b) a disposable electrochemical paper-based analytical devices (EPADs). Three components of EPADs (inner solution zone, sensing membrane, reference/sample zone) are stacked for the cation determinations. Adapted from W.-J. Lan; X. U. Zou; M. M. Hamedi; J. Hu; C. Parolo; E. J. Maxwell; P. Bühlmann; G. M. Whitesides, *Anal. Chem.*, 2014, **86**, 19, 9548-9553 (ref. 213). Copyright 2014 American Chemical Society; (c) a disposable planer paper-based potentiometric ion-sensing platform (reproduced with permission from ref. 214. Copyright© 2016 Wiley-VCH Verlag GmbH & Co. KGaA, Weinheim); (d) a fully inkjet-printed paper-based potentiometric ion-sensing device for Na^+ or K^+. Adapted from N. Ruecha; O. Chailapakul; K. Suzuki; D. Citterio, *Anal. Chem.*, 2017, **89**, 19, 10608-10616 (ref. 215). Copyright 2017 American Chemical Society).

A strip-type sensor is the most common platforms to fabricate paper-based ISEs, therefore, a number of excellent strip-type paper-based ISEs have been reported for point-of-care and in-field testing application until now[216-217]. On the other hands, a separated reference electrode is required for the potentiometric measurement (**Figure 1-21a**).[212] In 2013, both a working electrode and a reference electrode for potentiometric ion sensing were embedded into a paper substrate[218], followed by wax-patterned paper-based analytical devices (EPADs)

for the potentiometric determination of electrolytes (**Figure 1-21b**)[213]. Afterward, the function of ISEs were completely embedded into a disposable planar paper-based ion sensing platform by Bühlmann's research group for the determination of Cl^- and K^+ in serum (**Figure 1-21c**).[214] More recently, our research group has applied inkjet printing technology for all fabrication steps of paper-based ISEs (**Figure 1-21d**).[215]

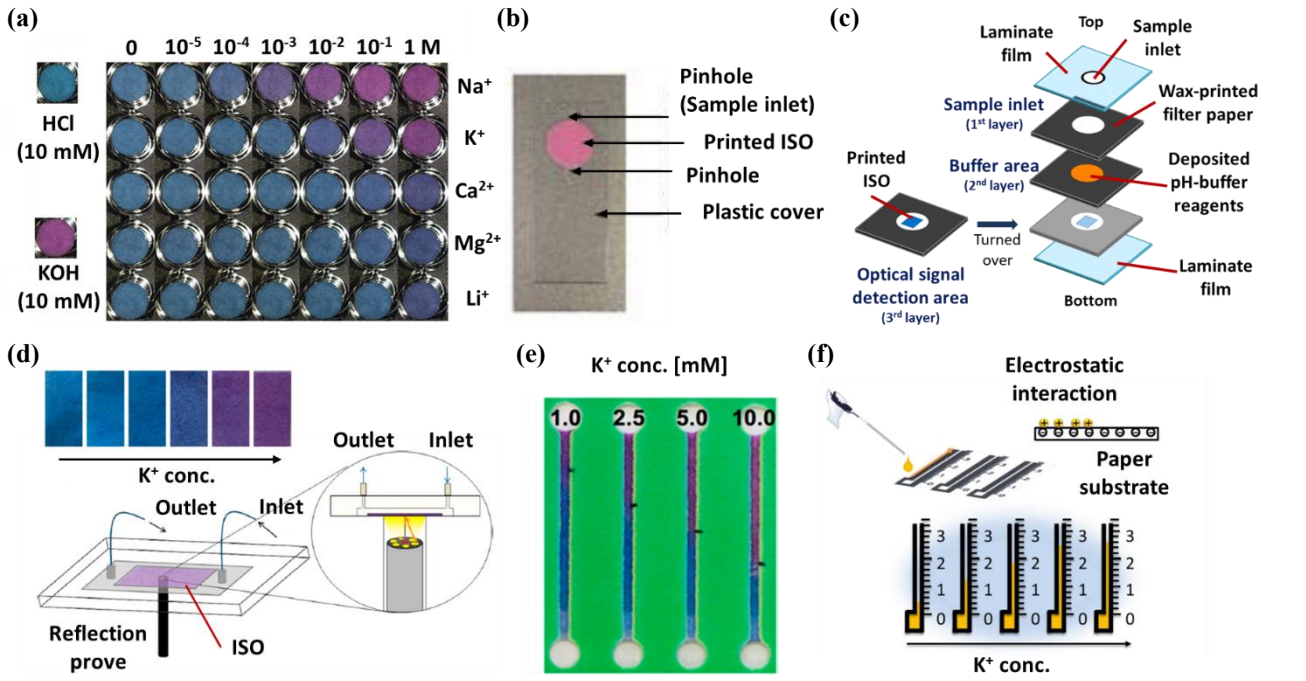

Figure 1-22. Designs of colorimetric (μ)PADs combined with ISOs: (a) a planar paper strip of plasticizer-free paper-based ISOs for determination of pH-buffered Na^+ (adapted from ref. 74 with permission from The Royal Society of Chemistry), (b) a plasticizer-free anion-selective paper-based ISO. Assay components were inkjet-printed onto a paper substrate (reproduced with permission from ref. 75. Copyright© 2017 Wiley-VCH Verlag GmbH & Co. KGaA, Weinheim); (c) a vertically-assembled μPAD (vPAD) with a classical plasticized PVC-based ISO (adapted from ref. 78 with permission from The Royal Society of Chemistry); (d) a paper-based classical ISO for the continuous colorimetric sensing of K^+ (adapted from Talanta, P. Kassal; M. Sigurnjak; I. M. Steinberg, 193, "Paper-based ion-selective optodes for continuous sensing: Reversible potassium ion monitoring", 51-55 (ref.222), Copyright 2019, with permission from Elsevier); (e) colorimetric distance-based μPADs for the determination of K^+ (adapted from C. T. Gerold; E. Bakker; C. S. Henry, *Anal. Chem.,* 2018, **90**, 7, 4894-4900 (ref. 223). Copyright 2018 American Chemical Society); (f) colorimetric distance-based μPADs for K^+ determination with an ISO-modified capillary (adapted from Y. Soda; D. Citterio; E. Bakker, *ACS Sens*., 2019, **4**, 3, 670-677 (ref. 221). Copyright 2019 American Chemical Society).

In accordance with the advantageous features of colorimetric (μ)PADs (*i.e.* observable by unaided eyes, simplicity), the function of ISOs has been frequently applied to paper-based sensing platforms. Compared to

paper-based ISEs, the implementation of ISOs into paper-based sensing platforms is are much less plentiful. In 1990s, a cellulose derivative (cellulose acetate) was used instead of a conventional organic polymer (e.g. polyvinyl chloride) to fabricate a pH-sensitive optomembrane.[219-220] The sensing components, such as a pH indicator, plasticizer, were mixed together with a cellulose derivative. In one special arrangement, a semi-selective colorimetric indicator has been combined with a selective receptor for Cu^{2+}, doped into a polymer inclusion membrane (PIM) composed of a plasticized polyvinyl chloride. This membrane fabricated by a dropping cast method was attached to cellulosic filter paper vertically stacked by hot lamination.[152] Since Meyerhoff's research group established a new class of paper-based ISO without a traditional plasticized organic polymeric membrane (**Figure 1-22a**)[74], the implementation of ISOs into a paper substrate has gained for ion-selective determination of cations, anions, cations.[75-79, 221-224] More recently, Meyerhoff's research group also first introduced inkjet printing technology for the deposition of the sensing reagents together with pH-controlling function (**Figure 1-22b**).[75] A mimic plasticized polymer phase for the ISO-based detection (*i.e.* hydrophobic micro-environment) has been successfully formed by both the highly lipophilic ISO components themselves and a hydrophobic part of cellulose.[74-77] Interestingly, observable reaction basically relied on the transfer-based heterogeneous sensing, resembled in the traditional response function of carrier-based ISOs. Afterward, our research group applied a classical PVC-based ISO to μPADs together with pH-buffering function (**Figure 1-22c**).[78] Moreover, same research group fabricated polymetric ISO nanoparticles by means of inkjet-printing technology for paper-based sensing platforms, and reaction behavior was addressed by the use of a classical equilibrium-based theory.[79] More recently, paper-based classical ISOs leaded continuous colorimetric sensing of K^+ with reflectometry (**Figure 1-22d**).[223] In order to simplify colorimetric readout, equipment-free distance-based quantification was achieved by corroboration of Henry's and Bakker's research groups (**Figure 1-22e**).[224] Micelle-composed ISO nanosphere (nano-optode) was simply applied for colorimetric detection of K^+. Later, inkjet-printing technology was adapted to the well-defined and reproducible deposition of ISO nanosphere for the colorimetric determination of Ca^{2+} in drinking and tap water samples.[222] The water-monodisperse nano-optodes enabled patterning onto wax-patterned microfluidic

channels with simple office inkjet printer. Another approach for colorimetric distance-based readout was accomplished by the use of target-induced dyes released from a plasticized PVC film in a separated capillary (**Figure 1-22f**).[221] Released positively-charged colorimetric dyes were adsorbed onto the negatively-charged surface of a paper substrate, resulting in chromogenic length corresponding to the analyte concentration.

1.3.3. Analyte loss during cation assay

The majority of academic studies on the development of (μ)PADs have supported for the implementation of particular detection mechanism into paper-based sensing platform. Hence, the optimization of device geometry and the effect of a cellulosic paper substrate on the (bio)chemical assay have drawn less attention until now. Recently, instead of traditional one-factor-at-time (OFAT) approaches, design of experiments (DOE) have been applied for the selection of the optimum experimental conditions with limited experimental effort.[225-227] In these publications[226-227], the device sensitivity strongly relied on not only the amount of sensing reagents but also device geometry. In other research[176], the correlation between total area of flow channel (*i.e.* channel width × channel length) and amount of transported cation analytes has been investigated by the use of a simple assay model with μPADs (**Figure 1-24**). Although flow rate in μPADs is affected by various influence factors, such as ambient condition (e.g. temperature, humidity), channel width, and others, the amount of transported analytes depended on the total area of channel. In other words, we have to consider the total area of μPADs to yield greater device sensitivity.

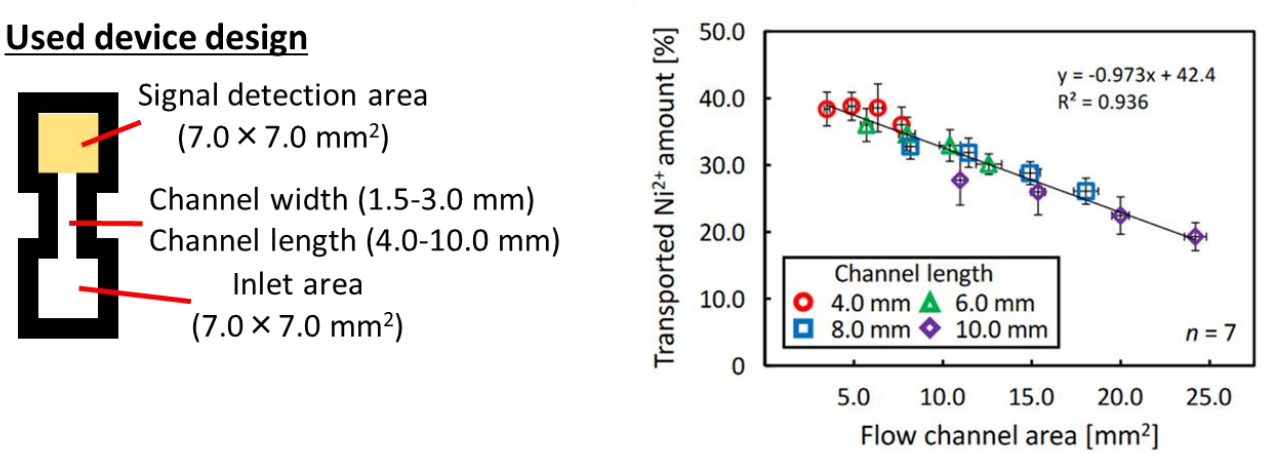

Figure 1-24. Estimation of amount of cationic analyte (Ni^{2+}) transported in μPADs, corresponding to the total area of flow channel (adapted from ref. 176 with permission from The Royal Society of Chemistry).

Regarding paper-based ion sensing, loss of cation analyte (e.g. Ni^{2+}, Cu^{2+}, Zn^{2+}) and anion analytes (e.g. PO_4^{3-}) during transport in μPADs has been quantitatively discussed under various influence factors such as device geometry, user handling, and physico-chemical nature of analyte (**Figure 1-25a**).[172, 176] It is known that the surface of cellulosic paper is negatively charged because carboxyl and hydroxyl groups are abundant. Typically, carboxyl groups are generated by oxidization of 6-position hydroxy group during bleaching process.[228] Therefore, amount of carboxyl group on the surface of cellulose relies on the used oxidative treatment and types of used paper. This carboxyl groups mainly contribute to ion-exchange behavior between the anionic paper and cationic analytes occurs (chelating-like bonding). In this adsorption of cation analytes, the amount of transported cation analytes was independent on the counter ions (e.g. Cl-, NO_3^-) as described in **Figure 1-25a**. Although this binding strength is affected by chemical conditions of sample liquid (e.g. sample pH, ionic strength), it depends on types of cations as shown in **Figure 1-25b**.[229] On the other hands, anionic analyte (e.g. PO_4^{3-}) showed higher transport amount due to electrostatic repulsion with the cellulosic substrate.[173]

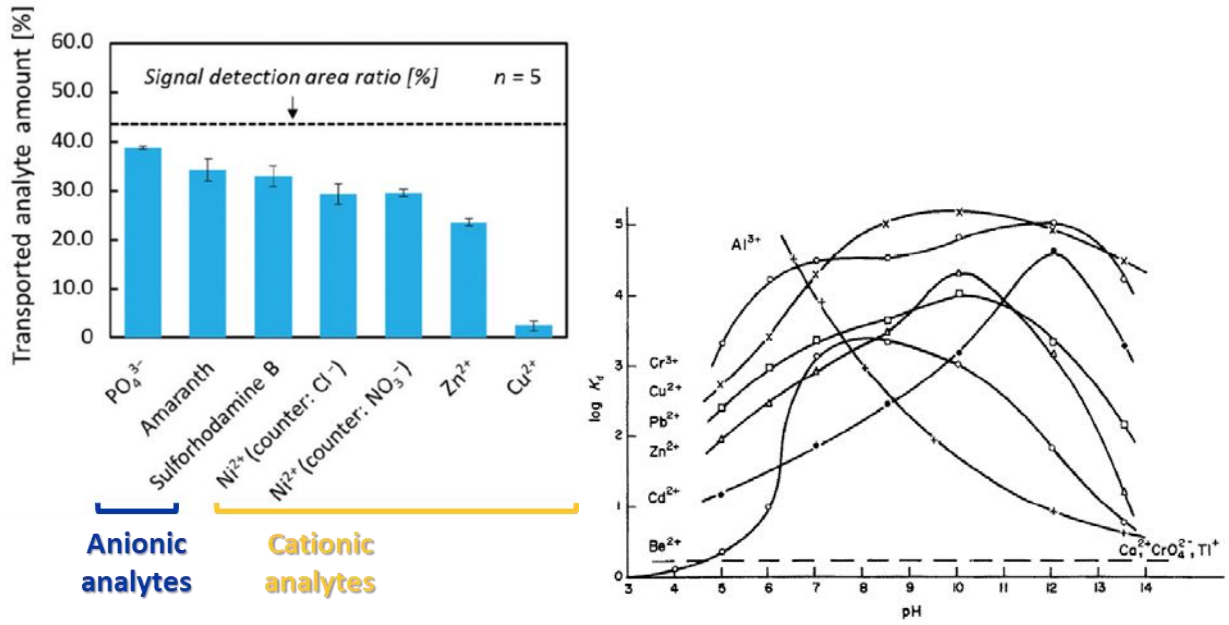

Figure 1-24. (a) Amount of cationic/anionic analytes transported in μPADs corresponding to types of target analytes (adapted from ref. 176 with permission from The Royal Society of Chemistry); (b) distribution coefficient (K_d) of metal ion traces corresponding to sample pH; note that short-fibered cellulose was used in this experiment (adapted from Burba P. and Willmer P. G, 30, 5, "CELLULOSE: A BIOPOLYMERIC SORBENT HEAVY-METAL TRACES IN WATERS", 381-383 (ref. 229), Copyright 1983, with permission from Elsevier).

The electrostatic adsorption behavior of metal cations can be described by a Langmuir adsorption isotherm model (**Figure 1-25**).[230] Based on the Langmuir equation, absorption amount (W) can be expressed by the use of an equilibrium concentration (C) as follows: $W = \frac{\alpha W_S C}{1+\alpha C}$, where α and W_s represent an associated equilibrium constant and saturated adsorption amount, respectively. Note that the Langmuir equation is frequently applied to a binary system the sorption of cations (e.g. Na^+, Ca^{2+}) by kraft pulps. In this Langmuir model, the velocity of adsorption/desorption relies on amounts of bunding sites and free targets. In addition, the adsorption depends also on the structure of fibers, which is highly complex consisting of cellulose layers.

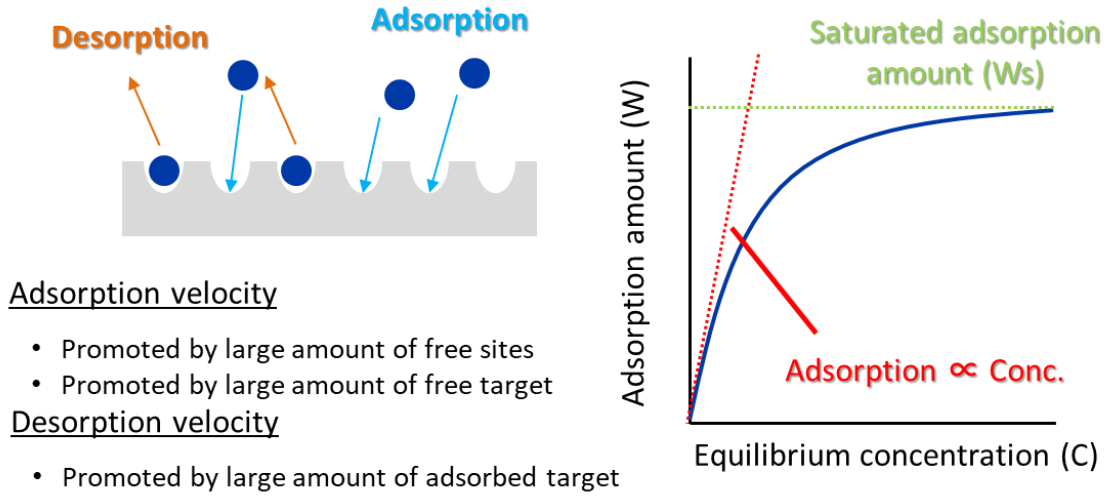

Figure 1-24. Schematic adsorption and desorption process based on a Langmuir adsorption isotherm model.

1.4. Summary of the research motivation

This thesis describes the integration of an ionophore-based ISOs into a paper-based sensing platform for optical cation detection (e.g. Na^+ and Ca^{2+}) to solve historical drawbacks of ISOs as mentioned before. For this issue, three classes of ISOs, which are a plasticized polymetric film-based optodes, plasticizer-free optodes, and micelle-composed optode nanospheres, have been applied to (μ)PADs by means of an inkjet-printing technology. Focus of the current thesis can be categorized into two main missions: (i) the elimination of the inherent pH-dependence during ISO-based assay (**Chapter 2 and 3**) and (ii) simplification of colorimetric signal readout for semi-quantification of cations (**Chapter 4**). The outline of this thesis is summarized in **Scheme 1-1**.

Chapter 1 describes general background of advancing ionophore-based optical sensors and (μ)PADs targeting the detection of ion species. The state-of-the-art and challenging of colorimetric (μ)PADs for ion sensing have been discussed by reviewing the recent literatures. The colorimetric detection of heavy metals and nitrite with (μ)PADs are frequently reported since excellent classical indicators are abundant. Thus, development of (μ)PADs for the colorimetric detection of alkali-earth and alkali metals have drawn significant attention. Although alternatives of classical indicators, such as metal-chelating fluorophores[133] and a DNAzyme coupled with chromogenic enzymatic reaction[134], have been adapted to μPAD-based quantification of these electrolytes, sensor varieties are still limited. For this reason, the function of the ISO system has been frequently applied to a paper-based sensing platform because ISO-based chemical sensors potentially provide ion-selective detection of interest and appropriate dynamic response range.[75-79, 219-222]

Chapter 2 describes that both a classical PVC-based ISO and the pH-buffering function have been integrated with vertically-assembled PADs (vPADs). Functionalized paper layers individually containing printed classical film-based ISOs and pH-buffering reagents have leaded the colorimetric Na^+ detection with no pretreatment (e.g. pH controlling, separate pH measurement prior to the assay), resulting in the elimination of the pH dependence. Moreover, the establishment of an ion-exchange equilibrium was achieved by eliminating evaporation of sample liquid through whole device lamination because the response function of

equilibrium-based ISOs refers to not "analyte amounts" but "analyte concentrations (strictly, analyte activities)", in contrast to conventional colorimetric μPAD-based assay. Since classical film-based ISOs have been first applied to an active sensor substrate (*i.e.* cellulosic paper), the comparison of the ISO response between "on a paper substrate" and "on a conventional plastic film (*i.e.* non-active sensor substrate)" has been quantitatively demonstrated by the use of a well-known theory on the working principle.

Chapter 3 describes a new class of paper-based ISOs for pH-independent assay for fluorescent detection of Ca^{2+}. Since the pH dependence of ISOs rooted the use of H^{+}-sensitive chromoionophores, positively-charged solvatochromic dyes (SDs) have been introduced to plasticizer-free ISO sensing system for the first time. All sensing components, such as SDs, ionophores, and ion-exchangers, were directly inkjet-printed onto wax-patterned paper wells to fabricate plasticizer-free paper-based ISOs. The proposed paper-based ISOs have served to eliminate a traditional plasticized polymeric membrane, resulting in reduction of the assay time. As an early stage of practical analytical applications, quantification of Ca^{2+} concentration in drinking water has been demonstrated with the proposed paper devices.

Chapter 4 describes an instrument-free "distance-based" quantitative signal readout approach for ISOs. In the same manner with previously reported articles[222], ISO nanospheres in the form of surfactant-composed micelles (nano-optodes) [44, 46] were used to achieve a distance-based readout model. For reliable and highly-reproducible distance-based readout, all assay reagents including prepared nano-optodes and pretreatment reagents have been inkjet-printed onto microfluidic channels by means of a simple desktop thermal inkjet printer for the first time. To meet with the criteria recommended by both World Health Organization (WHO) and International Organization for Standardization, pre-deposition of electrolytes (*i.e.* $MgCl_2$) providing an increased ionic strength environment after sample application resulted in improved assay sensitivity by reducing the interaction between cationic analytes and the paper substrate. Besides, it can be found that this adsorption of cation analytes onto the paper substrate also served to accomplish distance-based quantification. Finally, the developed distance-based paper devices have quantified the concentration of Ca^{2+}

in drinking and tap water samples, which are comparable to conventional analytical technique (complexometric titration).

Chapter 5 summarizes the result of this thesis research and a future outlook of paper-based ion-sensing platform with ionophore-based ISOs.

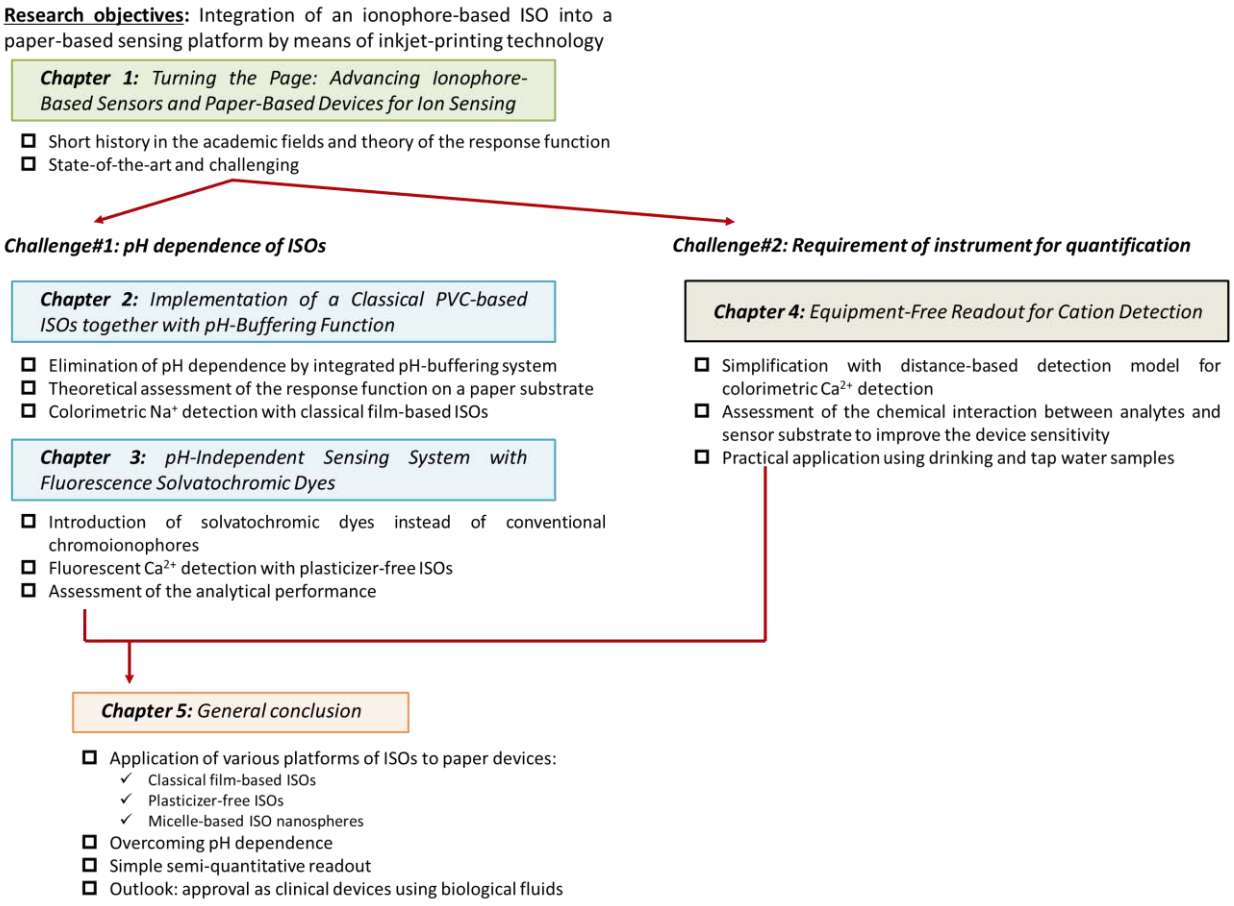

Scheme 1-1. Outline of the current thesis for the implementation of an ionophore-based ISO into paper-based sensing platform by means of inkjet-printing technology

References

1. Spichiger, U.; Freiner, D.; Bakker, E.; Rosatzin, T.; Simon, W., Optodes in clinical chemistry: potential and limitations. *Sens. Act. B* **1993,** *11* (1-3), 263-271.

2. Potentiometric Polyion Sensors: New Measurement Technology for Monitoring Blood Heparin Concentrations During Open Heart Surgery. *Clin. Chem.* **1995,** *41* (9), 1355.

3. Johnson, R. D.; Gavalas, V. G.; Daunert, S.; Bachas, L. G., Microfluidic ion-sensing devices. *Anal. Chim. Acta* **2008,** *613* (1), 20-30.

4. Gholivand, M. B.; Babakhanian, A.; Kaki, S.; Mohammadi, M.; Moradi, P., A New Bulk Optical PVC Membrane Sensor: Determination of Aluminum in Tea Leaf, Mushroom, Potato and Al-Mg Syrup Samples. *Sens. Lett.* **2013,** *11* (9), 1651-1657.

5. Crespo, G. A., Recent advances in ion-selective membrane electrodes for in situ environmental water analysis. *Electrochim. Acta* **2017,** *245*, 1023-1034.

6. Bakker, E.; Bühlmann, P.; Pretsch, E., Carrier-Based Ion-Selective Electrodes and Bulk Optodes. 1. General Characteristics. *Chem. Rev.* **1997,** *97* (8), 3083-3132.

7. Mistlberger, G.; Crespo, G. A.; Bakker, E., Ionophore-Based Optical Sensors. *Annu. Rev. Anal. Chem.* **2014,** *7* (1), 483-512.

8. Xie, X.; Bakker, E., Ion selective optodes: from the bulk to the nanoscale. *Anal. Bioanal. Chem.* **2015,** *407* (14), 3899-3910.

9. Mikhelson, K.; Peshkova, M., Advances and trends in ionophore-based chemical sensors. *Russian Chem. Rev.* **2015,** *84* (6), 555.

10. Zhai, J.; Bakker, E., Complexometric titrations: new reagents and concepts to overcome old limitations. *Analyst* **2016,** *141* (14), 4252-4261.

11. Bühlmann, P.; Pretsch, E.; Bakker, E., Carrier-Based Ion-Selective Electrodes and Bulk Optodes. 2. Ionophores for Potentiometric and Optical Sensors. *Chem. Rev.* **1998,** *98* (4), 1593-1688.

12. Charlton, S.; Fleming, R. L.; Zipp, A., Solid-phase colorimetric determination of potassium. *Clin. Chem.* **1982,** *28* (9), 1857-1861.

13. Morf, W. E.; Seiler, K.; Lehmann, B.; Behringer, C.; Hartman, K.; Simon, W., Carriers for chemical sensors: design features of optical sensors (optodes) based on selective chromoionophores. *Pure Appl. Chem.* **1989,** *61* (9), 1613-1618.

14. Seiler, K.; Morf, W. E.; Rusterholz, B.; Simon, W., Design and characterization of a novel ammonium ion selective optical sensor based on neutral ionophores. *Anal. Sci.* **1989,** *5* (5), 557-561.

15. Morf, W. E.; Seiler, K.; Rusterholz, B.; Simon, W., Design of a novel calcium-selective optode membrane based on neutral ionophores. *Anal. Chem.* **1990,** *62* (7), 738-742.

16. Bakker, E.; Lerchi, M.; Rosatzin, T.; Rusterholz, B.; Simon, W., Synthesis and characterization of neutral hydrogen ion-selective chromoionophores for use in bulk optodes. *Anal. Chim. Acta* **1993,** *278* (2), 211-225.

17. Xie, X., Renovating the chromoionophores and detection modes in carrier-based ion-selective optical sensors. *Anal. Bioanal. Chem.* **2016,** *408* (11), 2717-2725.

18. Kurihara, K.; Ohtsu, M.; Yoshida, T.; Abe, T.; Hisamoto, H.; Suzuki, K., Micrometer-sized sodium ion-selective optodes based on a “tailed” neutral ionophore. *Anal. Chem.* **1999,** *71* (16), 3558-3566.

19. Hisamoto, H.; Kim, K.-H.; Manabe, Y.; Sasaki, K.; Minamitani, H.; Suzuki, K., Ion-sensitive and selective active waveguide optodes. *Anal. Chim. Acta* **1997,** *342* (1), 31-39.

20. Hisamoto, H.; Nakashima, Y.; Kitamura, C.; Funano, S.-i.; Yasuoka, M.; Morishima, K.; Kikutani, Y.; Kitamori, T.; Terabe, S., Capillary-Assembled Microchip for Universal Integration of Various Chemical Functions onto a Single Microfluidic Device. *Anal. Chem.* **2004,** *76* (11), 3222-3228.

21. Mizuta, T.; Maeno, K.; Sueyoshi, K.; Endo, T.; Hisamoto, H., Regioselective Immobilization of a PVC Membrane Composed of an Ionic Liquid-based Dye on Convex-shaped PDMS Surface for Multiplexed Microanalytical Devices. *Anal. Sci.* **2018,** *34* (5), 517-519.

22. Clark, H. A.; Hoyer, M.; Philbert, M. A.; Kopelman, R., Optical nanosensors for chemical analysis inside single living cells. 1. Fabrication, characterization, and methods for intracellular delivery of PEBBLE sensors. *Anal. Chem.* **1999,** *71* (21), 4831-4836.

23. Clark, H. A.; Kopelman, R.; Tjalkens, R.; Philbert, M. A., Optical nanosensors for chemical analysis inside single living cells. 2. Sensors for pH and calcium and the intracellular application of PEBBLE sensors. *Anal. Chem.* **1999,** *71* (21), 4837-4843.

24. Brasuel, M.; Kopelman, R.; Miller, T. J.; Tjalkens, R.; Philbert, M. A., Fluorescent nanosensors for intracellular chemical analysis: decyl methacrylate liquid polymer matrix and ion-exchange-based potassium PEBBLE sensors with real-time application to viable rat C6 glioma cells. *Anal. Chem.* **2001,** *73* (10), 2221-2228.

25. Park, E. J.; Brasuel, M.; Behrend, C.; Philbert, M. A.; Kopelman, R., Ratiometric optical PEBBLE nanosensors for real-time magnesium ion concentrations inside viable cells. *Anal. Chem.* **2003,** *75* (15), 3784-3791.

26. Buck, S. M.; Xu, H.; Brasuel, M.; Philbert, M. A.; Kopelman, R., Nanoscale probes encapsulated by biologically localized embedding (PEBBLEs) for ion sensing and imaging in live cells. *Talanta* **2004,** *63* (1), 41-59.

27. Si, D.; Epstein, T.; Koo Lee, Y.-E.; Kopelman, R., Nanoparticle PEBBLE sensors for quantitative nanomolar imaging of intracellular free calcium ions. *Anal. Chem.* **2012,** *84* (2), 978-986.

28. Dubach, J. M.; Harjes, D. I.; Clark, H. A., Fluorescent ion-selective nanosensors for intracellular analysis with improved lifetime and size. *Nano Lett.* **2007,** *7* (6), 1827-1831.

29. Balaconis, M. K.; Clark, H. A., Biodegradable Optode-Based Nanosensors for in Vivo Monitoring. *Anal. Chem.* **2012,** *84* (13), 5787-5793.

30. Bychkova, V.; Shvarev, A., Surface area effects on the response mechanism of ion optodes: a preliminary study. *Anal. Chem.* **2009,** *81* (17), 7416-7419.

31. Bychkova, V.; Shvarev, A., Fabrication of Micrometer and Submicrometer-Sized Ion-Selective Optodes *via* a Solvent Displacement Process. *Anal. Chem.* **2009,** *81* (6), 2325-2331.

32. Telting-Diaz, M.; Bakker, E., Mass-produced ionophore-based fluorescent microspheres for trace level determination of lead ions. *Anal. Chem.* **2002,** *74* (20), 5251-5256.

33. Tsagkatakis, I.; Peper, S.; Retter, R.; Bell, M.; Bakker, E., Monodisperse plasticized poly (vinyl chloride) fluorescent microspheres for selective ionophore-based sensing and extraction. *Anal. Chem.* **2001,** *73* (24), 6083-6087.

34. Wygladacz, K.; Bakker, E., Imaging fiber microarray fluorescent ion sensors based on bulk optode microspheres. *Anal. Chim. Acta* **2005,** *532* (1), 61-69.

35. Ngeontae, W.; Xu, C.; Ye, N.; Wygladacz, K.; Aeungmaitrepirom, W.; Tuntulani, T.; Bakker, E., Polymerized Nile Blue derivatives for plasticizer-free fluorescent ion optode microsphere sensors. *Anal. Chim. Acta* **2007,** *599* (1), 124-133.

36. Wygladacz, K.; Radu, A.; Xu, C.; Qin, Y.; Bakker, E., Fiber-optic microsensor array based on fluorescent bulk optode microspheres for the trace analysis of silver ions. *Anal. Chem.* **2005,** *77* (15), 4706-4712.

37. Tsagkatakis, I.; Peper, S.; Bakker, E., Spatial and spectral imaging of single micrometer-sized solvent cast fluorescent plasticized poly (vinyl chloride) sensing particles. *Anal. Chem.* **2001,** *73* (2), 315-320.

38. Ye, N.; Wygladacz, K.; Bakker, E., Absorbance characterization of microsphere-based ion-selective optodes. *Anal. Chim. Acta* **2007,** *596* (2), 195-200.

39. Peper, S.; Ceresa, A.; Qin, Y.; Bakker, E., Plasticizer-free microspheres for ionophore-based sensing and extraction based on a methyl methacrylate-decyl methacrylate copolymer matrix. *Anal. Chim. Acta* **2003,** *500* (1-2), 127-136.

40. Retter, R.; Peper, S.; Bell, M.; Tsagkatakis, I.; Bakker, E., Flow cytometric ion detection with plasticized poly (vinyl chloride) microspheres containing selective ionophores. *Anal. Chem.* **2002,** *74* (20), 5420-5425.

41. Wygladacz, K.; Qin, Y.; Wroblewski, W.; Bakker, E., Phosphate-selective fluorescent sensing microspheres based on uranyl salophene ionophores. *Anal. Chim. Acta* **2008,** *614* (1), 77-84.

42. Xie, X.; Crespo, G. A.; Zhai, J.; Szilágyi, I.; Bakker, E., Potassium-selective optical microsensors based on surface modified polystyrene microspheres. *Chem. Commun.* **2014,** *50* (35), 4592-4595.

43. Wang, L.; Xie, X.; Cao, T.; Bosset, J.; Bakker, E., Surface-Doped Polystyrene Microsensors Containing Lipophilic Solvatochromic Dye Transducers. *Chem. Euro. J.* **2018,** *24* (31), 7921-7925.

44. Xie, X.; Mistlberger, G.; Bakker, E., Ultrasmall Fluorescent Ion-Exchanging Nanospheres Containing Selective Ionophores. *Anal. Chem.* **2013,** *85* (20), 9932-9938.

45. Xie, X.; Zhai, J.; Crespo, G. A.; Bakker, E., Ionophore-Based Ion-Selective Optical NanoSensors Operating in Exhaustive Sensing Mode. *Anal. Chem.* **2014,** *86* (17), 8770-8775.

46. Xie, X.; Zhai, J.; Bakker, E., pH Independent Nano-Optode Sensors Based on Exhaustive Ion-Selective Nanospheres. *Anal. Chem.* **2014,** *86* (6), 2853-2856.

47. Xie, X.; Bakker, E., Determination of Effective Stability Constants of Ion-Carrier Complexes in Ion Selective Nanospheres with Charged Solvatochromic Dyes. *Anal. Chem.* **2015,** *87* (22), 11587-11591.

48. Xie, X.; Gutiérrez, A.; Trofimov, V.; Szilagyi, I.; Soldati, T.; Bakker, E., Charged Solvatochromic Dyes as Signal Transducers in pH Independent Fluorescent and Colorimetric Ion Selective Nanosensors. *Anal. Chem.* **2015,** *87* (19), 9954-9959.

49. Xie, X.; Szilagyi, I.; Zhai, J.; Wang, L.; Bakker, E., Ion-Selective Optical Nanosensors Based on Solvatochromic Dyes of Different Lipophilicity: From Bulk Partitioning to Interfacial Accumulation. *ACS Sens.* **2016,** *1* (5), 516-520.

50. Xie, X.; Zhai, J.; Jarolímová, Z.; Bakker, E., Determination of pKa Values of Hydrophobic Colorimetric pH Sensitive Probes in Nanospheres. *Anal. Chem.* **2016,** *88* (6), 3015-3018.

51. Xie, X.; Bakker, E., Light-Controlled Reversible Release and Uptake of Potassium Ions from Ion-Exchanging Nanospheres. *ACS Appl. Mater. Interfaces* **2014,** *6* (4), 2666-2670.

52. Zhai, J.; Xie, X.; Bakker, E., Ionophore-based ion-exchange emulsions as novel class of complexometric titration reagents. *Chem. Commun.* **2014,** *50* (84), 12659-12661.

53. Zhai, J.; Xie, X.; Bakker, E., Solvatochromic Dyes as pH-Independent Indicators for Ionophore Nanosphere-Based Complexometric Titrations. *Anal. Chem.* **2015,** *87* (24), 12318-12323.

54. Zhai, J.; Xie, X.; Bakker, E., Anion-Exchange Nanospheres as Titration Reagents for Anionic Analytes. *Anal. Chem.* **2015,** *87* (16), 8347-8352.

55. Zhai, J.; Xie, X.; Bakker, E., Ion-Selective Optode Nanospheres as Heterogeneous Indicator Reagents in Complexometric Titrations. *Anal. Chem.* **2015,** *87* (5), 2827-2831.

56. Du, X.; Xie, X., Non-equilibrium diffusion controlled ion-selective optical sensor for blood potassium determination. *ACS Sens.* **2017,** *2* (10), 1410-1414.

57. Reichardt, C., Solvatochromic dyes as solvent polarity indicators. *Chem. Rev.* **1994,** *94* (8), 2319-2358.

58. Buncel, E.; Rajagopal, S., Solvatochromism and solvent polarity scales. *Acc. Chem. Res.* **1990,** *23* (7), 226-231.

59. Wolfbeis, O. S., Fluorescence-based ion sensing using potential-sensitive dyes. *Sens. Act. B* **1995,** *29* (1-3), 140-147.

60. Murkovic, I.; Lobnik, A.; Mohr, G. J.; Wolfbeis, O. S., Fluorescent potential-sensitive dyes for use in solid state sensors for potassium ion. *Anal. Chim. Acta* **1996,** *334* (1-2), 125-132.

61. Krause, C.; Werner, T.; Huber, C.; Wolfbeis, O. S., Emulsion-based fluorosensors for potassium featuring improved stability and signal change. *Anal. Chem.* **1999,** *71* (23), 5304-5308.

62. Huber, C.; Werner, T.; Krause, C.; S. Wolfbeis, O., Novel chloride-selective optode based on polymer-stabilised emulsions doped with a lipophilic fluorescent polarity-sensitive dye. *Analyst* **1999,** *124* (11), 1617-1622.

63. Huber, C.; Klimant, I.; Krause, C.; Werner, T.; Wolfbeis, O. S., Nitrate-selective optical sensor applying a lipophilic fluorescent potential-sensitive dye. *Anal. Chim. Acta* **2001,** *449* (1-2), 81-93.

64. Wang, L.; Xie, X.; Zhai, J.; Bakker, E., Reversible pH-independent optical potassium sensor with lipophilic solvatochromic dye transducer on surface modified microporous nylon. *Chem. Commun.* **2016,** *52* (99), 14254-14257.

65. Hirayama, E.; Sugiyama, T.; Hisamoto, H.; Suzuki, K., Visual and colorimetric lithium ion sensing based on digital color analysis. *Anal. Chem.* **2000,** *72* (3), 465-474.

66. Suzuki, K.; Hirayama, E.; Sugiyama, T.; Yasuda, K.; Okabe, H.; Citterio, D., Ionophore-based lithium ion film optode realizing multiple color variations utilizing digital color analysis. *Anal. Chem.* **2002,** *74* (22), 5766-5773.

67. Capitan-Vallvey, L. F.; Lopez-Ruiz, N.; Martinez-Olmos, A.; Erenas, M. M.; Palma, A. J., Recent developments in computer vision-based analytical chemistry: A tutorial review. *Anal. Chim. Acta* **2015,** *899*, 23-56.

68. Kalinichev, A. V.; Frosinyuk, A.; Peshkova, M. A.; Mikhelson, K. N., The impact of ion association in the optode phase to the dynamic range and the sensitivity of the response of ion-selective bulk optodes. *Sens. Act. B* **2017,** *249*, 123-130.

69. Cantrell, K.; Erenas, M.; de Orbe-Payá, I.; Capitán-Vallvey, L., Use of the hue parameter of the hue, saturation, value color space as a quantitative analytical parameter for bitonal optical sensors. *Anal. Chem.* **2009,** *82* (2), 531-542.

70. Battisti, A.; Minei, P.; Pucci, A.; Bizzarri, R., Hue-based quantification of mechanochromism towards a cost-effective detection of mechanical strain in polymer systems. *Chem. Commun.* **2017,** *53* (1), 248-251.

71. Erenas, M. M.; de Orbe-Payá, I.; Capitan-Vallvey, L. F., Surface Modified Thread-Based Microfluidic Analytical Device for Selective Potassium Analysis. *Anal. Chem.* **2016,** *88* (10), 5331-5337.

72. Zhai, J.; Xie, X.; Cherubini, T.; Bakker, E., Ionophore-Based Titrimetric Detection of Alkali Metal Ions in Serum. *ACS Sens.* **2017,** *2* (4), 606-612.

73. Thajee, K.; Wang, L.; Grudpan, K.; Bakker, E., Colorimetric ionophore-based coextraction titrimetry of potassium ions. *Anal. Chim. Acta* **2018,** *1029*, 37-43.

74. Wang, X.; Qin, Y.; Meyerhoff, M. E., Paper-based plasticizer-free sodium ion-selective sensor with camera phone as a detector. *Chem. Commun.* **2015,** *51* (82), 15176-15179.

75. Wang, X.; Mahoney, M.; Meyerhoff, M. E., Inkjet-Printed Paper-Based Colorimetric Polyion Sensor Using a Smartphone as a Detector. *Anal. Chem.* **2017,** *89* (22), 12334-12341.

76. Wang, X.; Zhang, Q.; Nam, C.; Hickner, M.; Mahoney, M.; Meyerhoff, M. E., An Ionophore-Based Anion-Selective Optode Printed on Cellulose Paper. *Angew. Chem. Int. Ed.* **2017,** *56* (39), 11826-11830.

77. Ferguson, S. A.; Wang, X.; Mahoney, M.; Meyerhoff, M. E., Detection and Quantification of Polyquaterniums via Polyion-Sensitive Ion-Selective Optodes Inkjet Printed on Cellulose Paper. *Anal. Sci.* **2018,** *34* (1), 45-50.

78. Shibata, H.; Henares, T. G.; Yamada, K.; Suzuki, K.; Citterio, D., Implementation of a plasticized PVC-based cation-selective optode system into a paper-based analytical device for colorimetric sodium detection. *Analyst* **2018,** *143* (3), 678-686.

79. Soda, Y.; Shibata, H.; Yamada, K.; Suzuki, K.; Citterio, D., Selective Detection of K^+ by Ion-Selective Optode Nanoparticles on Cellulosic Filter Paper Substrates. *ACS Appl. Nano Mater.* **2018,** *1* (4), 1792-1800.

80. Ahuja, P.; Peshkova, M. A.; Hemphill, B. D.; Gratzl, M., Minimizing color interference from biological samples in optode-based measurements. *Sens. Act. B* **2014,** *204*, 319-325.

81. Krauss, S. T.; Nauman, A. Q.; Garner, G. T.; Landers, J. P., Color manipulation through microchip tinting for colorimetric detection using hue image analysis. *Lab Chip* **2017,** *17* (23), 4089-4096.

82. Mohamed, A. A.; Shalaby, A. A., Digital imaging devices as sensors for iron determination. *Food Chem.* **2019,** *274*, 360-367.

83. Doumas, B. T., Landmark Papers in Clinical Chemistry. *Amsterdam: Elsevier B.V.,* **2006.**

84. Nery, E. W.; Kubota, L. T., Sensing approaches on paper-based devices: a review. *Anal. Bioanal. Chem.* **2013,** *405* (24), 7573-7595.

85. Mahadeva, S. K.; Walus, K.; Stoeber, B., Paper as a Platform for Sensing Applications and Other Devices: A Review. *ACS Appl. Mater. Interfaces* **2015,** *7* (16), 8345-8362.

86. Xu, Y.; Liu, M.; Kong, N.; Liu, J., Lab-on-paper micro- and nano-analytical devices: Fabrication, modification, detection and emerging applications. *Microchim. Acta* **2016,** *183* (5), 1521-1542.

87. Fernandes, S. C.; Walz, J. A.; Wilson, D. J.; Brooks, J. C.; Mace, C. R., Beyond Wicking: Expanding the Role of Patterned Paper as the Foundation for an Analytical Platform. *Anal. Chem.* **2017,** *89* (11), 5654-5664.

88. Salentijn, G. I.; Grajewski, M.; Verpoorte, E., Reinventing (Bio)chemical Analysis with Paper. *Anal. Chem.* **2018,** *90* (23), 13815-13825.

89. Carlisle, R. P., Scientific American inventions and discoveriees : all the milestones in ingenuity - from the discovery of fire to the invention of the microwave oven. *John Wiley* **2004**.

90. Comer, J. P., Semiquantitative Specific Test Paper for Glucose in Urine. *Anal. Chem.* **1956,** *28* (11), 1748-1750.

91. Free, A. H.; Adams, E. C.; Kercher, M. L.; Free, H. M.; Cook, M. H., Simple Specific Test for Urine Glucose. *Clin. Chem.* **1957,** *3* (3), 163-168.

92. Campbell, R. L., Daniel B. Wagner, and James P. O'connell Solid phase assay with visual readout. **1987**, US Patent 4,703,017.

93. Bloomster, R. W. R. a. T. G. Solid phase assay employing capillary flow. **1989**, US Patent 4,855,240.

94. Yagoda, H., Applications of Confined Spot Tests in Analytical Chemistry: Preliminary Paper. *Ind. Eng. Chem. Anal. Ed.* **1937,** *9* (2), 79-82.

95. Müller, R. H.; Clegg, D. L., Automatic Paper Chromatography. *Anal. Chem.* **1949,** *21* (9), 1123-1125.

96. Dieterich, K. Testing-paper and method of making same. **1902**, US Patent 691,249,1902.

97. Martinez, A. W.; Phillips, S. T.; Butte, M. J.; Whitesides, G. M., Patterned Paper as a Platform for Inexpensive, Low-Volume, Portable Bioassays. *Angew. Chem. Inter. Ed.* **2007,** *46* (8), 1318-1320.

98. Martinez, A. W.; Phillips, S. T.; Wiley, B. J.; Gupta, M.; Whitesides, G. M., FLASH: A rapid method for prototyping paper-based microfluidic devices. *Lab Chip* **2008,** *8* (12), 2146-2150.

99. Jokerst, J. C.; Emory, J. M.; Henry, C. S., Advances in microfluidics for environmental analysis. *Analyst* **2012,** *137* (1), 24-34.

100. Cate, D. M.; Adkins, J. A.; Mettakoonpitak, J.; Henry, C. S., Recent Developments in Paper-Based Microfluidic Devices. *Anal. Chem.* **2015,** *87* (1), 19-41.

101. Yang, Y.; Noviana, E.; Nguyen, M. P.; Geiss, B. J.; Dandy, D. S.; Henry, C. S., based microfluidic devices: emerging themes and applications. *Anal. Chem.* **2016,** *89* (1), 71-91.

102. Nilghaz, A.; Guan, L.; Tan, W.; Shen, W., Advances of Paper-Based Microfluidics for Diagnostics—The Original Motivation and Current Status. *ACS Sens.* **2016,** *1* (12), 1382-1393.

103. Yamada, K.; Shibata, H.; Suzuki, K.; Citterio, D., Toward practical application of paper-based microfluidics for medical diagnostics: state-of-the-art and challenges. *Lab Chip* **2017,** *17* (7), 1206-1249.

104. Mahato, K.; Srivastava, A.; Chandra, P., Paper based diagnostics for personalized health care: Emerging technologies and commercial aspects. *Biosens. Bioelectron.* **2017,** *96*, 246-259.

105. Gong, M. M.; Sinton, D., Turning the page: advancing paper-based microfluidics for broad diagnostic application. *Chem. Rev.* **2017,** *117* (12), 8447-8480.

106. Sharma, N.; Barstis, T.; Giri, B., Advances in paper-analytical methods for pharmaceutical analysis. *Euro. J. Pharm. Sci.* **2018,** *111*, 46-56.

107. López-Marzo, A. M.; Merkoçi, A., based sensors and assays: a success of the engineering design and the convergence of knowledge areas. *Lab Chip* **2016,** *16* (17), 3150-3176.

108. Ren, K.; Zhou, J.; Wu, H., Materials for Microfluidic Chip Fabrication. *Acc. Chem. Res.* **2013,** *46* (11), 2396-2406.

109. Nge, P. N.; Rogers, C. I.; Woolley, A. T., Advances in Microfluidic Materials, Functions, Integration, and Applications. *Chem. Rev.* **2013,** *113* (4), 2550-2583.

110. Tobjörk, D.; Österbacka, R., Paper Electronics. *Adv. Mater.* **2011,** *23* (17), 1935-1961.

111. Yetisen, A. K.; Akram, M. S.; Lowe, C. R., Paper-based microfluidic point-of-care diagnostic devices. *Lab Chip* **2013,** *13* (12), 2210-2251.

112. Larsson, P. A.; Gimåker, M.; Wågberg, L., The influence of periodate oxidation on the moisture sorptivity and dimensional stability of paper. *Cellulose* **2008,** *15* (6), 837-847.

113. Larsson, P. A.; Wågberg, L., Influence of fibre–fibre joint properties on the dimensional stability of paper. *Cellulose* **2008,** *15* (4), 515-525.

114. Samyn, P., Wetting and hydrophobic modification of cellulose surfaces for paper applications. *J. Mater. Sci.* **2013,** *48* (19), 6455-6498.

115. Bechtold, T.; Manian, A. P.; Öztürk, H. B.; Paul, U.; Široká, B.; Široký, J.; Soliman, H.; Vo, L. T.; Vu-Manh, H., Ion-interactions as driving force in polysaccharide assembly. *Carbohydr. Polym.* **2013,** *93* (1), 316-323.

116. Credou, J.; Berthelot, T., Cellulose: from biocompatible to bioactive material. *J. Mater. Chem. B* **2014,** *2* (30), 4767-4788.

117. Moon, R. J.; Martini, A.; Nairn, J.; Simonsen, J.; Youngblood, J., Cellulose nanomaterials review: structure, properties and nanocomposites. *Chem. Soc. Rev.* **2011,** *40* (7), 3941-3994.

118. Kalia, S.; Kaith, B.; Kaur, I., Cellulose fibers: bio-and nano-polymer composites: green chemistry and technology. *Springer Science & Business Media*, **2011**.

119. Klemm, D.; Heublein, B.; Fink, H. P.; Bohn, A., Cellulose: fascinating biopolymer and sustainable raw material. *Angew. Chem. Inter. Ed.* **2005,** *44* (22), 3358-3393.

120. Roy, D.; Semsarilar, M.; Guthrie, J. T.; Perrier, S., Cellulose modification by polymer grafting: a review. *Chem. Soc. Rev.* **2009,** *38* (7), 2046-2064.

121. Yamada, K.; Henares, T. G.; Suzuki, K.; Citterio, D., Paper-Based Inkjet-Printed Microfluidic Analytical Devices. *Angew. Chem. Inter. Ed.* **2015,** *54* (18), 5294-5310.

122. He, Y.; Wu, Y.; Fu, J.-Z.; Wu, W.-B., Fabrication of paper-based microfluidic analysis devices: a review. *RSC Adv.* **2015,** *5* (95), 78109-78127.

123. Xia, Y.; Si, J.; Li, Z., Fabrication techniques for microfluidic paper-based analytical devices and their applications for biological testing: A review. *Biosens. Bioelectron.* **2016,** *77*, 774-789.

124. Lu, Y.; Shi, W.; Jiang, L.; Qin, J.; Lin, B., Rapid prototyping of paper‐based microfluidics with wax for low‐cost, portable bioassay. *Electrophoresis* **2009,** *30* (9), 1497-1500.

125. Abe, K.; Suzuki, K.; Citterio, D., Inkjet-printed microfluidic multianalyte chemical sensing paper. *Anal. Chem.* **2008,** *80* (18), 6928-6934.

126. Abe, K.; Kotera, K.; Suzuki, K.; Citterio, D., Inkjet-printed paperfluidic immuno-chemical sensing device. *Anal. Bioanal. Chem.* **2010,** *398* (2), 885-893.

127. Komuro, N.; Takaki, S.; Suzuki, K.; Citterio, D., Inkjet printed (bio)chemical sensing devices. *Anal. Bioanal. Chem.* **2013,** *405* (17), 5785-5805.

128. Morbioli, G. G.; Mazzu-Nascimento, T.; Stockton, A. M.; Carrilho, E., Technical aspects and challenges of colorimetric detection with microfluidic paper-based analytical devices (μPADs)-A review. *Anal. Chim. Acta* **2017,** *970*, 1-22.

129. Lin, Y.; Gritsenko, D.; Feng, S.; Teh, Y. C.; Lu, X.; Xu, J., Detection of heavy metal by paper-based microfluidics. *Biosens. Bioelectron.* **2016,** *83*, 256-266.

130. Almeida, M. I. G. S.; Jayawardane, B. M.; Kolev, S. D.; McKelvie, I. D., Developments of microfluidic paper-based analytical devices (μPADs) for water analysis: A review. *Talanta* **2018,** *177*, 176-190.

131. Sriram, G.; Bhat, M. P.; Patil, P.; Uthappa, U. T.; Jung, H.-Y.; Altalhi, T.; Kumeria, T.; Aminabhavi, T. M.; Pai, R. K.; Kurkuri, M. D., based microfluidic analytical devices for colorimetric detection of toxic ions: A review. *TrAC Trends Anal. Chem.* **2017,** *93*, 212-227.

132. Sriram, G.; Bhat, M. P.; Patil, P.; Uthappa, U. T.; Jung, H.-Y.; Altalhi, T.; Kumeria, T.; Aminabhavi, T. M.; Pai, R. K.; Madhuprasad; Kurkuri, M. D., Paper-based microfluidic analytical devices for colorimetric detection of toxic ions: A review. *TrAC Trends Anal. Chem.* **2017,** *93*, 212-227.

133. Meredith, N. A.; Quinn, C.; Cate, D. M.; Reilly, T. H.; Volckens, J.; Henry, C. S., Paper-based analytical devices for environmental analysis. *Analyst* **2016,** *141* (6), 1874-1887.

134. Macherey-Nagel Web page. https://www.mn-net.com/tabid/4928/default.aspx.

135. Merk Web page. www.merckmillipore.jp/test-kits.

136. Yetisen, A. K.; Jiang, N.; Tamayol, A.; Ruiz-Esparza, G. U.; Zhang, Y. S.; Medina-Pando, S.; Gupta, A.; Wolffsohn, J. S.; Butt, H.; Khademhosseini, A., Paper-based microfluidic system for tear electrolyte analysis. *Lab Chip* **2017,** *17* (6), 1137-1148.

137. Zhang, Y.; Fan, J.; Nie, J.; Le, S.; Zhu, W.; Gao, D.; Yang, J.; Zhang, S.; Li, J., Timing readout in paper device for quantitative point-of-use hemin/G-quadruplex DNAzyme-based bioassays. *Biosens. Bioelectron.* **2015,** *73*, 13-18.

138. Wang, H.; Li, Y.-j.; Wei, J.-f.; Xu, J.-r.; Wang, Y.-h.; Zheng, G.-x., Paper-based three-dimensional microfluidic device for monitoring of heavy metals with a camera cell phone. *Anal. Bioanal. Chem.* **2014,** *406* (12), 2799-2807.

139. Hossain, S. M. Z.; Brennan, J. D., β-Galactosidase-Based Colorimetric Paper Sensor for Determination of Heavy Metals. *Anal. Chem.* **2011,** *83* (22), 8772-8778.

140. Rattanarat, P.; Dungchai, W.; Cate, D. M.; Siangproh, W.; Volckens, J.; Chailapakul, O.; Henry, C. S., A microfluidic paper-based analytical device for rapid quantification of particulate chromium. *Anal. Chim. Acta* **2013,** *800*, 50-55.

141. Cate, D. M.; Nanthasurasak, P.; Riwkulkajorn, P.; L'orange, C.; Henry, C. S.; Volckens, J., Rapid detection of transition metals in welding fumes using paper-based analytical devices. *Ann. Occup. Hyg.* **2014,** *58* (4), 413-423.

142. Rattanarat, P.; Dungchai, W.; Cate, D.; Volckens, J.; Chailapakul, O.; Henry, C. S., Multilayer Paper-Based Device for Colorimetric and Electrochemical Quantification of Metals. *Anal. Chem.* **2014,** *86* (7), 3555-3562.

143. Li, M.; Cao, R.; Nilghaz, A.; Guan, L.; Zhang, X.; Shen, W., "Periodic-table-style" paper device for monitoring heavy metals in water. *Anal. Chem.* **2015,** *87* (5), 2555-2559.

144. Alahmad, W.; Tungkijanansin, N.; Kaneta, T.; Varanusupakul, P., A colorimetric paper-based analytical device coupled with hollow fiber membrane liquid phase microextraction (HF-LPME) for highly sensitive detection of hexavalent chromium in water samples. *Talanta* **2018,** *190*, 78-84.

145. Asano, H.; Shiraishi, Y., Microfluidic Paper-based Analytical Device for the Determination of Hexavalent Chromium by Photolithographic Fabrication Using a Photomask Printed with 3D Printer. *Anal. Sci.* **2018,** *34* (1), 71-74.

146. Devadhasan, J. P.; Kim, J., A chemically functionalized paper-based microfluidic platform for multiplex heavy metal detection. *Sens. Act. B* **2018,** *273*, 18-24.

147. Sun, X.; Li, B.; Qi, A.; Tian, C.; Han, J.; Shi, Y.; Lin, B.; Chen, L., Improved assessment of accuracy and performance using a rotational paper-based device for multiplexed detection of heavy metals. *Talanta* **2018,** *178*, 426-431.

148. Sun, H.; Jia, Y.; Dong, H.; Fan, L.; Zheng, J., Multiplex quantification of metals in airborne particulate matter via smartphone and paper-based microfluidics. *Anal. Chim. Acta* **2018,** *1044*, 110-118.

149. Meredith, N. A.; Volckens, J.; Henry, C. S., Paper-based microfluidics for experimental design: screening masking agents for simultaneous determination of Mn(ii) and Co(ii). *Anal. Methods* **2017,** *9* (3), 534-540.

150. Rahbar, M.; Nesterenko, P. N.; Paull, B.; Macka, M., Geometrical alignment of multiple fabrication steps for rapid prototyping of microfluidic paper-based analytical devices. *Anal. Chem.* **2017,** *89* (22), 11918-11923.

151. Mentele, M. M.; Cunningham, J.; Koehler, K.; Volckens, J.; Henry, C. S., Microfluidic Paper-Based Analytical Device for Particulate Metals. *Anal. Chem.* **2012,** *84* (10), 4474-4480.

152. Jayawardane, B. M.; Coo, L. d.; Cattrall, R. W.; Kolev, S. D., The use of a polymer inclusion membrane in a paper-based sensor for the selective determination of Cu(II). *Anal. Chim. Acta* **2013,** *803*, 106-112.

153. Cate, D. M.; Noblitt, S. D.; Volckens, J.; Henry, C. S., Multiplexed paper analytical device for quantification of metals using distance-based detection. *Lab Chip* **2015,** *15* (13), 2808-2818.

154. Henares, T. G.; Yamada, K.; Takaki, S.; Suzuki, K.; Citterio, D., "Drop-slip" bulk sample flow on fully inkjet-printed microfluidic paper-based analytical device. *Sens. Act. B* **2017,** *244*, 1129-1137.

155. Hofstetter, J. C.; Wydallis, J. B.; Neymark, G.; Reilly III, T. H.; Harrington, J.; Henry, C. S., Quantitative colorimetric paper analytical devices based on radial distance measurements for aqueous metal determination. *Analyst* **2018,** *143* (13), 3085-3090.

156. Liu, L.; Xie, M.-R.; Fang, F.; Wu, Z.-Y., Sensitive colorimetric detection of Cu^{2+} by simultaneous reaction and electrokinetic stacking on a paper-based analytical device. *Microchem. J.* **2018,** *139*, 357-362.

157. Bandara, G. C.; Heist, C. A.; Remcho, V. T., Chromatographic separation and visual detection on wicking microfluidic devices: quantitation of Cu^{2+} in surface, ground, and drinking water. *Anal. Chem.* **2018,** *90* (4), 2594-2600.

158. Zhang, L.; Guan, L.; Lu, Z.; Li, M.; Wu, J.; Cao, R.; Tian, J., Barrier-free patterned paper sensors for multiplexed heavy metal detection. *Talanta* **2019,** *196*, 408-414.

159. Huangfu, C.; Zhang, Y.; Jang, M.; Feng, L., A μPAD for Simultaneous Monitoring of Cu^{2+}, Fe^{2+} and Free Chlorine in Drinking Water. *Sens. Act. B* **2019**, *293*, 350-356

160. Chabaud, K. R.; Thomas, J. L.; Torres, M. N.; Oliveira, S.; McCord, B. R., Simultaneous colorimetric detection of metallic salts contained in low explosives residue using a microfluidic paper-based analytical device (μPAD). *Forensic Chem.* **2018,** *9*, 35-41.

161. Shimada, Y.; Kaneta, T., Highly sensitive paper-based analytical devices with the introduction of a large-volume sample via continuous flow. *Anal. Sci.* **2018,** *34* (1), 65-70.

162. Asano, H.; Shiraishi, Y., Development of paper-based microfluidic analytical device for iron assay using photomask printed with 3D printer for fabrication of hydrophilic and hydrophobic zones on paper by photolithography. *Anal. Chim. Acta* **2015,** *883*, 55-60.

163. Ogawa, K.; Kaneta, T., Determination of Iron Ion in the Water of a Natural Hot Spring Using Microfluidic Paper-based Analytical Devices. *Anal. Sci.* **2016,** *32* (1), 31-34.

164. Han, J.; Qi, A.; Zhou, J.; Wang, G.; Li, B.; Chen, L., Simple Way To Fabricate Novel Paper-Based Valves Using Plastic Comb Binding Spines. *ACS Sens.* **2018,** *3* (9), 1789-1794.

165. Giannoulas, G.; Tsogas, G. Z.; Giokas, D. L., Single-point calibration and standard addition assays on calibrant-loaded paper-based analytical devices. *Talanta* **2019,** *201*, 149-155.

166. Satarpai, T.; Shiowatana, J.; Siripinyanond, A., Paper-based analytical device for sampling, on-site preconcentration and detection of ppb lead in water. *Talanta* **2016,** *154*, 504-510.

167. Buking, S.; Saetear, P.; Tiyapongpattana, W.; Uraisin, K.; Wilairat, P.; Nacapricha, D.; Ratanawimarnwong, N., Microfluidic paper-based analytical device for quantification of lead using reaction band-length for identification of bullet hole and its potential for estimating firing distance. *Anal. Sci.* **2018,** *34* (1), 83-89.

168. Feng, L.; Li, X.; Li, H.; Yang, W.; Chen, L.; Guan, Y., Enhancement of sensitivity of paper-based sensor array for the identification of heavy-metal ions. *Anal. Chim. Acta* **2013,** *780*, 74-80.

169. Mujawar, L. H.; Felemban, A. A.; El-Shahawi, M. S., Hexamethyldisilazane Modified Paper as an Ultra-sensitive Platform for Visual Detection of Hg^{2+}, Co^{2+}, Zn^{2+} and the Application to Semi-quantitative Determination of Hg^{2+} in Wastewater. *Anal. Sci.* **2016,** *32* (5), 491-497.

170. Cai, L.; Fang, Y.; Mo, Y.; Huang, Y.; Xu, C.; Zhang, Z.; Wang, M., Visual quantification of Hg on a microfluidic paper-based analytical device using distance-based detection technique. *AIP Adv.* **2017,** *7* (8), 085214.

171. Cao, R.; Zhang, X.; Tan, W.; Shen, W., Precipitation assay meets low wettability on paper: a simple approach for fabricating patterned paper sensors. *Cellulose* **2018,** *25* (1), 583-592.

172. Nguyen, M. P.; Meredith, N. A.; Kelly, S. P.; Henry, C. S., Design considerations for reducing sample loss in microfluidic paper-based analytical devices. *Anal. Chim. Acta* **2018,** *1017*, 20-25.

173. Cate, D. M.; Dungchai, W.; Cunningham, J. C.; Volckens, J.; Henry, C. S., Simple, distance-based measurement for paper analytical devices. *Lab Chip* **2013,** *13* (12), 2397-2404.

174. Yamada, K.; Citterio, D.; Henry, C. S., "Dip-and-read" paper-based analytical devices using distance-based detection with color screening. *Lab Chip* **2018,** *18* (10), 1485-1493.

175. Li, J.-j.; Hou, C.-j.; Huo, D.-q.; Shen, C.-h.; Luo, X.-g.; Fa, H.-b.; Yang, M.; Zhou, J., Detection of trace nickel ions with a colorimetric sensor based on indicator displacement mechanism. *Sens. Act. B* **2017,** *241*, 1294-1302.

176. Ota, R.; Yamada, K.; Suzuki, K.; Citterio, D., Quantitative evaluation of analyte transport on microfluidic paper-based analytical devices (μPADs). *Analyst* **2018,** *143* (3), 643-653.

177. Kudo, H.; Yamada, K.; Watanabe, D.; Suzuki, K.; Citterio, D., Paper-Based Analytical Device for Zinc Ion Quantification in Water Samples with Power-Free Analyte Concentration. *Micromachines* **2017,** *8* (4).

178. Ostad, M. A.; Hajinia, A.; Heidari, T., A novel direct and cost effective method for fabricating paper-based microfluidic device by commercial eye pencil and its application for determining simultaneous calcium and magnesium. *Microchem. J.* **2017,** *133*, 545-550.

179. Karita, S.; Kaneta, T., Chelate titrations of Ca^{2+} and Mg^{2+} using microfluidic paper-based analytical devices. *Anal. Chim. Acta* **2016,** *924*, 60-67.

180. Kang, S.-M.; Jang, S.-C.; Huh, Y. S.; Lee, C.-S.; Roh, C., A highly facile and selective Chemo-Paper-Sensor (CPS) for detection of strontium. *Chemosphere* **2016,** *152*, 39-46.

181. Jayawardane, B. M.; McKelvie, I. D.; Kolev, S. D., Development of a Gas-Diffusion Microfluidic Paper-Based Analytical Device (μPAD) for the Determination of Ammonia in Wastewater Samples. *Anal. Chem.* **2015,** *87* (9), 4621-4626.

182. Phansi, P.; Sumantakul, S.; Wongpakdee, T.; Fukana, N.; Ratanawimarnwong, N.; Sitanurak, J.; Nacapricha, D., Membraneless Gas-Separation Microfluidic Paper-Based Analytical Devices for Direct Quantitation of Volatile and Nonvolatile Compounds. *Anal. Chem.* **2016,** *88* (17), 8749-8756.

183. Peters, K. L.; Corbin, I.; Kaufman, L. M.; Zreibe, K.; Blanes, L.; McCord, B. R., Simultaneous colorimetric detection of improvised explosive compounds using microfluidic paper-based analytical devices (μPADs). *Anal. Methods* **2015,** *7* (1), 63-70.

184. Cho, Y. B.; Jeong, S. H.; Chun, H.; Kim, Y. S., Selective colorimetric detection of dissolved ammonia in water via modified Berthelot's reaction on porous paper. *Sens. Act. B* **2018,** *256*, 167-175.

185. Loh, L. J.; Bandara, G. C.; Weber, G. L.; Remcho, V. T., Detection of water contamination from hydraulic fracturing wastewater: a μPAD for bromide analysis in natural waters. *Analyst* **2015,** *140* (16), 5501-5507.

186. Hashimoto, Y.; Kaneta, T., Chromatographic paper-based analytical devices using an oxidized paper substrate. *Anal. Methods* **2019,** *11* (2), 179-184.

187. Li, X.; Tian, J.; Garnier, G.; Shen, W., Fabrication of paper-based microfluidic sensors by printing. *Colloids Surf. B* **2010,** *76* (2), 564-570.

188. Li, X.; Tian, J.; Shen, W., Progress in patterned paper sizing for fabrication of paper-based microfluidic sensors. *Cellulose* **2010,** *17* (3), 649-659.

189. Klasner, S. A.; Price, A. K.; Hoeman, K. W.; Wilson, R. S.; Bell, K. J.; Culbertson, C. T., Paper-based microfluidic devices for analysis of clinically relevant analytes present in urine and saliva. *Anal. Bioanal. Chem.* **2010,** *397* (5), 1821-1829.

190. Xiao, L.; Liu, X.; Zhong, R.; Zhang, K.; Zhang, X.; Zhou, X.; Lin, B.; Du, Y., A rapid, straightforward, and print house compatible mass fabrication method for integrating 3D paper-based microfluidics. *Electrophoresis* **2013,** *34* (20), 3003-3007.

191. Jayawardane, B. M.; Wei, S.; McKelvie, I. D.; Kolev, S. D., Microfluidic Paper-Based Analytical Device for the Determination of Nitrite and Nitrate. *Anal. Chem.* **2014,** *86* (15), 7274-7279.

192. de Tarso Garcia, P.; Garcia Cardoso, T. M.; Garcia, C. D.; Carrilho, E.; Tomazelli Coltro, W. K., A handheld stamping process to fabricate microfluidic paper-based analytical devices with chemically modified surface for clinical assays. *RSC Adv.* **2014,** *4* (71), 37637-37644.

193. Lopez-Ruiz, N.; Curto, V. F.; Erenas, M. M.; Benito-Lopez, F.; Diamond, D.; Palma, A. J.; Capitan-Vallvey, L. F., Smartphone-Based Simultaneous pH and Nitrite Colorimetric Determination for Paper Microfluidic Devices. *Anal. Chem.* **2014,** *86* (19), 9554-9562.

194. Bhakta, S. A.; Borba, R.; Taba Jr, M.; Garcia, C. D.; Carrilho, E., Determination of nitrite in saliva using microfluidic paper-based analytical devices. *Anal. Chim. Acta* **2014,** *809*, 117-122.

195. Kao, P.-K.; Hsu, C.-C., Battery-Operated, Portable, and Flexible Air Microplasma Generation Device for Fabrication of Microfluidic Paper-Based Analytical Devices on Demand. *Anal. Chem.* **2014,** *86* (17), 8757-8762.

196. Cardoso, T. M. G.; Garcia, P. T.; Coltro, W. K. T., Colorimetric determination of nitrite in clinical, food and environmental samples using microfluidic devices stamped in paper platforms. *Anal. Methods* **2015,** *7* (17), 7311-7317.

197. Wang, B.; Lin, Z.; Wang, M., Fabrication of a Paper-Based Microfluidic Device To Readily Determine Nitrite Ion Concentration by Simple Colorimetric Assay. *J. Chem. Edu.* **2015,** *92* (4), 733-736.

198. Lo, S.-J.; Chen, K.-H.; Yao, D.-J., An approach to enhance self-compensation capability in paper-based devices for chemical sensing. *Talanta* **2015,** *145*, 29-34.

199. Ismail, A.; Araújo, M. O.; Chagas, C. L. S.; Griveau, S.; D'Orlyé, F.; Varenne, A.; Bedioui, F.; Coltro, W. K. T., Colorimetric analysis of the decomposition of S-nitrosothiols on paper-based microfluidic devices. *Analyst* **2016,** *141* (22), 6314-6320.

200. Jiang, Y.; Hao, Z.; He, Q.; Chen, H., A simple method for fabrication of microfluidic paper-based analytical devices and on-device fluid control with a portable corona generator. *RSC Adv.* **2016,** *6* (4), 2888-2894.

201. de Oliveira, R. A. G.; Camargo, F.; Pesquero, N. C.; Faria, R. C., A simple method to produce 2D and 3D microfluidic paper-based analytical devices for clinical analysis. *Anal. Chim. Acta* **2017,** *957*, 40-46.

202. Zhang, X.-X.; Song, Y.-Z.; Fang, F.; Wu, Z.-Y., Sensitive paper-based analytical device for fast colorimetric detection of nitrite with smartphone. *Anal. Bioanal. Chem.* **2018,** *410* (11), 2665-2669.

203. Vidal, E.; Lorenzetti, A. S.; Lista, A. G.; Domini, C. E., Micropaper-based analytical device (μPAD) for the simultaneous determination of nitrite and fluoride using a smartphone. *Microchem. J.* **2018,** *143*, 467-473.

204. Chiang, C.-K.; Kurniawan, A.; Kao, C.-Y.; Wang, M.-J., Single step and mask-free 3D wax printing of microfluidic paper-based analytical devices for glucose and nitrite assays. *Talanta* **2019,** *194*, 837-845.

205. Jayawardane, B. M.; McKelvie, I. D.; Kolev, S. D., A paper-based device for measurement of reactive phosphate in water. *Talanta* **2012,** *100*, 454-460.

206. Jayawardane, B. M.; Wongwilai, W.; Grudpan, K.; Kolev, S. D.; Heaven, M. W.; Nash, D. M.; McKelvie, I. D., Evaluation and Application of a Paper-Based Device for the Determination of Reactive Phosphate in Soil Solution. *J. Environ. Quality* **2014,** *43* (3), 1081-1085.

207. Fu, E., Enabling robust quantitative readout in an equipment-free model of device development. *Analyst* **2014,** *139* (19), 4750-4757.

208. Tian, T.; Li, J.; Song, Y.; Zhou, L.; Zhu, Z.; Yang, C. J., Distance-based microfluidic quantitative detection methods for point-of-care testing. *Lab Chip* **2016,** *16* (7), 1139-1151.

209. Walter, B., Dry reagent chemistries in clinical analysis. *Anal. Chem.* **1983,** *55* (4), 498A-514A.

210. Dumschat, C.; Borchardt, M.; Diekmann, C.; Cammann, K.; Knoll, M., Potentiometric test strip. *Sens. Act. B* **1995,** *24* (1), 279-281.

211. Eggenstein, C.; Borchardt, M.; Dumschat, C.; Gründig, B.; Cammann, K.; Spener, F.; Knoll, M., Potentiometric biosensor in double matrix membrane technology. *Biosens. Bioelectron.* **1995,** *10* (6), 595-600.

212. Novell, M.; Parrilla, M.; Crespo, G. A.; Rius, F. X.; Andrade, F. J., Paper-Based Ion-Selective Potentiometric Sensors. *Anal. Chem.* **2012,** *84* (11), 4695-4702.

213. Lan, W.-J.; Zou, X. U.; Hamedi, M. M.; Hu, J.; Parolo, C.; Maxwell, E. J.; Bühlmann, P.; Whitesides, G. M., Paper-Based Potentiometric Ion Sensing. *Anal. Chem.* **2014,** *86* (19), 9548-9553.

214. Hu, J.; Stein, A.; Bühlmann, P., A Disposable Planar Paper-Based Potentiometric Ion-Sensing Platform. *Angew. Chem. Inter. Ed.* **2016,** *55* (26), 7544-7547.

215. Ruecha, N.; Chailapakul, O.; Suzuki, K.; Citterio, D., Fully Inkjet-Printed Paper-Based Potentiometric Ion-Sensing Devices. *Anal. Chem.* **2017,** *89* (19), 10608-10616.

216. Zdrachek, E.; Bakker, E., Potentiometric Sensing. *Anal. Chem.* **2019,** *91* (1), 2-26.

217. Hu, J.; Stein, A.; Bühlmann, P., Rational design of all-solid-state ion-selective electrodes and reference electrodes. *TrAC Trends Anal. Chem.* **2016,** *76*, 102-114.

218. Lan, W.-J.; Maxwell, E. J.; Parolo, C.; Bwambok, D. K.; Subramaniam, A. B.; Whitesides, G. M., Paper-based electroanalytical devices with an integrated, stable reference electrode. *Lab Chip* **2013,** *13* (20), 4103-4108.

219. Wróblewski, W.; Roźniecka, E.; Dybko, A.; Brzózka, Z., Cellulose based bulk pH optomembranes. *Sens. Act. B* **1998,** *48* (1), 471-475.

220. Cardwell, T. J.; Cattrall, R. W.; Deady, L. W.; Dorkos, M.; O'Connell, G. R., A fast response membrane-based pH indicator optode. *Talanta* **1993,** *40* (5), 765-768.

221. Soda, Y.; Citterio, D.; Bakker, E., Equipment-Free Detection of K^+ on Microfluidic Paper-Based Analytical Devices Based on Exhaustive Replacement with Ionic Dye in Ion-selective Capillary Sensors. *ACS Sens.* **2019,** *4* (3), 670-677.

222. Shibata, H.; Hiruta, Y.; Citterio, D., Fully inkjet-printed distance-based paper microfluidic devices for colorimetric calcium determination using ion-selective optodes. *Analyst* **2019,** *144* (4), 1178-1186.

223. Kassal, P.; Sigurnjak, M.; Steinberg, I. M., Paper-based ion-selective optodes for continuous sensing: Reversible potassium ion monitoring. *Talanta* **2019,** *193*, 51-55.

224. Gerold, C. T.; Bakker, E.; Henry, C. S., Selective Distance-Based K+ Quantification on Paper-Based Microfluidics. *Anal. Chem.* **2018,** *90* (7), 4894-4900.

225. Avoundjian, A.; Jalali-Heravi, M.; Gomez, F. A., Use of chemometrics to optimize a glucose assay on a paper microfluidic platform. *Anal. Bioanal. Chem.* **2017,** *409* (10), 2697-2703.

226. Hamedpour, V.; Postma, G. J.; van Den Heuvel, E.; Jansen, J. J.; Suzuki, K.; Citterio, D., Chemometrics-assisted microfluidic paper-based analytical device for the determination of uric acid by silver nanoparticle plasmon resonance. *Anal. Bioanal. Chem.* **2018,** *410* (9), 2305-2313.

227. Hamedpour, V.; Leardi, R.; Suzuki, K.; Citterio, D., Fabrication of paper-based analytical devices optimized by central composite design. *Analyst* **2018,** *143* (9), 2102-2108.

228. Kong, F.; Hu, Y. F., Biomolecule immobilization techniques for bioactive paper fabrication. *Anal. Bioanal. Chem.* **2012,** *403* (1), 7-13.

229. Burba, P.; Willmer, P., Cellulose: a biopolymeric sorbent for heavy-metal traces in waters. *Talanta* **1983,** *30* (5), 381-383.

230. Duong, T. D.; Nguyen, K. L.; Hoang, M., Competitive sorption of Na^+ and Ca^{2+} ions on unbleached kraft fibres -A kinetics and equilibrium study. *J. Colloid Interface Sci.* **2006,** *301* (2), 446-451.

Chapter 2

Integration of a classical film-based optode system into paper-based sensing platform

This chapter is based on "Implementation of a plasticized PVC-based cation-selective optode system into a paper-based analytical device for colorimetric sodium detection",

Hiroyuki Shibata, Terence G. Henares, Kentaro Yamada, Koji Suzuki and Daniel Citterio,

Analyst, **2018**, *143*, 678-686.

Summary

On the example of a colorimetric sodium assay, this work demonstrates the implementation of a classical cation-exchange optode relying on an ionophore-doped plasticized PVC membrane into a paper-based analytical device (PAD). An ion-selective optode (ISO) system has been arranged into a vertically-assembled PAD (vPAD) integrating a pH-buffering function. Capillary force-driven sample liquid transportation through the paper matrix enabled pH-adjustment prior to the optical detection of the analyte cation. Functionalized paper layers with inkjet-deposited ISO membranes were combined with whole device lamination to attain a stable ion-exchange equilibrium required for the theoretical behavior of ISOs. Whole device lamination limited rapid evaporation of sample liquid on vPADs to avoid an increase of target concentration. Sigmoidal response curves between 10^{-5} and 1 M of Na^+ at pH 5.0–7.0 have been confirmed on vPADs, following the theory defined by the cation-exchange equilibrium reaction. Finally, the influence of the cellulosic paper substrate matrix acting as a cation-exchanger on the optode response behavior has been evaluated and compared with conventional plastic film optodes.

2.1. Introduction

Ion-selective optodes (ISOs), often regarded as optical counterparts of ion-selective electrodes (ISEs), have been applied for optical detection of ion species targeting a wide array of application fields.[1-3] Their detection mechanism is typically based on an equilibrium reaction between a water-immiscible polymeric membrane and an aqueous sample phase.[1] Selective recognition of the ion of interest is achieved by an ion-specific receptor (ionophore) doped into the organic polymeric membrane. Extraction of the target ion into the organic phase is accompanied either by protonation (for anionic target ions) or deprotonation (for cationic target ions) of a co-doped lipophilic pH indicator (chromoionophore), generating an optical signal from the ISO membrane. Their advantageous features, including high selectivity and ease of optical signal detection, gave birth to a variety of ISO configurations such as thin films, particles and suspensions.[2-5]

Over the past decade, porous filter paper has drawn attention as an attractive substrate material for the fabrication of analytical devices due to multiple advantages including: (i) low-cost, (ii) ease of device manufacturing, (iii) portability, and (iv) safe disposability by incineration, among others.[6-8] In 2007, the Whitesides research group has first introduced the concept of microfluidically patterned paper as a new chemical assay platform,[9] now commonly referred to as microfluidic paper-based analytical devices (μPADs).[10] The porous structure and hydrophilic nature of cellulose-composed paper enables pump-free passive sample transportation by capillary action, in contrast to conventional microfluidic systems requiring active pumping. Such capabilities of μPADs have greatly expanded their application fields including to medical diagnosis, environmental analysis and food quality monitoring, among others.[11-17]

Colorimetry is undoubtedly the most well-established signalling approach among classical chemical analyses. Not surprisingly, a large fraction of μPADs reported in the literature relies on colorimetric detection,[7] because of the abundance of chemistries for this detection technique and the ease of signal recognition (*i.e.* observable by unaided eyes) fitting well the philosophy of μPADs (low-cost and user-friendliness). Accordingly, a wide range of analytical targets including ion species has become detectable by colorimetric μPADs.[13, 15, 18] Focus has mostly been on the detection of heavy metal cations relying on

classical colorimetric indicators.[19-23] In one special arrangement, a semi-selective colorimetric indicator has been combined with a selective carrier for Cu^{2+}, incorporated into a polymer inclusion membrane (PIM) made from plasticized PVC.[21] This membrane was attached to filter papers vertically stacked by hot lamination. μPADs for the biologically most abundant electrolytes (e.g. Na^+, K^+, Cl^-) are much less plentiful, because no selective classical colorimetric indicators are available for these ion species. Alternatively, metal-chelating fluorophores[24] and a DNAzyme coupled with chromogenic enzymatic reaction[25] were used to achieve μPAD-based quantification of tear electrolytes (Na^+, K^+, Ca^{2+}) and serum K^+, respectively.

Despite the well-established ISO-based analytical technique and the importance of biological electrolyte detection,[26-27] this system is scarcely integrated into μPADs. While the sensitivity required for blood electrolyte analysis with very narrow physiological ranges might be challenging for a μPAD relying on colorimetric signaling, there are biological samples showing significant variations of electrolyte levels (e.g. tear fluid, urine, saliva), for which monitoring at point-of-care is of interest. In addition to the application to biological fluids, ISO-based μPADs could also come handy in the field of drinking water monitoring or the analysis of environmental water samples, among others. Given the large number of highly selective ionophores available,[28] their implementation into user-friendly μPADs with optical colorimetric signal detection offers great potential to extend the palette of target analytes detectable by low-cost approaches. In 2015, the Meyerhoff research group has first reported the colorimetric ISO-based detection of Na^+ on a filter paper disc,[29] where they surprisingly demonstrated that the traditional plasticized organic polymer matrix was not needed. In 2016, Capitan-Vallvey and co-workers applied classical film-based cation exchange ISOs for the determination of K^+ onto a cotton thread substrate.[30] Although quantitative analysis of the target ions was achieved with these systems, they require sample pH control by the user, since the optical signal generated by the cation exchange reaction is inevitably influenced by the pH of the aqueous sample phase in the same manner as with classical ISOs.[1-3] Only very recently, Meyerhoff's group addressed this bottleneck by pre-depositing pH-buffering components together with an inkjet-dispensed polymer matrix-free ISO on a filter paper strip for detection of anions (F^-, Cl^-)[31] or polyions[32]. Nevertheless, the implementation of a classical plasticized PVC-based ion-selective optode system onto a paper platform has to the best of our knowledge

never been reported.

In this context, the current work describes a μPAD for cation detection (Na^+ as a proof-of-concept target) relying on a classical ion exchange reaction-based ISO membrane. For the sake of user-friendliness, the pH-buffering function was integrated into vertically-assembled μPADs (vPADs). Shorter flow path lengths on vPADs (several hundreds of μm per paper layer) compared to lateral-flow configurations (several mm to cm) bring along several advantages: (i) only low sample volume required, (ii) quick sample liquid transportation, and (iii) compact device size.[33] Fabrication of microfluidic structure and deposition of ISO reagents were performed by using printing technologies (wax and inkjet printing) since they allow for well-defined and reproducible micropatterning of μPAD components.[34-36] The developed ISO-based vPAD successfully integrated multiple advantageous features, including automated sample pH adjustment by the pre-deposited buffer salt reagent, flexibility of pH value condition in the ISO reaction, prevention of evaporative loss of sample liquid and good selectivity for Na^+ over potentially interfering cations (K^+, Ca^{2+}, Mg^{2+}, Li^+). Besides evaluation of the analytical performance, a basic study on the influence of the cellulosic paper matrix on the optode response function was performed for the first time.

2.2. Theory of the detection principle

ISOs rely on an equilibrium cation-exchange reaction between the plasticized polymeric organic optode membrane phase containing the sensing reagents and the aqueous sample phase. The equilibrium reaction of the used ISO for Na^+ detection is given by **eq (2.1)**:[1-2]

$$Na^+_{(aq)} + CH^+_{(org)} + L_{(org)} + R^-_{(org)} \leftrightharpoons H^+_{(aq)} + C_{(org)} + LNa^+_{(org)} + R^-_{(org)} \quad (2.1)$$

where C is the chromoionophore (CH1), L the Na^+ ionophore (DD16C5), R^- the ion-exchanger (KTpClPB), and the indices “aq” and “org” indicate the aqueous sample phase and organic membrane phase, respectively. Extraction of the monovalent sodium ion (Na^+) into the organic membrane phase by the ionophore is

accompanied by deprotonation of the chromoionophore in order to maintain the electro-neutrality within the optode membrane phase. The degree of deprotonation of the chromoionophore (α) is related to the activity of the target analyte ion ($a_{\mathrm{Na^+}}$) in the aqueous sample phase as expressed by the following equation (**eq. 2.2**):

$$a_{\mathrm{Na^+}} = \frac{1}{K_{exch}}\left(\frac{\alpha}{1-\alpha}a_{\mathrm{H^+}}\right) \times \frac{R_{\mathrm{T}} - (1-\alpha)C_{\mathrm{T}}}{L_{\mathrm{T}} - (R_{\mathrm{T}} - (1-\alpha)C_{\mathrm{T}})} \tag{2.2}$$

where, K_{exch} is the equilibrium constant of the reaction shown in **eq (2.1)**, $a_{\mathrm{H^+}}$ is the proton activity in the aqueous sample solution, R_{T}, C_{T}, and L_{T} are the total concentration of ion-exchanger, chromoionophore and ionophore in the optode membrane, respectively. The optical property of ISOs is determined by the ratio of the chromoionophore's protonated and deprotonated form. The degree of deprotonation of the chromoionophore (α) is calculated according to **eq (2.3)** based on the experimentally determined absorbance of the chromoionophore in the optode phase: [1-2]

$$\alpha = \frac{A_{\mathrm{P}} - A}{A_{\mathrm{P}} - A_{\mathrm{D}}} \tag{2.3}$$

where A represents the experimentally measured absorbance at any given protonation state, and A_{P} and A_{D} stand for the absorbance in the fully protonated and deprotonated states, respectively.

Throughout this study, the hue value of the HSV (hue-saturation-value) color coordinate system was used as the colorimetric signal of the vPADs. In analogy to **eq (2.3)**, the hue parameter is linked to α by the following **eq (2.4)**:[37]

$$\alpha = \frac{H_{\mathrm{P}} - H}{H_{\mathrm{P}} - H_{\mathrm{D}}} \tag{2.4}$$

Here H_{P} and H_{D} are the experimentally obtained hue values of the fully protonated and deprotonated chromoionophore, and H is the hue value at any given state. Throughout this work, H_{D} and H_{P} were measured

by using aqueous solutions of 0.1 M KOH and 0.1 M HCl as the sample, respectively.

2.3. Experimental section

2.3.1. Reagents and instruments

All reagents were used without further purification. High molecular weight poly(vinyl chloride) (PVC), chromoionophore I (CH1), and tetramethylammonium hydroxide pentahydrate (TMAOH) were purchased from Sigma-Aldrich (St Louis, MO). Potassium tetrakis(4-chlorophenyl)borate (KTpClPB) was purchased from TCI (Tokyo, Japan). Bis(2-ethylhexyl)sebacate (DOS), cyclohexanone, sodium chloride (NaCl), potassium chloride (KCl), lithium chloride monohydrate ($LiCl \cdot H_2O$), calcium chloride dihydrate ($CaCl_2 \cdot 2H_2O$), magnesium chloride hexahydrate ($MgCl_2 \cdot 6H_2O$), cobalt(II) chloride hexahydrate ($CoCl_2 \cdot 6H_2O$), 0.1 N hydrochloric acid (HCl), potassium hydroxide (KOH), sodium hydroxide (NaOH) and citric acid were purchased from Wako Pure Chemical Industries (Osaka, Japan). 2-Morpholinoethanesulfonic acid (MES), *N*-(2-hydroxyethyl)-1-piperazineethanesulfonic acid (HEPES) and DD16C5 (sodium ionophore IV) were purchased from Dojindo Laboratories (Kumamoto, Japan). Ultrapure water (>18 MΩ cm) was obtained from a PURELAB flex water purification system (ELGA, Veolia Water, Marlow, U.K.) and used for the preparation of all solutions. Advantec No. 5C filter paper was purchased from Toyo Roshi (Tokyo, Japan). Hot lamination films (100 μm thickness, film material: polyethylene terephthalate and polyvinyl alcohol as a thermoplastic adhesive) were obtained from Jointex (Tokyo, Japan).

2.3.2. Preparation and characterization of paper layers

Advantec 5C filter paper cut into A4-size was fed into a ColorQube 8570 printer (Xerox, Norwalk, CT) to pattern wax barriers designed in PowerPoint (Microsoft) as shown in **Figure 2-1a**, followed by heating at 150 °C for 3 min on a hot plate (Nissin NHS-450ND, Nissinrika, Tokyo, Japan). The wax patterned paper substrates were then subjected to reagent deposition to fabricate the vPAD for colorimetric Na^+ detection

composed of 3 paper layers as illustrated in **Figure 2-1b and c**.

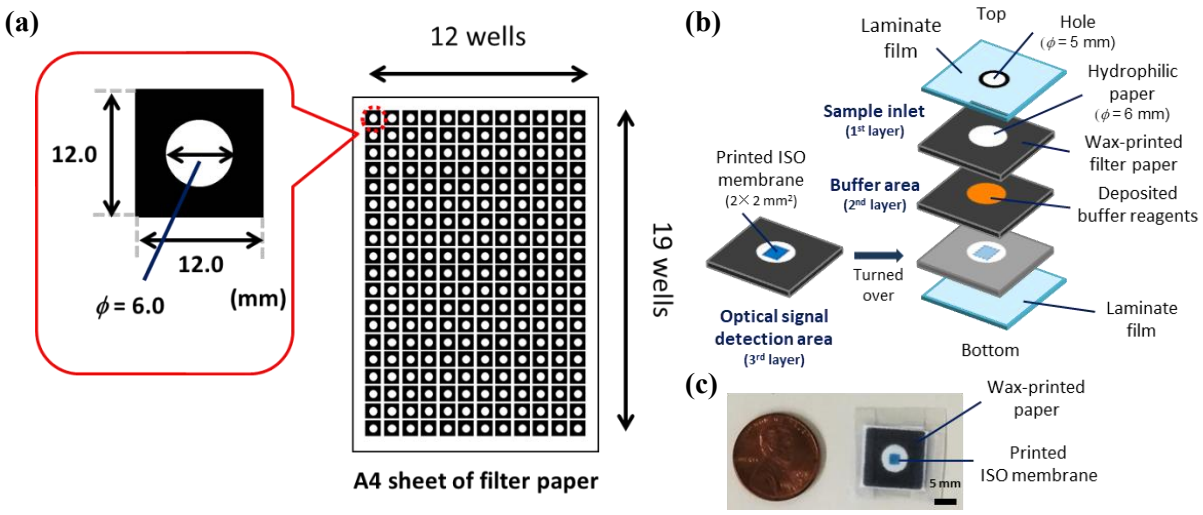

Figure 2-1. (a) Schematic illustration of the wax barrier pattern printed on an A4 size filter paper sheet. The dimensions in the red box represent the settingsinthe PowerPoint graphic software; (b) Schematic design of the developed vertically microfluidic paper-based analytical devices (vPADs) for ISO-based Na+ detection; (c) actual photograph of a vPAD.

For the preparation of a sample inlet ("1st layer" in **Figure 2-1b**), no reagent deposition was performed, whereas the buffer area ("2nd layer" in **Figure 2-1b**) was prepared by pipetting 7 µL of an aqueous pH-buffer solution (1 M citric acid-TMAOH pH 5.0, 1 M MES-TMAOH pH 6.0, or 1 M HEPES-TMAOH pH 7.0) onto the hydrophilic paper zone, followed by complete drying at room temperature. The optical detection area ("3rd layer" in **Figure 2-1b**) was prepared by depositing the ISO reagent ink (18.0 mg of PVC, 72.0 mg of DOS, 2.40 mg of KTpClPB, 1.28 mg of CH1 and 2.56 mg of DD16C5 dissolved in 2.0 g of cyclohexanone) onto the centre of the paper zone by means of a piezoelectrically actuated Dimatix DMP-2831 inkjet printer (Dimatix-Fujifilm Inc., Santa Clara, CA) in 30 printing cycles (2 × 2 mm^2 square, 40 µm of drop spacing). To meet the ink volume requirements and to decrease the ink dead volume, a 5 mL disposable pipette tip was used as the ink reservoir in place of the original Dimatix cartridge. During inkjet deposition, the printing table was heated at 40 °C to promote solvent evaporation. Optical microscope images were acquired on a DVM2500 digital microscope (Leica, Wetzlar, Germany) and scanning electron micrographs were recorded with a JSM-7600 instrument (JEOL, Tokyo Japan).

2.3.3. Assembly of vPADs

As-processed A4 size wax-patterned paper substrates were cut into individual spots. Before lamination, sample inlet holes (ϕ = 5 mm) were cut into the top lamination film layer with a Silhouette Cameo electronic knife blade cutting device (Silhouette, Lehi, UT) in double cutting mode. After sandwiching the three paper layers by the lamination films (note that the ISO-printed side is visible from the bottom side), hot lamination was performed on a QHE325 laminator (Meikoshokai, Tokyo, Japan). The instrument settings for substrate thickness and feeding speed were "150 µm" and "slow", respectively.

2.3.4. Na^+ assay with vPADs

15 µL of sample solution was applied onto the inlet area of the vPADs, followed by equilibration for 20 min under ambient condition to carry out the ISO reaction. The developed optical signals were captured with a Canoscan 8800F color scanner (Canon, Tokyo, Japan) from the bottom side. Numerical color intensity values of the ISO region (**Figure 2-2**) on the RGB (Red-Green-Blue) color scale were extracted from the scanned images with the ImageJ software (NIH, Bethesda, MD) to quantify the colorimetric response. The acquired RGB color intensity values were further converted to the HSV color coordinates,[38] and the hue value was used as the principal colorimetric signal parameter throughout this work. The deprotonation degree of CH1 (α) was calculated based on **eq (2.4)** using experimental hue values.[37]

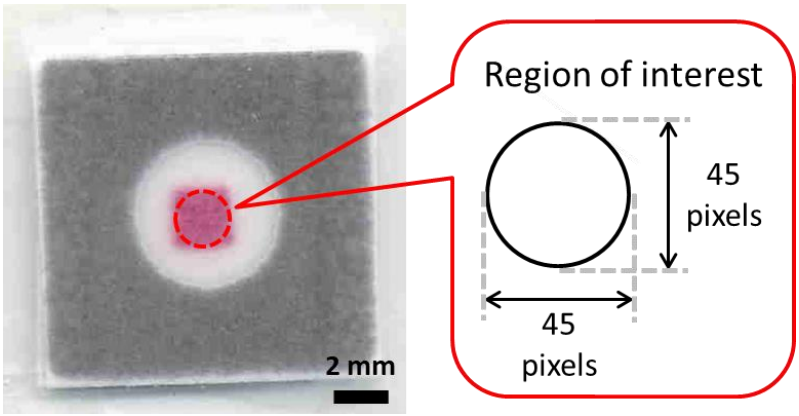

Figure 2-2. Color measurementarea on a scanned device image (600 dpi) for quantitative evaluation of ISO response. The dimensions of the ROI (region of interest) represent the settingsinthe ImageJ software

2.3.5. Theoretical sigmoidal curve fitting of ISO response

Activities of metal ions were estimated according to the expanded Debye-Hückel equation.[39] Theoretical curve fitting for the experimentally acquired ISO response data was performed based on **eq (2.2)** using known experimental parameter values (a_{H^+}, C_C, C_R, C_L shown in **Table 2-1**) and estimates of the equilibrium constant (K_{exch}) obtained with the "Solver" function of Excel (Microsoft).

Table 2-1. Experimental parameters used for calculation of $K_{exch.}$

Parameters	Values
a_{H^+}	1.0×10^{-6} mol/L
C_C	2.72×10^{-2} mol/kg
C_R	5.04×10^{-2} mol/kg
C_L	5.91×10^{-2} mol/kg

2.4. Results and discussion

2.4.1. Inkjet-printing of ISO membranes onto paper substrates

While a 1:2 molar ratio of polymer matrix (PVC) and plasticizer (DOS) is commonly chosen,[40] a 1:4 (PVC:DOS) ratio has been selected in this work, for the sake of optimal viscosity for inkjet-printing and shorter response time of the Na^+-selective devices. In addition, a preliminary experiment revealed that 30 printing cycles of the ISO reagent ink were sufficient to obtain color intensities enabling reproducible hue-based signal processing (refer to **Figure 2-3** for the detailed experimental setup and results, respectively). Inkjet-deposited ISOs exhibit well-defined optode areas on the surface of the filter paper (**Figure 2-4a**). The printed ISO reagents mainly reside in the filter paper within a depth of 150 μm from the printed surface, as seen in the cross-sectional microscope image shown in **Figure 2-4b**. The morphology of the printed-optode membrane prepared on the paper substrate was further studied by scanning electron microscopy (SEM). In contrast to the rough structure of the unmodified filter paper (**Figure 2-4c**), formation of smooth film areas

linking cellulosic fibres are observable on the ISO-modified paper surface (**Figure 2-4d**). It should be noted however, that due to the high porosity and surface area of the filter paper substrate, no continuous optode film is formed despite of the 30 printing cycles. This is an advantageous feature to partially maintain the liquid wicking character of the originally hydrophilic substrate.

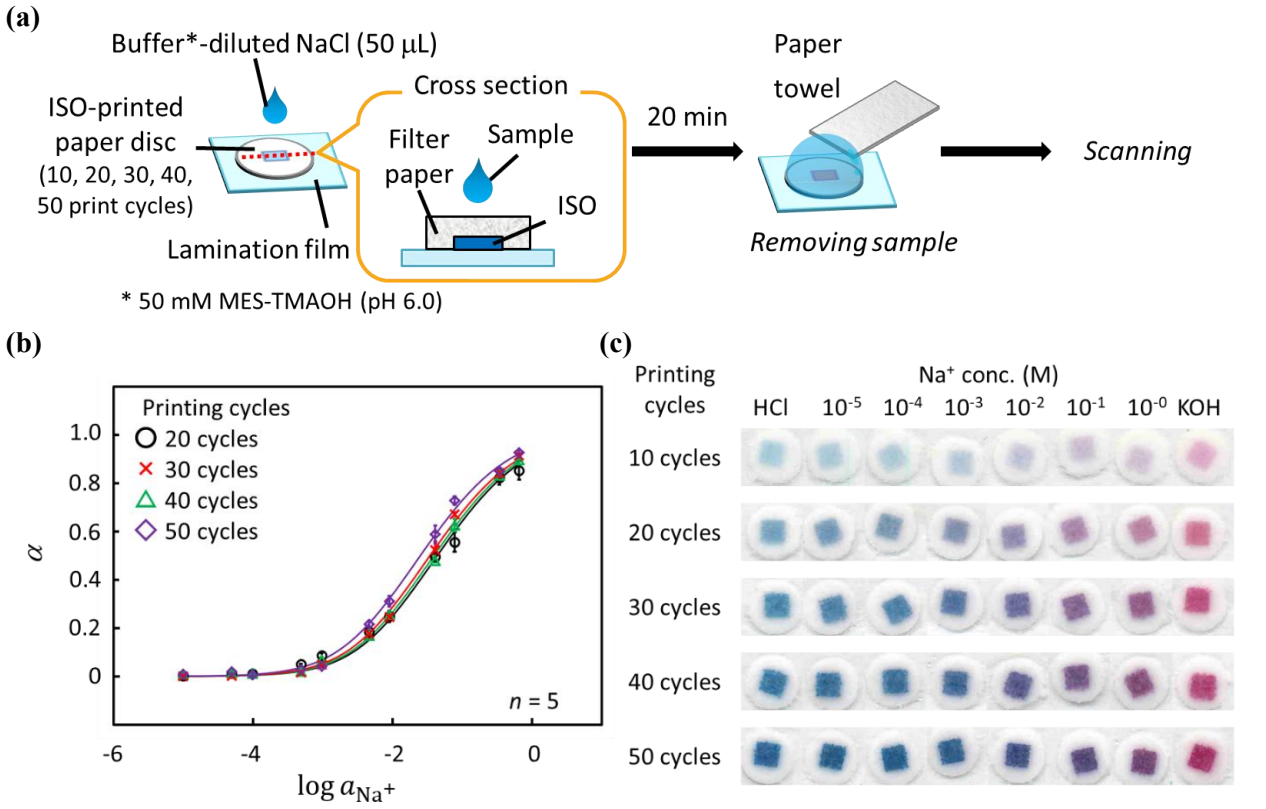

Figure 2-3. (a) Experimental procedure for optimization of ISO inkjet-printing cycles based ona spot test; (b) Scanned images of paper-based ISOs at 10, 20, 30, 40, 50 printing cyclesafter exposure to various concentrations of Na^+; (c) Hue-based (converted to α) response curvesobtained by scanning the results of 20, 30, 40, 50 printing cycles shown in part (b); each data point has been obtained by measurements with 5 individual single-use paper discs; error bars indicate the standard deviations.

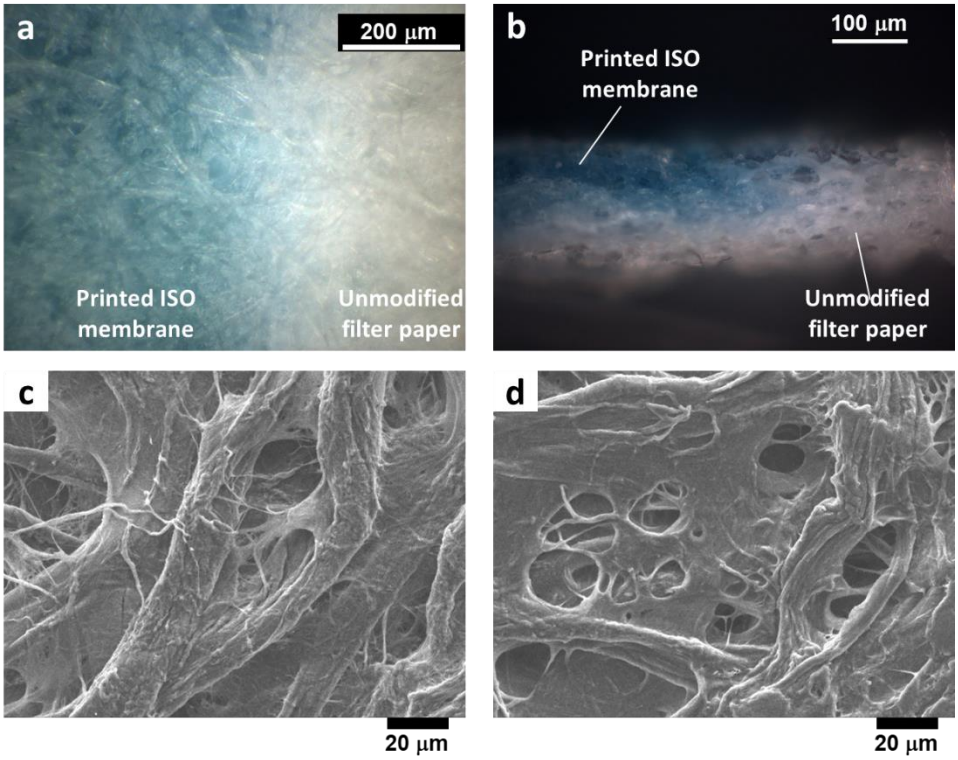

Figure 2-4. Microscope images of filter paper substrates: optical microscope images of (a) ISO-modified paper surface and (b) cross-section of ISO-modified paper; SEM images of (c) unmodified filter paper and of (d) filter paper after deposition of 30 printing cycles of ISO reagent ink.

2.4.2. Prevention of sample liquid evaporation by device lamination

Since the ISO-based Na^+ detection relies on the ion-exchange equilibrium reaction between the immiscible aqueous sample phase and the organic optode phase, evaporation of the aqueous sample liquid during the system equilibration must be prevented. Sample liquid evaporation would inevitably shift the reaction equilibrium, making quantitative analyses dependent on external factors (e.g. temperature- and humidity-dependent evaporation loss). Whole device lamination has been reported as an efficient approach to reduce evaporation of the sample liquid on µPADs.[21, 33, 41-42] In this study, the effect of vPAD lamination on the preservation of the sample liquid in the optical signal detection area was evaluated by making use of the hydration state-dependent color change of $CoCl_2$ (blue dehydrated form and red hydrated form). After deposition of 15 µL of aqueous $CoCl_2$ solution onto a reagent-free vPAD (**Figure 2-5**), the bottom paper layer maintained the red color after 30 min (**Figure 2-5c, top row**). On the other hand, non-laminated devices

prepared by stacking three paper layers with staples (**Figure 2-5b**) resulted in more rapid liquid evaporation, as indicated by the significant color change observed after 20 min (**Figure 2-5c, bottom row**). The results of a hue-based quantitative evaluation are shown in **Figure 2-6**. Non-laminated vPADs lead to a completely dry state 40 min after sample introduction, while no significant evaporation of sample liquid occurs within the first 25 min for the laminated devices. Thus, it can be concluded that in the case of fully laminated vPADs, an ISO-based assay with an equilibration time of 20 min can be performed without influence of sample evaporation.

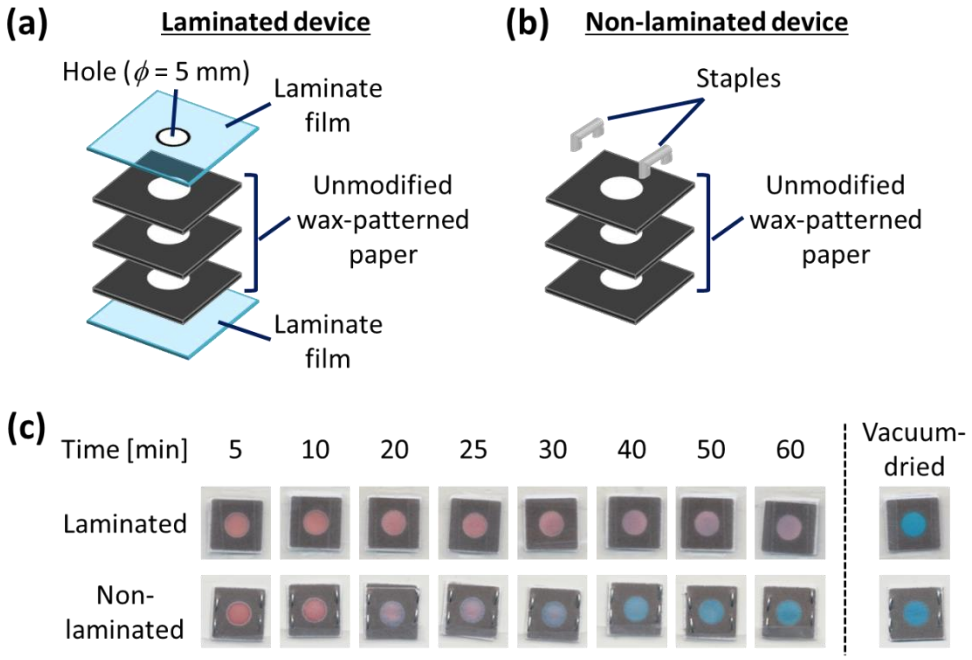

Figure 2-5. Evaluation of sample liquid evaporation prevention by device lamination: (a) design of laminated device (vPAD without ISO and pH-buffer reagents); (b) design of non-laminated device prepared by stacking paper layers with staples; (c) qualitative evaluation of the wetting state of the bottom paper layer of laminated and non-laminated devices (application of 15 µL of 0.3 g mL^{-1} aqueous $CoCl_2$ solution to sample inlet followed by scanning after indicated time); the "vacuum-dried" result represents the completely dry state.

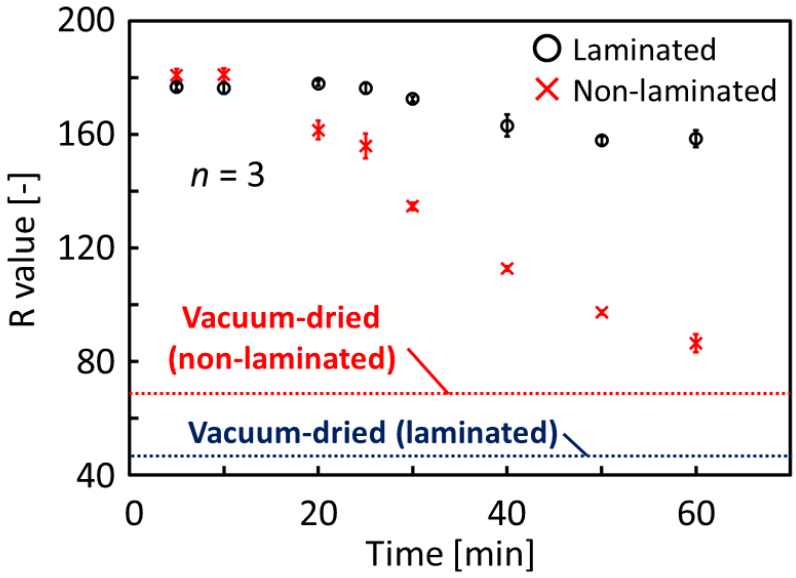

Figure 4-6. Quantitativeevaluation of the wettingstate of the bottom paper layer of laminated and non-laminated devices as shown in **Figure 4-5** of the main text (application of 15 µL of 0.3 g mL^{-1} aqueous $CoCl_2$ solution to sample inlet followed by scanning after indicated time); the "vacuum-dried" result representsthe completely dry state; each data point has been obtained by measurements with 3 individual single-use devices; error bars indicate the standard deviations.

2.4.3. On device pH-control in vPADs

A drawback of cation-exchange-based ISO systems is the inherent pH-dependency of the optical signal, making it necessary to either adjust the pH of the sample to a known fixed value or to perform simultaneous pH-measurements.[1-2] This pH-dependency is obvious from the ion-exchange equilibrium involved **eq (2.1)** and also reflected in the corresponding theoretical ISO response function including the proton activity of the aqueous sample phase (**eq (2.2)**). In order to overcome the pH-dependency of the ISO response, the developed vPAD integrates a buffer component (MES-TMAOH, pH 6.0) in the 2nd paper layer for on-device pH-control (**Figure 2-1b**). The successful integration of the pH-control function has been experimentally validated by comparing the colorimetric response obtained after application of pure aqueous NaCl solutions to vPADs integrating the buffer component in the 2nd paper layer, or of pH-buffered (50 mM MES-TMAOH, pH 6.0) NaCl solutions to vPADs lacking the buffer component (**Figure 2-7**). Actual scanned images of the colorimetric Na^+ assays are shown in **Figure 2-7b**. The corresponding ISO response functions shown in **Figure 2-7** indicate a good agreement for the results of the two experiments. Therefore, it can be concluded

that on-device pH-buffering of the sample prior to the ISO assay is achievable by the buffer component pre-deposited onto an internal paper layer.

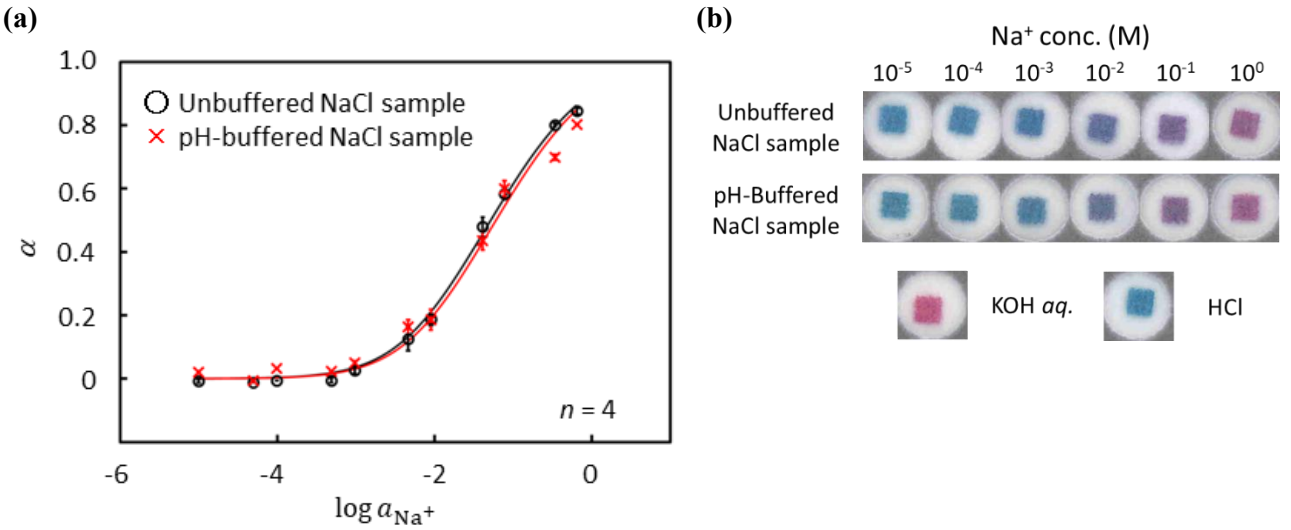

Figure 2-7. (a) Response curves obtained by application of unbuffered (black circles) or buffered (red crosses; MES-TMAOH, 50 mM, pH 6.0) aqueous NaCl samples applied to vPADs with (black circles) or without (red crosses) integrated pH-buffering function; sample volume 15 µL; equilibration time 20 min; each data point has been obtained by measurements with 4 individual single-use devices; error bars indicate the standard deviations: (b) actual scanned images of colorimetric ISO response on vPADs exposed to corresponding sample liquid solutions.

A positive "side-effect" of the pH-dependency of cation-exchange-based ISO systems is the possibility to modulate their dynamic response range by the pH of the aqueous sample phase. This characteristic was also demonstrated for the vPADs by pretreating the 2nd paper layer for on-device pH-control (**Figure 2-1b**) with 7 µL of pH-buffer solutions of different pH-values, followed by the application of unbuffered aqueous NaCl solutions. **Figure 2-8a** shows that the dynamic response range shifts to lower Na^+ activities with increasing pH-values, and vice versa (actual scanned images are shown in **Figure 2-8b**).

Finally, the pH-buffering capacity of the vPAD-integrated buffer system was examined by applying 10^{-5}-1 M aqueous NaCl samples of different pH-values to devices including a pH 6.0 buffer area as the 2nd paper layer for on-device pH-control. Typical response curves obtained with these samples are shown in **Figure 2-9** (actual scanned images are shown in **Figure 2-9b**). The lack of significant differences between the three response curves demonstrates that the integrated pH-control function is tolerant to different sample pH

conditions (pH 5.0-7.0 tested) even in pH-buffered samples.

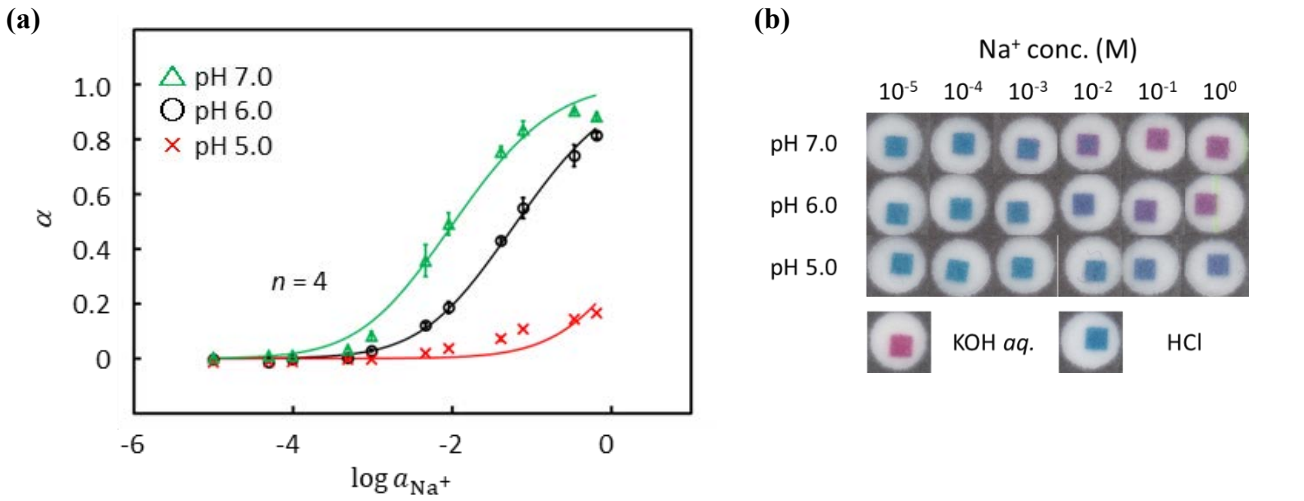

Figure 2-8. (a) pH-Dependent response curves of ISO vPADs with integrated pH-buffering function (red crosses: 1 M citric acid-TMAOH pH 5.0; black circles: 1 M MES-TMAOH pH 6.0; green triangles: 1 M HEPES-TMAOH pH 7.0) upon application of unbuffered aqueous Na^+ solutions; sample volume 15 µL; equilibration time 20 min; each data point has been obtained by measurements with 4 individual single-use devices; error bars indicate the standard deviations: (b) actual scanned images of colorimetric ISO response on vPADs exposed to corresponding sample liquid solutions.

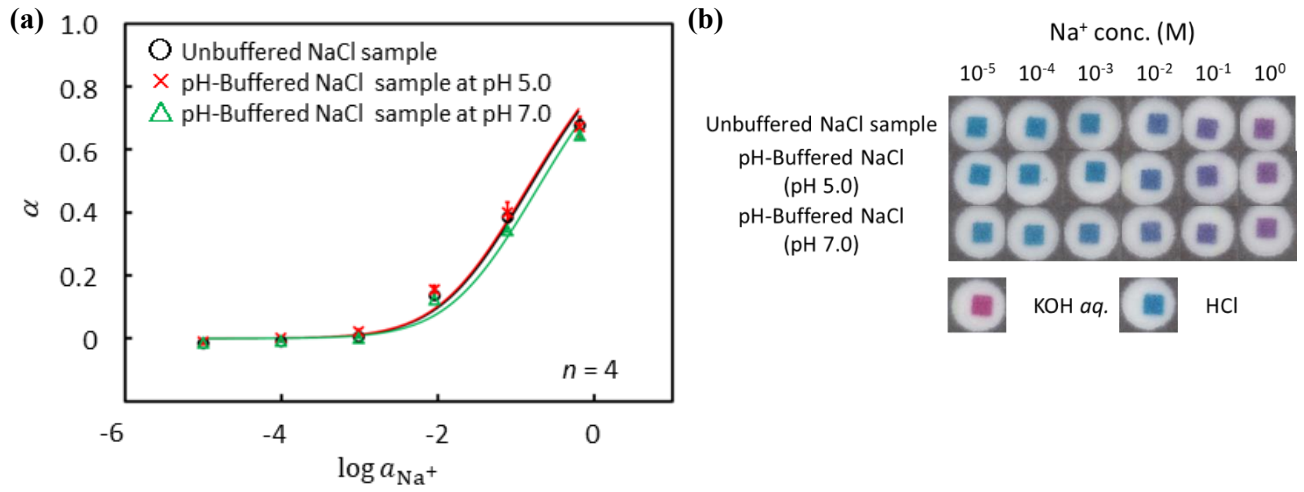

Figure 4-9. (a) Tolerance of the integrated pH-buffering function (buffer area pretreated with 7 µL of 1 M MES-TMAOH pH 6.0) of the vPADs against unbuffered (black circles) and weakly buffered aqueous NaCl solutions (red crosses: 10 mM citric acid-TMAOH pH 5.0; green triangles: 10 mM HEPES-TMAOH pH 7.0); sample volume 15 µL; equilibration time 20 min; each data point has been obtained by measurements with 4 individual single-use devices; error bars indicate the standard deviations: (b) actual scanned images of colorimetric ISO response on vPADs exposed to corresponding sample liquid solutions.

2.4.4. Selectivity of vPADs

The selectivity of the vPAD for Na+ detection has been investigated by determining the optical selectivity coefficient (K_{opt}) based on the separate solution method.[1-2] **Figure 2-10a** shows the ISO vPAD response obtained with unbuffered aqueous solutions of various alkali and alkaline earth metal ions, including NaCl, KCl, $CaCl_2$, $MgCl_2$ and LiCl (actual scanned images are shown in **Figure 2-10b**). As expected from the known selectivity of the used Na^+-ionophore DD16C5[43] and confirmed by the response curves shown in **Figure 2-10**, Ca^{2+}, Mg^{2+} and Li^+ generated no significant colorimetric signal up to tested concentrations of as high as 1 M. Also not surprisingly, only K^+ resulted in a weak colorimetric signal at the highest tested concentration of 1 M. The log K_{opt} value for Na^+ over K^+ was found to be −2.10. This selectivity value is comparable to the one reported for the ISE counterpart using the same ionophore (log K_{pot}: −2.5).[43]

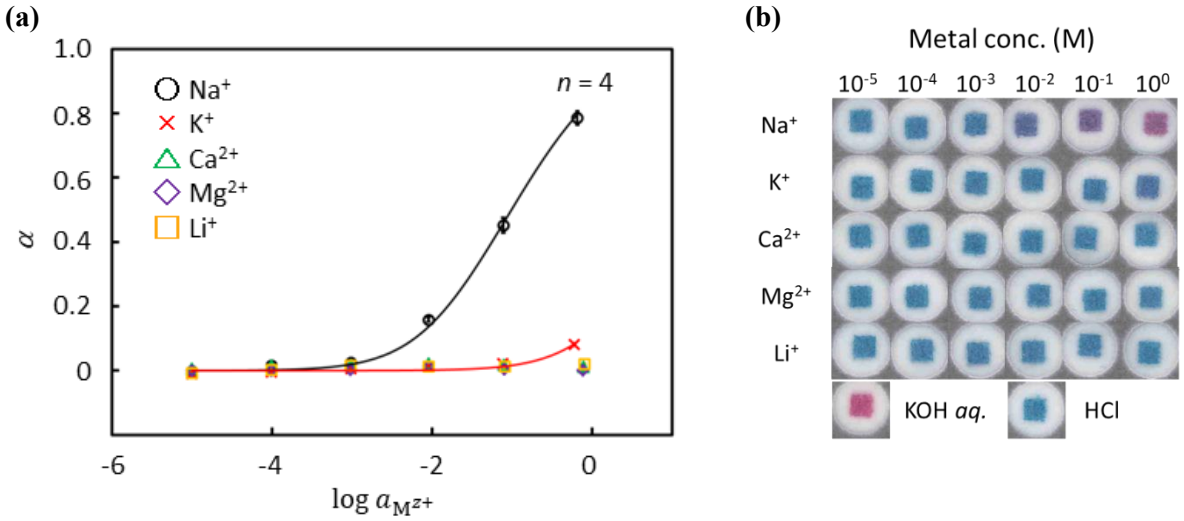

Figure 2-10. (a) Selectivity evaluation of vPADs for ISO-based Na^+ detection over other alkali and alkaline earth metal cations (K^+, Ca^{2+}, Mg^{2+}, Li^+); all metal cation samples were applied as chloride salts; sample volume 15 µL; equilibration time 20 min; each data point has been obtained by measurements with 4 individual single-use devices; error bars indicate the standard deviations: (b) actual scanned images of colorimetric ISO response on vPADs exposed to corresponding sample liquid solutions.

Device lamination is essential to maintain the selectivity for Na^+. As can be observed from the data shown in **Figure 2-11**, the response behaviour of ISO vPADs, including their selectivity, is significantly influenced

by device lamination. Non-laminated devices (**Figure 2-5b**) resulted in more pronounced response to K^+ at elevated activities (**Figure 2-11**, yellow diamonds) in comparison to laminated vPADs (**Figure 2-11**, red crosses). In addition, non-laminated devices exhibited a dynamic response to Na^+ at lower activities (**Figure 2-11**, green triangles) compared to the laminated vPADs (**Figure 2-11**, black circles). These changes in the ISO vPAD response properties are another indication of the importance of device lamination, since they are attributed to the evaporation of the sample liquid. Evaporative loss of sample liquid results in concentration of solute species in the aqueous sample phase, and thus, a shift in equilibrium, promoting ion extraction into the organic ISO phase. Lamination contributes not only to maintaining the selectivity, but also renders devices more robust against fluctuation caused for example by environmental conditions such as humidity and temperature.

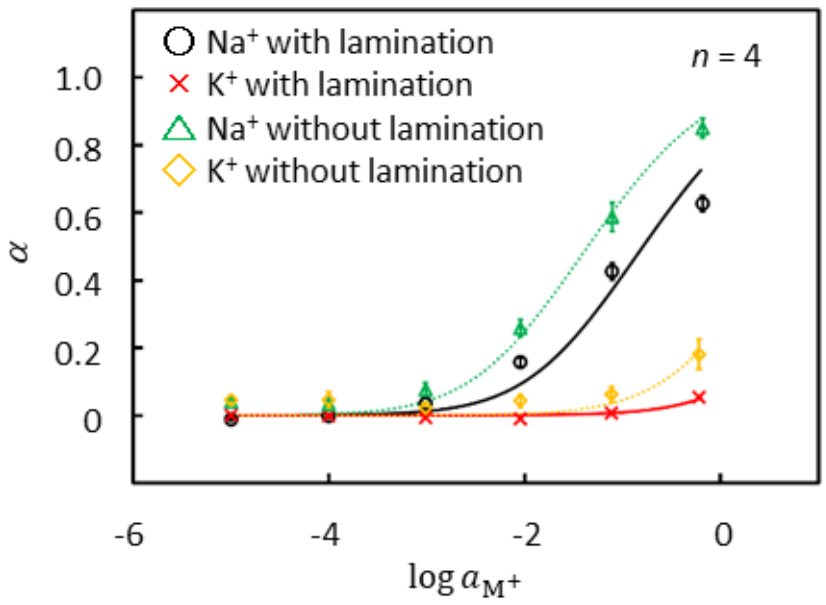

Figure 4-11. Comparison of selectivity and dynamic response range between laminated vPADs (**Figure 2-5a**) and non-laminated devices (**Figure 2-5b**); sample volume 15 µL; equilibration time 20 min; each data point has been obtained by measurements with 4 individual single-use devices; error bars indicate the standard deviations.

2.4.5. Influence of the cellulose matrix on ISO response

Finally, to investigate the influence of the cellulosic substrate on the ion-exchange reaction, the paper-based ISO system was compared with a classical membrane ISO approach, where optode films were

prepared on a transparent plastic substrate. The classical film-based ISOs were fabricated on a transparent lamination sheet by inkjet-printing, following the same procedure as the paper-based system. A spot test using the printed ISO film and pH-buffered NaCl solutions was carried out (detailed procedure is shown in **Figure 2-12**). As shown in **Figure 2-13**, the response curve obtained from the plastic film-based spot test (**Figure 2-13a**, green triangles) exhibited colorimetric response at a lower activity range of Na^+ (log K_{exch}: −3.88) as compared to the assay on vPADs (**Figure 2-13a**, black circles) with a log K_{exch} value of −4.53. On the other hand, the response curve and log K_{exch} value (−4.48) obtained in a simple filter paper spot test using pH-buffered NaCl solutions (**Figure 2-13a**, red crosses) was nearly identical to the one obtained with the vPAD assembly (actual scanned images for all 3 cases are shown in **Figure 2-13b**). The close agreement of the ISO response on vPADs with that of simple paper spot tests suggests that the deviation from the classical plastic film-based configuration is caused by the cellulosic substrate material, rather than the vPAD-specific multilayer-structured configuration.

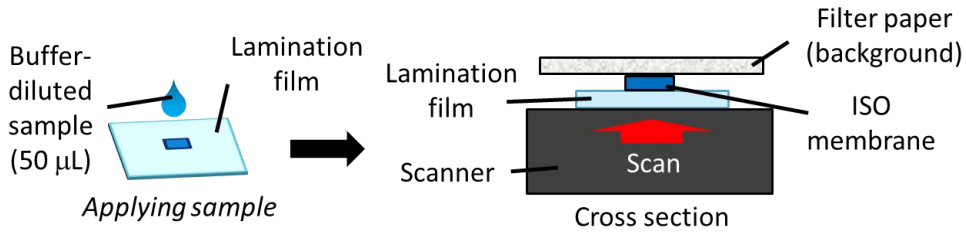

Figure 2-12. Experimental procedure for the spot test with classical membrane-type optodes on a lamination film. The ISO membranes were first prepared on an A4 sheet of lamination film with the Dimatix DMP-2831 inkjet printer in the same way as on the filter paper platform. 50 µL of aqueous NaCl solutions prepared in MES-TMAOH buffer (pH 6.0, 50 mM) were directly applied to the ISO-printed lamination film. After 20 min of equilibration, the remaining sampleliquidwas removed with a paper towel, and the ISO-printed lamination film was scanned from the bottom sideagainst a filter paperbackground, simulating the vPAD arrangement.

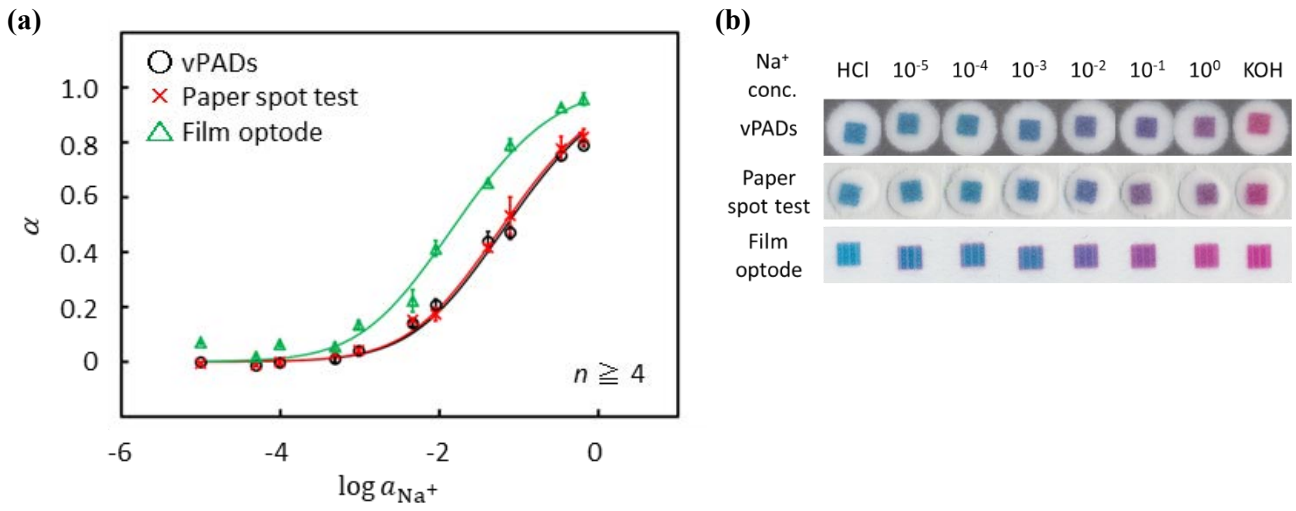

Figure 2-13. (a) Comparison of ISO response curves obtained on vPADs with integrated pH-buffering function (pH 6.0) and unbuffered aqueous NaCl solutions, spot tests using ISOs-printed on paper discs and ISOs printed on lamination film with pH-buffered solutions (50 mM MES-TMAOH pH 6.0); sample volume 15 µL for vPADs, 50 µL for spot tests; equilibration time 20 min; data points of vPADs or paper spot test/film optodes have been obtained by measurements with 4 and 5 individual single-use devices, respectively; error bars indicate the standard deviations: (b) actual scanned images of colorimetric ISO response to corresponding devices and samples.

Generally, cellulosic paper contains several ionizable groups having different pK_a values and different affinities to cations depending on the chemical nature of the respective ionizable functional group.[44-45] Due to the major presence of carboxyl groups, the surface of cellulosic paper is negatively charged.[31, 44, 46-47] Carboxylic acids are weakly dissociated (pK_a ≈ 4-5),[44] with the negative charge on the cellulose surface being dependent on sample pH.[31] Thus, carboxylic acid residues play an important role as functional anionic groups to interact with metal ions.[45] In a paper-based ISO assay performed near neutral or slightly acidic pH, carboxyl groups can be involved in cation-exchange processes, as schematically shown in **Scheme 2-1**. Electrolytes present in the sample solution (e.g. Ca^{2+}, Mg^{2+} and Na^+) are interacting with these carboxyl groups on cellulose, based on reversible, and spontaneous sorption.[44-45] Previous studies mentioned that Donnan distribution can be adapted to the validation of the distribution coefficient of ions in cellulosic fibre slurries.[44-45] The interaction of metal ions with the cellulosic surface is affected by the pH and the ionic strength of the sample liquid. Hence, independent of the existence of an ISO membrane, the concentration of cations (e.g. Na^+) in an aqueous sample phase applied to a paper-based device can be reduced by sorption to

the paper surface during sample transport through the porous cellulose fibre network, potentially giving rise to different response functions when comparing the optode behaviour on a plastic film and on a cellulose substrate. In the current case, the amount of Na^+ sorption onto the cellulose surface of the used filter paper (Advantec 5C) was experimentally evaluated. For this purpose, the ion-exchange capacity (IEC) of the filter paper was determined by acid–base titration. The experimentally determined IEC value of the filter paper used in this work is comparable to reported values of the amount of carboxyl groups on other cellulose-based materials.[44, 46] The average weight of a paper disc of the size corresponding to the hydrophilic region of each paper layer used for vPAD assembly was determined to be 2.1 mg (estimated from the total weight of 10 paper discs). Thus, the experimentally estimated total amounts of ionizable groups present in the hydrophilic area (*i.e.* no wax-modified area) of a vPAD or a paper disc used for the spot tests are approximately 0.67 µmol or 0.23 µmol, respectively. Putting these IEC values of the filter paper in relation to the total amounts of Na^+ applied as sample solutions (vPADs: 150 pmol–15 µmol, spot tests: 500 pmol-50 µmol) maximum paper-induced target cation depletion between 100-0.5% is theoretically thinkable. However, these numbers do not take into consideration a possible competition for carboxylate sites from the TMA^+ cations present at high concentration in the pH-buffering system, which makes a total depletion of Na^+ rather unlikely in reality. In any case, the IEC of cellulose alone does not allow to explain the experimentally observed differences in ISO response curves obtained on plastic and paper substrates (**Figure 2-13**).

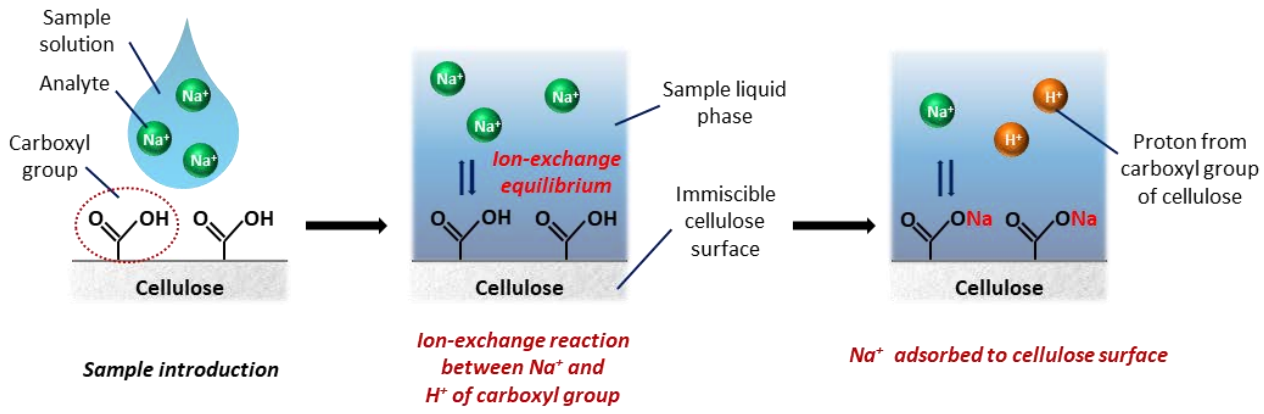

Scheme 2-1. Cation-exchange reaction between analyte cations (Na+) and protons of carboxyl groups present on the

surface of cellulose.

There remains another important factor potentially influencing ISO response curves obtained on ion-exchange inert plastic substrates and on filter paper with inherent ion-exchange capacity. With ISO systems transferred to cellulosic paper surfaces, there exists the possibility of competing cation-exchange reactions between the target cation of the aqueous sample phase (e.g. Na^+) and protons from cellulosic carboxyl groups instead of protons from the chromoionophore present in the optode membrane phase. With an ISO membrane deposited on cellulose fibres, carboxylic acid residues become an integral part of the organic optode phase. Since carboxyl groups have significantly lower pK_a values compared to a chromoionophore typically used in an ISO membrane (pK_a of CH1 in plasticized PVC membrane: 12.0),[48] the cation-exchange between the target ions and protons of carboxyl groups is preferred over the actual ISO cation-exchange reaction, which leads to apparent shifts in log K_{exch} values. Translated to the concept of classical cation-exchange optodes, this situation corresponds not only to an optode membrane phase with amounts of cation exchanger in addition to the added anionic additive (KTpClPB), but also to the situation where two proton acceptors/donors with different pK_a values are present (cellulosic carboxyl groups and chromoionophore), one of them not directly contributing to the optical signal. The fact that the paper matrix in combination with a deposited ISO membrane does provide a cation exchange function is indicated by the small, but significant colorimetric response observed for anionic additive-free ISO membranes deposited on filter paper, in contrast to the complete absence of such response with identical ISO membranes printed onto a lamination film (**Figure 2-14**).

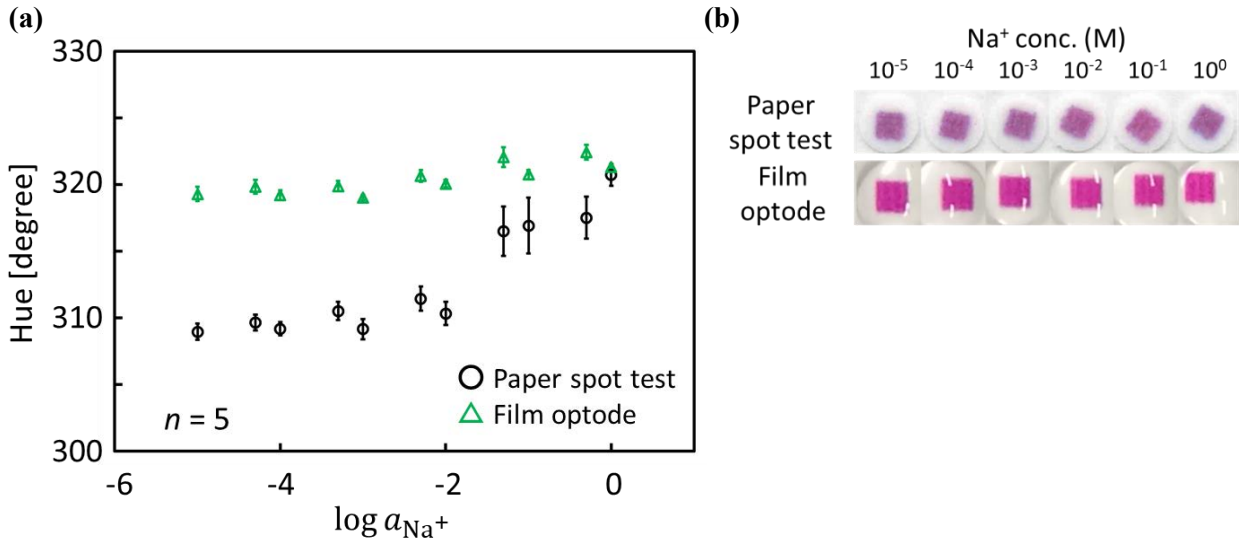

Figure 2-14. Response behaviourof spot tests with ISO membranes deposited onto filter paper (top row) or lamination film (bottom row) in the absence of anionic additive (KTpClPB) exposed to pH-buffered (pH 6.0) NaCl solutions: (a) hue-based response curvesand (b) corresponding images acquiredwith a color scanner (paper) or an iPhone 5S (film); sample volume 50 µL; equilibration time 20 min; each data point has been obtained by measurements with 5 individual spots; error bars indicate the standard deviations.

2.5. Conclusion

The implementation of the classical plasticized PVC-based ISO system onto a cellulosic paper platform for colorimetric cation detection has been successfully demonstrated on the example of a Na^+-selective vertically-assembled paper-based analytical device (vPAD). Whole device lamination allowed for prevention of evaporation loss of sample liquid and preserved the selectivity for Na^+ over other potentially interfering cations (K^+, Ca^{2+}, Mg^{2+}, Li^+). It has been shown that the hue-based ISO response curves obtained on a paper platform can be fitted to the known ion-selective cation-exchange optode function. However, a shift of the response function to higher analyte activities in comparison to classical film optodes deposited on solid plastic substrates has been observed. It has been experimentally shown that the cause for this shift most likely lies in the cation-exchange properties of the cellulosic paper matrix. Although further experimentation is required to fully clarify this phenomenon and to eventually eliminate the substrate material caused differences in optode response, we believe that the current work contributes to the expansion of the applicability of the well-known plasticized PVC optode system.

References

1. Bakker, E.; Bühlmann, P.; Pretsch, E., Carrier-Based Ion-Selective Electrodes and Bulk Optodes. 1. General Characteristics. *Chem. Rev.* **1997,** *97* (8), 3083-3132.

2. Mistlberger, G.; Crespo, G. A.; Bakker, E., Ionophore-Based Optical Sensors. *Annual Review of Anal. Chem.* **2014,** *7* (1), 483-512.

3. Mikhelson, K.; Peshkova, M., Advances and trends in ionophore-based chemical sensors. *Russian Chem. Rev.* **2015,** *84* (6), 555.

4. Xie, X.; Bakker, E., Ion selective optodes: from the bulk to the nanoscale. *Anal. Bioanal. Chem.* **2015,** *407* (14), 3899-3910.

5. Zhai, J.; Bakker, E., Complexometric titrations: new reagents and concepts to overcome old limitations. *Analyst* **2016,** *141* (14), 4252-4261.

6. Mahadeva, S. K.; Walus, K.; Stoeber, B., Paper as a Platform for Sensing Applications and Other Devices: A Review. *ACS Appl. Mater. Interfaces* **2015,** *7* (16), 8345-8362.

7. Xu, Y.; Liu, M.; Kong, N.; Liu, J., Lab-on-paper micro- and nano-analytical devices: Fabrication, modification, detection and emerging applications. *Microchim. Acta* **2016,** *183* (5), 1521-1542.

8. Fernandes, S. C.; Walz, J. A.; Wilson, D. J.; Brooks, J. C.; Mace, C. R., Beyond Wicking: Expanding the Role of Patterned Paper as the Foundation for an Analytical Platform. *Anal. Chem.* **2017,** *89* (11), 5654-5664.

9. Martinez, A. W.; Phillips, S. T.; Butte, M. J.; Whitesides, G. M., Patterned Paper as a Platform for Inexpensive, Low-Volume, Portable Bioassays. *Angew. Chem. Int. Ed.* **2007,** *46* (8), 1318-1320.

10. Martinez, A. W.; Phillips, S. T.; Wiley, B. J.; Gupta, M.; Whitesides, G. M., FLASH: A rapid method for prototyping paper-based microfluidic devices. *Lab on Chip* **2008,** *8* (12), 2146-2150.

11. Yetisen, A. K.; Akram, M. S.; Lowe, C. R., Paper-based microfluidic point-of-care diagnostic devices. *Lab on Chip* **2013,** *13* (12), 2210-2251.

12. Cate, D. M.; Adkins, J. A.; Mettakoonpitak, J.; Henry, C. S., Recent Developments in Paper-Based Microfluidic Devices. *Anal. Chem.* **2015,** *87* (1), 19-41.

13. Lin, Y.; Gritsenko, D.; Feng, S.; Teh, Y. C.; Lu, X.; Xu, J., Detection of heavy metal by paper-based microfluidics. *Biosens. Bioelectron.* **2016,** *83*, 256-266.

14. Nilghaz, A.; Guan, L.; Tan, W.; Shen, W., Advances of Paper-Based Microfluidics for Diagnostics—The Original Motivation and Current Status. *ACS Sens.* **2016,** *1* (12), 1382-1393.

15. Sriram, G.; Bhat, M. P.; Patil, P.; Uthappa, U. T.; Jung, H.-Y.; Altalhi, T.; Kumeria, T.; Aminabhavi, T. M.; Pai, R. K.; Madhuprasad; Kurkuri, M. D., Paper-based microfluidic analytical devices for colorimetric detection of toxic ions: A review. *TrAC Trends Anal. Chem.* **2017,** *93*, 212-227.

16. Yamada, K.; Shibata, H.; Suzuki, K.; Citterio, D., Toward practical application of paper-based microfluidics for medical diagnostics: state-of-the-art and challenges. *Lab on Chip* **2017,** *17* (7), 1206-1249.

17. Yang, Y.; Noviana, E.; Nguyen, M. P.; Geiss, B. J.; Dandy, D. S.; Henry, C. S., Paper-Based Microfluidic Devices: Emerging Themes and Applications. *Anal. Chem.* **2017,** *89* (1), 71-91.

18. Meredith, N. A.; Quinn, C.; Cate, D. M.; Reilly, T. H.; Volckens, J.; Henry, C. S., Paper-based analytical devices for environmental analysis. *Analyst* **2016,** *141* (6), 1874-1887.

19. Hossain, S. M. Z.; Brennan, J. D., β-Galactosidase-Based Colorimetric Paper Sensor for Determination of Heavy Metals. *Anal. Chem.* **2011,** *83* (22), 8772-8778.

20. Mentele, M. M.; Cunningham, J.; Koehler, K.; Volckens, J.; Henry, C. S., Microfluidic Paper-Based Analytical Device for Particulate Metals. *Anal. Chem.* **2012,** *84* (10), 4474-4480.

21. Jayawardane, B. M.; Coo, L. d.; Cattrall, R. W.; Kolev, S. D., The use of a polymer inclusion membrane in a paper-based sensor for the selective determination of Cu(II). *Anal. Chim. Acta* **2013,** *803*, 106-112.

22. Li, M.; Cao, R.; Nilghaz, A.; Guan, L.; Zhang, X.; Shen, W., "Periodic-Table-Style" Paper Device for Monitoring Heavy Metals in Water. *Anal. Chem.* **2015,** *87* (5), 2555-2559.

23. Kudo, H.; Yamada, K.; Watanabe, D.; Suzuki, K.; Citterio, D., Paper-Based Analytical Device for Zinc Ion Quantification in Water Samples with Power-Free Analyte Concentration. *Micromachines* **2017,** *8* (4).

24. Yetisen, A. K.; Jiang, N.; Tamayol, A.; Ruiz-Esparza, G. U.; Zhang, Y. S.; Medina-Pando, S.; Gupta, A.; Wolffsohn, J. S.; Butt, H.; Khademhosseini, A.; Yun, S.-H., Paper-based microfluidic system for tear electrolyte analysis. *Lab Chip* **2017,** *17* (6), 1137-1148.

25. Zhang, Y.; Fan, J.; Nie, J.; Le, S.; Zhu, W.; Gao, D.; Yang, J.; Zhang, S.; Li, J., Timing readout in paper device for quantitative point-of-use hemin/G-quadruplex DNAzyme-based bioassays. *Biosens. Bioelectron.* **2015,** *73*, 13-18.

26. Yu, S. P.; Canzoniero, L. M. T.; Choi, D. W., Ion homeostasis and apoptosis. *Curr. Opin. Cell Biol.* **2001,** *13* (4), 405-411.

27. Lewenstam , A., Routines and Challenges in Clinical Application of Electrochemical Ion-Sensors. *Electroanalysis* **2014,** *26* (6), 1171-1181.

28. Bühlmann, P.; Pretsch, E.; Bakker, E., Carrier-Based Ion-Selective Electrodes and Bulk Optodes. 2. Ionophores for Potentiometric and Optical Sensors. *Chem. Rev.* **1998,** *98* (4), 1593-1688.

29. Wang, X.; Qin, Y.; Meyerhoff, M. E., Paper-based plasticizer-free sodium ion-selective sensor with camera phone as a detector. *Chem. Commun.* **2015,** *51* (82), 15176-15179.

30. Erenas, M. M.; de Orbe-Payá, I.; Capitan-Vallvey, L. F., Surface Modified Thread-Based Microfluidic Analytical Device for Selective Potassium Analysis. *Anal. Chem.* **2016,** *88* (10), 5331-5337.

31. Wang, X.; Zhang, Q.; Nam, C.; Hickner, M.; Mahoney, M.; Meyerhoff, M. E., An Ionophore-Based Anion-Selective Optode Printed on Cellulose Paper. *Angew. Chem. Inter. Ed.* **2017,** *56* (39), 11826-11830.

32. Wang, X.; Mahoney, M.; Meyerhoff, M. E., Inkjet-Printed Paper-Based Colorimetric Polyion Sensor Using a Smartphone as a Detector. *Anal. Chem.* **2017,** *89* (22), 12334-12341.

33. Vella, S. J.; Beattie, P.; Cademartiri, R.; Laromaine, A.; Martinez, A. W.; Phillips, S. T.; Mirica, K. A.; Whitesides, G. M., Measuring Markers of Liver Function Using a Micropatterned Paper Device Designed for Blood from a Fingerstick. *Anal. Chem.* **2012,** *84* (6), 2883-2891.

34. Komuro, N.; Takaki, S.; Suzuki, K.; Citterio, D., Inkjet printed (bio)chemical sensing devices. *Anal. Bioanal. Chem.* **2013,** *405* (17), 5785-5805.

35. Cate, D. M.; Noblitt, S. D.; Volckens, J.; Henry, C. S., Multiplexed paper analytical device for quantification of metals using distance-based detection. *Lab Chip* **2015,** *15* (13), 2808-2818.

36. Yamada, K.; Henares, T. G.; Suzuki, K.; Citterio, D., Paper-Based Inkjet-Printed Microfluidic Analytical Devices. *Angew. Chem. Inter. Ed.* **2015,** *54* (18), 5294-5310.

37. Cantrell, K.; Erenas, M. M.; de Orbe-Payá, I.; Capitán-Vallvey, L. F., Use of the Hue Parameter of the Hue, Saturation, Value Color Space As a Quantitative Analytical Parameter for Bitonal Optical Sensors. *Anal. Chem.* **2010,** *82* (2), 531-542.

38. Capitán-Vallvey, L. F.; López-Ruiz, N.; Martínez-Olmos, A.; Erenas, M. M.; Palma, A. J., Recent developments in computer vision-based analytical chemistry: A tutorial review. *Anal. Chim. Acta* **2015,** *899*, 23-56.

39. Meier, P. C., Two-parameter debye-hückel approximation for the evaluation of mean activity coefficients of 109 electrolytes. *Anal. Chim. Acta* **1982,** *136*, 363-368.

40. Bakker, E.; Lerchi, M.; Rosatzin, T.; Rusterholz, B.; Simon, W., Synthesis and characterization of neutral hydrogen ion-selective chromoionophores for use in bulk optodes. *Anal. Chim. Acta* **1993,** *278* (2), 211-225.

41. Cassano, C. L.; Fan, Z. H., Laminated paper-based analytical devices (LPAD): fabrication, characterization, and assays. *Microfluid. Nanofluid.* **2013,** *15* (2), 173-181.

42. Tenda, K.; Ota, R.; Yamada, K.; Henares, G. T.; Suzuki, K.; Citterio, D., High-Resolution Microfluidic Paper-Based Analytical Devices for Sub-Microliter Sample Analysis. *Micromachines* **2016,** *7* (5).

43. Suzuki, K.; Sato, K.; Hisamoto, H.; Siswanta, D.; Hayashi, K.; Kasahara, N.; Watanabe, K.; Yamamoto, N.; Sasakura, H., Design and Synthesis of Sodium Ion-Selective Ionophores Based on 16-Crown-5 Derivatives for an Ion-Selective Electrode. *Anal. Chem.* **1996,** *68* (1), 208-215.

44. Duong, T. D.; Hoang, M.; Nguyen, K. L., Sorption of Na^{+}, Ca^{2+} ions from aqueous solution onto unbleached kraft fibers—kinetics and equilibrium studies. *J. Colloid Interface Sci.* **2005,** *287* (2), 438-443.

45. Christa, F.-B.; Thomas, B., Sorption of alkaline earth metal ions Ca^{2+} and Mg^{2+} on lyocell fibres. *Carbohydr. Polym.* **2009,** *76* (1), 123-128.

46. Murphy, A.; Gorey, B.; de Guzman, K.; Kelly, N.; Nesterenko, E. P.; Morrin, A., Microfluidic paper analytical device for the chromatographic separation of ascorbic acid and dopamine. *RSC Adv.* **2015,** *5* (113), 93162-93169.

47. Yamada, K.; Henares, T. G.; Suzuki, K.; Citterio, D., Distance-Based Tear Lactoferrin Assay on Microfluidic Paper Device Using Interfacial Interactions on Surface-Modified Cellulose. *ACS Appl. Mater. Interfaces* **2015,** *7* (44), 24864-24875.

48. Qin, Y.; Bakker, E., Quantitive binding constants of H^{+}-selective chromoionophores and anion ionophores in solvent polymeric sensing membranes. *Talanta* **2002,** *58* (5), 909-918.

Chapter 3
pH-Independent cation sensing system with fluorescence solvatochromic dyes

Summary

A challenge for paper-based cationic ion sensors relying on carrier-based ion-selective optodes (ISOs) is pH-cross respon-sivity during the cation assay due to the use of H^+-sensitive chromoionophores as optical signal transducers. Herein, this work demonstrates the pH-independent fluorescence cation detection with a paper-based plasticizer-free ISO. To achieve pH-independent cation assay, instead of a traditional H^+-sensitive chromoionophore, a solvatochromic dye (SD) has been applied to the paper-based ISO by means of inkjet printing technology. The detection principle basically depends on trans-fer-based ion-exchange reaction directly between the positive-ly-charged SDs and the target cations, which no longer involves H^+ during the cation detection. In the current work, Ca^{2+} was selected as a model cation to proof the concept. The proposed paper-based ISOs with the SDs clearly showed that concentra-tion response curves were not affected by the sample pH (pH 6.0, 7.0, and 8.0). The dynamic range for Ca^{2+} detection was from 10^{-5} to 1 M of Ca^{2+} samples. Additionally, excellent selectivity relying on the used ionophores has been confirmed with the developed paper-based ISOs. The capability of the developed plasticizer-free paper-based ISOs has been proposed to overcome pH dependence for determination of Ca^{2+} in mineral water without conventional pH-buffering process by using chemical components.

3.1. Introduction

The quantification of ion species is one of the crucial components in not only biomedical science but also physiology, and environmental monitoring.[1-4] Ion-selective optodes (ISOs) have been extensively gained as powerful optical chemical sensors for many years potentially to consider alternatives to ion-selective electrodes (ISEs).[1-4] Such classical optodes are typically composed of a plasticized organic polymeric membrane (e.g. polyvinyl chloride), doped with a lipophilic pH indicator generating optical signal (chromoionophore), an ion-specific ligand (ionophore), and an ion-exchanger.[1-2] The function of cation-selective optodes is undoubtedly well-established, relying on an ion-exchange equilibria reaction between cationic analytes and protons (H^+) of H^+-responsive chromoionophores. However, the response of classical optodes is accompanied by sample pH changes, and this pH-cross response is admittedly a historical drawback to extend their application fields.

To overcome the pH dependence, solvatochromic dyes (SDs), which are also called as polarity-sensitive dyes, have been introduced as signal transducers instead of conventional chromoionophores.[5-13] Positively-charged SDs exhibit different absorption/emission spectra (*i.e.* color) corresponding to the solvent polarity (solvatochromic effect). In 2014, charged SDs were rediscovered for carrier-based ISOs by Bakker's research group.[5] The basis for the sensor response with SDs is no longer traditional extraction competition between cationic analytes and the H^+. Instead, cationic analytes are extracted into the lipophilic optode phase, corresponding to the amount of the positively-charged SDs expelled from the organic phase.[14] As a result, pH-independent cation quantification was achieved due to the application introduction of SDs to ISOs.

Recently, point-of-care testing (POCT) or on-site analysis have played as important roles in the field of analytical chemistly.[15-16] Since 2007 when a microfluidically-patterned paper was first established by Whitesides' research group[17-18], paper has been drawn significant attention as cost-effective attractive analytical platform due to its multiplex advantages; i) low-cost, ii) safe disposability by incineration, iii) portability, iv) ease of fabrication. Besides, a cellulosic porous structure of the paper serves passive pump-free transport of sample liquid by capillary force. Such advantageous capability of paper-based assay enables a

wide variety of measurement for biomedical science, physiology, and environmental monitoring.[19-24]

In accordance with the advantages of colorimetric paper-based analytical devices (e.g. observable with unaided eyes), the function of ionophore-based ISOs has been frequency adapted to cellulosic paper materials for selective determination of cations, anions, and polyions.[25-34] More recently, our research group has introduced classical plasticized polymetric ISO have been applied to paper-based sensing platform by means of inkjet printing technology for determination of Na^+ or K^+.[29-30] On the other hands, Meyerhoff's research group first discovered new class of paper-based ISOs without traditional plasticized organic polymeric materials.[31-34] A mimic plasticized polymer phase for the ISO-based detection (*i.e.* hydrophobic micro-environment) has been successfully formed by both the highly lipophilic ISO components themselves and a hydrophobic part of cellulose. Interestingly, obtained reaction basically relied on transfer-based heterogeneous sensing.[31] Nevertheless, the detection function of paper-based ISOs has been suffering from pH-cross reactivity due to the use of the H^+-sensitive chromoionophores.

Here, we demonstrate a pH-independent paper-based ISO without a traditional plasticized organic polymer, relying on an inkjet-printed positively-charged SD. In this work, Ca^{2+} was selected as a model ion to show for the first time that pH-independent system of paper-based ISOs has been successfully overcome without pH-buffering reagents. The lipophilic sensing components of SD-based ISOs (SD-ISOs) were inkjet-printed onto a wax-patterned paper substrate and resulted in forming a "dry" hydrophobic sensing layer[31-32]. Printing technologies in the entire process of the device fabrication are expected for well-defined and reproducible micropatterning during the device fabrication.[35-37] Finally, the developed paper-based SD-ISOs have successfully quantified Ca^{2+} based on fluorescence detection without pH-buffering process, and their obtained quantitative result was comparable to a conventional complexometric titration method.

3.2. Experimental section

3.2.1. Reagents and instruments

All reagents were used without further purification. Tetrakis[3,5-bis(trifluoromethyl)phenyl] borate, sodium salt (NaTFPB), 2-morpholinoethanesulfonic acid (MES), and *N*-(2-hydroxyethyl)-1-piperazineethanesulfonic acid (HEPES) were purchased from Dojindo (Kumamoto, Japan). Calcium ionophore IV and tetramethylammonium hydroxide pentahydrade (TMAOH) were purchased from Sigma-Aldrich (St. Louis, MO). Cyclohexanone, sodium chloride (NaCl), potassium chloride (KCl), calcium chloride dihydrate ($CaCl_2 \cdot 2H_2O$), and magnesium chloride hexahydrate ($MgCl_2 \cdot 6H_2O$) were purchased from Wako Pure Chemical Industries (Osaka, Japan).

Ultrapure water (>18 MΩ cm) was obtained from a PURELAB flex water purification system (ELGA, Veolia Water, Marlow, U.K.) and used for the preparation of all solutions. Advantec No. 5C and Whatman Grade 541 filter paper were purchased from Toyo Roshi (Tokyo, Japan) and GE Healthcare (Buckinghamshire, U.K), respectively. Hot lamination films (150 μm thickness) were obtained from Jointex (Tokyo, Japan). A single-lens mirrorless digital camera was purchased from Nikon (Tokyo, Japan). A UV hand lump (UVGL-25 Compact UV Lamp 4W) was purchased from UVP (CA, USA). Field-emission scanning electron microscopy (SEM) analysis was performed on a JSM-7600F microscope (JEOM, Tokyo Japan).

3.2.2. Fabrication of Ca^{2+} paper sensor

ColorQube 8580 printer (Xerox, Norwalk, CT, USA) was used to pattern a wax barrier on a filter paper cut into A4-size before. Identical patterns of wax designed in PowerPoint (Microsoft) were printed, shown in **Figure 3-1**. For fabrication of the hydrophobic barrier, the wax-patterned paper was heated at 150 °C for 3 min on a hot plate (Nissin NHS-450ND, Nissinrika, Tokyo, Japan). Hot-lamination of only the unprinted backside was performed on a QHE325 laminator (Meikoshokai, Tokyo, Japan) to prevent leakage of sample liquid during the Ca^{2+} assay. For the device lamination, a sheet of baking paper was inserted between the

laminate film and the top side of the wax-patterned paper to prevent them from adhesion to each other. The instrument settings of hot lamination for substrate thickness and feeding speed were "150 μm" and "slow", respectively. The wax-patterned paper substrates were then subjected to reagent deposition to fabricate the paper-based SD-ISOs for fluorescent Ca^{2+} detection as illustrated in **Figure 3-2a and b**.

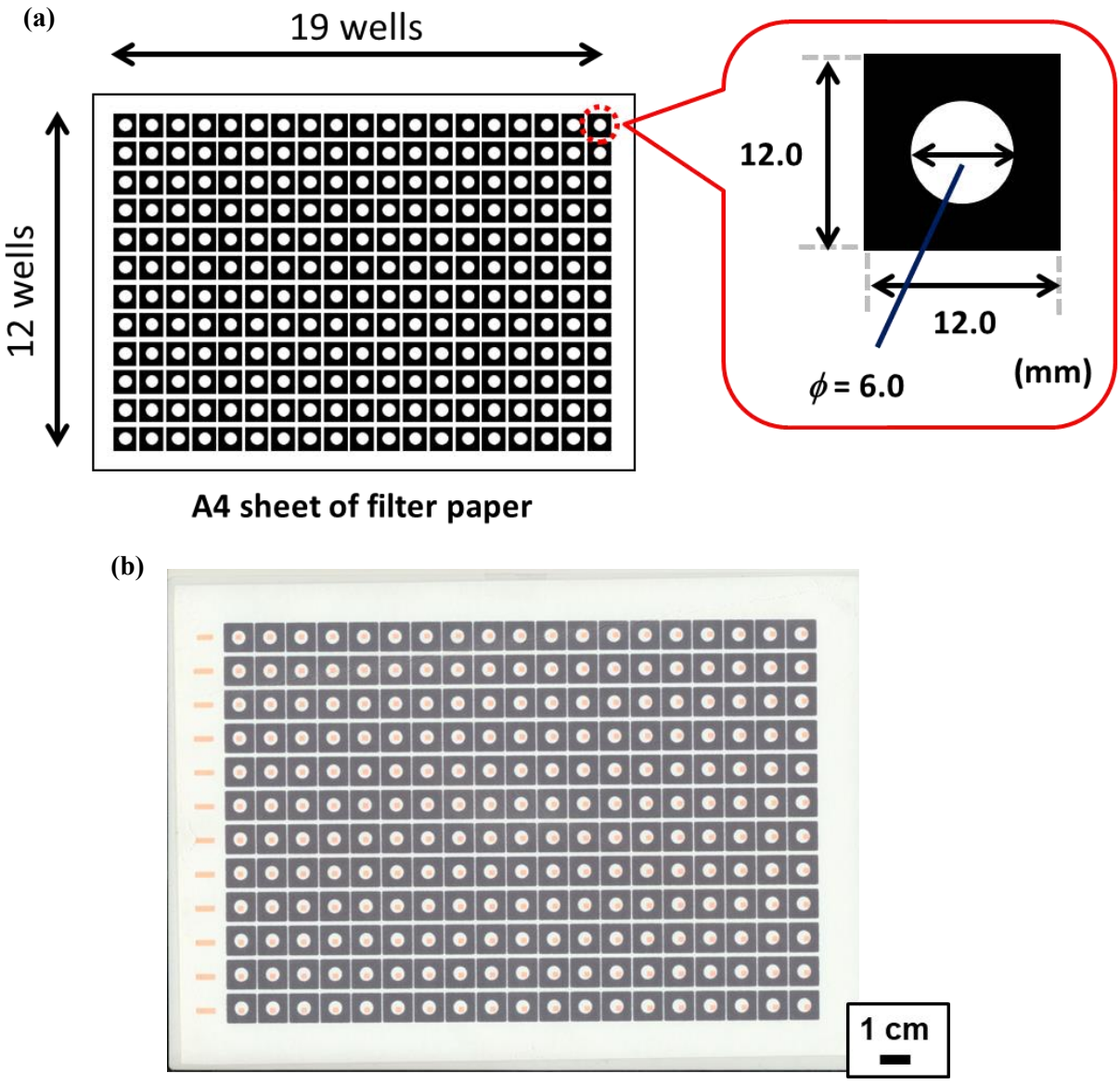

Figure 3-1. (a) Schematic illustration of the wax barrier pattern printed on an A4 size filter papersheet.29 The dimensions in the red box exhibit the settings in the PowerPoint graphic software; (b) actual photograph of paper-based ISOs after deposition of ISO components with Dimatix DMP-2831 inkjet printer.

Sensing printing ink for fluorescence detection of Ca^{2+} was prepared by dissolving 0.9 mg of SD, 2.7 mg of NaTFPB (ion-exchanger) and 3.24 mg of Ca ionophore IV in 2.0 mL of cyclohexanone. The used SD ((*E*)-1-ethyl-4-(-4-(ethyl(2-(stearoyloxy)ethyl)amino)styryl)pyridinium)) was synthesized according to the previous report[9]. The prepared printing ink was dispensed onto the center of the wax-patterned unmodified paper zone (inlet area in **Figure 3-2a**) by means of piezoelectrically-actuated Dimatix DMP-2831 inkjet printer (Dimatix-Fujifilm Inc., Santa Clara) in 20 printing cycles (2×2 mm^2 square, 40 μm of the dropping space setting). In inkjet printing steps, 4 nozzles were selected from 16 nozzles of a cartridge (DMC-11610) to achieve homogeneously printing, and a customized ink reservoir was used instead of the original Dimatix cartridge.[29] During inkjet deposition with the Dimatix printer, its printing table was heated at 40°C to promote the evaporation of the ink solvent.

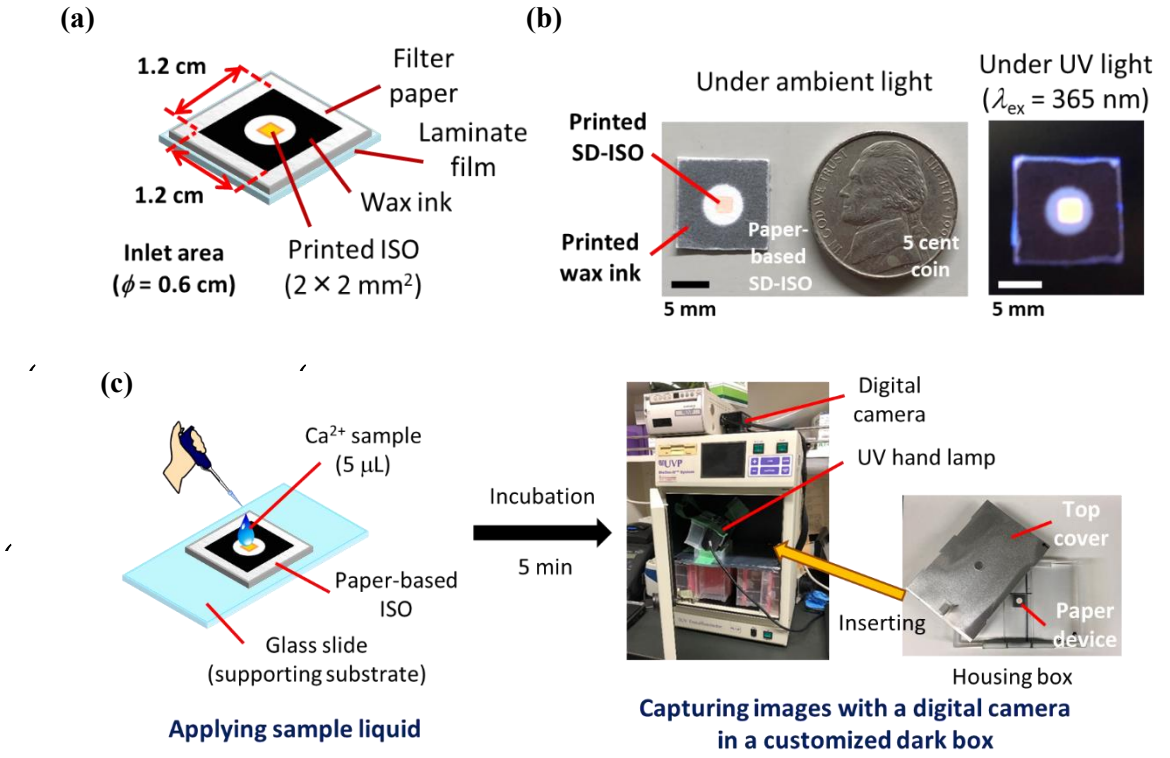

Figure 3-2. Schematic design of the developed Ca^{2+}-selective paper-based SD-ISO and assay procedure; (a) the device dimension designed on the software; (b) actual photograph of a paper-based SD-ISO under ambient light or UV light (λ_{ex} = 365 nm); (c) schematic procedure for the fluorescent detection of Ca^{2+} with a digital camera in a customized dark box. The focus of the digital camera was adjusted by using a paper-based SD-ISO without exposure to Ca^{2+} samples.

3.2.3. Fluorescent Ca^{2+} assay with paper devices

Figure 3-2c shows the schematic protocol for the fluorescence Ca^{2+} detection with the developed paper-based SD-ISO. Sample liquid solution of 5 μL was applied onto the paper device, followed by equilibration for 5 min under ambient condition to achieve the ISO reaction. The incubated paper-based SD-ISO was fixed on a customized housing case, and the fluorescent signal corresponding to concentration of Ca^{2+} was captured with a digital camera under irradiation with a UV hand lump (λ_{ex} = 365 nm) in a customized dark box. The settings of the digital camera were as follows: exposure time 1 s; ISO value 800; *f* value 11. The images of paper devices were captured as NEF format. Using the converted JPEG file, the numerical red intensity values of the SD-ISO region (**Figure 3-3**) on an RGB (Red-Green-Blue) color model were extracted from the obtained digital images with a ImageJ software (NIH, Bethesda, MD) to quantify the concentration of Ca^{2+}. Curve fitting for the experimentally acquired device response data was performed with Igor Pro software (WaveMetrics, Lake Oswegeo, OR) based on a sigmoidal equation.

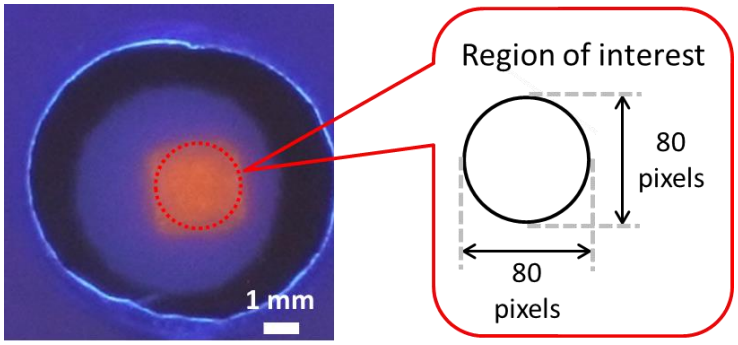

Figure 3-3. Color measurement area on a digital image for quantitative validation of ISO response. The dimensions of the ROI (region of interest) represent the settings in the ImageJ software.

3.3. Result and discussion

3.3.1. Fluorescence assay with Ca^{2+}-selective paper-based SD-ISO

It has been known that the sensing function of carrier-based ISOs with SDs relies on the ion-exchange equilibrium reaction as shown in following **Scheme 3-1**.[9, 14] In this work, the working principle can be

expressed in a simplified manner based on the equilibrium reaction using eq. (3.1).

$$Ca^{2+}_{(aq)} + 2SD^{+}_{(org)} + 3L_{(org)} + 2R^{-}_{(org)} \rightleftarrows Ca^{2+}_{(aq)} + 2SD^{+}_{(su)} + L_3Ca^{2+}_{(org)} + 2R^{-}_{(org)} \quad (3.1)$$

where, subscripts of (org), (aq).and (su) designate the organic sensing phase on/in the modified cellulosic paper, the surrounding aqueous sample phase and the interface between the organic sensing phase and the aqueous sample phase respectively; L is calcium ionophore IV; SD^+ is positively-charged solvatochromic dye; R^- is an ion-exchanger. After extraction of cationic analytes (*i.e.* Ca^{2+} in this work) from the aqueous sample phase, positively-charged SDs must be expelled from an organic sensing phase into the hydrophilic aqueous phase (refer to **Scheme 3-1**). Here, the optical spectrum property of the used SD (e.g. fluorescence, absorbance) is significantly sensitive to solvent polarity, which results in the "on-off" fluorescence signal corresponding to the concentration of Ca^{2+}.[9, 11] The long alkyl chain linkers conjugated with the SDs serve to retain on the cellulosic surface, preventing the leakage of SDs into the aqueous sample phase. As described in **Scheme 3-1**, the conceptual reaction scheme of SD-ISOs in the current work relies on the transfer-based heterogeneous sensing with two water-unmixable phases, in the same manner with previously reported articles[31-34].

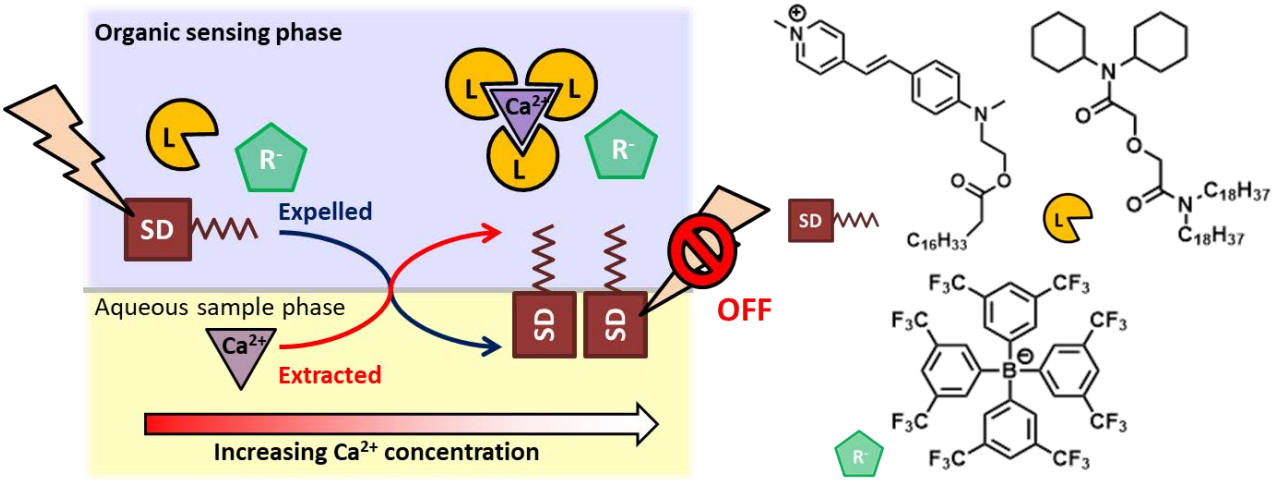

Scheme 3-1. Schematic illustration of conceptual reaction principle of thee plasticizer-free Ca^{2+}-selective ISO on a paper substrate, relying on positively-charged SD and Calcium ionophore IV.

Fluorescence measurements to detect Ca^{2+} were performed with the Ca^{2+}-selective paper-based SD-ISOs (**Figure 3-4**). Fluorescent signal emitted from the paper device under irradiation of UV light with a UV hand lump was quantified by digital color analysis based on the mean values of R. **Figure 3-4a** obviously shows a concentration-dependent decrease in the fluorescence signal of the printed SDs after the incubation for 5 min, corresponding to the anticipated detection mechanism as demonstrated in **Scheme 3-1**. The experimentally acquired means of the R values exhibited a good correlation with the concentration of Ca^{2+} (pH-buffered at 7.0) in the dynamic range of from 10^{-5} mol/L[1] to 1 mol/L (**Figure 3-4b**). Moreover, the obtained R-based response curve for Ca^{2+} was not affected by the different volumes of the applied sample (5, 7, 10 μL) as shown in **Figure 3-5**. Therefore, it should be noted that the response of SD-ISOs in the current work relied on not the "amount" but the "concentration" of the target cations (*i.e.* Ca^{2+}), indicating that the anticipated ion-exchange equilibrium reaction was occurred in the same manner with previously-reported articles[9, 11, 14].

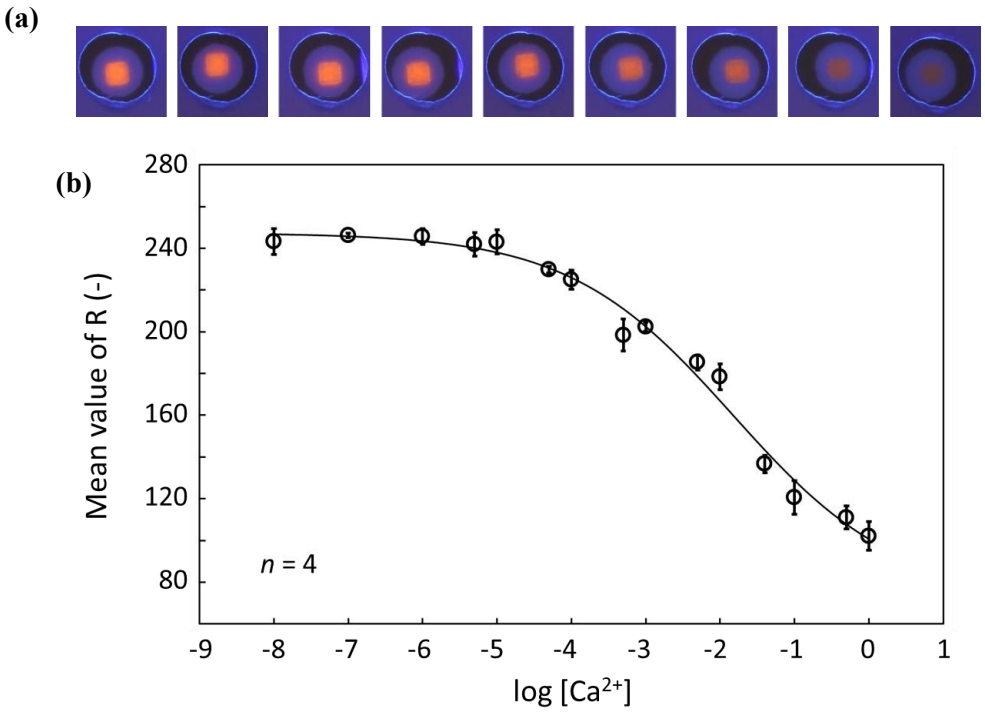

Figure 3-4. (a) Scanned images of concentration-dependent response for Ca^{2+} on paper-based SD-ISOs under the irradiation of the UV light (λ_{ex} = 365 nm) from a UV hand lump. (b) R-based response curve obtained by Ca^{2+}-selective paper-based SD-ISOs exposed to various concentrations of pH-buffered Ca^{2+} samples (50 mM MES-TMAOH buffer, pH 7.0); sample volume 5 μL; incubation time 5 min; each data point has been obtained by measurements with 4 individual single-use devices; error bars indicate the standard deviations.

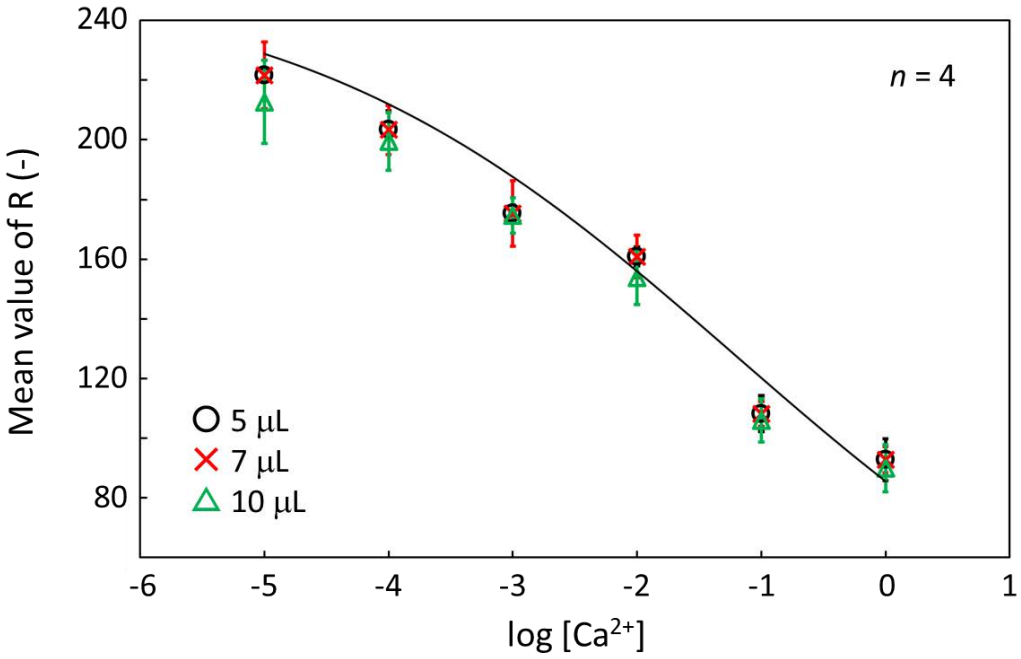

Figure 3-5. R-based response curve obtained from paper-based SD-ISOs exposed to various applied volumes of pH-buffered Ca^{2+} samples (50 mM HEPES-TMAOH buffer, pH 7.0); sample volume 5, 7, and 10 µL; incubation time 5 min; the response curve represented by the solid line was obtained by using underlying data of 5 µL (circles); each data point has been obtained by measurements with 4 individual single-use devices; error bars indicate the standard deviations.

To estimate the morphology of the SD-ISOs printed on the paper substrate, a filter paper after deposition of the SD-ISO components was compared with an unmodified filter paper by using a SEM (**Figure 3-6**). In contrast to the smooth surface of the unmodified paper (**Figure 3-6a**), the rough surface of the ISO-modified paper (**Figure 3-6**) was clearly observable due to the presence of the printed lipophilic sensing reagents in analogy to a published article[32]. Hence, it can be concluded that the homogenous hydrophobic micro-environment layer was successfully formed on the surface of the paper fiber by the SD-ISO reagents themselves. As others have already reported on ISOs with the same SDs[9], however, no obvious analyte-dependent fluorescence signal has not been confirmed on a hydrophobic plastic film (nylon) without a plasticizer. The reason for this issue is that the SDs were not able to easily transfer from a solid nylon film to the aqueous phase[9]. Nevertheless, a cellulosic paper allowed for this transfer of the SDs to achieve the ion-exchange reaction as demonstrated **Scheme 3-1**. Although both the structure and property of the cellulosic

filter paper are rather complex than the traditional materials for ISOs (e.g. plasticized organic polymer), it should be known that a cellulosic paper substrate is composed of a crystalline and an amorphous form.[38-40] The lipophilic ISO components may be adsorbed onto/in the amorphous part since tightly binding between each cellulose molecular in the region of the crystalline cellulose prevents the penetration of other chemicals.[31-34] The concentration-dependent response for Ca^{2+} on paper substrate was achievable regardless of the features of the filter paper (see **Figure 3-7** for Ca^{2+} assay on the different types of the paper substrate). Although the corresponding fluorescent signal was slightly different probably because of the chemical or physical distinctions, however, the obtained dynamic ranges were nearly identical. Consequently, it can be concluded that cellulosic sensor material enabled the movement of the SDs from the hydrophobic sensing phase into the aqueous sample phase for transfer-based reaction as illustrated in **Scheme 3-1**.

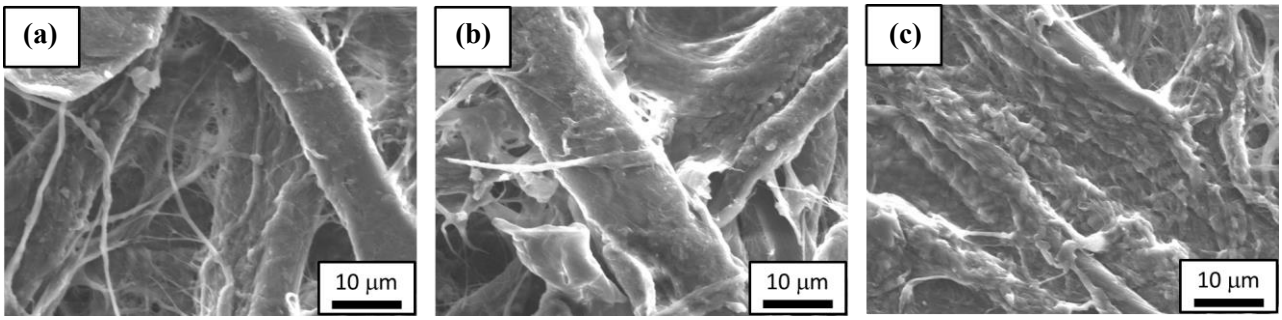

Figure 3-6. SEM images of (a) unmodified filter paper, (b) filter paper after printing reagent-free cyclohexanone at 20 printing cycles, (c) filter paper after deposition of 20 printing cycles of SD-based ISO components with a Dimatix DMP-2831 inkjet printer.

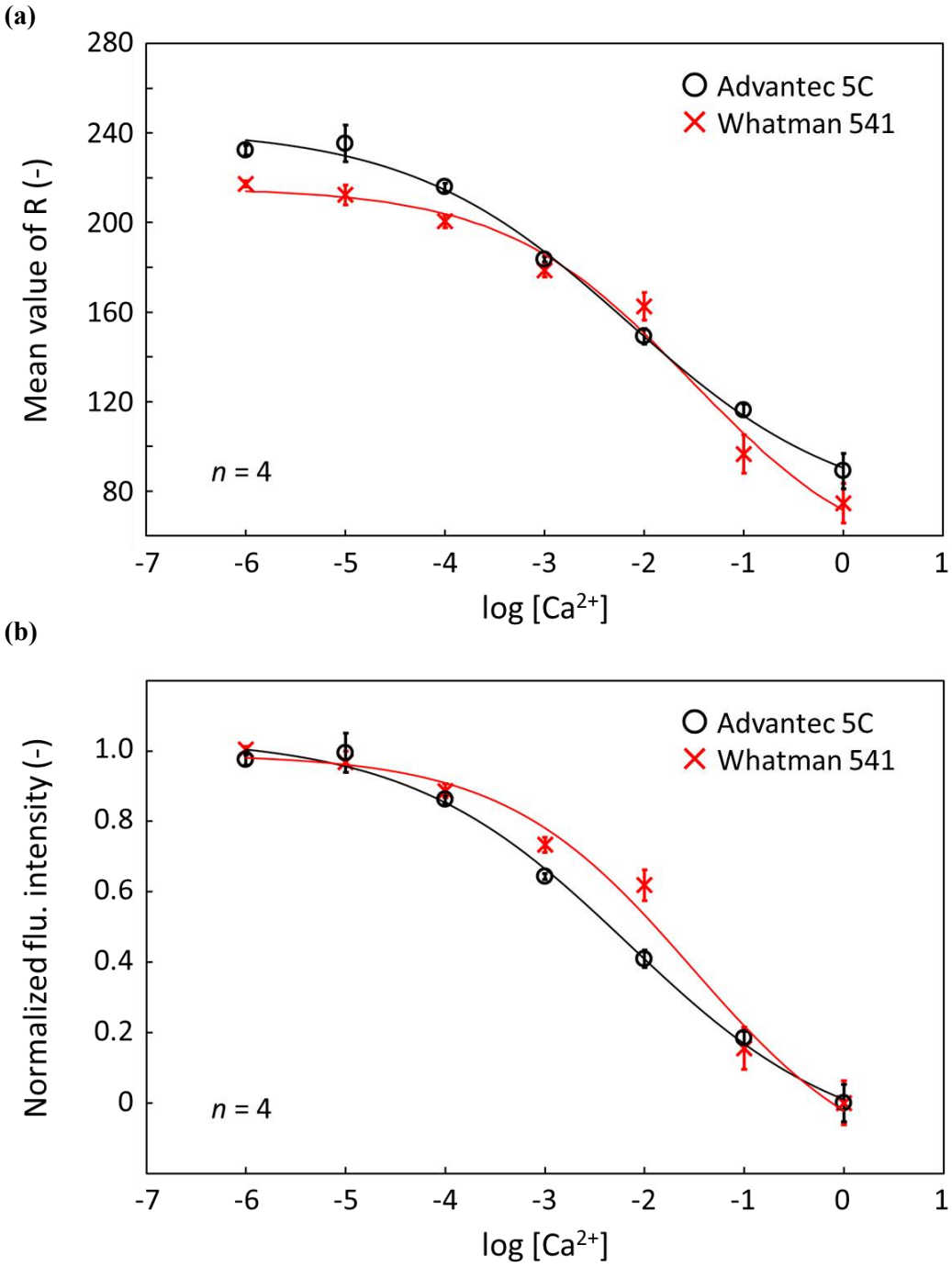

Figure 3-7. Ca^{2+} concentration response curves obtained from paper-based SD-ISOs fabricated by using different kinds of filter paper, which are calculated from (a) mean values of R or (b) normalized fluorescence intensity; sample volume: 5 μL; corresponding Ca^{2+} samples were prepared in 50 mM HEPES-TMAOH buffer (pH 7.0); incubation time 5 min; each data point has been obtained by measurements with 4 individual single-use devices; error bars indicate the standard deviations; normalized fluorescence intensities were estimated by using maximum (experimental result of 1 mol/L) and minimum (blank) experimental results.

3.3.2. pH independence of paper-based SD-ISOs

In a proof-of-concept experiment, Ca^{2+} samples prepared with different pH-buffering solutions (pH 6.0: 50 mM MES-TMAOH buffer, pH 7.0: 50 mM HEPES-TMAOH buffer, pH 8.0: 50 mM HEPES-TMAOH buffer) were applied onto the proposed paper devices (**Figure 3-8**). From **Figure 3-8**, it can be clearly shown that the fluorescence response for the corresponding concentration of Ca^{2+} did indeed not rely on the sample pH (6.0-8.0 tested). Since the used SDs cannot be protonated compared to the traditional H^+-responsive chromoionophore[9, 41], the ion-exchange reaction directly between the positively-charged SDs and the target cations (*i.e.* Ca^{2+}) was achievable, which no longer involved the H^+ during the Ca^{2+} detection. Therefore, pH-independent fluorescent Ca^{2+} assay was successfully performed with the developed Ca^{2+}-selective paper devices owing to the introduction of the positively-charged SDs.

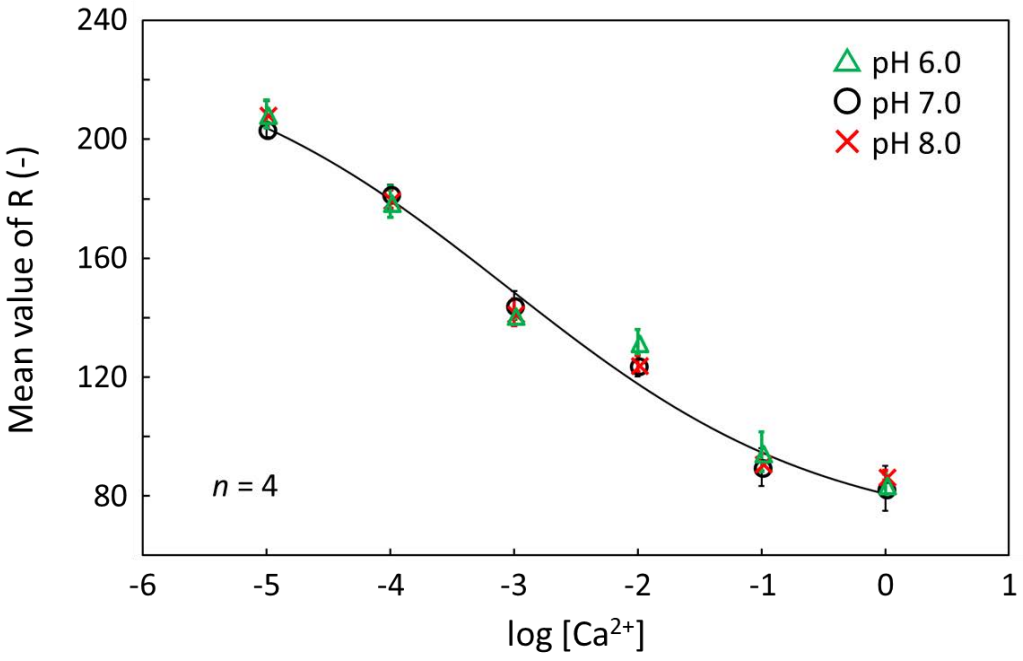

Figure 3-8. R-based response curve obtained by Ca^{2+}-selective paper devices exposed to Ca^{2+} samples pH-buffered at different pH conditions (red crosses: 50 mM MES-TMAOH buffer at pH 6.0; black circles: 50 mM HEPES-TMAOH buffer at pH 7.0; green triangles: 50 mM HEPES-TMAOH buffer at pH 8.0); a solid line represents sigmoidal fitting curve for results of pH 7.0 (circles); sample volume 5 µL; incubation time 5 min; each data point has been obtained by measurements with 4 individual single-use devices; error bars indicate the standard deviations.

This pH independence serves to eliminate the traditional pH-buffering process with chemical reagents prior to the ISO-based assay, corresponding theoretical response function of the SD-ISOs as described in the above section. To confirm this advantageous feature, the response curve for pH-unbuffered Ca^{2+} samples (*i.e.* prepared with ultrapure water) were experimentally evaluated by using the paper devices with any pre-deposited pH-buffering salts (**Figure 3-9**). The obtained fluorescent response shows identical dynamic concentration range from 10^{-5} to 1 mol/L. Therefore, it can be concluded that elimination of the pH-buffering of the sample is achievable by introduction of the SDs instead of the traditional H^+-sensitive chromoionophores.

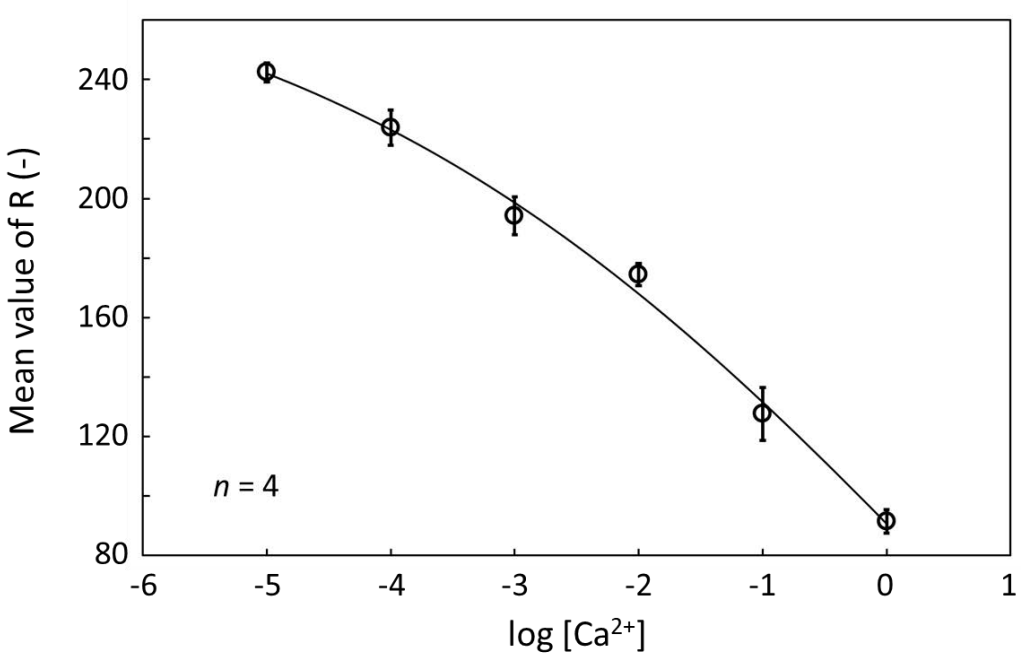

Figure 3-9. R-based response curve obtained by Ca^{2+}-selective paper-based SD-ISOs exposed to various concentrations of Ca^{2+} samples without pH-buffering; sample volume 5 µL; incubation time 5 min; each data point has been obtained by measurements with 4 individual single-use devices; error bars indicate the standard deviations.

3.3.3. Selectivity study over other cations

The selectivity of the proposed paper devices for Ca^{2+} detection has been investigated with pH-buffered cation samples (50 mM HEPES-TMAOH buffer, pH 7.0) of common alkali and alkaline earth metal ions

including $MgCl_2$, NaCl, KCl (**Figure 3-10**). **Figure 3-10** demonstrates that the selectivity feature owing to the used Ca^{2+}-ionophore was observable. Here, the SD-ISOs without any addition of the ionophores did not show concentration response for Ca^{2+} (**Figure 3-11**). Based on the Separation Solution Method by using experimentally acquired mean values of R, observable legalism selectivity coefficient of the proposed paper-based Ca^{2+}-selective optodes were found to be -2.3 over Mg^{2+} and <-3 over other cations (Na^+ and K^+). Compared with classical membrane-based or ISEs[42] or emulsion-based ISOs[43] with the same ionophore, the selectivity of the developed paper devices was slightly reduced probably due to the different polarity environment of the receptors[43]. Consequently, selective recognition of Ca^{2+} was successfully accompanied with the ion-specific ionophores (calcium ionophore IV).

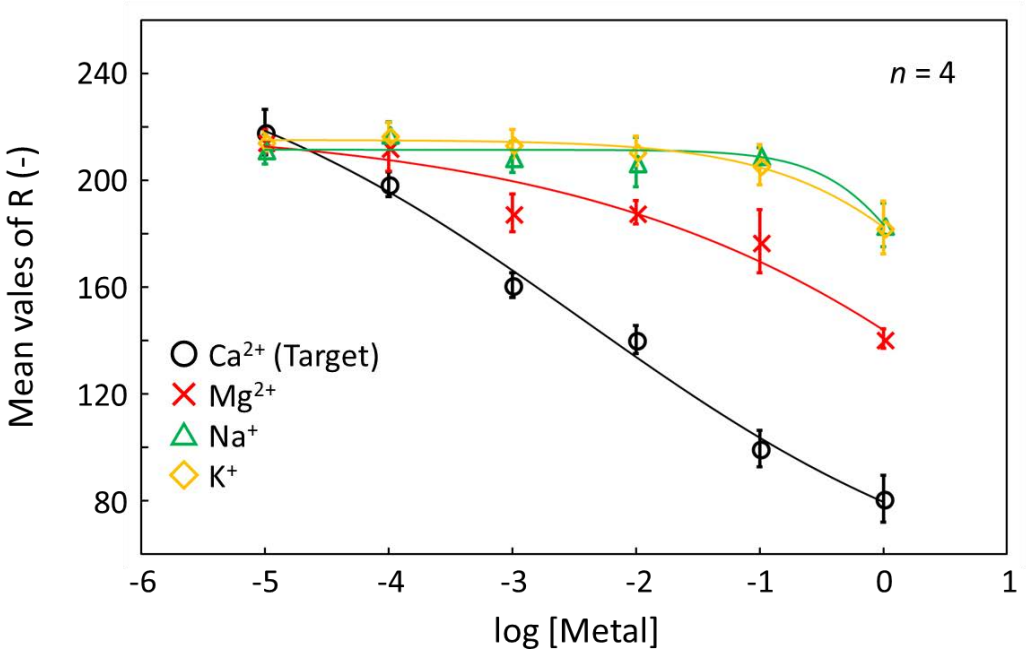

Figure 3-10. Selectivity evaluation of Ca^{2+}-selective paper-based SD-ISOs over other alkali and alkaline earth metal cations (Mg^{2+}, Na^+, K^+); all metal cation samples were prepared with chloride salts; All sample solutions were pH-buffered with HEPES-TMAOH buffer (50 mM, pH 7.0); sample volume 5 µL; incubation time 5 min; each data point has been obtained by measurements with 4 individual single-use devices; error bars indicate the standard deviations.

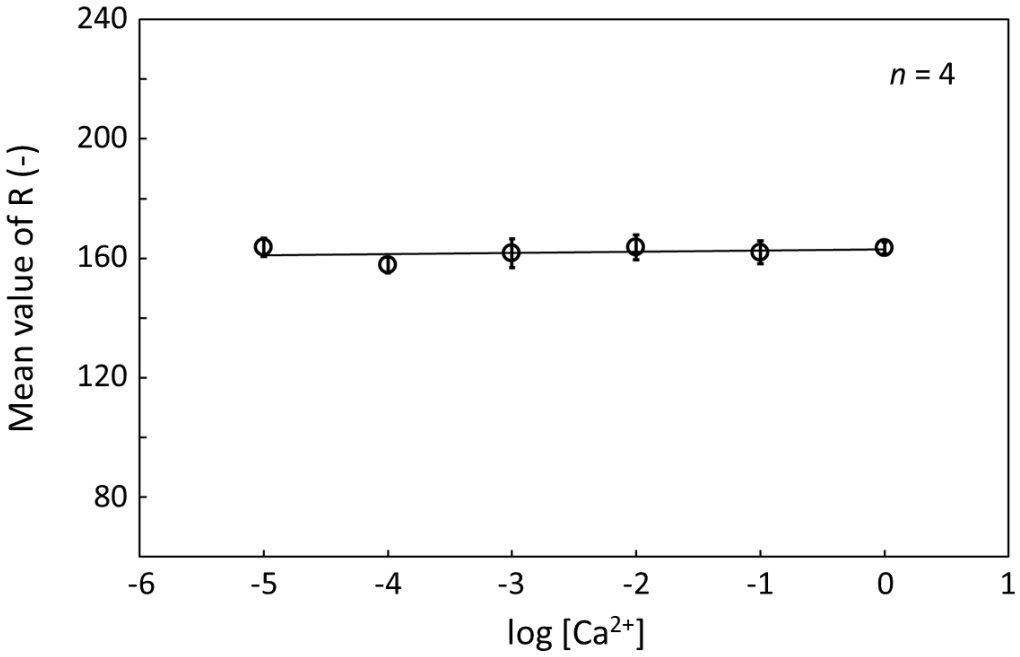

Figure 3-11. R-based response curve obtained from ionophore-free paper-based SD-ISOs exposed to various concentrations of pH-buffered Ca^{2+} samples (50 mM HEPES-TMAOH buffer, pH 7.0); sample volume 5 μL; incubation time 5 min; each data point has been obtained by measurements with 4 individual single-use devices; error bars indicate the standard deviations.

3.3.4. Practical application

Finally, we selected here a mineral water purchased at a local supermarket as an early stage practical application. The level of Ca^{2+} concentration in the mineral water was estimated by using the developed paper-based SD-ISOs or complexometric titration. The quantitative results obtained from the paper devices and the titration were 0.20±0.04 mM (n = 3) and 0.18±0.01 mM (n = 3), respectively. It should be noted that the capability of the proposed devices to determine Ca^{2+} in the mineral water was comparable to the conventional titration methods, which no longer required any pretreatments prior to the assay.

3.4. Conclusion

The implementation of the positively-charged SDs onto a plasticizer-free paper-based ISO system for fluorescent cation detection has been successfully demonstrated on the example of Ca^{2+} as the model of the

target cations. The use of the SDs instead of conventional H^+-responsive leaded to overcome the pH-independence of paper-based ISOs without pre-deposited pH-buffering components. The proposed paper devices have provided the fluorescence response corresponding to the concentration of Ca^{2+} in the range of 10^{-5}-1 mol L^{-1}, and a good selectivity capability owing to the used ionophore. As simple application, the Ca^{2+} level in mineral water has been quantified with the developed paper devices, which is comparable to a conventional complexometric titration method. It has been experimentally shown that a homogenous hydrophobic micro-environment layer was observable on a cellulosic fiber of paper substrate, which is applicable to transfer-based heterogeneous sensing with two water-unmixable phases in the same manner with previously reported articles. Interestingly, the structure of a cellulosic paper also allowed for the transfer of the SDs from the organic sensing phase into the aqueous sample phase. Although further experimentation is required to fully clarify this phenomenon, we believe that the current work contributes to the expansion of the applicability of paper-based cation sensors.

References

1. Bakker, E.; Bühlmann, P.; Pretsch, E., Carrier-Based Ion-Selective Electrodes and Bulk Optodes. 1. General Characteristics. *Chem. Rev.* **1997,** *97*, 3083.

2. Mistlberger, G.; Crespo, G. A.; Bakker, E., Ionophore-Based Optical Sensors. *Annu. Rev. Anal. Chem.* **2014,** *7*, 483.

3. Xie, X.; Bakker, E., Ion Selective Optodes: From the Bulk to the Nanoscale. *Anal. Bioanal. Chem.* **2015,** *407*, 3899.

4. Mikhelson, K.; Peshkova, M., Advances and trends in ionophore-based chemical sensors. *Russian Chem. Rev.* **2015,** *84* (6), 555.

5. Xie, X.; Zhai, J.; Bakker, E., Potentiometric response from ion-selective nanospheres with voltage-sensitive dyes. *J. Am. Chem. Soc.* **2014,** *136* (47), 16465-16468.

6. Zhai, J.; Xie, X.; Bakker, E., Solvatochromic Dyes as pH-Independent Indicators for Ionophore Nanosphere-Based Complexometric Titrations. *Analytical Chemistry* **2015,** *87* (24), 12318-12323.

7. Xie, X.; Gutiérrez, A.; Trofimov, V.; Szilagyi, I.; Soldati, T.; Bakker, E., Charged Solvatochromic Dyes as Signal Transducers in pH Independent Fluorescent and Colorimetric Ion Selective Nanosensors. *Anal. Chem.* **2015,** *87* (19), 9954-9959.

8. Xie, X.; Bakker, E., Determination of Effective Stability Constants of Ion-Carrier Complexes in Ion Selective Nanospheres with Charged Solvatochromic Dyes. *Anal. Chem.* **2015,** *87* (22), 11587-11591.

9. Wang, L.; Xie, X.; Zhai, J.; Bakker, E., Reversible pH-independent optical potassium sensor with lipophilic solvatochromic dye transducer on surface modified microporous nylon. *Chem. Commun.* **2016,** *52* (99), 14254-14257.

10. Du, X.; Xie, X., Non-Equilibrium Diffusion Controlled Ion-Selective Optical Sensor for Blood Potassium Determination. *ACS Sens.* **2017,** *2* (10), 1410-1414.

11. Lu, W.; Xiaojiang, X.; Tianchi, C.; Jérôme, B.; Eric, B., Surface-Doped Polystyrene Microsensors Containing Lipophilic Solvatochromic Dye Transducers. *Chem.: A Eur. J.* **2018,** *24* (31), 7921-7925.

12. Du, X.; Yang, L.; Hu, W.; Wang, R.; Zhai, J.; Xie, X., A Plasticizer-Free Miniaturized Optical Ion Sensing Platform with Ionophores and Silicon-Based Particles. *Anal. Chem.* **2018,** *90* (9), 5818-5824.

13. Du, X.; Huang, M.; Wang, R.; Zhai, J.; Xie, X., A Rapid Point-of-Care Optical Ion Sensing Platform Based on Target-Induced Dye Release from Smart Hydrogels. *Chem. Commun.* **2019**.

14. Xie, X., Renovating the chromoionophores and detection modes in carrier-based ion-selective optical sensors. *Anal. Bioanal. Chem.* **2016,** *408* (11), 2717-2725.

15. Dincer, C.; Bruch, R.; Kling, A.; Dittrich, P. S.; Urban, G. A., Multiplexed point-of-care testing–xPOCT. *Trends in Biotech.* **2017,** *35* (8), 728-742.

16. Majors, C. E.; Smith, C. A.; Natoli, M. E.; Kundrod, K. A.; Richards-Kortum, R., Point-of-care diagnostics to improve maternal and neonatal health in low-resource settings. *Lab on Chip* **2017,** *17* (20), 3351-3387.

17. Martinez, A. W.; Phillips, S. T.; Butte, M. J.; Whitesides, G. M., Patterned Paper as a Platform for Inexpensive, Low Volume, Portable Bioassays. *Angew. Chem., Int. Ed.* **2007,** *46*, 1318.

18. Martinez, A. W.; Phillips, S. T.; Wiley, B. J.; Gupta, M.; Whitesides, G. M., FLASH: a rapid method for prototyping paper-based microfluidic devices. *Lab on Chip* **2008,** *8* (12), 2146-2150.

19. Yetisen, A. K.; Akram, M. S.; Lowe, C. R., Paper-Based Microfluidic Point-of-Care Diagnostic Devices. *Lab Chip* **2013,** *13*, 2210.

20. Cate, D. M.; Adkins, J. A.; Mettakoonpitak, J.; Henry, C. S., Recent Developments in Paper-Based Microfluidic Devices. *Anal. Chem.* **2015,** *87*, 19.

21. Nilghaz, A.; Guan, L.; Tan, W.; Shen, W., Advances of Paper-Based Microfluidics for Diagnostics□ The Original Motivation and Current Status. *ACS Sens.* **2016,** *1* (12), 1382-1393.

22. Yang, Y.; Noviana, E.; Nguyen, M. P.; Geiss, B. J.; Dandy, D. S.; Henry, C. S., based microfluidic devices: Emerging themes and applications. *Anal. Chem.* **2016,** *89* (1), 71-91.

23. Yamada, K.; Shibata, H.; Suzuki, K.; Citterio, D., Toward Practical Application of Paper-Based Microfluidics for Medical Diagnostics: State-of-the-Art and Challenges. *Lab Chip* **2017,** *17*, 1206.

24. Tian, T.; Bi, Y.; Xu, X.; Zhu, Z.; Yang, C., Integrated paper-based microfluidic devices for point-of-care testing. *Anal. Methods* **2018,** *10* (29), 3567-3581.

25. Gerold, C. T.; Bakker, E.; Henry, C. S., Selective Distance-Based K+ Quantification on Paper-Based Microfluidics. *Anal. Chem.* **2018,** *90* (7), 4894-4900.

26. Kassal, P.; Sigurnjak, M.; Steinberg, I. M., Paper-based ion-selective optodes for continuous sensing: reversible potassium ion monitoring. *Talanta* **2018**.

27. Shibata, H.; Hiruta, Y.; Citterio, D., Fully inkjet-printed distance-based paper microfluidic devices for colorimetric calcium determination using ion-selective optodes. *Analyst* **2019**.

28. Soda, Y.; Citterio, D.; Bakker, E., Equipment-Free Detection of K^+ on Microfluidic Paper-based Analytical Devices Based on Exhaustive Replacement with Ionic Dye in Ion-selective Capillary Sensors. *ACS Sens.* **2019**.

29. Shibata, H.; Henares, T. G.; Yamada, K.; Suzuki, K.; Citterio, D., Implementation of a plasticized PVC-based cation-selective optode system into a paper-based analytical device for colorimetric sodium detection. *Analyst* **2018,** *143* (3), 678-686.

30. Soda, Y.; Shibata, H.; Yamada, K.; Suzuki, K.; Citterio, D., Selective Detection of K^+ by Ion-Selective Optode Nanoparticles on Cellulosic Filter Paper Substrates. *ACS Appl. Nano Mater.* **2018,** *1* (4), 1792-1800.

31. Wang, X.; Qin, Y.; Meyerhoff, M. E., Paper-Based Plasticizer-Free Sodium Ion-Selective Sensor with Camera Phone as a Detector. *Chem. Commun.* **2015,** *51*, 15176.

32. Wang, X.; Zhang, Q.; Nam, C.; Hickner, M.; Mahoney, M.; Meyerhoff, M. E., An Ionophore-Based Anion-Selective Optode Printed on Cellulose Paper. *Angew. Chem., Int. Ed.* **2017,** *56*, 11826.

33. Wang, X.; Mahoney, M.; Meyerhoff, M. E., Inkjet-Printed Paper-Based Colorimetric Polyion Sensor Using a Smartphone as a Detector. *Anal. Chem.* **2017,** *89*, 12334.

34. Ferguson, S. A.; Wang, X.; Mahoney, M.; Meyerhoff, M. E., Detection and Quantification of Polyquaterniums via Polyion-Sensitive Ion-Selective Optodes Inkjet Printed on Cellulose Paper. *Anal. Sci.* **2018,** *34* (1), 45-50.

35. Abe, K.; Suzuki, K.; Citterio, D., Inkjet-printed microfluidic multianalyte chemical sensing paper. *Anal. Chem.* **2008,** *80* (18), 6928-6934.

36. Komuro, N.; Takaki, S.; Suzuki, K.; Citterio, D., Inkjet Printed (Bio)chemical Sensing Devices. *Anal. Bioanal. Chem.* **2013,** *405*, 5785.

37. Yamada, K.; Henares, T. G.; Suzuki, K.; Citterio, D., Paper-Based Inkjet-Printed Microfluidic Analytical Devices. *Angew. Chem., Int. Ed.* **2015,** *54*, 5294.

Chapter 4
Simplification of Semi-quantitative Readout for Colorimetric Cation Detection

This chapter is based on "Fully inkjet-printed distance-based paper microfluidic devices for colorimetric calcium determination using ion-selective optodes",

Hiroyuki Shibata, Yuki Hiruta and Daniel Citterio,

Analyst, **2019**, *144*, 1178-1186.

Summary

Although the determination of calcium ions (Ca^{2+}) is of high importance to monitor water hardness, currently available devices for on-site analysis suffer from a lack of user-friendliness and sensitivity. This work demonstrates fully inkjet-printed and low-cost microfluidic paper-based analytical devices (μPADs) for the simple naked-eye colorimetric determination of calcium ions (Ca^{2+}) in drinking and tap water samples. The quantification of Ca^{2+} relies on visual readout of the length of a color-changed detection channel modified with ionophore-doped ion-selective optode nanospheres (nano-optodes), eliminating the requirement of a scanner or a camera. All fabrication steps for deposition of assay reagents have been performed by means of a simple desktop thermal inkjet printer, which is expected to contribute to highly batch-to-batch reproducible device preparation. The detectable Ca^{2+} concentrations between 0.05 mM and 5 mM cover the range recommended by the International Organization for Standardization (0.05-2.5 mM) and the World Health Organization (WHO) guideline for Ca^{2+} quantification in drinking water (less than 5 mM). The lowest concentration of Ca^{2+} detectable by the naked eye was found to be 0.05 mM, which is below the value achieved with previously reported paper-based devices. μPAD quantified Ca^{2+} concentrations in tap or drinking waters were within 15% error of the results obtained with a classical complexometric titration. Hence,

distanced-based μPADs relying on nano-optodes are sensitive and reproducible tools for equipment-free on-site assaying of Ca^{2+} in real samples.

4.1. Introduction

Calcium (Ca) is found as an important trace mineral and nutrient in natural or drinking waters, and together with magnesium (Mg) determines the water hardness. The World Health Organization (WHO) published a report on the public health significance of water hardness, addressing its benefits and risks.[1] Although no strict criteria for Ca^{2+} levels in the context of drinking water quality have been defined in this guideline, the WHO alternatively established a recommendation for Ca^{2+} levels in drinking water to be below 5 mM and a taste threshold for Ca^{2+} in the range of 2.5-7.5 mM.[1] Quantitative and selective quantification of Ca relies on a wide variety of classical analytical methods, such as complexometric titration, spectrophotometry and atomic absorption spectrometry (AAS).[1-3] As a standardised protocol provided by the International Organization for Standardization, classic complexometric titrations using cation-responsive chromogens and chelating reagents are applied to the direct determination of calcium levels in the range of 0.05-2.5 mmol/L.[4] While this analytical approach is inexpensive and relatively simple, it is difficult to be adapted to on-site or in-field assays because of the necessity of specific experimental equipment (e.g. burette) and the multistep nature of the assay including sample pretreatment with a strongly basic solution (pH ≈ 12) for masking interfering cations.[4-5] On the other hand, spectrophotometry and AAS allow for selective, sensitive, and reliable measurement of the target ions of interest. However, they are expensive, labour intensive, and complicated for untrained users.

Since Whitesides' research group first established the concept of microfluidically patterned paper,[6-7] microfluidic paper-based analytical devices (μPADs) have emerged as a new class of analytical platform over conventional paper strips for point-of-need analysis.[3, 8-14] In this context, the naturally porous structure of cellulosic paper plays an important role as a sustainable, inexpensive, ready-to-use, and safely disposable substrate platform for (semi-)quantitative assays applied to both clinical and environmental monitoring.

Passive sample transportation through capillary forces enables sophisticated (bio)chemical assays, including sample pretreatment steps, and μPADs have evolved into analytical tools helping to overcome some limitations of conventional analytical instruments in terms of cost, portability and user-friendliness. Colorimetric μPADs are of particularly high interest, because they allow for unaided eye observable quantitative signal readout.[15] Not surprisingly, various metal ions (especially heavy metals) have been colorimetrically determined on μPADs due to the wide availability of classical colorimetric indicators. [3, 12-14, 16-20] With regard to the colorimetric detection of Ca^{2+}, complexometric titration reagents, such as chelating reagents, cation-responsive chromogens, and masking reagents, have typically been adapted to the cellulosic substrate.[21-23] Kaneta's research group for example, fully integrated the classical complexometric titration system into a μPAD for the visual determination of Ca^{2+} and Mg^{2+} in natural or drinking waters without the requirement for burettes and optical signal quantification tools (e.g. camera, scanner).[22] Nevertheless, paper-based assays for visual detection of Ca^{2+} in drinking water and tap water suffer from relatively poor limits of detection (LOD), with an LOD of 0.21 mM reported for a μPAD relying on software-assisted colorimetric readout,[21] or of 5 mM by naked eye visual detection.[22]

As one of the sophisticated optical chemical sensors targeting ionic species, ionophore-based ion-selective optodes (ISOs) continue to attract significant attention.[24-26] Classical ISOs are typically composed of lipophilic sensing components, such as a pH indicator as optical transducer (chromoionophore), an ion-specific ligand (ionophore), and an organic salt additive (ion-exchanger), embedded into a plasticised polymeric membrane.[24, 27] Due to the versatile capabilities of ISOs, their detection function has been integrated into cellulosic material platforms, such as a cotton thread[28] and paper substrates.[29-36] More recently, our research group introduced the classical polymer film-based ISOs into μPADs with the aid of inkjet printing technology.[29] In a later stage, we reported the use of inkjet-generated polymeric particle-based ISOs on paper strips.[30] Meyerhoff's research group on the other hand, first established a new class of ISOs without the conventional plasticised polymeric materials on paper substrates,[31] and first applied inkjet printing technology for the deposition of the corresponding ISO components.[32-34] Although paper-based ISOs have served to determine various electrolytes,

they require optical signal readout tools (e.g. scanner, camera, reflectometry). Only in 2018, Henry's and Bakker's research groups succeeded in the elimination of the conventional color intensity or color hue readout by adapting a distance-based signal readout motif to ISOs with micelle-based nanospheres (nano-optodes) pipetted onto μPADs.[35] Nevertheless, inkjet printing technology has to best of our knowledge never been applied to the highly-reproducible and well-defined deposition of all assay reagents onto practical μPADs.

The present work demonstrates distance-based μPADs for the naked-eye quantification of Ca^{2+} in drinking or tap waters with high batch-to-batch reproducibility and assay accuracy without any external equipment. For this purpose, nano-optodes composed of the surfactant Pluronic® F-127 have been applied to the fabrication of distance-based μPADs by means of inkjet printing technology. Notably, the nano-optodes no longer require the use of volatile organic solvents in the paper device fabrication process (e.g. tetrahydrofuran, cyclohexanone).[25, 37-38] Therefore, it is possible to use simple desktop thermal inkjet printing for their deposition onto wax-patterned paper substrates. All fabrication steps leading to the distance-based μPADs, from the microfluidic patterning of the paper substrate (wax printing) to the deposition of all required assay reagents (inkjet printing), were performed with standard printing technology, which is expected to contribute to highly reproducible and scalable fabrication with minimum consumption of chemical reagents.[39-40] Additionally, the developed μPADs show a lower naked-eye observable LOD (0.05 mM) than a commercial colorimetric paper dipstick (0.1 mM), and they are applicable to practical sample analysis of Ca^{2+} with sufficient accuracy (no more than 15% error).

4.2. Materials and methods

4.2.1. Reagents and instruments

All reagents were used without further purification. Chromoionophore I (CH1), calcium ionophore IV and tetramethylammonium hydroxide pentahydrade (TMAOH) were purchased from Sigma-Aldrich (St. Louis, MO). Pluronic® F-127 (F127) was purchased from BASF (Ludwigshafen, Germany). Tetrahydrofuran (THF) was purchased from Kanto Chemical (Tokyo, Japan). Bis(2-ethylhexyl) sebacate (DOS), sodium chloride

(NaCl), potassium chloride (KCl), calcium chloride dihydrate ($CaCl_2 \cdot 2H_2O$) and magnesium chloride hexahydrate ($MgCl_2 \cdot 6H_2O$) were purchased from Wako Pure Chemical Industries (Osaka, Japan). *N*-(2-hydroxyethyl)-1-piperazineethanesulfonic acid (HEPES), sodium tetrakis[3,5-bis(trifluoromethyl)phenyl]borate (NaTFPB), 0.01 N EDTA (ethylenediaminetetraacetate) titration solution (f = 1.001), and 2-hydroxy-1-(2-hydroxy-4-sulfo-1-naphthylazo)-3-naphthoic acid (NN) were purchased from Dojindo Laboratories (Kumamoto, Japan). Colorimetric paper dipsticks for Ca^{2+} assays were purchased from Merck Milllipore (Darmstadt, Germany).

Ultrapure water (>18 MΩ cm) was obtained from a PURELAB flex water purification system (ELGA, Veolia Water, Marlow, U.K.) and used for the preparation of all solutions. Advantec No. 5C filter paper was purchased from Toyo Roshi (Tokyo, Japan). Hot lamination films (150 μm thickness, film material: polyethylene terephthalate and polyvinyl alcohol as a thermoplastic adhesive) were obtained from Jointex (Tokyo, Japan). For inkjet printing of the reagents for Ca^{2+} detection, a thermally-actuated Canon iP2700 inkjet printer (Canon, Tokyo, Japan) was used. For this purpose, the standard color cartridge of the Canon printer was cut open and the sponge inside and color inks were removed, followed by washing with copious amounts of deionised water. Dynamic light scattering (DLS) measurements to evaluate the hydrodynamic diameter of nano-optodes were performed by a Zetasizer Nano ZS from Malvern (Worcestershire, UK). Optical microscope images were acquired on a DVM2500 digital microscope (Leica, Wetzlar, Germany).

4.2.2. Preparation of Ca^{2+}-selective nano-optode suspension

The preparation of the ion-selective optode nanospheres (nano-optodes) according to previously published articles[37-38] and the evaluation of their physical properties by DLS are described in **Figure 4-1**. 4.28 mg of NaTFPB, 1.68 mg of CH1, 3.2 mg of DOS, 3.0 mg of F127 and 3.90 mg of calcium ionophore IV were dissolved in 1.2 mL of THF to obtain a homogeneous solution. 1.0 mL of this prepared cocktail was injected into 4.5 mL of deionized water on a vortex with a spinning speed of 1000 r/min, followed by organic solvent removal with a stream of N_2 gas for 40 min. The suspension of nano-optodes contained nanosphere particles

of approximately 200 nm in diameter with a polydispersity index (PDI) of 0.273. This solution was directly used for inkjet printing without any further processing.

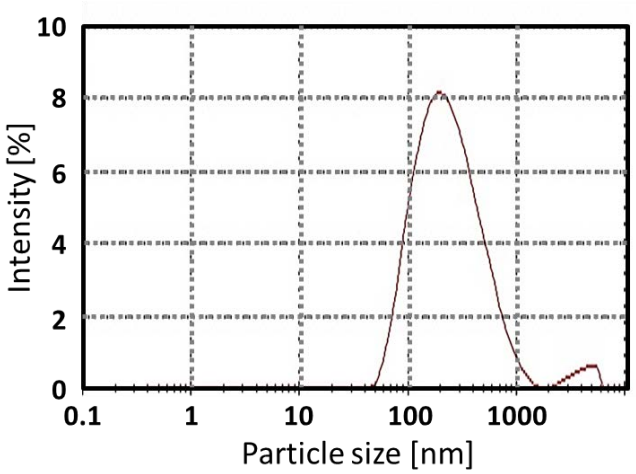

Figure 4-1. Hydrodynamic diameter of the prepared nano-optodes measured by dynamic light scattering (DLS). The suspension of nano-optodes contained nanosphere particles of approximately 200 nm in diameter with a polydispersity index (PDI) of 0.273.

4.2.3. Device fabrication for distance-based Ca^{2+} quantification

A ColorQube 8570 printer (Xerox, Norwalk, CT, USA) was used to pattern wax barriers on filter paper sheets cut into A4-size before use. 32 identical wax patterns designed in PowerPoint (Microsoft) were transferred to one single sheet of paper, as shown in **Figure 4-2**. For melting the wax into the depth of the paper to produce hydrophobic barriers, printed patterns were heated on a hot plate (Nissin NHS-450ND, Nissinrika, Tokyo, Japan) at 150°C for 3 min. To prevent contamination from paper feeding rollers of the printer during inkjet printing steps, the back side of wax-patterned paper was laminated. The wax-patterned and back side-laminated paper substrates were then subjected to reagent deposition to obtain the distance-based μPADs for colorimetric determination of Ca^{2+} as described below and illustrated in **Figure 4-3**.

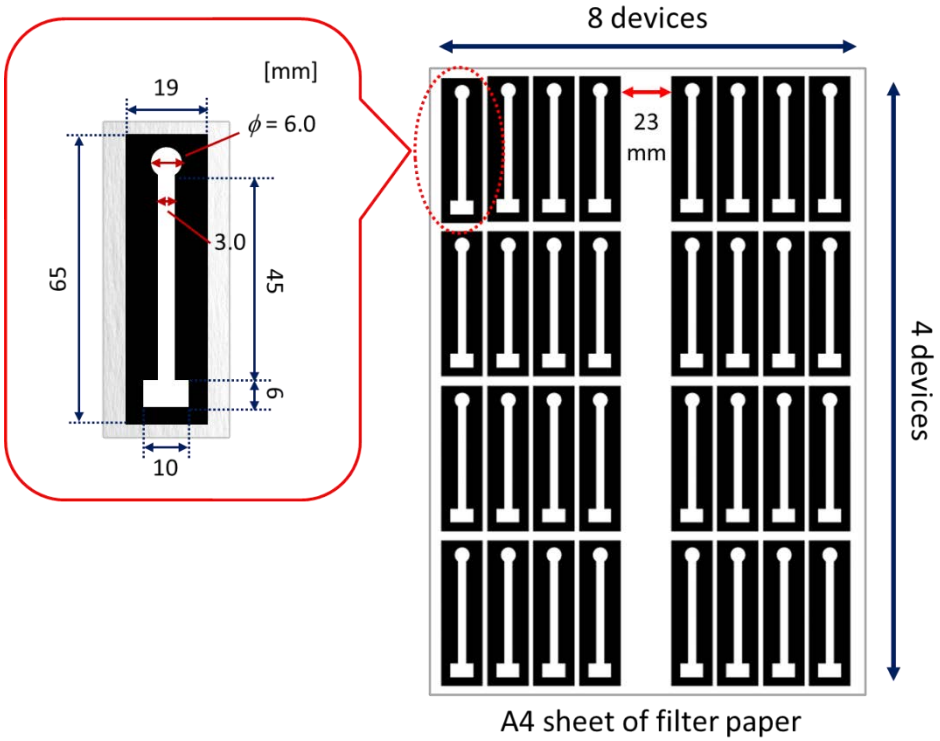

Figure 4-2. Schematic illustration of the wax barrier patterns printed on an A4-size filter paper sheet. The dimensions in the red box represent the settings in the PowerPoint graphic software.

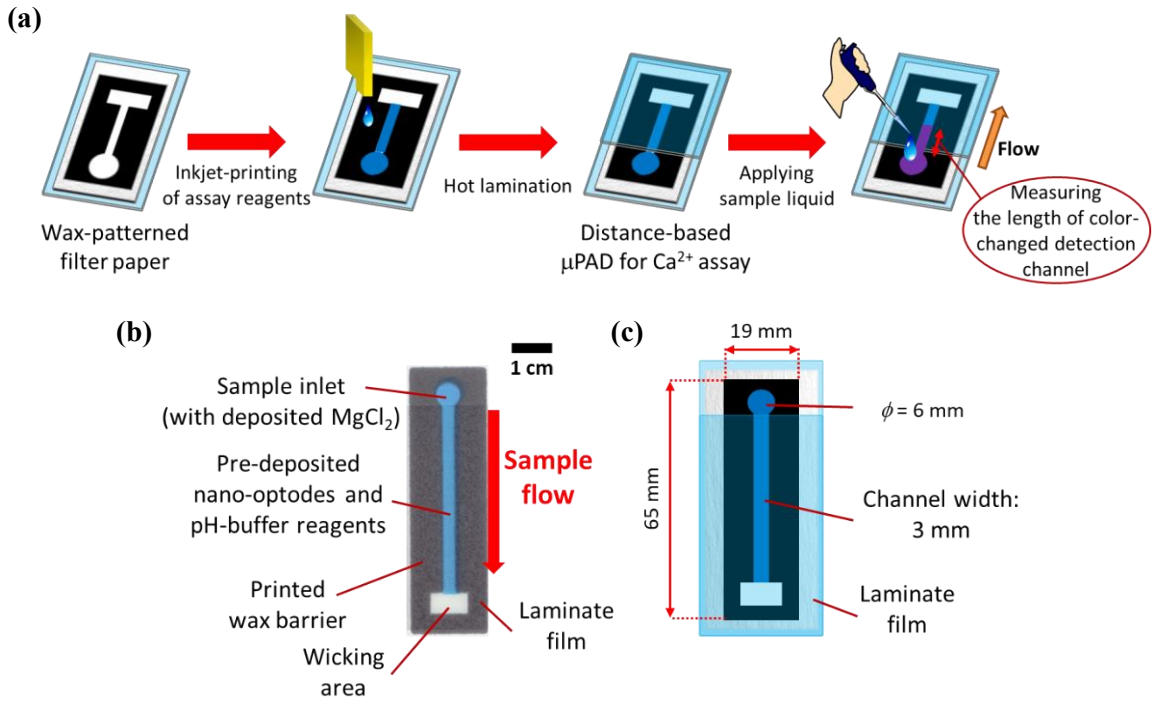

Figure 4-3. (a) Schematic procedure of device fabrication by printing technology and Ca^{2+} assay with a Ca^{2+}-selective distance-based μPAD; (b) Design of distance-based μPAD for nano-optode based Ca^{2+} detection, and (c) corresponding dimensions representing the settings in the PowerPoint graphic software.

As sample pretreatment reagents, pH-buffering solution (250 mM HEPES-TMAOH buffer, pH 7.0) and 10 mM aqueous $MgCl_2$ solution, were separately inkjet-deposited from a black ink cartridge in 1 and 3 print cycles, respectively. Then, Ca^{2+}-selective nano-optodes were inkjet-printed from a magenta ink cartridge in 20 printing cycles. After the inkjet printing step, the printed sides of the μPADs were laminated with exception of the sample inlet area to limit evaporation of sample liquid during assays.

4.2.4. Distance-based Ca^{2+} assay with μPADs

30 μL of aqueous $CaCl_2$ solution was applied to the sample inlet of the μPAD, followed by incubation under ambient condition to perform the nano-optode reaction (45 min). The generated colorimetric signals were captured as JPEG images of 600 dpi resolution with a Canoscan 9000F MarkII color scanner (Canon, Tokyo, Japan). The obtained images were processed by separating the color into the red, green and blue channels. The red channel was used to quantify the colorimetric change of paper devices. The length of the color-changed nano-optode section of the detection channel was measured with the ImageJ software (NIH, Bethesda, MD). The colorimetric response profile recorded along the detection channel shown in **Figure 4-4** was obtained by using the data smoothing function of ImageJ. It is noted here that the distance-based μPADs are intended for equipment-free naked-eye signal readout. The use of scanned images and image processing software exclusively serves the purpose of device characterization. Curve fitting of the experimentally acquired response data was performed with the Igor Pro 4.01 software package (WaveMetrics, Lake Oswegeo, OR) based on a sigmoidal equation and estimates for the concentration of Ca^{2+} were obtained with the "Solver" function of Excel (Microsoft).

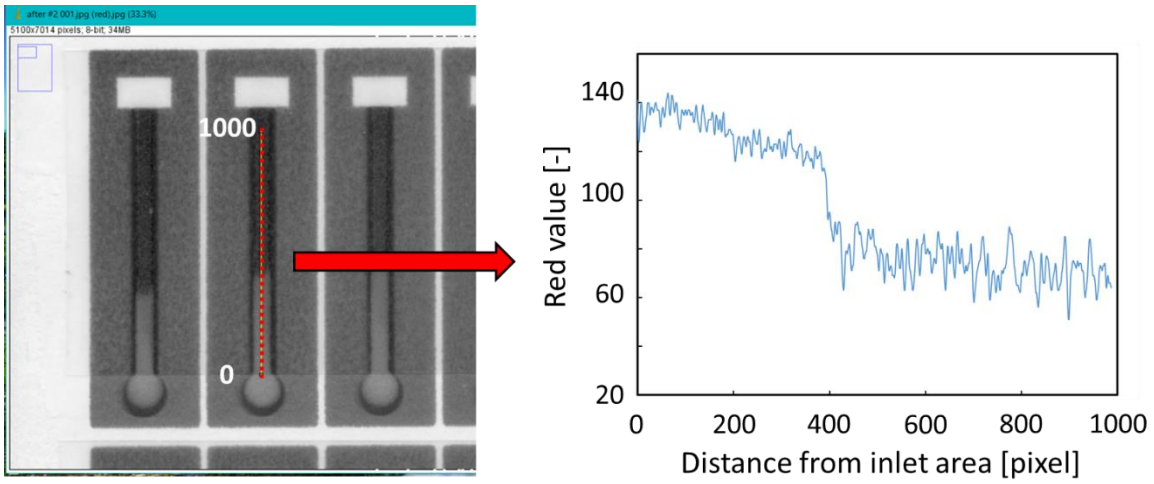

Figure 4-4. Procedure for obtaining colorimetric response profiles along a detection channel of color-developed μPADs; after extraction of the red color channel from a scanned image, the "smoothing" function of Image J was applied.

4.2.5. Ca^{2+} assay in water samples

All used mineral waters were purchased at a local convenience store. Tap water samples were collected from various local sources, followed by storage in plastic bottles. Complexometric titration to quantify the Ca^{2+} levels in water samples was performed with NN as the colorimetric indicator and 0.01 N aqueous EDTA titration solution as chelating reagent under strong basic condition using 8 N KOH. For spiking tests using tap water, spiked water samples (added Ca^{2+} levels: 0.3, 0.5, 0.7 mM) were prepared by mixing as-collected tap water with aqueous Ca^{2+} standard solutions in a 99:1 (v/v) ratio.

4.3. Results and discussion

4.3.1. Optimization of distance-based Ca^{2+} assays

A preliminary experiment revealed that 20 printing cycles (*i.e.* the amount of nano-optodes deposited with an inkjet printer) of the nano-optode ink was sufficient to obtain visual colorimetric changes (refer to **Figure 4-5** for the detailed experimental procedure and results). In the same manner with previously reported articles[16-17], the device sensitivity relied on the amount of printed nano-optodes (**Figure 4-5c**), indicating potential to moderate the dynamic range corresponding to analytical applications (e.g. biological fluids).

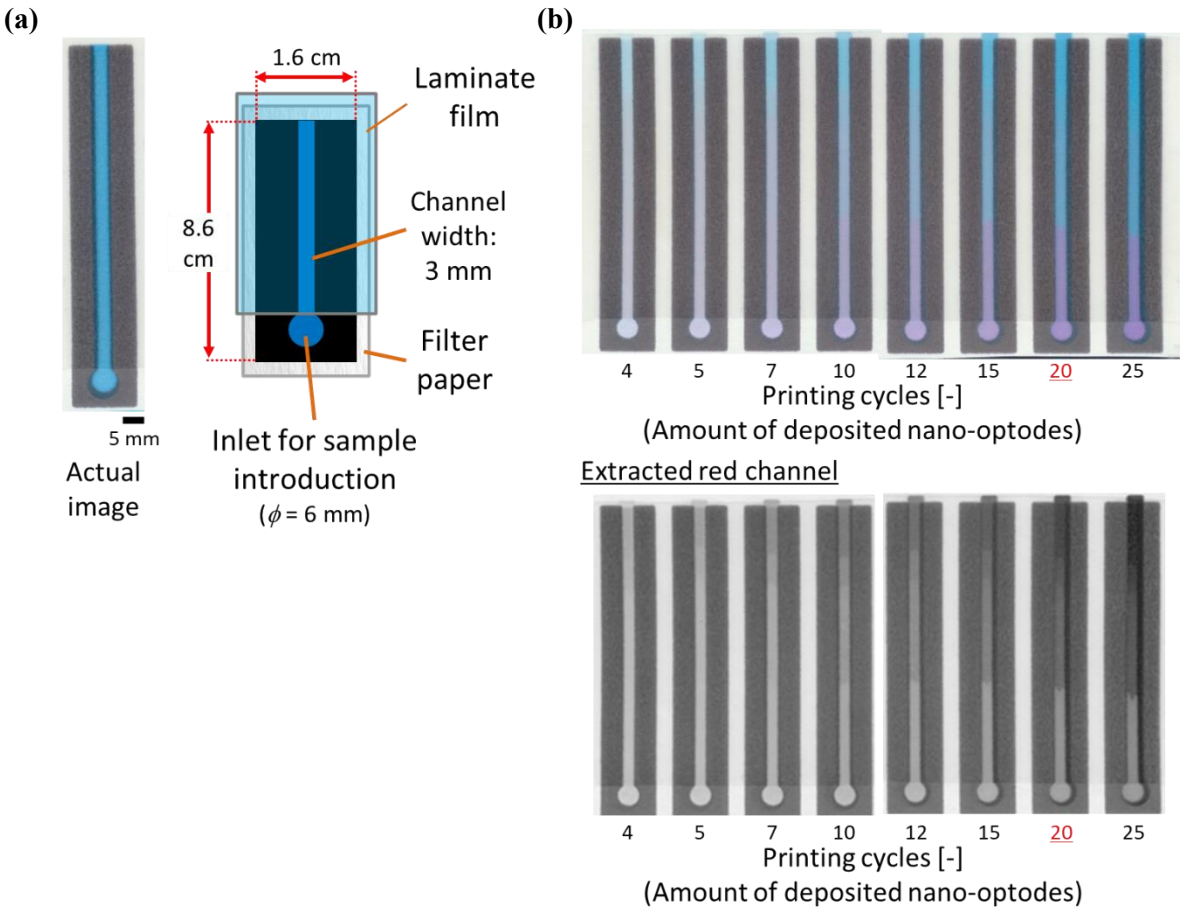

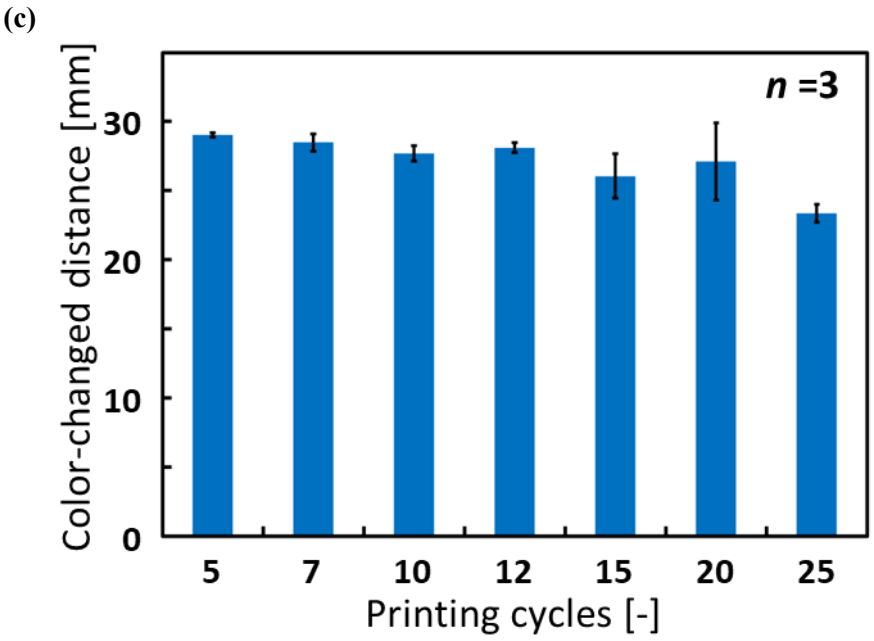

Figure 4-5. (a) Design of the developed distance-based μPADs for evaluation of the amount of nano-optodes: actual scanned image of a μPAD (left) and the corresponding dimensions (right). (b) Scanned images of distance-based μPADs with different amounts of printed nano-optodes (number of printing cycles: 4, 5, 7, 10, 12, 15, 20 and 25) 45 min after application of 30 μL of pH-buffered (50 mM HEPES-TMAOH buffer pH 7.0) 1.0 mM Ca^{2+} solution; (c) quantitative result of visible colorimetric signal corresponding to amount of printed nano-optodes (printing cycles).

However, it should be noted that **Figure 4-5c** did not show the significant difference depending on the amount of printed nano-optodes because the contribution of analyte extraction by nano-optodes was less than the interaction between cation analytes (*i.e.* Ca^{2+}) and a cationic paper surface (refer to **Section 4.3.4**). Typically, device geometry is also essential to consider the device sensitivity since large total area of a flow channel results in the decreased sensitivity. Hence, we confirmed the effect of a channel width on the response curves (**Figure 4-6**). The narrower channel width provided the longer visual colorimetric with same mass of Ca^{2+} in applied sample liquid because the areas of both a flow channel and nano-optodes were reduced. Although device sensitivity can be tuned by changing the channel width, narrower channel width resulted in the prolonged assay time because of the slow flow rate.

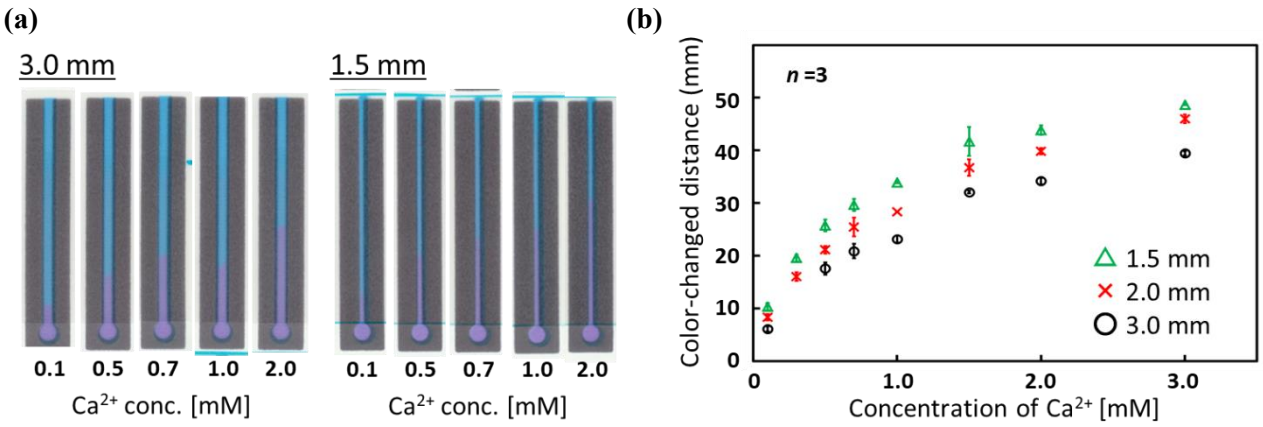

Figure 4-6. (a) Scanned images of distance-based μPADs with a different channel width (1.5, 2.0, and 3.0 mm) after application of 30 μL of pH-buffered (50 mM HEPES-TMAOH buffer pH 7.0) Ca^{2+} solution; (b) quantitative result of visible colorimetric signal corresponding to the paper devices with a different width.

Notably, the hydrophobic wax barriers defining the fluidic structure of the devices were not affected by the pre-deposited surfactant (nano-optode suspension), since no leakage of applied sample liquid was observed (refer to **Figure 4-7** for the detailed experimental procedure and results). Whereas manual deposition of nano-optode suspension by pipetting causes the occurrence of a coffee-ring effect after the evaporation of the water solvent,[35] inkjet-dispensed nano-optodes exhibit well-defined and homogeneous optode areas on the surface of the paper substrate (**Figure 4-8a, b**). The printed nano-optodes mainly reside in the filter paper

within a depth of approximately 120 µm from the printed surface, as seen in the cross-sectional microscope image shown in **Figure 4-8c**. Additionally, the advantageous capabilities of the filter paper substrate, such as its high porosity and surface area, were maintained for the unhindered liquid wicking character of the original hydrophilic substrate.

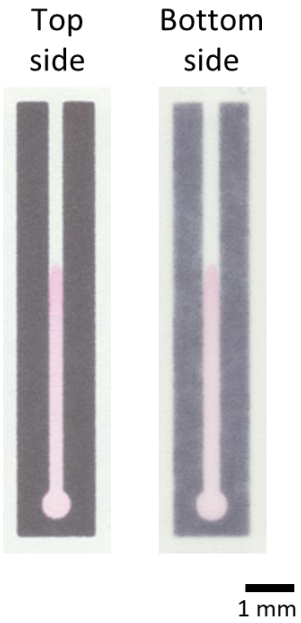

Figure 4-7. Evaluation of wax barrier resistance against the presence of surfactants: 30 µL of aqueous solution containing a food dye (0.02wt% acid red) was applied to an unlaminated µPAD containing surfactant (F-127) micelles printed from a magenta cartridge at 20 cycles to mimic the conditions found in Ca^{2+}-selective distance-based µPADs; the F-127 micelle ink suspension was prepared according to the same procedure as described for the preparation of Ca^{2+}-selective nano-optodes, however without the addition of sensing reagents (ionophore, chromoionophore, ion-exchanger).

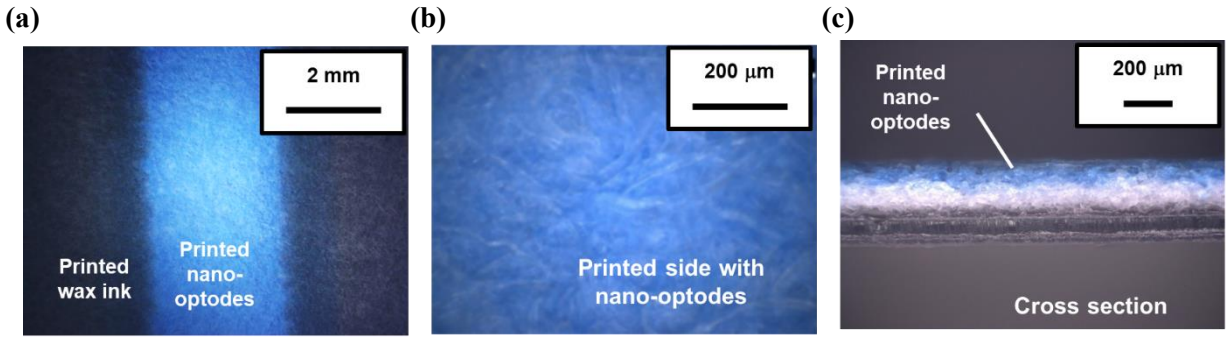

Figure 4-8. Microscope images of nano-optode filter paper substrates: (a) nano-optode modified paper surface of the flow channel; (b) scale-up of the nano-optode modified paper surface; and (c) cross section of nano-optode modified paper.

The appropriate amounts of chemical reagents for distance-based Ca^{2+} assays (e.g. pH-buffering reagents, pre-deposited $MgCl_2$ salt) were investigated. First, the influence of the amount of deposited pH-buffering reagents (250 mM HEPES-TMAOH buffer at pH 7.0) was evaluated. For this purpose, 4 different numbers of printing cycles (1, 2, 3 and 5 cycles) were tested with distance-based μPADs (results shown in **Figure 4-9**). The deposition of two or more printing cycles of the pH-buffer solution resulted in a high background signal indicated by the magenta color observable also in the absence of Ca^{2+}. This is probably because an excess quantity of cationic buffer components (*i.e.* TMA^+) affects the cation-exchange reaction of the nano-optodes by an uptake of buffer cations into the nano-optode phase and hence, the deprotonation of chromoionophore even in the absence of target cations. Therefore, one single printing cycle was selected as the optimal amount of deposited pH-buffering solution in device fabrication. Next, the effect of the amount of deposited $MgCl_2$ for improved sensitivity of μPADs was studied (refer to **Figure 4-10** for the quantitative response curves). In this work, $MgCl_2$ was deposited in the inlet area to compete in the non-specific interaction between the target cations (Ca^{2+}) and the cellulosic surface during capillary force-driven sample wicking, which results in improved sensitivity for the distance-based Ca^{2+} assay. The reason for this is further explained in the section discussing the interference study. $MgCl_2$ has been selected because the used Ca^{2+} ionophore has excellent selectivity against Mg^{2+},[41] so that the presence of this cation does not contribute to a colorimetric signal. The experimental results of **Figure 4-10** show that the response curves for Ca^{2+} are vertically shifted towards longer color-changed distances with increasing amounts of printed $MgCl_2$. However, excess amounts of deposited $MgCl_2$ (*i.e.* over 5 printing cycles) resulted in a high background signal upon the corresponding μPADs being exposed to the blank and 1 mmol L^{-1} of Ca^{2+} samples (refer to **Figure 4-11**), due to the extraction of Mg^{2+} into the Ca^{2+}-selective nano-optodes. Therefore, three printing cycles were selected as the appropriate amount of deposited $MgCl_2$ in subsequent experiments.

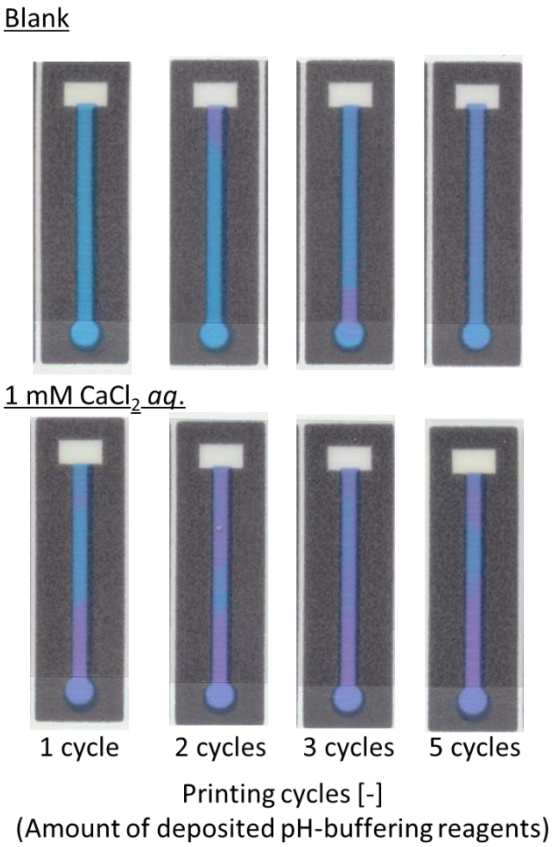

Figure 4-9. Evaluation of amounts of pH-buffering reagents (250 mM HEPES-TMAOH buffer pH 7.0) printed onto the inlet areas and the flow channels of µPADs (printing cycles of pH-buffering reagents: 1, 2, 3, 5 cycles); 30 µL of blank (pure H_2O) or 1 mM aqueous $CaCl_2$ solution was applied onto a µPAD.

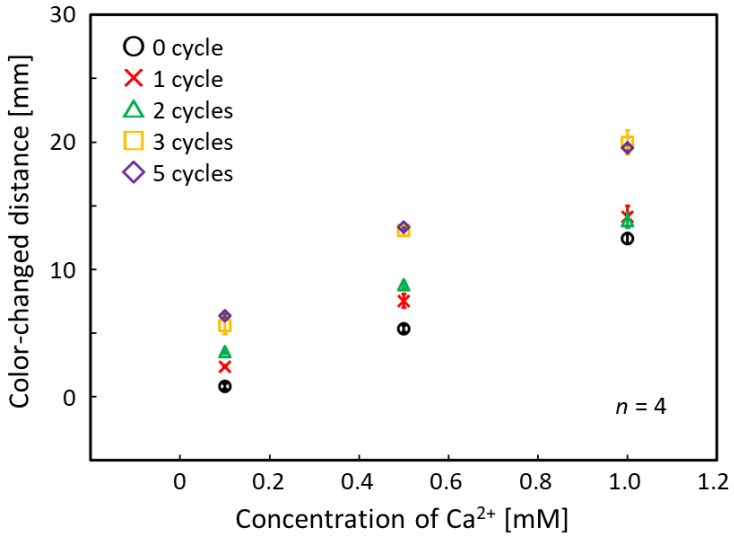

Figure 4-10. Evaluation of the amounts of $MgCl_2$ printed onto the inlet area of µPADs (printing cycles of $MgCl_2$: 0, 1, 3, 5 cycles); each data point has been obtained by measurements with 4 individual single-use distance-based µPADs; 30 µL of aqueous $CaCl_2$ solution was applied onto a µPAD; error bars indicate the standard deviations; incubation time: 45 min.

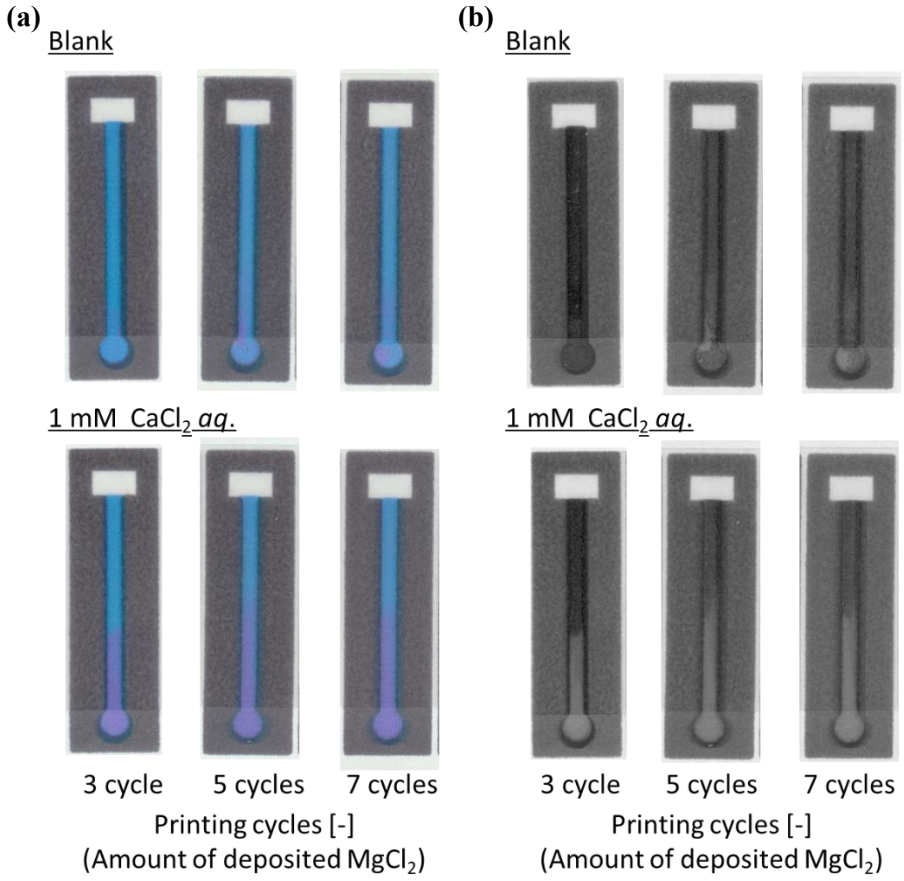

Figure 4-11. (a) Scanned images and (b) extracted red channel of distance-based μPADs with different amounts of printed $MgCl_2$ (number of printing cycles: 3, 5, 7) 45 min after application of 30 μL of blank sample (water) and 1.0 mM Ca^{2+} solution.

4.3.2. Distance-based Ca^{2+} assay

To confirm the distance-based colorimetric response of the developed μPADs, aqueous Ca^{2+} samples of various concentrations have been applied onto the paper devices (**Figure 4-12**). The developed μPADs showed a good correlation between the concentration of Ca^{2+} and the length of the color-developed nano-optode channel in the concentration range of 0-5.0 mM (**Figure 4-12**), making them ideally suited for the quantification of Ca^{2+} in drinking water samples according to the WHO (less than 5 mM) and International Organization for Standardization (0.05-2.5 mM) established recommendations. The batch-to-batch reproducibility of distance-based μPADs has been estimated by using response curves obtained with μPADs independently prepared on different days (**Figure 4-13a**). This data, together with the Pearson's correlation

analysis (r = 0.995-0.998) comparing the different batches with each other (**Figure 4-14**), confirms the high fabrication reproducibility of distance-based paper devices, which were independently fabricated on different days**.** For achieving calibration-free Ca^{2+} quantification by simply relying on a single color-changed distance measurement, this batch-to-batch reproducibility is one one of the most critical criteria for the successful practical application of μPADs. Additionally, it was also experimentally confirmed that the response curve obtained with the aid of scanned images and digital color analysis shows no significant difference from naked-eye visual readout by independent untrained volunteer users (**Figure 4-13b**). The corresponding Pearson's correlation analysis is summarized in **Figure 4-15**.

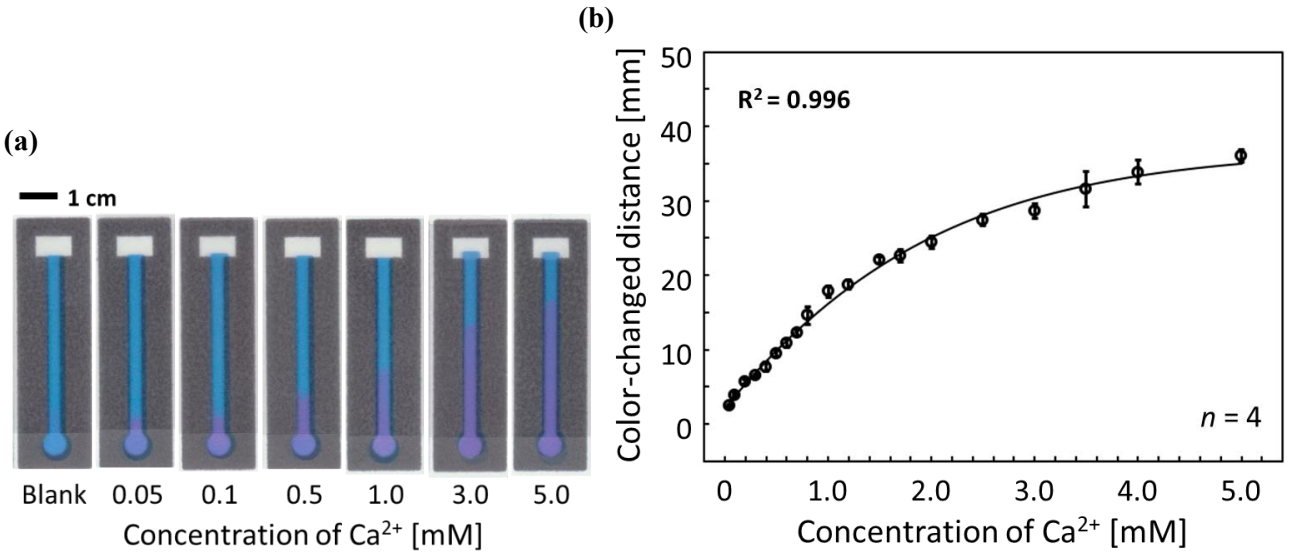

Figure 4-12. (a) Scanned images of color-developed μPADs after application of the corresponding Ca^{2+} solutions of various concentrations (30 μL of aqueous $CaCl_2$); (b) software-assisted response curve of a μPAD-based Ca^{2+} assay; the response curve represented by the solid line was obtained with a non-linear curve fit: $y = -124 + \frac{165}{1+\exp(-\frac{x-2.21}{1.99})}$; each data point has been obtained by measurements with 4 individual single-use devices; 30 μL of aqueous $CaCl_2$ solution applied; error bars indicate the standard deviations; incubation time: 45 min.

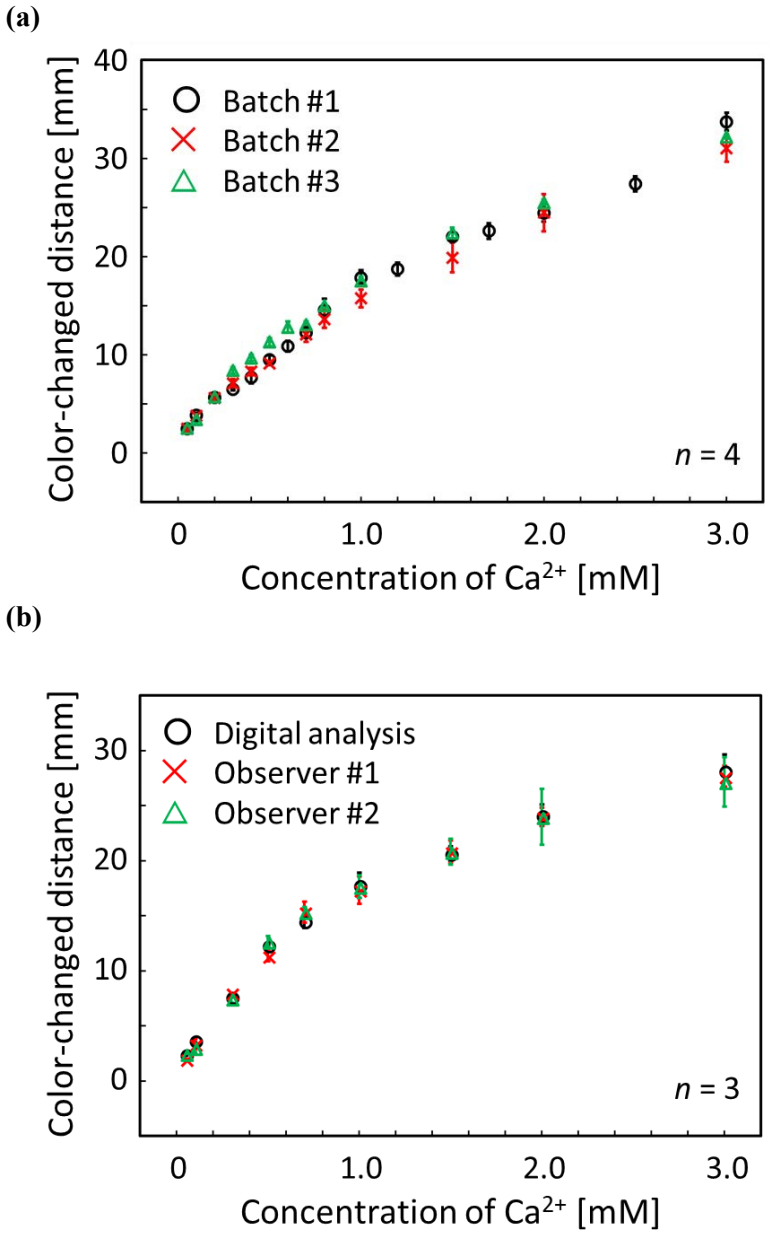

Figure 4-13. (a) Reproducibility evaluation of distance-based µPADs independently fabricated on different days for software-assisted Ca^{2+} quantification; each data point has been obtained by measurements with 4 individual single-use devices; 30 µL of aqueous $CaCl_2$ solution applied; error bars indicate the standard deviations; incubation time: 45 min; circle plots (batch #1) are identical to the data of **Figure 4-11b**; (b) response curves for distance-based Ca^{2+} detection obtained by scanner and software-assisted digital color analysis (circles) and individual user naked-eye readout (crosses and triangles); each data point has been obtained by measurements with 3 individual single-use devices; 30 µL of aqueous $CaCl_2$ solution applied; error bars indicate the standard deviations; incubation time: 45 min.

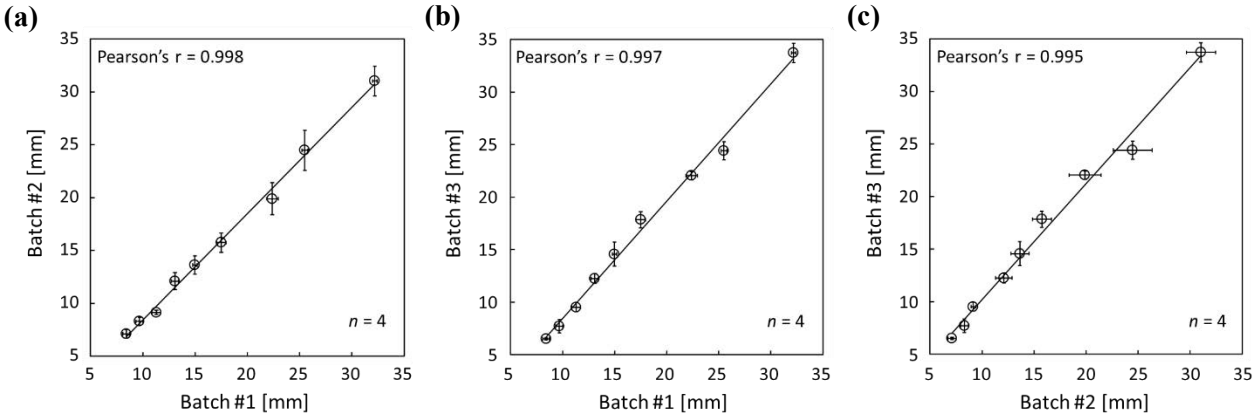

Figure 4-14. Comparison between different batches of fabricated μPADs; the underlying data is identical to **Figure 4-13a**.

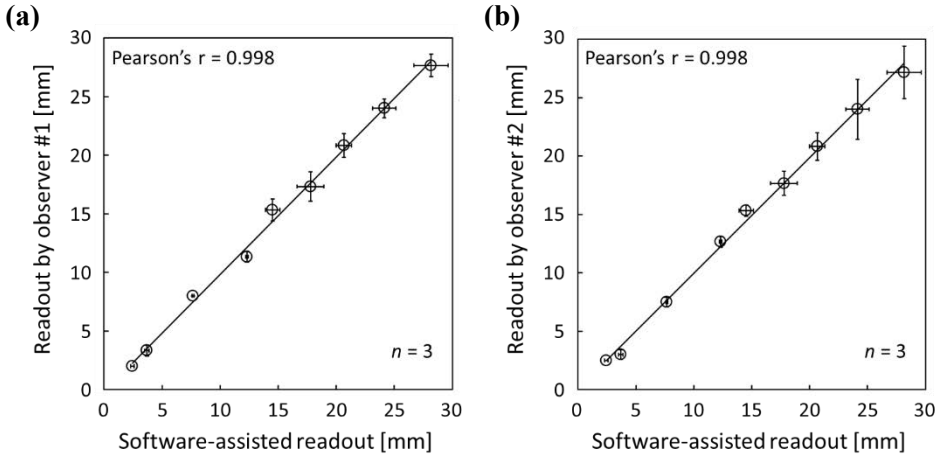

Figure 4-15. Comparison of Ca^{2+} assay results with distance-based μPADs between software-assisted readout and readouts by two individual observers; the underlying data is identical to **Figure 4-13b**.

To address the analytical capabilities of the μPADs, the lowest naked-eye detectable concentrations were compared with those achieved with commercial colorimetric paper dipsticks. The assay procedure applied for commercial paper dipsticks and the colorimetric changes corresponding to various Ca^{2+} concentrations are shown in **Figure 4-16**. In this study, the LOD was defined as the lowest concentration observable by naked eye as a visual color change instead of the classical 3σ method, since a blank sample does not generate any optical signal on distance-based μPADs (*i.e.* blank signal distance = 0 mm). From **Table 4-1**, it can be concluded that the developed distance-based μPADs resulted in lower LOD (0.05 mM) than commercial colorimetric paper dipsticks for the Ca^{2+} assay shown in **Figure 4-16b** (0.1 mM). Furthermore, it should be

noted that commercial paper dipsticks require a multi-step procedure, including sample pretreatment by reagent addition (**Figure 4-16a**). Thus, the distance-based µPADs represent sensitive and user-friendly tools for the instrument-free and single-step determination of Ca^{2+} concentrations.

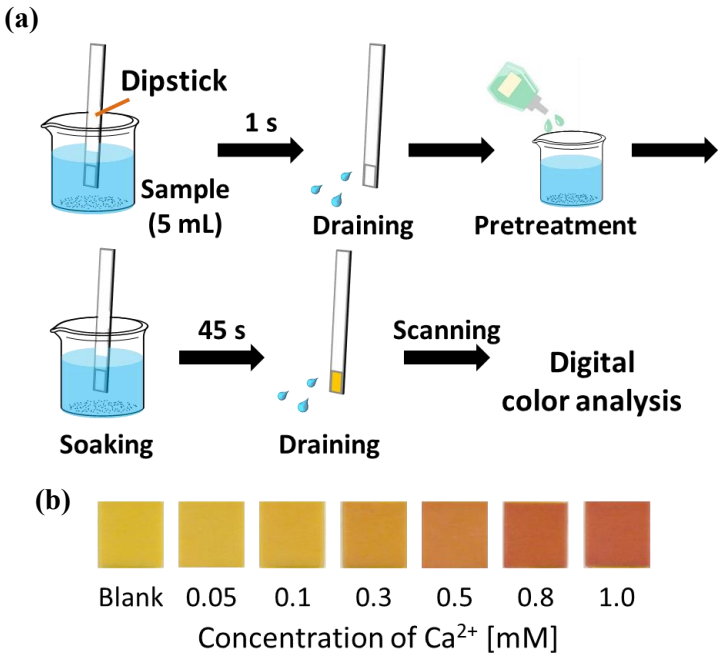

Figure 4-16. (a) Assay procedure applied for commercial colorimetric paper dipstick for Ca^{2+} according to the attached user manual; (b) Scanned images of the commercial test strips after exposure to the corresponding Ca^{2+} concentrations.

Table 4-1. Determination of the lowest naked-eye detectable Ca^{2+} concentration with commercial paper dipsticks.

Observer #	Concentration of Ca^{2+} [mM]				
	0	0.05	0.1	0.2	0.3
#1	-	-	✓	✓	✓
#2	-	-	✓	✓	✓
#3	-	-	✓	✓	✓
#4	-	-	✓	✓	✓

"-" and "✓" stand for "unobservable color change" and "observable color change", respectively, read out by 4 independent users; before comparing each sample exposed dipstick to a reference dipstick (*i.e.* exposed to blank), the color code reference of the user manual was used for user instruction.

Despite their improved sensitivity for selective naked-eye determination of Ca^{2+} in mineral or tap water, the proposed distance-based paper devices require a relatively long assay time (45 min) to acquire the

quantitative optical signal. It is a general drawback that distance-based detection motifs need a prolonged time for assay completion due to the slow transport of sample liquid by capillary force: up to 45 min have also been reported by others for several centimetres of detection channel length.[16-17, 20] In addition, distance-based colorimetric signalling relies on analyte depletion during sample transport, either by binding to a specific receptor[16] or by interaction with the paper substrate, as it is the case in the current work. This can only be achieved with sample liquids being slowly transported through the cellulose fibre network of the paper substrate.

On the other hand, the distance-based colorimetric signal achieved with the present system is stable over time (up to approximately 2 h) so that a user is not forced to continuously monitor the device during an assay, which allows for so-called "walk-away assays" that require nothing more than the application of the sample. While it is clear that in general a more rapid assay time is desirable, the 45 min assay time is not hindering practical use of the proposed devices. A possible perspective to reduce assay times is the shortening of flow channels. However, this would result in narrowing of the dynamic response range and reducing the signalling resolution. Alternatively, converting a color intensity-based approach into a distance readout referred to as "dip-and-read distance-based assay" as we have recently reported,[20] might allow nearly instantaneous signal detection, although probably at lower resolution. Furthermore, dipping time dependent result variations would have to be expected, due to the dissolution of buffer salts required for maintaining a constant pH value.

4.3.3. Interference study on distance-based Ca^{2+} assay

The selectivity of the Ca^{2+}-selective μPADs has been qualitatively validated by using aqueous samples of various metal cations (Na^+, K^+, Li^+, Mg^{2+}, Zn^{2+}, Cu^{2+}, Ni^{2+}, Hg^{2+} and Al^{3+}). In this assay, different concentrations of each interfering ion were evaluated on the μPADs and scanned images of devices exposed to the corresponding cation samples are summarized in **Table 4-2**. **Table 4-2** lists the experimentally evaluated maximal concentrations of interfering ions that do not result in a visually recognizable development of a

color-changed area. Such tolerance against potentially interfering cations (e.g. Na^+, K^+, Mg^{2+}) is comparable to the performance of plasticised PVC-based ISOs using the same ionophore.[41] Additionally, a competitive assay was performed by quantifying the concentration of Ca^{2+} (1 mM) in the presence of a mixture of Na^+ or Mg^{2+} in aqueous solution (refer to **Figure 4-17**). 30 µL of aqueous Ca^{2+} sample (1 mM) containing various concentrations of Na^+ or Mg^{2+} (0, 0.5, 1, 3 and 5 mM) was applied onto the fabricated Ca^{2+}-selective µPAD. After the incubation for 45 min under ambient condition, the generated distance-based signal was quantified with ImageJ software in the same manner as for Ca^{2+} assays. The color-changed distance was slightly extended by the presence of these cations at concentrations above 3 mM or 1 mM for Na^+ or Mg^{2+}, respectively. It is assumed that changes in the color-changed distance in mixed sample solutions containing Na^+ or Mg^{2+} are not caused by a lack of selectivity of the nano-optodes on the paper substrate, as confirmed by the data in **Table 4-2**. As others have already reported,[35] elevated ionic strengths of samples potentially cause a corresponding increase in viscosity with a decrease in flow velocity, resulting in the extension of length-based signals. However, the amounts of added cations (Na^+ or Mg^{2+}) in the current work are rather unlikely to result in an increase in the viscosity of the applied sample liquid.[35] Therefore, the presence of 1 mM or higher Mg^{2+} or 3 mM or higher Na^+ is assumed to cause an extended color-changed distance mainly due to increased competition for anionic binding sites on the paper surface between the Ca^{2+} target analyte and the other cations, as further outlined below.

Table 4-2. Tolerance levels for potentially interfering cations.

Interfering ions	Tolerance [mM]	Interfering ions	Tolerance [mM]
Na^+	100	Cu^{2+}	1000
K^+	100	Ni^{2+}	100
Li^+	100	Hg^{2+}	100
Mg^{2+}	100	Al^{3+}	1000
Zn^{2+}	1		

Cl^- was used as counter anion for preparation of all samples

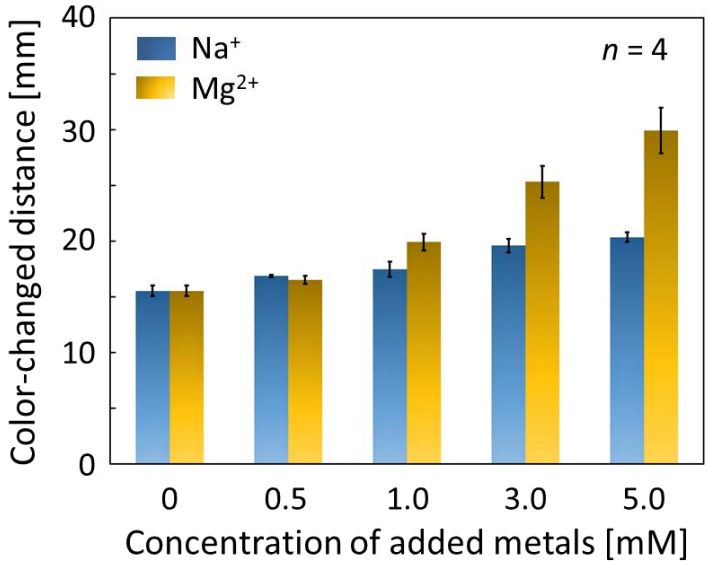

Figure 4-17. Result of Ca^{2+} concentration readout in the presence of potentially interfering cations (Na^+ and Mg^{2+}). The amount of Ca^{2+} was fixed at 1 mmol L^{-1}, whereas the amount of the interfering cations was varied (from 0 mM to 5 mM); each data point has been obtained by measurements with 4 individual single-use distance-based μPADs; error bars indicate the standard deviations.

4.3.4. Detection principle of distance-based readoutforCa^{2+}

Typically, non-specific adsorption onto a cellulosic surface results from reversible noncovalent interactions, such as van der Waals, electrostatic or hydrophobic interactions or hydrogen bonding.[42] The strength of this interaction varies corresponding to the experimental conditions (e.g. target analytes, pH, ionic strength, and others). It is postulated that the adsorption of Ca^{2+} to the paper substrate is the primary cause for the analyte concentration-dependent changes in color-changed distance, rather than the depletion of the target cation by extraction into the optode phase. To verify this hypothesis, various concentrations of pH-buffered

Ca^{2+} samples were applied onto a simple paper channel with/without sensing reagents (*i.e.* nano-optodes) as shown in **Figure 4-18a**. To visualize sample transport in a reagent-free paper channel (**condition 1**), Ca^{2+}-selective nano-optodes were inkjet-printed onto the channel after exposure to Ca^{2+} samples. The quantitative data of **Figure 4-18b** clearly shows that distance-based readout was achieved also in the absence of nano-optodes during sample flow through the detection channel (**condition 1**). Hence, it can be concluded that distance-based quantification in this work relies on the non-specific adsorption of Ca^{2+} onto the paper substrate. On the other hands, it can be found that concentration-corresponding distances obtained from reagent-free paper channels (**condition 1**) were slightly shorter than the result of **condition 2** probably because of the slow flow rate of applied sample. Additionally, the color change of nano-optodes of **condition 1** is weaker than **condition 2**, indicating the less amount of reacted nano-optodes. In **condition 1**, nano-optodes extracted the target analytes only during printing process (1 printing cycle for several seconds).

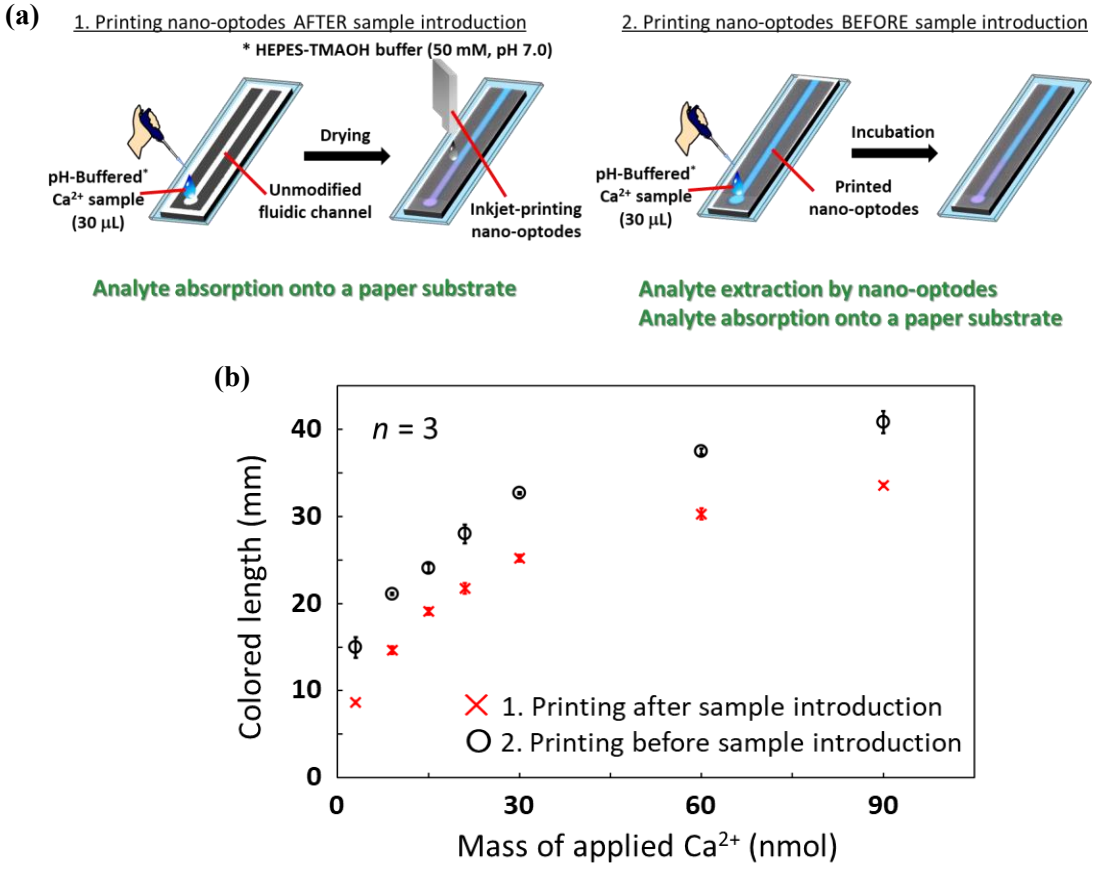

Figure 4-18. (a) Experimental procedure to verify the adsorption of Ca^{2+} onto a paper substrate; (b) software-assisted response curve for corresponding Ca^{2+} detection; each data point has been obtained by measurements with 3 individual

single-use devices; 30 μL of pH-buffered Ca^{2+} sample applied; error bars indicate the standard deviations.

For simple estimation of the flow rate based on capillary force, Lucas-Washburn equation, which exhibits the timi-dependent distance moved by the liquid front (L), has been generally used[43]:$L = \sqrt{\frac{r\gamma \cos\theta}{2\eta} t}$, where, r represents the pore size of a paper substrate, γ represents the surface tension of sample liquid, η represents the viscosity of sample liquid, θ represents the contact angle between the penetrating liquid and the solid, and t represents time. Here, Lucas-Washburn equation's terms can be categorized into the two factors related to the character of (i) a microfluidic material (e.g. r and θ) and (ii) the applied sample liquid (e.g. γ and η). In the **condition 1**, the presence of the hydrophobic sensing reagents (*i.e.* nano-optodes) on a paper channel prevented rapid sample flow by increasing the contact angle (θ), resulting in the shorter color-changed length. Then, we address the effect of the whole device lamination on the response curve (**Figure 4-19**). Although unlaminated devices (red triangles) did not have the sufficient capacity to maintain the applied sample droplet on the inlet area, the response curve of laminated devices (black circles) was vertically shifted. This is because pressing process during the device lamination decreased pore size of a paper substrate (r), resulting in slow flow rate to shorten the color-changed length. In contrast to the characters of a microfluidic material, the characters of the applied sample liquid did not provide significant difference on response curve, such as the viscosity of sample liquid corresponding to the target concentration[35] and the surface tension affected by the presence of surfactants with printed nano-optodes (**Figure 4-20**).

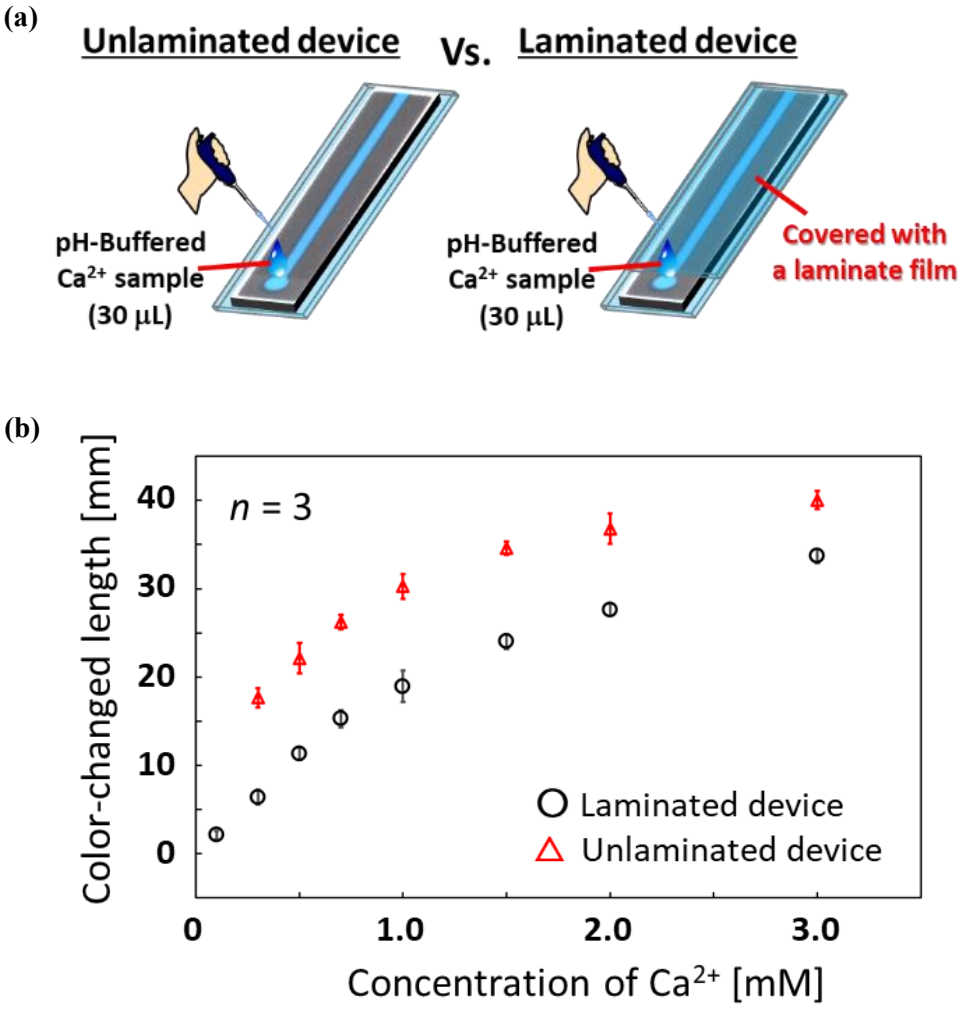

Figure 4-19. Estimation of whole device lamination effect on the Ca^{2+} response of distance-based readout; (a) schematic experimental procedure; (b) software-assisted response curve to comparison between laminated devices and unlaminated devices; each data point has been obtained by measurements with 3 individual single-use devices; 30 μL of pH-buffered Ca^{2+} solution applied; error bars indicate the standard deviations; incubation time: 45 min.

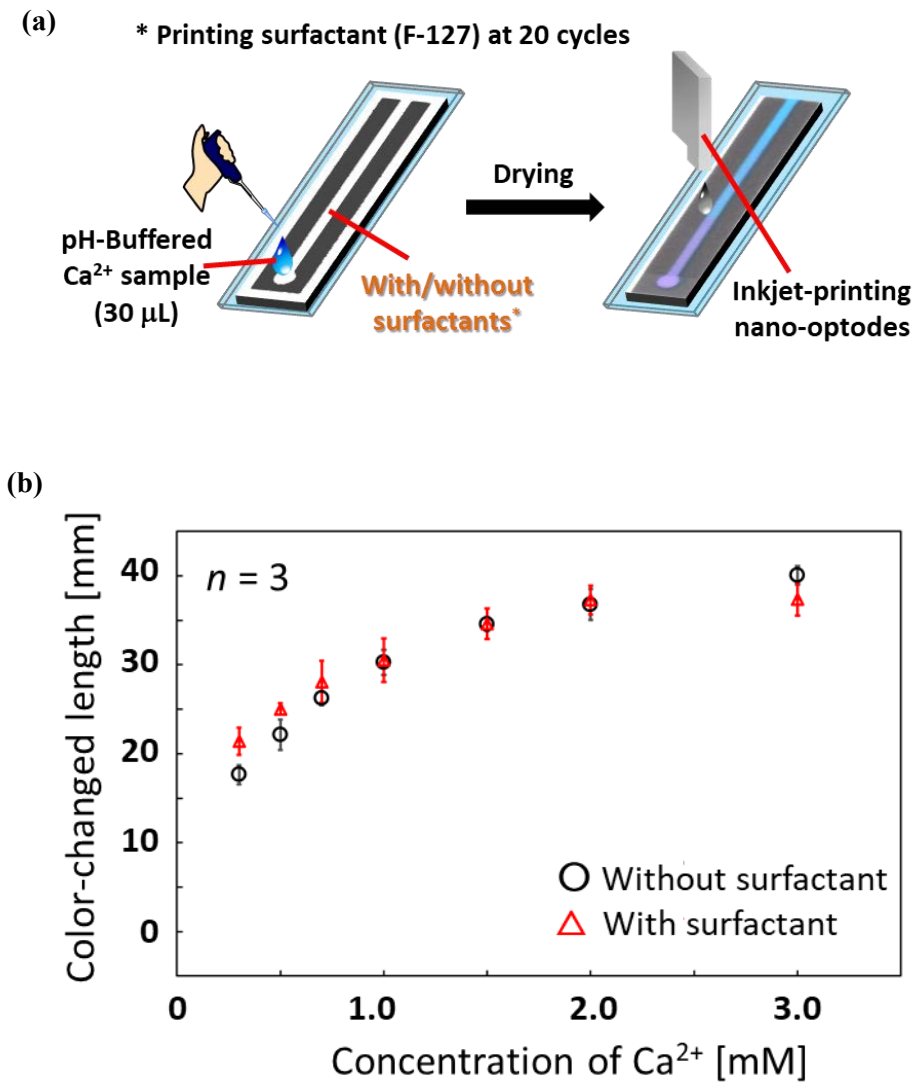

Figure 4-20. Estimation of the effect of printed surfactants on the device response; (a) experimental procedure; F-127 surfactants (0.56 g/L) were inkjet printed onto a reagent-free paper device at 20 printing cycles; (b) software-assisted response curve for distance-based Ca^{2+} detection by paper devices with/without surfactants of nano-optodes; each data point has been obtained by measurements with 3 individual single-use devices; 30 µL of pH-buffered Ca^{2+} solution applied; error bars indicate the standard deviations; incubation time: 45 min.

As mentioned before, distance-based detection in this work relied on the analyte adsorption onto the surface of a paper substrate. It is known that the degree of cation transport is modulated by the presence of ionizable sites on cellulosic paper surfaces (mostly carboxyl groups).[29-30, 44] In this work, the amount of binding sites derived from the ionizable groups on the paper surface (311 nmol) are significantly abundant compared with binding sites of printed nano-optodes (18 nmol). A significant amount of carboxyl groups (mmol/kg order[29, 45]) is produced by oxidation of cellulosic hydroxyl groups during the industrial paper

making process.[46] Therefore, the surface of filter paper is negatively charged as demonstrated in previously reported articles.[33, 47] The electrostatic interaction between a cationic analyte (e.g. Ca^{2+} in this work) and the anionic paper surface results in the adsorption of target cations onto the filter paper surface.[44, 48-49] In this adsorption process, the pre-deposited Mg^{2+} competes with the Ca^{2+} analyte for the available binding sites on the paper surface. In addition, the adsorption of metal cations, which is described by a Langmuir adsorption isotherm model, is affected by the ionic strength of the sample liquid.[50] Since the pre-deposited Mg^{2+} also contributes to an increase in ionic strength of the flowing liquid, this leads to decreased adsorption of metal cations onto the paper surface in the same manner with paper-based chromatographic separation[45]. The pre-deposited Mg^{2+} provides a relatively high but constant ion background, in order to avoid undesired modulation in non-specific Ca^{2+} adsorption due to sample-induced, non Ca^{2+}-related competition for binding sites or changes in ionic strength. The tolerance against interfering cations relies on the total amount of ionised electrolytes (*i.e.* pH-buffering reagents, $MgCl_2$ on the sample inlet). For drinking or natural water assays, the WHO guideline addresses the threshold values for multiple ions, including those potentially interfering with the current Ca^{2+} assay. The values of taste or health-based thresholds are all well below the amounts that can be tolerated by the developed μPAD[1] and are therefore expected not to interfere with the distance-based Ca^{2+} assay.

4.3.5. Ca^{2+} assays in mineral and tap water samples

The practical applicability of the developed distance-based μPADs was investigated by determining Ca^{2+} levels in mineral water or tap water samples without any sample pretreatment. **Table 4-3** summarises the concentrations of Ca^{2+} measured with μPADs and the classical complexometric titration method, with an intermethod result agreement ranging from +15% to -5%. The Pearson's correlation analysis (**Figure 4-21a**) and the Bland-Altmann method comparison plot (**Figure 4-21b**) indicate a good agreement between the two independent methos and confirm the suitability of the μPAD for reliable determination of Ca^{2+} levels in real water samples. In the case of Ca^{2+} analysis using mineral water sample #4, the observed standard deviation

(**Table 4-3**) was slightly higher than for other samples, due to lower device sensitivity in the higher concentration range. For the same reason, the corresponding sample is found outside the 95% limit of agreement in the Bland-Altmann plot of **Figure 4-21b**. Notably, the distance-based μPADs allow to detect low Ca^{2+} concentration levels (mM order), which are out of reach for recently published colorimetric μPADs that do not use optical signal readout instruments[22].

Table 4-3. Determination of Ca^{2+} concentrations in mineral or tap waters with distance-based μPADs and classical complexometric titration.

Sample	Distance-based μPADs (mM)[a]	Complexometric titration (mM)[b]	Error[c] (%)
Mineral water			
#1	0.43±0.03	0.43±0.01	0
#2	0.25±0.03	0.23±0.01	+6
#3	0.21±0.02	0.21±0.01	+2
#4	1.96±0.13	2.05±0.01	-5
Tap water			
#1	0.46±0.03	0.41±0.02	+10
#2	0.48±0.03	0.45±0.01	+6
#3	0.51±0.03	0.44±0.01	+15
#4	0.39±0.01	0.35±0.01	+12

[a] Each data has been obtained by measurements with 4 individual single-use devices, [b] each data has been obtained by 3 individual titrations, [c] error estimated by comparing with the experimental results obtained by complexometric titration as reference values.

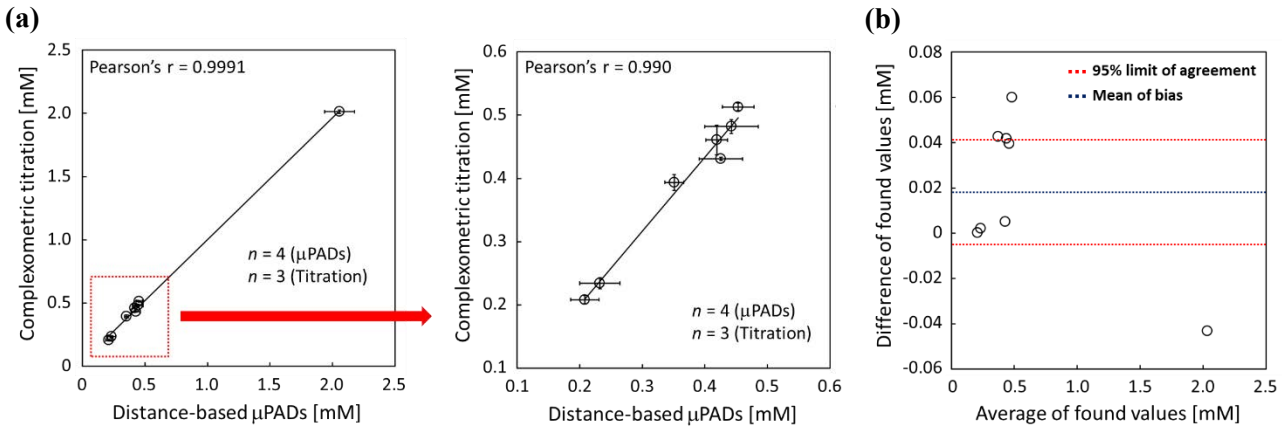

Figure 4-21. (a) Comparison between Ca^{2+} measurements by distance-based μPADs and complexometric titration; the plots and error bars represent the average and standard deviations of 4 (μPADs) and 3 (titration) repetitions; (b) Bland-Altmann analysis for eight Ca^{2+} samples quantified by μPADs and complexometric titration; the underlying data is identical to **Table 4-3**.

To further investigate the capability of the distance-based μPADs, quantification of Ca^{2+} levels in spiked tap water samples was carried out by multiple independent observers. The as-collected tap water (tap water #4 shown in **Table 4-3**) as well as 3 spiked samples were applied onto μPADs and the resulting length of the color-changed detection channel was measured by a ruler with sample exposed μPADs presented to observers in a random order. Before testing, the volunteers were instructed on the readout method using one example of a color-changed μPAD. **Figure 4-22** shows the visually read out results for various concentrations of Ca^{2+} in tap water or spiked tap water samples. Due to the subjective interpretation of the distance-based signals, some differences between individual observers are unavoidable. Overall, the visually detected distance-based signals were within +23% to -11% of the ImageJ software-assisted readout results. The color blurring in the detection of high-concentration Ca^{2+} occurred, potentially preventing obvious interpretation by users (for example, see **Figure 4-12a**). One of the approaches to overcome this issue is controlling the amount of sensing reagents (*i.e.* nano-optodes). Printing-based dispense enables to change the ejected ink volumes flexibly, corresponding to the color intensity on a software (e.g. magenta value). In previously reported article[17], graduation printing has been applied to improve the linearity of the response curve. In this work, increasing the amount of nano-optodes in the end of a detection channel potentially improve the visibility for

the signal interpretation. Another strategy is introduction of color manipulation. The visual colorimetric change based on ISOs relies on chromoionophores, therefore, introduction of chromoionophores with effective color variations (e.g. yellow to blue) potentially improves the visual interpretation in distance-based detection while we have to pay attention to pK_a of chromoionophores. For this purpose, digital color analysis (DCA) can help to simulate the optimum color variations for development of obvious visual readout.[51] In this publication, a screening indicator has been applied to produce the colorimetric change passing through a colorless gray point that serves to recognize visually at a certain point. As another technique, color screening filter is useful to manipulate the visual color by overlapping on the paper device.[52-53] Although this technique is affected by ambient light conditions (e.g. light source, wet/dry condition of the paper devices), it is relatively simple technique requiring no modification of the device design.

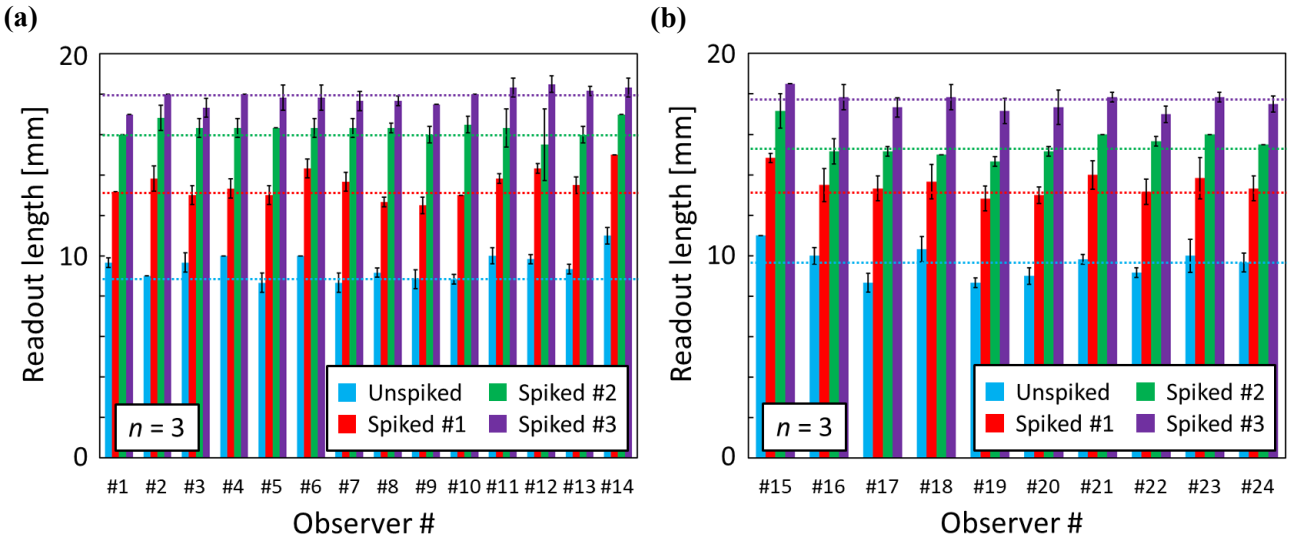

Figure 4-22. Naked-eye observer readout of length of color-changed detection channels from distance-based μPADs after Ca^{2+} assays of a tap water sample; different batches of μPADs were used for data shown in panels (a) and (b); the data represent the mean and standard deviations of 3 independent readouts by 24 observers; the corresponding color-change lengths obtained with the aid of scanned images and digital color analysis are indicated by the dotted horizontal lines with a color corresponding to the legend.

4.4. Conclusion

In this study, fully-printed distance-based microfluidic paper-based analytical devices (μPADs) for simple and reliable determination of Ca^{2+} levels by means of ionophore-doped ion-selective optode nanospheres (nano-optodes) have been demonstrated for the first time. Water-dispersible nano-optodes, which no longer require a volatile organic solvent, allowed for simple desktop thermal inkjet printing-based fabrication of μPADs. Highly batch-to-batch reproducible and reliable devices for naked-eye Ca^{2+}-selective assays have been obtained. The developed distance-based μPADs have been successfully applied to visual instrument-free quantification of Ca^{2+} in drinking or tap water samples, with no significant differences compared to classical complexometric titration. It has been experimentally shown that the tolerance of the paper-based devices against other potentially interfering cations was sufficient for Ca^{2+} determination in real world water samples. Notably, the μPADs provided improved lowest naked-eye detectable concentrations of Ca^{2+} (0.05 mM), compared to known colorimetric approaches. Although a relatively long assay time (45 min) is required to acquire the quantitative optical signal, we believe that our current work contributes to the further development of inexpensive, equipment-free, easy-to-handle, accurate and highly batch-to-batch reproducible analytical devices for on-site quantification of Ca^{2+} and other cations in real samples.

References

1. WHO, G., Guidelines for drinking-water quality. *World Health Organization* **2011,** *216*, 303-4.

2. Zulkifli, S. N.; Rahim, H. A.; Lau, W.-J., Detection of contaminants in water supply: A review on state-of-the-art monitoring technologies and their applications. *Sens. Act. B* **2018,** *255*, 2657-2689.

3. Almeida, M. I. G.; Jayawardane, B. M.; Kolev, S. D.; McKelvie, I. D., Developments of microfluidic paper-based analytical devices (μPADs) for water analysis: A review. *Talanta* **2018,** *177*, 176-190.

4. International Organization for Standardization, G., Water quality - Determination of calcium content -- EDTA titrimetric method. *ISO 6058,* **1984**.

5. Yappert, M. C.; DuPre, D. B., Complexometric titrations: Competition of complexing agents in the determination of water hardness with EDTA. *J. Chem. Educ* **1997,** *74* (12), 1422.

6. Martinez, A. W.; Phillips, S. T.; Butte, M. J.; Whitesides, G. M., Patterned paper as a platform for inexpensive, low‐volume, portable bioassays. *Angew. Chem. Inter.l Ed.* **2007,** *46* (8), 1318-1320.

7. Martinez, A. W.; Phillips, S. T.; Wiley, B. J.; Gupta, M.; Whitesides, G. M., FLASH: a rapid method for prototyping paper-based microfluidic devices. *Lab Chip* **2008,** *8* (12), 2146-2150.

8. Yetisen, A. K.; Akram, M. S.; Lowe, C. R., Paper based microfluidic point-of-care diagnostic devices. *Lab on Chip* **2013,** *13* (12), 2210-2251.

9. Yang, Y.; Noviana, E.; Nguyen, M. P.; Geiss, B. J.; Dandy, D. S.; Henry, C. S., Based Microfluidic Devices: Emerging Themes and Applications. *Anal. Chem.* **2016,** *89* (1), 71-91.

10. Nilghaz, A.; Guan, L.; Tan, W.; Shen, W., Advances of Paper-Based Microfluidics for Diagnostics The Original Motivation and Current Status. *ACS Sens.* **2016,** *1* (12), 1382-1393.

11. Yamada, K.; Shibata, H.; Suzuki, K.; Citterio, D., Toward practical application of paper-based microfluidics for medical diagnostics: state-of-the-art and challenges. *Lab Chip* **2017,** *17* (7), 1206-1249.

12. Meredith, N. A.; Quinn, C.; Cate, D. M.; Reilly, T. H.; Volckens, J.; Henry, C. S., Paper-based analytical devices for environmental analysis. *Analyst* **2016,** *141* (6), 1874-1887.

13. Lin, Y.; Gritsenko, D.; Feng, S.; Teh, Y. C.; Lu, X.; Xu, J., Detection of heavy metal by paper-based microfluidics. *Biosens. Bioelectron.* **2016,** *83*, 256-266.

14. Sriram, G.; Bhat, M. P.; Patil, P.; Uthappa, U. T.; Jung, H.-Y.; Altalhi, T.; Kumeria, T.; Aminabhavi, T. M.; Pai, R. K.; Kurkuri, M. D., Paper based microfluidic analytical devices for colorimetric detection of toxic ions: A review. *TrAC Trends Anal. Chem.* **2017,** *93*, 212-227.

15. Xu, Y.; Liu, M.; Kong, N.; Liu, J., Lab-on-paper micro-and nano-analytical devices: Fabrication, modification, detection and emerging applications. *Microchim. Acta* **2016,** *183* (5), 1521-1542.

16. Cate, D. M.; Dungchai, W.; Cunningham, J. C.; Volckens, J.; Henry, C. S., Simple, distance-based measurement for paper analytical devices. *Lab Chip* **2013,** *13* (12), 2397-2404.

17. Cate, D. M.; Noblitt, S. D.; Volckens, J.; Henry, C. S., Multiplexed paper analytical device for quantification of metals using distance-based detection. *Lab Chip* **2015,** *15* (13), 2808-2818.

18. Hossain, S. Z.; Brennan, J. D., β-Galactosidase-based colorimetric paper sensor for determination of heavy metals. *Anal. Chem.* **2011,** *83* (22), 8772-8778.

19. Tan, W.; Zhang, L.; Shen, W., Low-Cost Chemical-Responsive Adhesive Sensing Chips. *ACS Appl. Mater. Interfaces* **2017,** *9* (48), 42366-42371.

20. Yamada, K.; Citterio, D.; Henry, C. S., "Dip-and-read" paper-based analytical devices using distance-based detection with color screening. *Lab Chip* **2018**, *18*, 1485-1493.

21. Ostad, M. A.; Hajinia, A.; Heidari, T., A novel direct and cost effective method for fabricating paper-based microfluidic device by commercial eye pencil and its application for determining simultaneous calcium and magnesium. *Microchem. J.* **2017,** *133*, 545-550.

22. Karita, S.; Kaneta, T., Chelate titrations of Ca^{2+} and Mg^{2+} using microfluidic paper-based analytical devices. *Anal. Chim. Acta* **2016,** *924*, 60-67.

23. Jarujamrus, P.; Malahom, N.; Puchum, S.; Meelapsom, R.; Amatatongchai, M.; Siripinyanond, A.; Chairam, S.; Kulsing, C., Complexometric and argentometric titrations using thread-based analytical devices. *Talanta* **2018,** *183*, 228-236.

24. Mistlberger, G.; Crespo, G. A.; Bakker, E., Ionophore-Based Optical Sensors. *Annual Review of Anal. Chem.* **2014,** *7* (1), 483-512.

25. Xie, X.; Bakker, E., Ion selective optodes: from the bulk to the nanoscale. *Anal. Bioanal. Chem.* **2015,** *407* (14), 3899-3910.

26. Mikhelson, K.; Peshkova, M., Advances and trends in ionophore-based chemical sensors. *Russ. Chem. Rev.* **2015,** *84* (6), 555.

27. Bakker, E.; Bühlmann, P.; Pretsch, E., Carrier-Based Ion-Selective Electrodes and Bulk Optodes. 1. General Characteristics. *Chem. Rev.* **1997,** *97* (8), 3083-3132.

28. Erenas, M. M.; de Orbe-Payá I.; Capitan-Vallvey, L. F., Surface Modified Thread-Based Microfluidic Analytical Device for Selective Potassium Analysis. *Anal. Chem.* **2016,** *88* (10), 5331-5337.

29. Shibata, H.; Henares, T. G.; Yamada, K.; Suzuki, K.; Citterio, D., Implementation of a plasticized PVC-based cation-selective optode system into a paper-based analytical device for colorimetric sodium detection. *Analyst* **2018**.

30. Soda, Y.; Shibata, H.; Yamada, K.; Suzuki, K.; Citterio, D., Selective Detection of K^+ by Ion-Selective Optode Nanoparticles on Cellulosic Filter Paper Substrates. *ACS Appl. Nano Mater.* **2018**.

31. Wang, X.; Qin, Y.; Meyerhoff, M. E., based plasticizer-free sodium ion-selective sensor with camera phone as a detector. *Chem. Commun.* **2015,** *51* (82), 15176-15179.

32. Wang, X.; Zhang, Q.; Nam, C.; Hickner, M.; Mahoney, M.; Meyerhoff, M., Ionophore-based anion‐selective optode printed on cellulose paper. *Angew. Chem. Inter. Ed.* **2017,** *56* (39), 11826-11830.

33. Wang, X.; Mahoney, M.; Meyerhoff, M. E., Inkjet-Printed Paper-Based Colorimetric Polyion Sensor Using Smartphone as a Detector. *Anal. Chem.* **2017**, 89 (22), 12334-12341.

34. Ferguson, S. A.; Wang, X.; Mahoney, M.; Meyerhoff, M. E., Detection and Quantification of Polyquaterniums *via* Polyion-Sensitive Ion-Selective Optodes Inkjet Printed on Cellulose Paper. *Anal. Sci.* **2018,** *34* (1), 45-50.

35. Gerold, C. T.; Bakker, E.; Henry, C. S., Selective Distance-Based K+ Quantification on Paper-Based Microfluidics. *Anal. Chem.* **2018,** *90* (7), 4894-4900.

36. Kassal, P.; Sigurnjak, M.; Steinberg, I. M., Paper-based ion-selective optodes for continuous sensing: Reversible potassium ion monitoring. *Talanta* **2019,** *193*, 51-55.

37. Xie, X.; Mistlberger, G.; Bakker, E., Ultrasmall Fluorescent Ion-Exchanging Nanospheres Containing Selective Ionophores. *Anal. Chem.* **2013,** *85* (20), 9932-9938.

38. Xie, X.; Zhai, J.; Bakker, E., pH Independent Nano-Optode Sensors Based on Exhaustive Ion-Selective Nanospheres. *Anal. Chem.* **2014,** *86* (6), 2853-2856.

39. Komuro, N.; Takaki, S.; Suzuki, K.; Citterio, D., Inkjet printed (bio)chemical sensing devices. *Anal. Bioanal. Chem.* **2013,** *405* (17), 5785-5805.

40. Yamada, K.; Henares, T. G.; Suzuki, K.; Citterio, D., Paper‐Based Inkjet‐Printed Microfluidic Analytical Devices. *Angew. Chem. Inter. Ed.* **2015,** *54* (18), 5294-5310.

41. Bühlmann, P.; Pretsch, E.; Bakker, E., Carrier-Based Ion-Selective Electrodes and Bulk Optodes. 2. Ionophores for Potentiometric and Optical Sensors. *Chem. Rev.* **1998,** *98* (4), 1593-1688.

42. Credou, J.; Berthelot, T., Cellulose: from biocompatible to bioactive material. *J. Mater. Chem. B* **2014,** *2* (30), 4767-4788.

43. Ahmed, S.; Bui, M.-P. N.; Abbas, A., Paper-based chemical and biological sensors: Engineering aspects. *Biosens. Bioelectron.* **2016,** *77*, 249-263.

44. Ota, R.; Yamada, K.; Suzuki, K.; Citterio, D., Quantitative evaluation of analyte transport on microfluidic paper-based analytical devices (μPADs). *Analyst* **2018,** *143* (3), 643-653.

45. Murphy, A.; Gorey, B.; de Guzman, K.; Kelly, N.; Nesterenko, E.; Morrin, A., Microfluidic paper analytical device for the chromatographic separation of ascorbic acid and dopamine. *RSC Adv.* **2015,** *5* (113), 93162-93169.

46. Pelton, R., Bioactive paper provides a low-cost platform for diagnostics. *TrAC Trends Anal. Chem.* **2009,** *28* (8), 925-942.

47. Yamada, K.; Henares, T. G.; Suzuki, K.; Citterio, D., Distance-Based Tear Lactoferrin Assay on Microfluidic Paper Device Using Interfacial Interactions on Surface-Modified Cellulose. *ACS Appl. Mater. Interfaces* **2015,** *7* (44), 24864-24875.

48. Duong, T. D.; Hoang, M.; Nguyen, K. L., Sorption of Na^{+}, Ca^{2+} ions from aqueous solution onto unbleached kraft fibers kinetics and equilibrium studies. *J. Colloid Interface Sci.* **2005,** *287* (2), 438-443.

49. Duong, T. D.; Hoang, M.; Nguyen, K. L., Extension of Donnan theory to predict calcium ion exchange on phenolic hydroxyl sites of unbleached kraft fibers. *J. Colloid Interface Sci.* **2004,** *276* (1), 6-12.

50. Reddad, Z.; Gerente, C.; Andres, Y.; Le Cloirec, P., Adsorption of several metal ions onto a low-cost biosorbent: kinetic and equilibrium studies. *Environm. Sci. Tech.* **2002,** *36* (9), 2067-2073.

51. Hirayama, E.; Sugiyama, T.; Hisamoto, H.; Suzuki, K., Visual and colorimetric lithium ion sensing based on digital color analysis. *Anal. Chem.* **2000,** *72* (3), 465-474.

52. Yamada, K.; Citterio, D.; Henry, C. S., "Dip-and-read" paper-based analytical devices using distance-based detection with color screening. *Lab Chip* **2018,** *18* (10), 1485-1493.

53. Krauss, S. T.; Nauman, A. Q.; Garner, G. T.; Landers, J. P., Color manipulation through microchip tinting for colorimetric detection using hue image analysis. *Lab Chip* **2017,** *17* (23), 4089-4096.

Chapter 5
General conclusion

5.1. Summary of the results

Until now, the implementation of ionophore-based ion-selective optodes (ISOs) into paper-based sensing platforms has gained in the academic field to expand the feasibility of colorimetric paper devices targeting ion species. Because typical ISOs must refer to protons as reference ions to quantify cations of interest, it is known that pH-dependent sensing system is the most challenging for the development of ISO-based sensors. Moreover, the evaluation of the ISO response has been often performed by the use of spectral information (e.g. UV-vis absorbance measurement) or digital color analysis (e.g. camera, colorimetric scanner). For these reasons, both (i) elimination of pH dependence and (ii) equipment-free readout is significantly essential to develop ISO-integrated sensors for point-of-care testing (POCT) or on-site analysis. In the current thesis, various sensing platforms, which are composed of a classical film-based ISO (**Chapter 2**), a plasticizer-free ISO (**Chapter 3**), and a micelle-based ISO nanosphere (**Chapter 4**), have been applied to (microfluidic) paper-based analytical devices ((μ)PADs) by means of inkjet-printing technology.

Elimination of pH dependence during ISO-based assay has been accomplished by the introduction of pre-deposited pH-buffering reagents. For development of ISO-integrated μPADs, open microfluidic channel potentially provides poor selectivity because of an increase in the analyte concentration by the evaporation of applied sample liquid. For this reason, whole device lamination allowing for prevention of evaporation loss of sample liquid served to preserve the selectivity over other potentially interfering cations. Although the function of classical equilibrium-based ISOs has been embedded into μPADs, paper substrate caused a shift of the response function to higher analyte activities in comparison to classical film-based optodes deposited on solid plastic substrates (non-active substrate). It has been demonstrated that the cause for this shift primary lies in the cation-exchange adsorption properties of the cellulosic paper matrix.

Another approach to overcome pH dependence is the introduction of a fluorescent solvatochromic dye (SD) instead of a conventional H^+-responsive chromoionophore. In the current thesis, pH-independent sensing system has been first applied to paper-based assay with ISOs, regarded as plasticizer-free ISOs. The developed paper-based ISOs has eliminated a traditional pH-controlling step prior to the ISO-based assay, and they provided the excellent selectivity derived from used ion-specific ionophores. Although the feasibility of SD-based ISOs is still limited to simple matrix samples (e.g. drinking water in the current thesis), the use of SDs served to expand analytical application of paper-based ISOs.

To meet with equipment-free readout, distance-based detection model has been applied to ISO-integrated μPADs, and the applicability of the developed paper devices has been successfully demonstrated. Distance-based readout promises calibration-free semi-quantification by measuring the resultant length of the color-changed region of ISOs. It should be noted that highly reproducible device fabrication is essential to achieve distance-based quantification. For this purpose, all device fabrications of ISO-integrated μPADs have been performed by the use of printing technology (wax and inkjet-printing) for the first time. The printing ink of water-monodisperse micelle-based ISO nanospheres (nano-optodes) potentially enabled dispensing with a simple desktop thermal inkjet printer, and the use of volatile organic compounds (VOCs) which are unsuitable for industrial manufacturing can be avoided. Moreover, the introduction of pre-deposited electrolyte salts ($MgCl_2$) for an increase in ionic strength of sample liquid has provided the improved sensitivity because working principle of distance-based readout relied on the adsorption of analyte cations onto the cellulosic paper substrates. Although the developed paper devices require relatively long assay time, they have quantified the concentration of Ca^{2+} in drinking and tap water samples, which are comparable to conventional analytical technique (complexometric titration).

Finally, the current thesis has stated the potential of ionophore-based ISOs in fabrication of μPADs targeting ion sensing and overcoming historical drawbacks of ISO-based sensor by the use of μPADs. The main focus is on the fundamental study for the development of ISO-integrated (μ)PADs by addressing the chemical interaction between analyte cations and cellulosic paper substrates. The early stage of practical

applications of these techniques have experimentally demonstrated in cation sensing paper devices.

5.2. Future outlook

Scheme 5-1 demonstrates the summarized pathways toward the paper-based analytical devices targeting industrial products. Contrast to successful paper devices (e.g. dipsticks, immunochromatography test kit), the majority of μPADs are chemical still under development for commercialization in the market. In the current thesis, fundamental study on the integration of ionophore-based ISOs into paper-based sensing platform and an early stage of simple practical application with the developed ISO-integrated paper devices have been demonstrated. Although the feasibility of μPADs to detect ion species has been expanded by the establishment of ISOs on paper substrates, further studies must be required before industrial manufacturing. For example, ISO-based sensors typically require matrix simplification for the assay using complicated samples such as biological fluids (e.g. urine, blood). Therefore, it should be essential that not only the response function of paper-based ISOs but also pretreatment step prior to the ISO-based assay. In addition, reliability of paper-based ISOs was never discussed in the academic field until now. To overcome these issues, not focusing on applicability to practical use but careful fundamental study (e.g. working function on a sensor substrate) must be necessary. Once again, paper-based ISOs still require further studies to promise commercialization, however, paper-based ISO will gain by accompanying other analytical technique to improve device handling and reliability, such as smartphone or Raspberry Pi for automation of colorimetric readout.

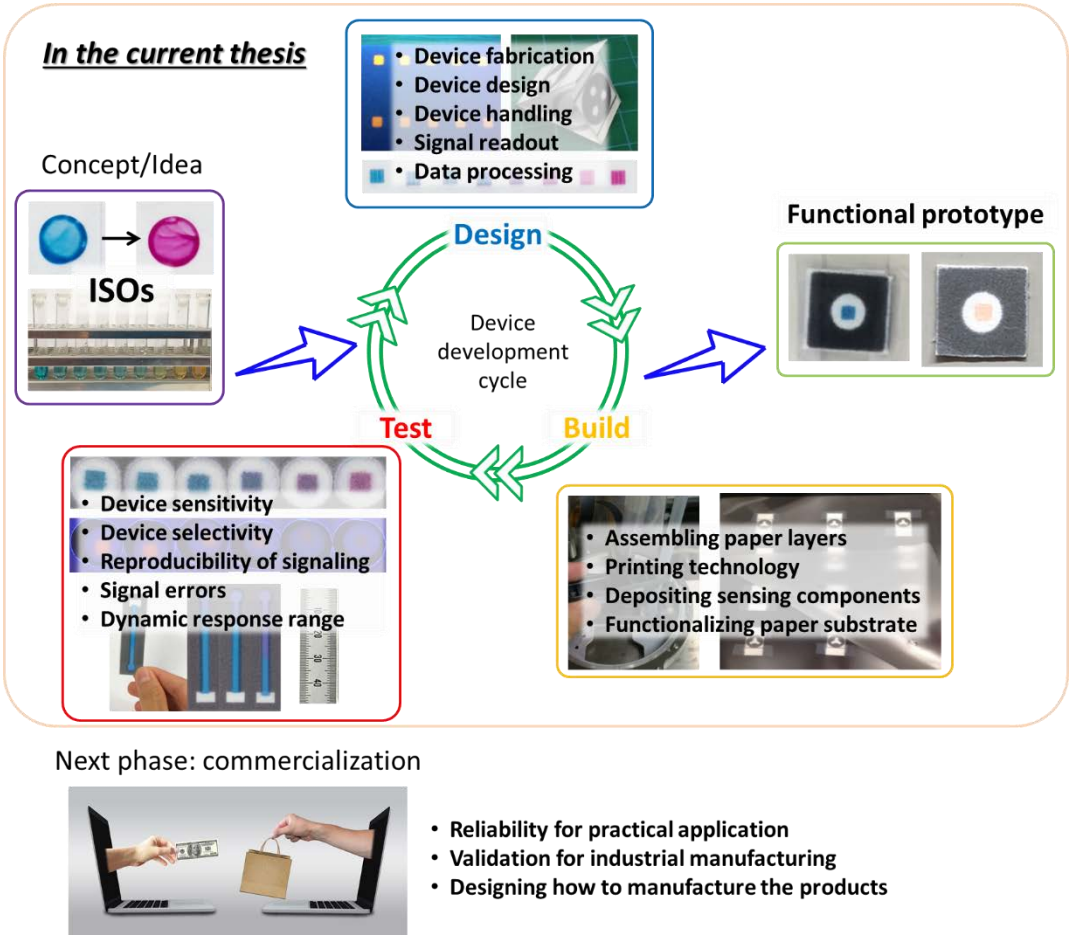

Scheme 5-1. Essential steps for development of paper-based analytical devices targeting industrial application

Achievement list

Original papers related to this thesis

(1) Hiroyuki Shibata; Terence G. Henares; Kentaro Yamada; Koji Suzuki; Daniel Citterio,
"Implementation of a Plasticized PVC-Based Cation-Selective Optode System into a Paper-Based Analytical Device for Colorimetric Sodium Detection", *Analyst*, **2018**, *143*, 678-686.

(2) Hiroyuki Shibata; Yuki Hiruta; Daniel Citterio,
"Fully inkjet-printed distance-based paper microfluidic devices for colorimetric calcium determination using ion-selective optodes", *Analyst*, **2019**, *144*, 1178-1186.

Other original papers

(1) Yoshiki Soda; Hiroyuki Shibata; Kentaro Yamada; Koji Suzuki; Daniel Citterio,
"Selective Detection of K^+ by Ion-Selective Optode Nanoparticles on Cellulosic Filter Paper Substrates",
ACS Applied Nano Materials, **2018**, *1*, 4, 1792–1800.

(2) Quoc Trung Hua; Hiroyuki Shibata; Yuki Hiruta; Daniel Citterio,
"Flow Control-Based 3D μPADs for Organophosphate Pesticide Detection", Analytical Science, **2019**, *35*, 4, 393-399.

(3) Shogo Fujisaki; Hiroyuki Shibata; Kenrato Yamada; Koji Suzuki; Daniel Citterio,
"Printed low-cost microfluidic analytical devices based on a transparent substrate", *Analyst*, **2019**, *144*, 2746-2754

Review articles

(1) Kentaro Yamada[†]; Hiroyuki Shibata[†]; Koji Suzuki; Daniel Citterio,
"Toward practical application of paper-based microfluidics for medical diagnostics: state-of-the-art and challenges", *Lab on a Chip*, **2017**, *17*, 1206-1249. ([†] equally contributed)

Other publications

(1) 石井 政憲、城戸 滉太、太田 力、柴田 寛之、山田 健太郎、鈴木 孝治、チッテリオ ダニエル
「インクジェット技術によるペーパーマイクロ流体デバイスの開発」
日本画像学会誌, **2016**, *55*, 94−105.

(2) Hiroyuki Shibata; Yuma Ikeda; Daniel Citterio,
"Inkjet-printed colorimetric paper-based gas sensor for the discrimination of volatile primary amines with amine-responsive dye-encapsulating polymer nanoparticles",
Biomimetic Sensing: Methods and Protocols, USA, 2018

International conference presentations

Oral presentations

(1) "Inkjet-printed colorimetric paper optode microfluidics for simple quantification of Calcium ions",
○Hiroyuki Shibata; Yuki Hiruta; Daniel Citterio,
Bio4Apps 2017, Tokyo (Japan), December 2017.

Poster presentations

(1) "Ion selective optodes for inkjet-printed microPADs"
○Hiroyuki Shibata; Terence G. Henares; Nobutoshi Komuro; Koji Suzuki; Daniel Citterio,
RSC Tokyo International Conference, Chiba (Japan), September 2015.

(2) "Inkjet-printed paper-based ion optode devices"
○Hiroyuki Shibata; Terence G. Henares; Nobutoshi Komuro; Koji Suzuki; Daniel Citterio,
Pacifichem, Honolulu (Hawaii), December 2015.

(3) "Printed paper-based ion-selective optode devices with integrated pH-buffer system",
○Hiroyuki Shibata; Terence G. Henares; Kentaro Yamada; Koji Suzuki; Daniel Citterio,
RSC Tokyo International Conference, Chiba (Japan), September 2016.

(4) "pH-Buffer-integrated ion-selective optodes on printed microfluidic paper-based analytical devices (microPADs)",
○Hiroyuki Shibata; Terence G. Henares; Kentaro Yamada; Koji Suzuki; Daniel Citterio,
Pittcon, Chicago (USA), March 2017.

(5) "Paper-based colorimetric sodium ion-selective devices integrated with pH-buffering function",
○Hiroyuki Shibata; Terence G. Henares; Kentaro Yamada; Koji Suzuki; Daniel Citterio,
International Workshop on Quantitative Biology, Kanagawa (Japan), April 2017.

(6) "Inkjet-printed calcium-selective microfluidic paper devices using distance-based quantification",
○Hiroyuki Shibata; Yuki Hiruta; Daniel Citterio,
RSC Tokyo International Conference, Chiba (Japan), September 2017.

(7) "Printed ionophore-based colorimetric microfluidic paper devices for determination of calcium ions using distance-based quantification",
○Hiroyuki Shibata; Yuki Hiruta; Daniel Citterio,
Pittcon, Orlando (USA), February 2018.

(8) "Printed distance-based paper microfluidics for colorimetric detection of calcium ions",
○Hiroyuki Shibata; Yuki Hiruta; Daniel Citterio,
Europt(r)ode XIV, Napoli (Italy), March 2018.

(9) "Paper-Based pH-Independent Optical Calcium Sensor with Lipophilic Solvatochromic Dye"
○Hiroyuki Shibata; Yuma Ikeda; Yuki Hiruta; Daniel Citterio,
RSC Tokyo International Conference, Chiba (Japan), September 2018

Domestic conference presentations

Oral presentations

(1) 「Ionophore-based colorimetric sodium ion sensing on pH-buffer integrated paper-based devices」
○Hiroyuki Shibata、 Terence Gaba Henares、Kentaro Yamada、Koji Suzuki、Daniel Citterio,
日本化学会 第 97 春季年会，慶應義塾大学 日吉キャンパス，横浜，2017 年 3 月.

(2) 「飲料水中のカルシウムイオン比色分析に向けた距離検出型ペーパーチップ」
○柴田 寛之、蛭田 勇樹、Citterio Daniel,
日本分析化学会 第 67 年会，東北大学 大学院 理学研究科・理学部キャンパス，仙台，2018 年 9 月.

Poster presentation

(1) ナトリウムイオン検出のためのイオン選択性オプトード法に基づいたマイクロ流体紙基板分析デバイス」
○柴田 寛之、ヘナレス ガバ テレンス、山田 健太郎、鈴木 孝治、チッテリオ ダニエル,
化学とマイクロ・ナノシステム学会 第 34 回研究会 (34th CHEMINAS),
幕張メッセ国際会議場，千葉，2016 年 9 月.

(2) 「印刷技術を用いた pH 緩衝作用が内蔵された紙基板イオン選択性オプトードデバイス」
○柴田 寛之、ヘナレス ガバ テレンス、山田 健太郎、鈴木 孝治、チッテリオ ダニエル,
日本分析化学会 第 65 年会，北海道大学，札幌，2016 年 9 月.

(3) 「イオン選択性オプトード法に基づいたナトリウムイオン分析に向けたマイクロ流体 紙基板分析デバイスの開発」
○柴田 寛之、Henares G. Terence、山田 健太郎、鈴木 孝治、Citterio Daniel,
日本分析化学会 ホテルニュー塩原，那須，2017 年 7 月.

(4) 「イオン選択性オプトード法によるカルシウムイオン分析に向けた距離検出型マイクロ流体紙基板分析デバイス」
○柴田 寛之、蛭田 勇樹、Citterio Daniel,
日本分析化学会 第 66 年会，東京理科大学 葛飾キャンパス，葛飾，2017 年 9 月.

(5) 「飲料水中のカルシウムイオン比色分析に向けた簡便かつ安価なペーパーチップの開発」
○柴田 寛之、蛭田 勇樹、Citterio Daniel,
日本分析化学会若手交流会，新富亭，宮城，2018 年 7 月.

Other conference activities

International conferences

(1) "Inkjet generated ion-selective optode particles for calibration-free sensing on paper-based analytical devices",
○Yoshiki Soda; Hiroyuki Shibata; Kentaro Yamada; Koji Suzuki; Daniel Citterio,
Pittcon, Chicago (USA), March 2017.

(2) "Inkjet generated ion-selective optode particles for calibration-free sensing on paper-based analytical devices"
○Yoshiki Soda; Hiroyuki Shibata; Kentaro Yamada; Koji Suzuki; Daniel Citterio,
International Workshop on Quantitative Biology, Kanagawa (Japan), April 2017.

(3) "Inkjet generated ion-selective optode particles for calibration-free sensing on paper-based analytical devices"
○Yoshiki Soda; Hiroyuki Shibata; Kentaro Yamada; Koji Suzuki; Daniel Citterio,
RSC Tokyo International Conference, Chiba (Japan), September 2017.

(4) "Paper device for simultaneous colorimetric quantification of salivary Na^+, K^+, Ca^{2+}"
○Yasuhiro Suenaga; Hiroyuki Shibata; Yuki Hiruta; Daniel Citterio,
RSC Tokyo International Conference, Chiba (Japan), September 2018.

(5) "Reader-free quantification of urinary hemoglobin on paperfluidic analytical device"
○Rika Sawano; Hiroyuki Shibata; Kento Maejima; Yuki Hiruta; Daniel Citterio,
RSC Tokyo International Conference, Chiba (Japan), September 2018.

(6) "Printed low-cost microfluidic analytical devices based on a transparent substrate"
○Shogo Fujisaki; Hiroyuki Shibata; Yoshiki Soda; Kentaro Yamada; Koji Suzuki; Daniel Citterio,
Flow Analysis XIV, Bangkok (Thailand), December 2018.

Domestic conferences

(1) 「インクジェットプリント技術によるオプティカルセンシング粒子の創製」,
○相田 佳毅、柴田 寛之、山田 健太郎、鈴木 孝治、チッテリオ ダニエル,
日本分析化学会 第 65 年会、北海道大学、札幌、2016 年 9 月

(2) 「Inkjet-generated ion-selective optode particles for calibration-free sensing on paper-based analytical devices」,
○Yoshiki Soda、Hiroyuki Shibata、Kentaro Yamada、Koji Suzuki、Daniel Citterio,
日本化学会 第 97 春季年会，慶應義塾大学 日吉キャンパス，横浜，2017 年 3 月

(3) 「印刷技術を用いた低コスト透明基板マイクロ流体分析デバイス」,
○藤崎 省吾、柴田 寛之、山田 健太郎、相田 佳毅、鈴木 孝治、チッテリオ ダニエル,
日本分析化学会 第 66 年会，東京理科大学 葛飾キャンパス，葛飾，2017 年 9 月

(4) 「唾液中の Na^+, K^+, Ca^{2+}の同時定量可能な比色分析用紙基板デバイスの開発」
○末永 泰広、柴田 寛之、蛭田 勇樹、Citterio Daniel,
日本分析化学会 第 67 年会，東北大学 大学院 理学研究科・理学部キャンパス，仙台，2018 年 9 月

Awards

(1) 「優秀発表賞」，学とマイクロ・ナノシステム学会 第 34 回研究会 (34th CHEMINAS)，2016 年 9 月

(2) “Lab on a Chip 2017 Most Downloaded Articles”, *Lab on a Chip*, **2017**, *17*, 2, 1206-1249.

(3) “Analyst Hot Article”, *Analyst*, **2018**, *143*, 678-686.

(4) “Best student poster 1st award”, Europt(r)ode XIV, March 2018.

Acknowledgement

First and foremost, I would like to express the deepest gratitude to my supervisor Prof. Daniel Citterio for his enormous efforts in guidance and encouragement throughout the progress of my work. He always showed me the right way to become an academic researcher and more importantly taught me how to perform the achademic research. This thesis would not have been possible without valuable guidance.

I would also like to express my great gratitude to my thesis committee, Prof. Yasuhiro Koike, Prof Seimei Shiratori, and Prof. Hiroaki Onoe for their precious reviews to edit this thesis. I gratefully acknowledge Prof. Koji Suzuki as a co-supervisor for his kind support and encouragement. Also, I am deeply grateful to Prof. Yuki Hiruta for his kind support and encouragement. Without his valuable guidance and persistent help, this thesis would not have been possible.

I would like to show my greatest appreciation to Dr. Terence Gaba Henares for his great guidance and helpful discussion. His advice and comments have been a great help in facing with difficulties to progress my work. Also, I wish to express that Mr. Nobutoshi Komuro made enormous contribution to consider the device design for optical cation detection based on ion-selective optodes. I am grateful for the assistance and encouragement given by the laboratory members. I would like to express my special thanks to Dr. Vahid Hamedpour and Mr. Yuma Ikeda for their support and encouragement as my friends.

I am deeply grateful to Prof. Eric Bakker of the Department of Inorganic and Analytical Chemistry, University of Geneva, for helpful discussion.

I would like to acknowledge a research scholarship from a Keio University Doctorate Student Grant-in-Aid Program. This work was financially supported by the Medical Research and Development Programs Focused on Technology Transfer: Development of Advanced Measurement and Analysis Systems (SENTAN), given by Japan Agency for Medical Research and Development; AMED.

Finally, I wish to show my greatest application to my family for their understanding and continued support during research life.